DEVELOPMENT OF A FINITE ELEMENT BASED INJURY METRIC FOR PULMONARY CONTUSION

BY

F. SCOTT GAYZIK, M.S.

A Dissertation Submitted to the Graduate Faculty of

VIRGINIA TECH – WAKE FOREST UNIVERSITY

SCHOOL OF BIOMEDICAL ENGINEERING & SCIENCES

in Partial Fulfillment of the Requirements

for the Degree of

DOCTOR OF PHILOSOPHY

Biomedical Engineering

August, 2008

Winston-Salem, North Carolina

Approved by:

Joel D. Stitzel, Ph.D., Advisor & Chair _____

Examining Committee:

J. Jason Hoth, M.D. _____

Stefan M. Duma, Ph.D. _____

H. Clay Gabler, Ph.D. _____

R. Shayn Martin, M.D. _____

ACKNOWLEDGEMENTS

I would like to thank my primary advisor, Joel Stitzel for his guidance and patience in working with me over the course of my doctoral studies. He has always impressed me with his insights and depth of knowledge of injury biomechanics and has motivated me to achieve successes that exceeded even my own expectations. I certainly could not have accomplished all that I have while working towards my degree had it not been for his efforts. I have grown as a scientist, engineer, and professional during my tenure at Wake Forest University and I owe a great deal of that progression to Dr. Stitzel's guidance.

Biomedical engineering is a collaborative effort, and I believe my committee speaks to that fact. Jason Hoth, who conducted all of the surgeries for the experiments presented in this thesis, was absolutely critical to completing this work. Dr. Hoth was very generous with his time and resources and I owe him a great deal of gratitude. I have also benefited from the clinical insights of Shayn Martin, who despite his busy schedule, was able to help conduct CIREN and NASS studies for this thesis and ongoing research in the Center for Injury Biomechanics.

I must also thank the members of my committee from Virginia Tech, Stefan Duma and Clay Gabler. While working in the CIB, I have had the pleasure of taking classes taught by Dr. Duma and Dr. Gabler. Their classes were informative and enjoyable and provided a strong foundation for my own research. I owe a great deal to the philosophy that is shared by all professors in the CIB that the students should conduct and present their research to the community. This belief helped me hone my presentation skills, conquer my fears, and it was a great motivator. Thanks to this philosophy, I earned my way to Lyon, Melbourne, San Diego, Los Angeles, Washington DC, Detroit, Chicago, and last but not least Terra Haute!

But the acknowledgments could not be complete without thanking my family, who have always been there to celebrate the successes and to provide support in the difficult times. Without a doubt, the single most important person in my life for the last four years has been my

wife, Caroline. We began dating shortly before I began my doctoral work and were married just as things began to get hectic. She has always been there to be a voice of calm and reason and to remind me that there is much more to life than work. Bottom line; I couldn't have done this without her. I must also thank my mother and father, who have always supported my decisions and provided unwavering support in my pursuit of this degree. And to my brother Adam, thank you for always being ready with a crazy, nonsensical joke or story to brighten my day and keep me from taking things too seriously. I'm still working on that biomechanical arm by the way.

Much of my experiences at Wake Forest University have also been shaped by colleagues who I have had the pleasure of working with, including Kerry Danelson, Kathryn Loftis, Melissa Daly, and Mao Yu. I thank you all for your help over the years and for making coming to work each day a pleasure.

Of course, it wasn't all work. Winston-Salem has become home over the last several years because of some truly wonderful friends. I must thank Todd Atwood, Michael Lawrence, Jesse and Alix Norris, and Brian and Amanda Rucker (and many more…) for making these years so special.

I have greatly enjoyed my time at Wake Forest University in the Center for Injury Biomechanics, so much so that I decided to stay! It was the people around me that made the experience what it was, so here's to what's next.

TABLE OF CONTENTS

List of Figures

List of Tables

Abstract

Motor vehicle crash (MVC) and its associated injuries remain a major public health problem world wide. In 2005 alone there were 6 million police-reported crashes in the United States resulting in 2.5 million injuries and 46,000 fatalities. The thorax is second only to the head in terms of frequency of injury following MVC, and pulmonary contusion (PC) is the most common intra-thoracic soft tissue injury sustained as a result of blunt chest trauma. The goal of this dissertation research is to mitigate this commonly-sustained and potentially life threatening injury. We have taken a computational approach to solving this problem by developing a predictive injury metric for PC using finite element analysis (FEA).

The dissertation begins with an epidemiological examination of the crash modes, vehicles, and patient demographics most commonly associated with PC. This study was conducted using real world crash data from the Crash Injury Research and Engineering Network (CIREN) database and data from government-sponsored vehicle crash tests. The CIREN data showed that a substantial portion of the crashes resulting in PC were lateral impacts (48%). Analysis of the thoracic loading of dummy occupants in lateral crash tests resulted in mean values of medial-lateral chest compression and deflection velocity of 25.3 ± 2.6 % and 4.6 ± 0.42 $m \cdot s^{-1}$ respectively. These data provided quantified loading conditions associated with crash-induced PC and a framework for the remaining research studies, which were focused on blunt impact experiments examining the relationship between insult and outcome in a living model of this injury.

A combined experimental and computational approach was used to develop injury metrics for PC. The animal model selected for this research was the Sprague-Dawley male rat. In the remaining studies that comprise this dissertation, an outcome measure of the inflammatory response in the lung parenchyma was correlated with a mechanical analog calculated via a finite element model of the lung.

For all studies, a precise and instrumented electronic piston was used to apply prescribed insults directly to the lungs of the subjects. In the first set of experiments, contusion volume was calculated from MicroPET (Micro Positron Emission Tomography) scans and normalized on the basis of liver uptake of 18F-FDG. The subjects were scanned at 24 hours, 7 days, and 28 days (15 scans), and the contused volume was measured. A tentative criteria based on first principal strain in the parenchyma between 9 and 36% was established. In subsequent experiments Computed Tomography was used to acquire volumetric contusion data. The second set of experiments introduced two important aspects of this dissertation; a semi-automated algorithm for CT segmentation and a technique to match the spatial distribution of contusion within the lung to finite element analysis results. The results of this study indicated that the product of first principal strain and strain rate ($\varepsilon_{max} \cdot \dot{\varepsilon}_{max}$) is the most appropriate output variable upon which to base an injury metric for PC. Digital analysis of histology from study subjects that underwent CT scanning prior to sacrifice was conducted and showed good agreement between CT and histology.

A final set of experiments was conducted to synthesize the techniques developed in previous studies to determine an injury metric for PC. A concurrent optimization technique was applied to the FEA model to match force vs. deflection traces from four distinct impact cohorts. The resulting predictive injury metrics for PC were $\varepsilon_{max} \cdot \dot{\varepsilon}_{max}$ exceeding 94.5 sec^{-1}, first principal strain (ε_{max}) exceeding 0.284 (true strain, dimensionless), and first principal strain rate ($\dot{\varepsilon}_{max}$) exceeding 470 sec^{-1}.

The method used in this dissertation and the resulting injury metrics for PC are based on quantified inflammatory response observed in a living model, specifically in the organ of interest. This injury metric improves upon current thoracic injury criteria that rely on gross measures of chest loading such as acceleration, or deflection, and are not specific to a particular injury. We anticipate that the findings of this work will lead to more data-driven improvements to vehicular safety systems and ultimately diminish the instance of PC and mitigate its severity.

CHAPTER I

INTRODUCTION

I.1. Significance

In civilian trauma, rapid deceleration from motor vehicle crash (MVC) or falls are the predominant mechanisms for pulmonary contusion (PC).[1] This injury is frequently encountered in acute care settings and is a factor in the management of 10-17% of all trauma admissions.[1, 2] As a body region, trauma sustained to the chest is second only to head trauma in the injuries sustained in MVC.[3, 4] The mortality associated with PC is difficult to determine but is estimated to be 5-25% for adults and as high as 43% for children.[2, 5, 6] Pulmonary contusion has been demonstrated as an independent predictor of serious complications including Acute Respiratory Distress Syndrome (ARDS) and pneumonia.[7] The outcome has historically been difficult to predict because of a lack of prospective studies of the lesion quantifying both the mechanical insult and the host outcome. In nearly all acute care cases, the outcome due to the injury is quantifiable but the magnitude of the insult is unknown.[8]

The sequelae of PC vary widely and include ventilation and perfusion mismatch, elevated intrapulmonary shunt, and edema caused by inflammation of lung tissue. These clinically manifest as hypoxia, hypercarbia, and an increased work of breathing.[1] Long term respiratory dysfunction has been reported to last for months to years following the initial insult.[9] Recent studies of PC suggest that the lung plays a role in the inflammatory

response of the host in both a local and system fashion.[10-13] This systemic response predisposes the injured patient to developing complications from relatively lesser insults such as sepsis or surgery, a hypothesis often referred to as the "two-hit" model of trauma.[14, 15]

Given these findings, PC is a common injury which can result in potentially life threatening complications, yet no organ-specific injury metric exists for this lesion. Current thoracic injury criteria are much debated and rely on gross measures of chest loading such as chest acceleration, chest deflection or combinations of these measures.[16, 17] Additionally, much of the research performed on the development of thoracic injury criteria is based on experimentation on post-mortem human subjects which, by virtue of the inflammatory etiology of PC, cannot be used to evaluate the severity of contusion. In this dissertation we employ a method to determine an injury metric for PC directly based on the inflammatory response following injury.

I.2. Animal Models of Lung Trauma

Numerous animal models of PC have been published in the literature. These can be broken down into those utilizing larger animals, including canine[18] and porcine[19, 20] models and those utilizing murine models.[10, 11, 13, 21-23] Recent studies have favored murine models because of their well understood physiology and anatomy. Additionally, their small size makes high throughput studies possible, yet they are large enough to achieve adequate resolution through imaging studies. The rat in particular has been used in a number of studies of PC. The clinical relevance of the rat model is well established in the literature. Like clinical findings, rat lung dysfunction has been shown to progress over time following a blunt insult, with significant departures from baseline values

observed within 30 minutes and peaking between 24 and 48 hours post insult.[10, 23] Histological findings of PC in rat models are consistent with histology from human specimens demonstrating intrabronchial hemorrhage, and positive influx of neutrophils.[12, 21] On a macroscopic scale, lung dysfunction can be assessed through monitoring the ratio of the partial pressure of arterial oxygen (PaO_2) to fraction of inspired oxygen (FiO_2). This ratio, known as the P/F ratio, has been shown to decrease as lung function deteriorates.[10, 11]

In the clinical setting, pathology of the lung is frequently assessed via medical imaging modalities such as CT and x-ray. Previously published studies in this dissertation employ both Positron Emission Tomography (PET) and Computed Tomography (CT) to quantify the volume of contusion resulting from a quantified insult to the rat lung.[22, 24]

I.3. Predictors of Traumatic Lung Injury

A repeatable means of determining the volume of contused lung tissue in a patient may lead to earlier, more effective treatment and improved outcome.[25] The ability to determine this data also has important implications for biomechanical studies wherein quantifying the outcome (in terms of a volumetric assessment of the lesion) is equally as important as quantifying the initial insult (in terms of a force vs. deflection loading history). In the clinical literature, studies quantifying contusion have been reported using both plain film x-ray[26] and CT.[8, 25] A study by Miller et al. (2001) using CT data demonstrated that patients with 20% contusion by volume or greater had a significantly greater risk of developing ARDS than patients with less than that amount. The volume of lung contusion may also increase the risk of developing pneumonia.[27] While these

studies provide valuable information for formulating treatment plans, they do not aid in engineering improved countermeasures because they are missing two critical pieces of information: 1. the magnitude of the insult that resulted in the injury and 2. the tolerance of the lung itself to injury. Quantifying these data was the central focus of this dissertation work.

I.4. Finite Element Analysis and the Formulation of Injury Metrics

The increasing capability of computers to solve mathematical simulations of dynamic impacts have made finite element analysis (FEA) an attractive tool for establishing human injury tolerance criteria. These models discretize the spatial and temporal domains of an object under load to calculate the internal deformations dynamically. FEA models are frequently used to predict injury based on local stress and strain within the tissue. Many constitutive equations describing the stress and strain behavior of tissue under dynamic loading have been integrated into commercially available finite element solvers. A previously published material model for lung [28] implemented in a commercially-available dynamic FEA software (LS-Dyna, LSTC, Livermore, CA) is used throughout this dissertation.

Examples of this trend can be found in studies examining injury tolerance of various organs in the body. A significant amount of effort has been spent in recent years developing finite element models of the brain for injury prediction purposes. The National Highway Traffic Safety Administration (NHTSA) is currently developing the Simulated Injury MONitor (SIMon) model for predicting distinct soft tissue injuries in the brain including diffuse axonal injury and subdural hematoma.[29] Mathematical correlates based on the deformation of elements comprising the model have been

identified and evaluated for these injuries. Zhang et al. used a statistical approach in determining an injury metric for mild traumatic brain injury and found that shear stress at the brainstem in excess of 6.6 kPa resulted in the most accurate prediction of injury vs. non injury cases.[30]

Similar approaches have been applied to determine injury thresholds for rib fractures when injury and non injury data are available,[31] and also at a localized level using machined bone specimens.[32] Other soft tissue injuries have been studied using FEA; and injury thresholds have been proposed for aortic rupture,[33] carotid artery dissection[34], globe rupture of the eye,[35] and injury to the abdominal viscera.[36] While tentative injury criteria have been established for the lung, a more rigorous approach using CT and injury data from impacts of varying degrees of severity are required to establish formalized finite element-based criteria for lung injury.

I.5. Overall Objective and Approach

The goal of this research was to develop finite element-based injury metrics for PC following blunt thoracic trauma. Development of these injury metrics were accomplished using a rat model of PC in conjunction with a finite element model of the rat lung. Synergy between the animal and computational models have resulted in a more thorough characterization of this injury than using either one of these models in isolation.

In **Chapter II**, the crash epidemiology of PC is examined in order to better understand the vehicles, crash modes, patient demographics, and loading conditions that are commonly associated with this injury. The results of this study: 1. were used as validation of the loading used in preliminary research in this area, 2. provided a foundation for the final set of experiments conducted in the development of injury

metrics, and 3. will be used as the basis for continuing research investigating PC in modeling work focused on full body models. This chapter was accepted to the Journal of Trauma in July 2008 and is currently in review.

Chapter III[22] is the foundation for much of the experimental work in this dissertation. This chapter introduces the experimental setup, the finite element model of the rat lung used throughout this dissertation, and an optimization approach to tune the output of the model to experimental data. The inflammatory response of study subjects was quantified by PET and correlated to FEA model results, resulting in preliminary values for injury metrics based on first principal strain.

Chapter IV[24] builds on the methods established in Chapter III. In this study, PC was quantified using CT rather than PET, which affords a number of advantages, including reduced acquisition time, and the ability to determine normalized values of contusion to compare across study subjects. In addition, a technique to quantify the volume and spatial distribution of the contusion within the study subjects was introduced. This technique allowed for registration with the FEA results to determine the most appropriate injury metric for PC. This registration technique found that the product of first principal strain and its strain rate ($\varepsilon_{\max} \cdot \dot{\varepsilon}_{\max}$) was the most appropriate finite element model output to predict this injury.

In **Chapter V,**[37, 38] pulmonary contusion in histologic specimens is analyzed. The results of an automated contusion quantification algorithm were compared to the results determined through CT segmentation from the same subjects at the same time points. The algorithm and segmentation results reflected the same trends across the data set and good agreement in subjects with contusion by volume approaching 20%. The image

processing algorithm was compared to a pathologist assessment of contusion and shows good sensitivity and specificity when 20% or more contusion is present in a given slide.

A final set of experiments and computational work that synthesizes the research of the previous studies is presented in **Chapter VI**. A concurrent optimization was used to tune the finite element model to four distinct loading conditions. These loading conditions were meant to represent mild, intermediate, and severe chest loading based on the data from Chapter II. The findings of the spatial matching technique presented in Chapter V were employed to determine finite element-based in jury metrics based on the product of first principal strain and strain rate. The dissertation concludes with a final chapter (**Chapter VII**) summarizing our epidemiological, experimental, and computational findings and provides indications for areas of further research.

Chapter I References

1 Cohn SM. Pulmonary contusion: review of the clinical entity. *J Trauma.* May 1997;42(5):973-979.

2 Allen GS, Coates NE. Pulmonary contusion: a collective review. *Am Surg.* Nov 1996;62(11):895-900.

3 Blansfield J, Danis D, Gervasini A, Sheehy S. *Manual of Trauma Care: The First Hour*. St. Louis, MO: Mosby; 1999.

4 Cavanaugh KJ. Thoracic biomechanics. In: Nahum A, Melvin J, eds. *Accidental Injury Biomechanics and Prevention*. New York, New York: Springer-Verlag; 1993.

5 Stellin G. Survival in trauma victims with pulmonary contusion. *Am Surg.* 1991;57(12):780-784.

6 Balci AE, Balci TA, Eren S, Ulku R, Cakir O, Eren N. Unilateral post-traumatic pulmonary contusion: findings of a review. *Surg Today.* 2005;35(3):205-210.

7 Miller PR, Croce MA, Kilgo PD, Scott J, Fabian TC. Acute respiratory distress syndrome in blunt trauma: identification of independent risk factors. *Am Surg.* Oct 2002;68(10):845-850; discussion 850-841.

8 Miller PR, Croce MA, Bee TK, et al. ARDS after pulmonary contusion: accurate measurement of contusion volume identifies high-risk patients. *J Trauma.* Aug 2001;51(2):223-228; discussion 229-230.

9 Kishikawa M, Yoshioka T, Shimazu T, Sugimoto H, Yoshioka T, Sugimoto T. Pulmonary contusion causes long-term respiratory dysfunction with decreased functional residual capacity. *J Trauma.* Sep 1991;31(9):1203-1208; discussion 1208-1210.

10 Hoth JJ, Stitzel JD, Gayzik FS, et al. The pathogenesis of pulmonary contusion: an open chest model in the rat. *J Trauma.* Jul 2006;61(1):32-44; discussion 44-35.

11 Knoferl MW, Liener UC, Seitz DH, et al. Cardiopulmonary, histological, and inflammatory alterations after lung contusion in a novel mouse model of blunt chest trauma. *Shock.* Jun 2003;19(6):519-525.

12 Raghavendran K, Davidson BA, Woytash JA, et al. The evolution of isolated bilateral lung contusion from blunt chest trauma in rats: cellular and cytokine responses. *Shock.* Aug 2005;24(2):132-138.

13 Hoth JJ, Hudson WP, Brownlee NA, et al. Toll-Like Receptor 2 Participates in the Response to Lung Injury in a Murine Model of Pulmonary Contusion. *Shock.* Jun 7 2007.

14 Murphy TJ, Paterson HM, Mannick JA, Lederer JA. Injury, sepsis, and the regulation of Toll-like receptor responses. Vol 75; 2004:400-407.

15 Moore FA, Moore EE. Evolving concepts in the pathogenesis of postinjury multiple organ failure. *Surg Clin North Am.* Apr 1995;75(2):257-277.

16 Kuppa SM, Eppinger R. Development of an improved thoracic injury criterion. *Stapp Car Crash Journal.* 1998;42:139-154.

17 Morgan RE, Eppinger R, Haffner MP, et al. Thoracic trauma assessment formulations for restrained drivers in simulated frontal impacts. *Stapp Car Crash Journal.* 1994;38:15-34.

18 Shepard GH, Ferguson JL, Foster JH. Pulmonary contusion. *Ann Thorac Surg.* Feb 1969;7(2):110-119.

19 Kelly ME, Miller PR, Greenhaw JJ, Fabian TC, Proctor KG. Novel resuscitation strategy for pulmonary contusion after severe chest trauma. *J Trauma.* Jul 2003;55(1):94-105.

20 Cohn SM. Experimental pulmonary contusion; Review of the literature and description of a new porcine model. *J Trauma.* 1996;41(3):565-571.

21 Wang ND, Stevens MH, Doty DB, Hammond EH. Blunt chest trauma: an experimental model for heart and lung contusion. *J Trauma.* Apr 2003;54(4):744-748.

22 Stitzel J, Gayzik F, Hoth J, et al. Development of a finite element based injury metric for pulmonary contusion, Part I: model development and validation. *Stapp Car Crash Journal.* 2005;49:271-289.

23 Raghavendran K, Davidson BA, Helinski JD, et al. A rat model for isolated bilateral lung contusion from blunt chest trauma. *Anesth Analg.* Nov 2005;101(5):1482-1489.

24 Gayzik FS, Hoth JJ, Daly M, Meredith JW, Stitzel JD. A finite element based injury metric for pulmonary contusion: Investigation of candidate injury metrics through correlation with computed tomography. *Stapp Car Crash Journal.* 2007;51:189-209.

25 Trupka A, Waydhas C, Hallfeldt KK, Nast-Kolb D, Pfeifer KJ, Schweiberer L. Value of thoracic computed tomography in the first assessment of severely injured

patients with blunt chest trauma: results of a prospective study. *J Trauma.* Sep 1997;43(3):405-411; discussion 411-402.

26 Tyburski JG, Collinge JD, Wilson RF, Eachempati SR. Pulmonary contusions: quantifying the lesions on chest X-ray films and the factors affecting prognosis. *J Trauma.* May 1999;46(5):833-838.

27 Antonelli M, Moro ML, Capelli O, et al. Risk factors for early onset pneumonia in trauma patients. *Chest.* Jan 1994;105(1):224-228.

28 Vawter D. A finite element model for macroscopic deformation of the lung. *J. Biomech. Eng.* 1980;102:1-7.

29 Takhounts E, Eppinger R, Campbell J, Tannous R. On the development of the SIMon finite element head model. *Stapp Car Crash Journal.* 2003;47:107-133.

30 Zhang L, Yang K, King A. A Proposed Injury Threshold for Mild Traumatic Brain Injury. *J Biomech Eng.* 2004;126:226-236.

31 Shen W, Niu Y, Stuhmiller JH. Biomechanically based criteria for rib fractures induced by high-speed impact. *J Trauma.* Mar 2005;58(3):538-545.

32 Stitzel JD, Cormier JM, Barretta JT, et al. Defining regional variation in the material properties of human rib cortical bone and its effect on fracture prediction. *Stapp Car Crash J.* Nov 2003;47:243-265.

33 Shah CS, Yang KH, Hardy W, Wang HK, King AI. Development of a computer model to predict aortic rupture due to impact loading. *Stapp Car Crash J.* Nov 2001;45:161-182.

34 Gayzik FS, Bostom O, Ortenwall P, Duma S, Stitzel JD. An experimental and computational study of blunt carotid artery injury. *Annu Proc Assoc Adv Automot Med.* 2006;50:13-32.

35 Stitzel JD, Duma SM, Cormier JM, Herring IP. A nonlinear finite element model of the eye with experimental validation for the prediction of globe rupture. *Stapp Car Crash J.* Nov 2002;46:81-102.

36 Lee JB, Yang KH. Development of a finite element model of the human abdomen. *Stapp Car Crash J.* Nov 2001;45:79-100.

37 Gayzik FS, Brownlee NA, Hoth JJ, Stitzel JD. An image analysis method for quantitating pulmonary contusion in histologic specimens. Paper presented at: Southeast Bioengineering Conference, 2006; Duke University.

38 Gayzik FS, Hoth JJ, Stitzel JD. Quantitative histology of contused lung tissue with comparison to computed tomography. *Biomed Sci Instrum.* 2008;44:Epub.

Submitted to: *Journal of Trauma* Second Submission, April 2008

CHAPTER II

CHARACTERIZATION OF CRASH-INDUCED THORACIC LOADING RESULTING IN PULMONARY CONTUSION

F. Scott Gayzik, M.S.[1,2]
Robert S. Martin, M.D.[1]
H. Clay Gabler, Ph.D.[2]
J. Jason Hoth, M.D.[1]
Stefan M. Duma, Ph.D.[2]
J. Wayne Meredith, M.D.[1]
Joel D. Stitzel, Ph.D.[1,2]

1. Wake Forest University School of Medicine, Winston-Salem, NC
2. Virginia Tech – Wake Forest University Center for Injury Biomechanics, Winston-Salem, NC and Blacksburg, VA

Abstract

Pulmonary contusion (PC) is commonly sustained in motor vehicle crash. This study utilizes the Crash Injury Research and Engineering Network (CIREN) database and vehicle crash tests to characterize the occupants and loading characteristics associated with PC. A technique to match CIREN cases to vehicle crash tests is applied to quantify the thoracic loading associated with this injury. The CIREN database and crash test data from the National Highway Traffic Safety Administration were used in this study. An analysis of CIREN data was conducted between three study cohorts: patients that sustained PC and any other chest injury (PC + & Chest +), patients with chest injury and an absence of PC (PC - & Chest +) and a control group without chest injury (PC - & Chest -). Forty-one lateral impact crash tests were analyzed and thoracic loading data from on-board crash tests dummies were collected. The incidence of PC in CIREN data was 21.7 %. Crashes resulting in PC demonstrated significantly greater mortality (23.9%) and Injury Severity Score (33.1 ± 15.7) than the control group. The portion of lateral impacts increased from 27 % to 48 % between the control group and PC + & Chest + cohort, prompting the use of lateral impact crash tests for the case matching portion of the study. Crash tests were analyzed in two configurations; vehicle-to-vehicle tests and vehicle-to-pole tests. The average maximum chest compression and deflection velocity from the dummy occupants were found to be 25.3 ± 2.6 % and 4.6 ± 0.42 $m \cdot s^{-1}$ for the vehicle-to-pole tests and 23.0 ± 4.8 % and 3.9 ± 1.1 $m \cdot s^{-1}$ for the vehicle-to-vehicle tests. Chest deflection vs. time followed a roughly symmetric and sinusoidal profile. Sixteen CIREN cases were identified that matched the vehicle crash tests. Of the 16 matched cases, 12 (75 %) sustained chest injuries, with half of these patients presenting with PC. Quantified loading at the chest wall indicative of PC and chest injury in MVC is valuable boundary condition data for bench-top studies or computer simulations focused on this injury. In addition, since PC often exhibits a delayed onset, knowing the population and crash modes highly associated with this injury may promote earlier detection and improved management of this injury.

II.1. Introduction

Motor vehicle crash (MVC) and associated injuries remain a major public health problem world wide. In the United States in 2005 there were 6 million police reported crashes resulting in nearly 2 million injuries and 40,000 fatalities.[1] Analysis of occupant injury following MVC reveals that thoracic trauma is second only to head trauma in terms of frequency.[2, 3] For patients sustaining blunt chest trauma, pulmonary contusion (PC) is the most commonly identified injury, affecting 10-17% of all trauma admissions.[4] The mortality associated with PC is difficult to determine but is estimated to be 5-25% for adults and as high as 43% for children.[5-7] PC has been demonstrated as an independent predictor of Acute Respiratory Distress Syndrome and pneumonia.[8]

It is well established that MVC is the most common cause for PC in the civilian population, yet there are currently no data in the literature characterizing the occupants, crash modes and thoracic loading most commonly associated with this injury. This paper utilizes the Crash Injury Research and Engineering Network (CIREN) database and matched vehicle crash tests to better characterize PC and associated thoracic injuries.

While PC has a mechanical etiology, the response to the insult demonstrates a strong inflammatory component.[9, 10] A survey of recent trauma and critical care research indicates that there is strong interest in mechanistic studies of PC.[11-16] These studies introduced animal models for the study of PC or described components of the host inflammatory response. The studies acknowledge MVC as a common cause of PC, yet little discussion is devoted to similarities between the loading applied to the model and that experienced by a vehicle occupant.

The purpose of this work is therefore to quantify the loading conditions resulting in PC and its sequelae following MVC-induced blunt chest trauma. The study proceeds in three parts. The first is to utilize the Crash Injury Research and Engineering Network (CIREN) database to investigate the occupants, vehicle types and crash modes most commonly associated with PC. The strength of the CIREN database is that it contains detailed information on both the crash that caused AIS 3 or greater injury of the enrolled patient and the individual's hospital course. CIREN data is collected through an in-depth case review process conducted by participating physicians, radiologists, engineers and crash investigators.

Following the CIREN database study, data from lateral impact vehicle crash tests were analyzed to quantify crash parameters of interest including the mean vehicle crush, mean crash-induced change in vehicle velocity (Delta-V) and occupant loading data from the chest of an anthropometric test device (ATD) hereafter referred to as a dummy. For reasons based on the outcome of the CIREN analysis, this analysis was restricted to passenger vehicles in lateral impact tests.

The final aspect of this study was to query the CIREN database for cases whose crash characteristics matched the analyzed vehicle crash tests. Matching was conducted through analysis of the Collision Deformation Classification (CDC) code from the CIREN case reconstruction and by matching exterior crush and Delta-V within one standard deviation of the values determined through analysis of the crash tests. The CDC code is a comprehensive crash classification standard established by the Society of Automotive Engineers (standard SAE-J224), including the direction of force, general area

of vehicle damage and specific horizontal location of damage along the struck side of the vehicle.

The hypothesis behind this unifying aspect of the study is that injury data from matching CIREN cases coupled with thoracic loading data from the dummy situated in the vehicle crash test will provide two important results: realistic loading data for future mechanistic studies of PC and associated thoracic injuries, and insight into injury mechanisms associated with MVC-induced PC and thoracic injury.

II.2. Materials and Methods

Databases

The CIREN network was established by the National Highway Traffic Safety Administration (NHTSA) in 1998. The CIREN database includes roughly 3,500 motor vehicle crashes, generally with maximum AIS of 3 or greater. CIREN's mission is to bring together engineering and medical knowledge during a case review at which time the crash mechanics, biomechanics and clinical aspects of injury are assessed. CIREN is one of the most detailed databases of injuries sustained in car crash-induced trauma and contains operative notes, radiographic images and photographs of crash victims.

NHTSA's Vehicle Crash Test Database is a comprehensive source of engineering data generated through vehicle crash testing. It includes acceleration, force and deflection traces from the vehicle, location and type of crash test dummies in the test vehicle, and additional media describing the tests such as crash test video and reports. This data is available online in a searchable archive maintained by NHTSA.[17]

CIREN Data Collection

The CIREN database is continually updated as additional case studies are completed from the eight centers throughout the United States. The CIREN database was downloaded containing all case information from 1996 through 2006. At the time of acquisition, the database contained 3567 total cases. Case occupants less than 15 years of age were not considered in the analysis, eliminating 963 cases.

The CIREN data was imported into SAS statistical analysis software, (version 9.1e, Cary, NC). The cases were sorted into one of three groups: occupants who had sustained a pulmonary contusion and any other chest injury (PC + & Chest +), occupants who did not present with PC but experienced some form of chest trauma (PC - & Chest +) and a control group who did not present with chest injury whatsoever (PC - & Chest -). The first group is by definition positive for chest injury since PC is a chest region injury. Individuals in this group may have sustained additional chest injuries but were placed in this category based on the presence of PC alone. Cases were categorized following analysis of the patient's Abbreviated Injury Score (AIS) for each injury. Injury codes are derived directly from the diagnosis provided by the patient's attending physicians and radiologists.

Patient demographics (age, gender, height, weight), injury characteristics (MAIS, ISS, mortality) and vehicle demographics were compared between cohorts. Vehicles were classified into three groups based on wheelbase length: with small or compact vehicles having a wheelbase less than 265 cm, intermediate or full size vehicles having a wheelbase between 265 cm and 291 cm, and large vehicles having wheelbases exceeding 291 cm. Crash characteristics including the Principal Direction of Force of the crash

(PDOF), Delta-V, and the complete CDC code allowed for thorough description of the crash characteristics of all cases in CIREN.

Statistical comparisons between groups were conducted via ANOVA, with Tukey's *post-hoc* test for pair wise comparisons between groups. Chi Square tests were used for comparisons between categorical data. A significance level of 0.05 was used in all statistical tests.

Crash Test Data Collection

Vehicle Crash test data were downloaded from NHTSA's research and development website.[17] This database contains a summary of nearly 6000 tests from model year 1965 to the present containing data on the crash configuration, vehicle model and type of dummy used in the test.

All data used in case comparisons originated from lateral impact crash tests. Tests from four distinct lateral impact crash test configurations were analyzed in order to broaden range of crashes investigated. Two of these, the Lateral Impact New Car Assessment Program (LINCAP) tests and the Federal Motor Vehicle Safety Standard 214 (FMVSS) tests, replicate vehicle-to-vehicle lateral impacts. The remaining two test configurations, FMVSS 201 pole and FMVSS 214 pole, replicate vehicle-to-pole type lateral impacts. The crash test configurations, parameters for each test, and unique test numbers used in this study are provided in Table II-1. A complete description of these lateral impact tests can be found in the literature.[18] The tests used in this study were commissioned by NHTSA for research purposes rather than specifically for regulatory purposes.

Table II-1. Summary of lateral impact tests used in matching protocol. Side impact comparisons are restricted to passenger cars. Tests shown in bold were included in the rib module loading study.

Test	Barrier	Impact Angle	Impact Speed	Test Dummy	Mean Wheelbase, cm	Mean Weight, kg	NHTSA Test numbers (n)
FMVSS 214	Moving Deformable Barrier (1367 kg)	27° CW from lateral, driver-side	54 km/hr (33.5 mph)	EuroSID-2 / EuroSID-2re	270 ± 12	1361 ± 229	3819, **3799, 4456, 4097, 4455,** 4380, 3803, (7)
LINCAP	Moving Deformable Barrier (1367 kg)	27° CW from lateral, driver-side	62 km/hr (38.5 mph)	EuroSID-2 / EuroSID-2re	267 ± 12	1433 ± 144	5483, **5482, 5461**, 5481, 5485, **4547**, 4551, **4862**, (**8**)
FMVSS 201 (lateral pole)	Rigid Pole (254 mm dia.)	Lateral impact, driver-side	29 km/hr (18 mph)	EuroSID-2 / EuroSID-2re	273 ± 3.7	1507 ± 103	**3708**, **3703**, 3707, **3740**, 3802, 3818, 3820, (**7**)
FMVSS 214 (oblique pole)	Rigid Pole (254 mm dia.)	15° CCW from lateral, driver-side	32 km/hr (20 mph)	EuroSID-2 / EuroSID-2re	270 ± 9.0	1484 ± 136	5300, 5439, **5458**, 5407, 5408, **5472**, 4860, 4389, 4498, 4378, 4497, **4423**, 4284, **4285**, 4365, **4246**, **4313**, 4859, 5317 (**19**)

The analysis was limited to crash tests of passenger vehicles (excluding light trucks and vans). In addition, only tests utilizing the EuroSID-2 (European Side Impact Dummy, 2nd generation) dummy, or an updated version of the same dummy, the EuroSID-2re, were used. Potentiometers embedded in the thorax of this model record the lateral thoracic displacement during the crash. Data from the selected tests were obtained through NHTSA's Signal Browser software and the vehicle crash test report.[17] Crash test data collected for this study included the vehicle Delta-V (calculated from on-board accelerometers) [19], crush profile and dummy rib deflection. Peak rib deflection was normalized by half the width of the dummy thorax module and is expressed in terms of a percent compression.[20] The maximum deflection velocity was determined by differentiation of the deflection trace. Chest module loading data is presented for a subset of crash tests that were either not equipped with side impact airbags, or in which the dummy did not contact the airbag.

Video and a written summary of each crash test were also downloaded through NHTSA's research and development web site. The data were used to verify the crash mode, cross check test data, and ensure that no malfunction of the dummy or instrumentation was noted in the test.

II.3. Matching CIREN Cases to Crash Test Cases

The pool of potential CIREN cases was restricted to passenger cars. This was done to reduce variability due to height of the occupant from the road and to more closely match the crash tests analyzed. Matched cases met three criteria. The case occupant was the front seat occupant on the near side lateral impact position. The CDC code, including direction of force, general area of damage, and other parameters describing the crash

configuration, was consistent with one of the four crash tests analyzed. The Delta-V and weighted average crush of the CIREN case vehicle were within one standard deviation of the mean of these values from the analyzed crash tests.

The specific coding used to match each test is provided in Table II-2. To be consistent with the vehicle crash test data and to avoid a potentially confounding factor, matching CIREN cases in which the occupant was protected by a side airbag were excluded.

Vehicle crush data in CIREN was conditioned prior to case matching. The average crush was weighted differently depending on the type of crash analyzed. To quantify the vehicle's crush profile, six equally spaced measurements of the deformation are taken along the extent of the vehicle damage. This standardized technique is applied to both the CIREN cases during vehicle inspection and following all crash tests. Rather than using the average of these crush measures to compare vehicle crush between CIREN cases and the crash tests, weighted averages were used for both the vehicle-to-vehicle and vehicle-to-pole crash tests. The formulas for calculating the weighted average crush are found in Table II-2. The purpose of the weighted average was to accurately reflect the specific type of crush. Depending on the CDC code classification (i.e., vehicle-to-vehicle or vehicle-to-pole type crash), the appropriate weighted crush was applied to the matching algorithm.

II.4. Results

CIREN Data

Group populations, patient demographics, injury characteristics, and vehicle characteristics from the CIREN database are shown in Table II-3. The incidence of PC in

Table II-2. Collision Deformation Classification (CDC) code and crush calculations used for matching Crash Injury Research and Engineering Network (CIREN) cases to selected lateral vehicle crash tests.

	Vehicle to Vehicle Type		Vehicle to Pole Type	
	FMVSS 214	**LINCAP**	**FMVSS 201 Pole**	**FMVSS 214 Pole**
Principal Direction of Force	Lateral ± 20°		Lateral ± 20°	
General Area of Deformation	Left or Right (L or R)*		Left or Right (L or R)*	
Specific Horizontal Location	Side Center (P,Y, or Z)		Side Center (P, Y, or Z)	
Specific Vertical Location	All, Everything Below Beltline, or Top of Frame to Top of Vehicle (A, H, E)		All, Everything Below Beltline, or Top of Frame to Top of Vehicle (A, H, E)	
Type of Damage	Wide		Narrow	
Weighted Average Crush Calculation (cm)	$10\%\cdot C_1 + 20\%\cdot C_2 + 20\%\cdot C_3 + 20\%\cdot C_4 + 20\%\cdot C_5 + 10\%\cdot C_6$		$10\%\cdot C_1 + 10\%\cdot C_2 + 30\%\cdot C_3 + 30\%\cdot C_4 + 10\%\cdot C_5 + 10\%\cdot C_6$	
Weighted Crush Range (cm)	12.2 – 20.0		10.4 – 26.9	
Delta-V Range (km/h)	24.1 – 27.7	26.8 – 32.0	30.1 – 35.2	32.3 – 38.3

* Depending on case occupant's seating position

Table II-3. Crash Injury Research and Engineering Network (CIREN) pulmonary contusion study results. Mean patient demographics, injury characteristics, and vehicle demographics. Significant differences from the control group (PC - & Chest injury -) are in bold, α = 0.05.

	PC - & Chest Injury – (n = 951)	PC - & Chest Injury + (n = 1087)	PC + & Chest Injury + (n = 566)	P value
Age (years)	37.2 ± 17.4	**46.6 ± 19.1**	39.0 ± 20.1	<.0001*
Male : Female	1.09 : 1	**0.88 : 1**	**1.17 : 1**	0.02[+]
Height (cm)	171.0 ± 10.2	169.6 ± 11.6	170.8 ± 12.7	0.01*
Weight (kg)	79.7 ± 23.1	81.1 ± 23.1	80.6 ± 37.2	0.51*
MAIS	3.1 ± 0.8	**3.5 ± 1.1**	**4.1 ± 0.9**	<.0001*
ISS	14.3 ± 9.1	**24.0 ± 17.7**	**33.1 ± 15.7**	<.0001*
Mortality (%)	3.2	**16.8**	**23.9**	<.0001[+]
Model year	1998 ± 3	**1997 ± 4**	1998 ± 4	<.0001*
Wheelbase (cm)	273 ± 28	273 ± 26	**269 ± 21**	0.03*
Weight (kg)	1426 ± 341	1404 ± 497	1394 ± 281	0.34*

the total CIREN population was 21.7 % (566 / 2604). Study cohorts were primarily examined relative to the control group (PC - & Chest -). The PC - & Chest + group were significantly older, and demonstrated a lower male to female ratio than the control group. In terms of the injury data, the MAIS, ISS and mortality were significantly elevated relative to the control group.

MAIS, ISS, and mortality were highest in the PC + & Chest + group. This group exhibited significantly greater injury data than the control group and PC - & Chest + group. The male to female ratio was also majority male in the PC + & Chest + group. No differences in height and weight were noted among population groups.

The incidence of PC was also investigated with respect to vehicle parameters. Significant differences were noted in the mean vehicle model year for the PC - & Chest + group, but the difference was one year. The mean wheelbase of all vehicles was in the

intermediate size range, but a significant reduction in wheelbase size was noted for the PC + group. This is reflected in Figure II-1, which shows the incidence of PC by vehicle class. The incidence of PC remains steady across the small and intermediate class and drops substantially in larger wheelbase vehicles.

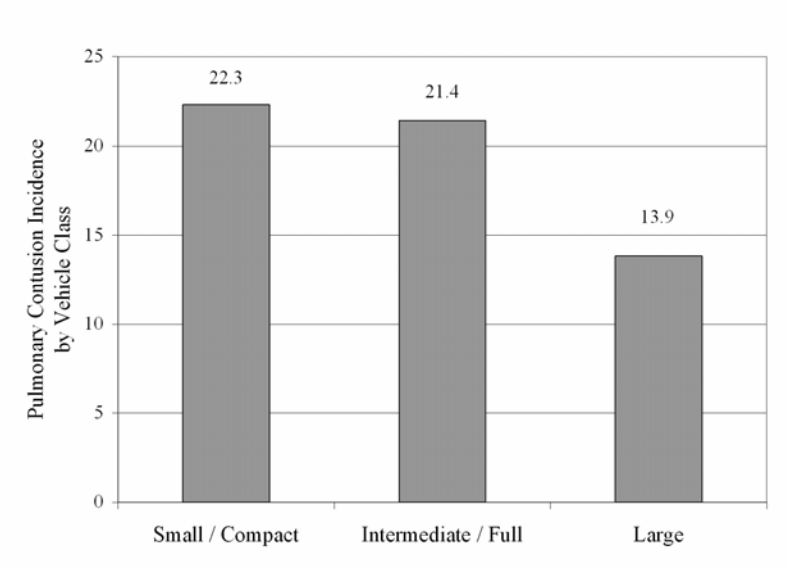

Figure II-1. Incidence of pulmonary contusion in the Crash Injury Research and Engineering Network (CIREN) Database by vehicle class.

Crash characteristics from the CIREN database are found in Figure II-2, which shows the crash classification based on the general area of damage (a part of the CDC code) for all cohorts. The most common crash mode for all groups was frontal, but the proportion of lateral crashes steadily increases across study cohorts. In the PC + & Chest + cohort, nearly half (48%) of crashes were lateral impacts.

Analyzing only those patients with PC in side impact reveals a strong influence between the impacted side of the vehicle and the location of the contused lung. Figure II-3 shows the breakdown of contusion classification based on struck side of the vehicle.

Contused lung is strongly dependent on struck side for both right and left impacts. Bilateral lung contusions constitute substantial portions of both right and left side impact.

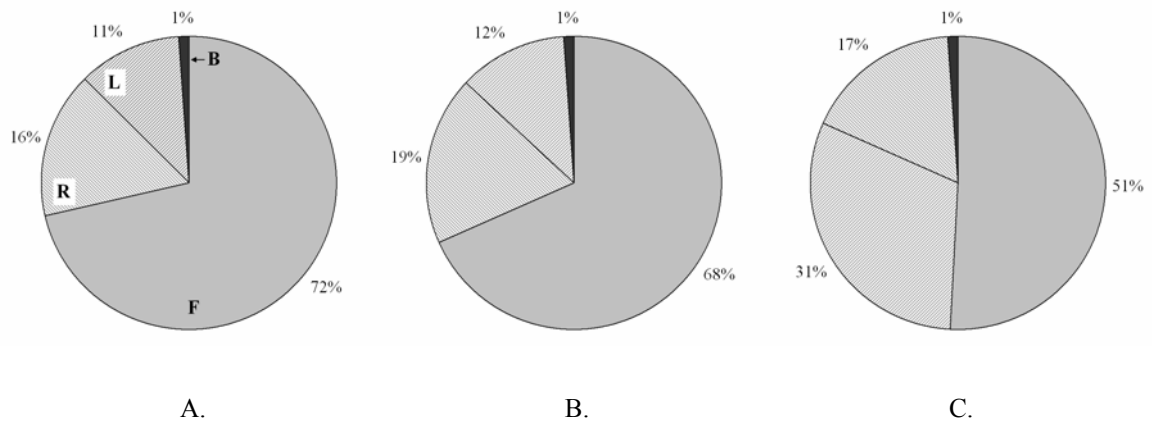

A. B. C.

Figure II-2. Crash mode distribution by study cohort. A. Without PC or Chest injury (PC - & Chest-), B. Without PC but with Chest injury (PC - & Chest +), C. With PC and Chest injury (PC +, Chest +). Labels indicate Frontal (F), Right (R), Left (L), and Rear (B) impacts.

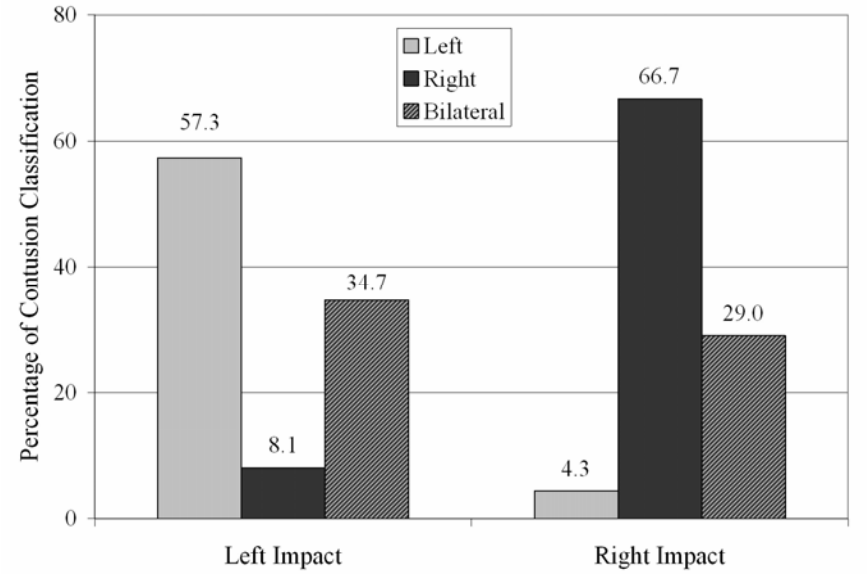

Figure II-3. Distribution of pulmonary contusion versus side of vehicle struck for lateral impact cases in the PC + & Chest injury + cohort.

The results of the CIREN portion of the study were used to focus the search criteria for the vehicle crash test database. The results of this study demonstrated a sharp increase in the portion of lateral impacts associated with PC. While the crash modes for

the PC + & Chest + cohort were essentially equally split between lateral and side impact, it is important to consider relative frequency of these crash modes. It is well documented that frontal impacts occur with more than twice the frequency of side impact crashes[1], yet side impact crashes represented nearly half of all PC cases in CIREN (Figure II-2). This disproportionate increase justified the study of thoracic loading in side impact.

Since the incidence of PC was highest in compact and intermediate vehicle types (Figure II-1), and since these vehicles are typically passenger cars, limiting the crash test analysis to passenger cars was deemed a justifiable approach. The mean height and weight of the three cohorts did not differ significantly and approximated the 50th percentile male values of 170 lbs (77.3 kg) and 69 in. (175.3 cm).[21]

Vehicle Crash Test Data

Forty-one lateral impact crash tests were examined for this study. Each test met all inclusion criteria for the study (passenger car, crash test configuration, and use of the specified dummy). Impact speed and impact angle were tightly controlled per the test stipulations. All vehicles selected for analysis were common models. Figure II-4 shows the average crush (non-weighted) and average Delta-V for lateral crashes in CIREN and for the analyzed crash tests. The mean non-weighted crush values from the crash tests were significantly below the same values from the CIREN database. The mean Delta-V aligned more closely, although it should be noted that the Delta-V for the crash tests was measured via on-board sensors while the Delta-V for the CIREN data was estimated from the vehicle crush profile.

All chest compression data was extracted from the left front seat occupant and therefore represents the near-side crash scenario. Figure II-5 shows exemplar traces of

the occupant loading at the chest wall for each crash test type analyzed. All traces show a roughly sinusoidal loading pattern. The mean and standard deviation of the maximum medial-lateral compression and maximum deflection velocity are provided in Table II-4.

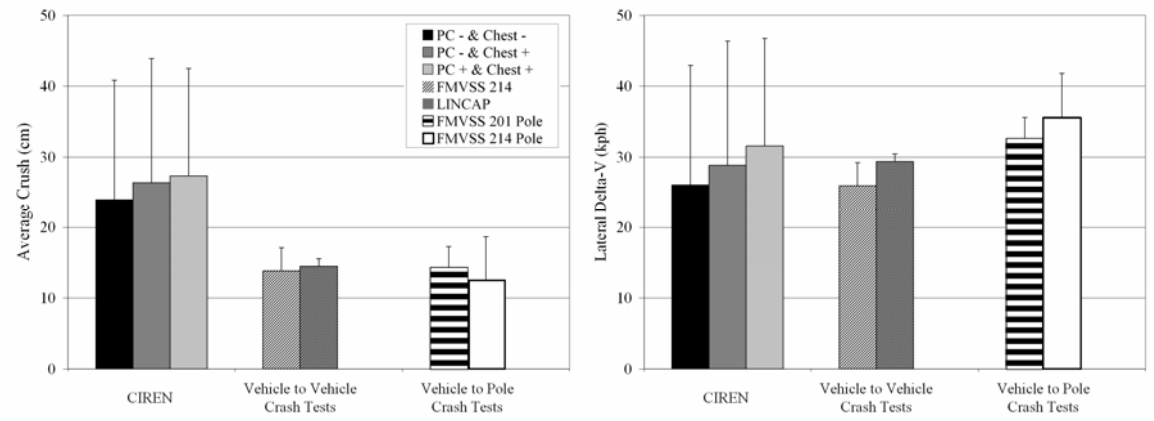

Figure II-4. Average crush (A) and Delta-V (B) for lateral impacts from CIREN database and analyzed crash tests with one standard deviation error bars shown. The legend is equivalent for (A) and (B).

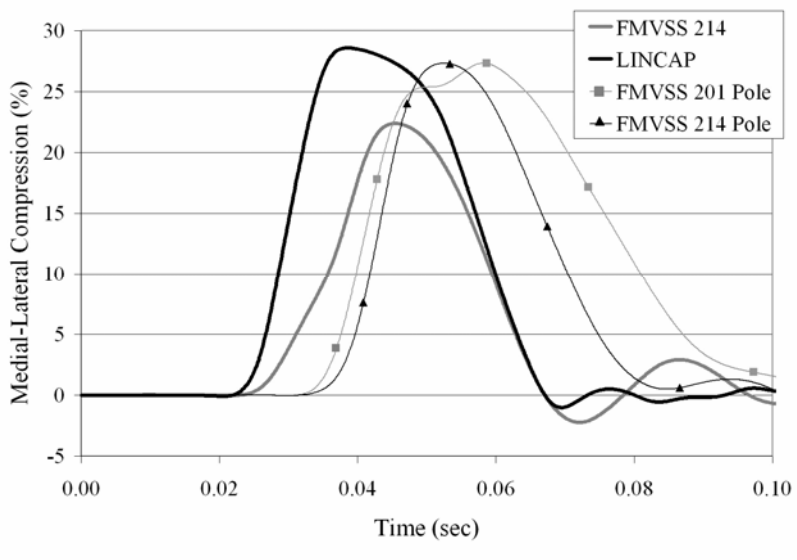

Figure II-5. Exemplar medial-lateral compression vs. time from dummy chest module in analyzed crash tests. Test numbers are 3799, 4547, 3708, and 4313 respectively, based on legend order.

Table II-4. Mean and standard deviation of rib module compression and velocity for analyzed cases. Sample size for each test is given. Tests included in this analysis are shown in bold in Table II-1. Statistically significant differences within test types denoted by * (t-test, α = 0.05).

Test Type	Vehicle to Vehicle Type		Vehicle to Pole Type	
Test (n)	FMVSS 214 (4)	LINCAP (4)	FMVSS 201 Pole (3)	FMVSS 214 Pole (6)
Maximum M-L Compression (%)	19.6 ± 3.2	26.4 ± 3.4	27.2 ± 1.0	24.7 ± 2.7
Maximum Deflection Velocity ($m \cdot s^{-1}$)	2.9 ± 0.3*	4.9 ± 0.4*	4.3 ± 0.3*	4.7 ± 0.4*

Crash test cases used for analysis of the rib module loading are shown in bold in Table II-1. Statistical tests (t-test, α = 0.05) for maximum compression and for maximum deflection velocity were conducted within each test type (i.e., within the vehicle-to-vehicle and vehicle-to-pole type tests). These tests indicated that maximum rib velocity was significantly different within tests but the compression was not.

Matched CIREN and Vehicle Crash Tests

Matching was performed independently for each crash test type (Table II-2). The inclusive ranges for matched Delta-V and weighted average crush for all test types are shown in Table II-2. The average weighted crush between the two vehicle-to-vehicle tests and the two vehicle-to-pole tests were not significantly different, so a common range was used for this parameter.

A total of 16 matching CIREN cases were identified. Thirteen cases matched the vehicle-to-vehicle type crash tests. The breakdown of specific matching cases is shown in Figure II-6. No cases were found to match all vehicle-to-pole test criteria because many pole-type cases in CIREN lacked a calculated Delta-V. When only the Delta-V criterion was dropped, three cases were found to match the pole tests. No differentiation

among the two vehicle-to-pole tests were made since the weighted crush was not found to be significantly different (Table II-2).

In terms of injury data, 4 of the 16 cases did not sustain chest injury, but all of these patients sustained pelvic fractures. All of the remaining 12 cases sustained a chest injury, and half of these cases presented with PC. Figure II-6-B shows the mean age by cohort. The mean age for the PC + & Chest injury + group, 33.4 ± 13.0 years, was found to be significantly less than the PC - & Chest + and PC- & Chest – cohorts (53.3 ± 23.9 years and 60.6 ± 32.3 years respectively) through t-test between cohorts ($\alpha = 0.05$). The control group was significantly shorter than the remaining cohorts ($p = 0.006$, ANOVA, $\alpha = 0.05$). No other demographic, injury, or vehicle data differed significantly by cohort. There was one fatality in the matched case group which matched the LINCAP-type test loading belonging to the PC - & Chest + cohort. The case occupant was an 89 year old male, right front seat passenger who was restrained. The majority of the patients in the matched cases were restrained by a three-point belt (14/16). There was no indication from the case vehicle reports that unrestrained occupants were out of position. All PC+ patients were restrained.

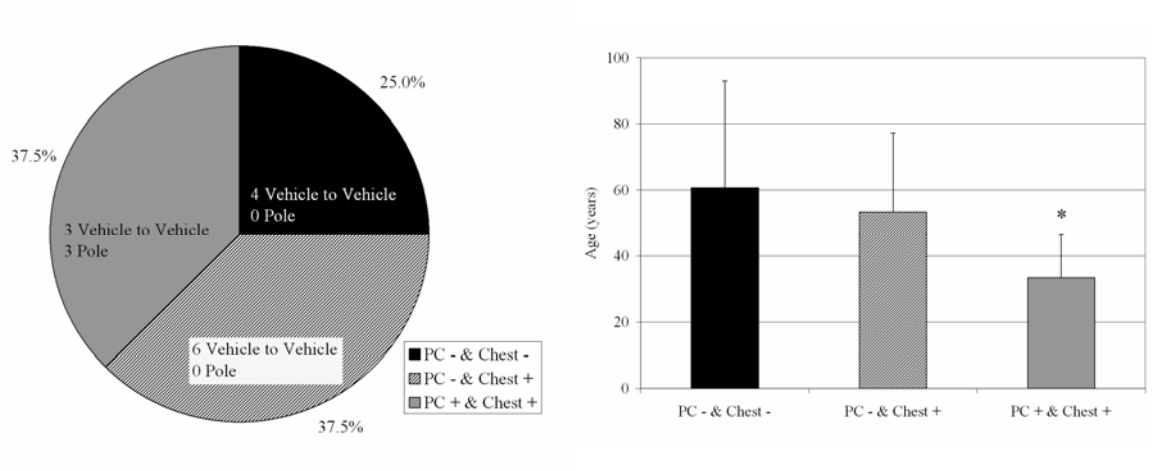

A. B.

Figure II-6. Matched case summary. (A) Breakdown of cohort population for cases in the Crash Injury Research and Engineering Network (CIREN) database that matched vehicle crash tests. Matching test configuration for each cohort is also shown. (B) Mean and standard deviation of patient age by study cohorts for matched case sub-population.

II.5. Discussion

The aims of this study were twofold: to characterize the occupants, injuries, and crash modes associated with PC and apply a case matching algorithm to the CIREN database to quantify the associated thoracic loading conditions via comparisons with similar laboratory-conducted crash tests. The results of this study provide several valuable contributions to the trauma research community regarding these aims. First, since PC can be an insidious injury exhibiting a delayed onset, knowing the population and crash modes associated with this injury could lead to earlier detection and improved management of the injury. Second, well-quantified loading conditions at the chest wall indicative of traumatic PC (and more generally, chest injury) will be a useful tool for designing future bench-top mechanistic studies of PC as well as for computer simulations focused on studying thoracic trauma. Additionally, this data will be useful to the

automotive safety community with respect to the goal of preventing or mitigating thoracic injuries.

Characterization of the CIREN population was achieved through analysis of mean demographic, injury and vehicle data for three distinct cohorts (Table II-3). These were a control group without chest injury, a group with some form of chest injury in the absence of PC (typically rib fractures), and a final group with PC. These three cohorts revealed several interesting trends. While there was no significant difference in age between the control group and the PC + & Chest + group, the PC - & Chest + group was found to be significantly older than the controls (37.2 ± 17.4 years vs. 46.6 ± 19.1 years). Since Delta-V was fairly uniform across all crash tests, these results suggest that age plays a role in the likelihood of developing PC following blunt chest trauma. In addition, significant gender differences were noted between cohorts in the characterization study with a greater number of males presenting with PC. As a whole, CIREN patient data was nearly evenly split between sexes (male to female ratio: 0.99:1). Males represented a larger proportion of drivers (54.7 %) and cases with male drivers were associated with a significantly greater Delta-V (43.3 ± 19.7 $km \cdot hr^{-1}$) than female drivers (40.2 ± 17.2 $km \cdot hr^{-1}$) (t-test, $\alpha = 0.05$). It appears that neither the occupants' physical size, vehicles wheelbase, or weight are a predictive factor for sustaining PC in vehicle crash since large differences between cohorts were not found in this study.

There were significant differences between cohort injury characteristics. Patients in the PC + & Chest + group exhibited significantly greater MAIS, ISS, and mortality. Our results suggest this difference is predominantly due to crash mode and crash severity. Figure II-4 shows that lateral Delta-V and average crush increase from the control group

and are greatest for the PC + & Chest + group. Lateral impact crash proportions are greatest for the PC + & Chest + cohort. In lateral impact scenarios the occupant is situated close to the point of momentum transfer of the impacting object.[19] This leads to severe loading of the near side of the occupant (typically the chest, pelvis, and/or head). As a result of the detailed injury analysis in the CIREN database, correlation of internal injuries to external loading was possible. The influence of the occupant's position within the vehicle on the resulting contusion is clear in Figure II-3, through the high correlation between the aspect of the contusion and the crash mode.

The chest loads associated with the crashes were calculated through analysis of the vehicle crash tests. The loading of the dummy chest module was quantified using two variables; maximum medial-lateral compression and the maximum deflection velocity. Table II-4 provides the averages of these values by test type. The data from the dummy chest module during the crash test in conjunction with the outcome data from matched CIREN cases provides a good estimate of the loading that caused these patients' chest injuries.

The approach taken here provides valuable information with regard to loading boundary conditions for blunt chest trauma models. The percent compression, deflection velocity and general shape of these loading curves are ideal input parameters for future experiments. In addition, as computer simulations of the human body for predicting injury become more prevalent, this type of data will be useful for recreating the appropriate injurious event.[22]

The average peak chest compression and rib deflection velocity (25.3 ± 2.6 % and 4.6 ± 0.42 $m \cdot s^{-1}$) was slightly greater in the pole tests than in vehicle-to-vehicle type tests

(23 ± 4.8 % and 3.9 ± 1.1 $m \cdot s^{-1}$). The difference in deflection velocity between pole and vehicle configurations were significant ($p = 0.05$, t-test, $\alpha = 0.05$), and the difference in compression approached significance ($p = 0.11$). Whether the data were examined from a pole-type or vehicle-type test, the loading data were roughly sinusoidal in nature, with a symmetric loading and unloading phase. Peak velocity was achieved prior to peak compression. Given the lung's relative compliance and coupling to the chest wall, these externally-measured loading parameters should be interpreted as loading conditions at the surface of the lung. Previous research on thoracic loading in side impact has shown that the door velocity-time profile heavily influences the severity of the loading.[23] While it is door deformation and movement that causes chest loading, measuring deflection directly from displacement sensors embedded in the chest module of the dummy captures this induced loading in the most direct manner possible.

It is useful to compare these findings to recent mechanistic studies of PC using animal models.[11-16] In four of these six studies, blast-rate loading was applied to the study subject, an insult characterized by extremely high deflection velocity (50 $m \cdot s^{-1}$) and low compression (< 5%).[24] Our results show that this type of loading is markedly different than that of MVC, which would be characterized by loading at a reduced deflection velocity with increased chest compression. While blast rate loading is appropriate for ballistic studies, our results indicate that the insult does not replicate loading in MVC. Two of the aforementioned studies applied chest loads that approximate what was found in this work.[11, 12] The former utilized an electronically-driven piston to directly strike the lung of the subject at 2.8 $m \cdot s^{-1}$ to a depth of 6.3 mm (correlates to roughly 30 % compression). The latter utilized a drop tower to achieve

loading speeds between 3.4 and 4.2 $m \cdot s^{-1}$ but did not control chest compression. Methods of blast type loading included the use of a captive-bolt handgun, nail driver, and blast wave generator. In the studies utilizing blast type loading, neither deflection velocity nor chest compression was reported.

Twelve of the sixteen matching CIREN cases (75 %) exhibited chest trauma and half of these cases presented with PC. Clearly, factors beyond chest wall loading alone influence the specific types of thoracic injuries that will be present following blunt chest trauma, but the results strongly indicate that the dummy chest loading data is indicative of PC. When considering all matched cases, regardless of which type of test each matched, statistical tests comparing the mean values of the sub-populations (categories in Table II-3) showed that only two parameters, age and height, were significantly different between groups. While hindered by the limited sample size of matched cases, these findings again suggest that age plays a role in determining thoracic injury outcome given a similar loading profile. This finding is consistent with studies focusing on the aging thorax, which show that aging is associated with structural and morphological changes that can increase susceptibility to disease and decrease the body's ability to withstand traumatic insults.[25, 26]

In an effort to normalize the study results, only passenger cars were considered in the matched case analysis. This was a reasonable restriction since the incidence of PC was higher in smaller vehicles (Figure II-1), and these vehicles tend to be passenger cars. Furthermore, in the majority of CIREN cases (76 %) the case vehicle was a passenger car. The study findings are also consistent with the observation that there are crash compatibility deficiencies between many passenger cars and light trucks and vans. In

56% (9/16) of matched cases, the striking vehicle was a light truck, van or SUV. In all PC + matched cases, the striking vehicle fell into this category or was a vehicle-to-pole type crash. These results suggest that loading was either uniform along the vertical extent of the vehicle or presented at the height of the occupant's chest. The dummy data also support these findings since the pole type exhibited a slightly greater peak compression and deflection velocity than the vehicle-to-vehicle tests. This is not meant to dismiss the severity of the vehicle-to-vehicle test data presented in this study. In fact, the lone patient fatality among the matched CIREN case subset was involved in a vehicle-to-vehicle lateral impact.

While CIREN data do not represent a broad, population-based sample, the database does have unique strengths (namely extensive injury and crash reconstruction data). These attributes make CIREN data especially well-suited for this type of study where the injury in question and vehicle crash data are closely linked and equally important to the conclusions.

The presence of multiple injuries could be viewed as a potentially confounding factor between cohorts. As evidenced by the elevated ISS of the PC + group, it is possible that shock induced release of pro-inflammatory mediators contributed to elevated diagnosis of PC in that cohort.[27] CIREN cases are frequently severe crashes and in many cases patients have suffered multi-system trauma. Thus while there is the possibility that a systemic inflammatory response could be misconstrued as PC, injury data is only entered in the database following detailed case review by the patient's attending physicians and radiologists, ensuring that the diagnoses in CIREN are as accurate as possible.

All the thoracic loading data presented in this work is derived from a 50th percentile male dummy. Crash tests meeting the inclusion criteria that utilized female dummies were unavailable. We do not believe that this result had a large influence on the results, although 10 of the 16 matched CIREN case occupants were female. The mean height and weight of the matched case individuals were 168 ± 9.4 cm and 72.6 ± 15 kg respectively, well within one standard deviation of the standard height and weight of the 50th percentile male (175.3 cm and 77.3 kg)[21] In addition, the dummy used in this work has demonstrated improved biofidelity over previous models[28] and NHTSA has adopted its latest iteration (EuroSID2-re) for use in federally-mandated vehicle side impact testing.

II.6. Conclusions

A study utilizing the CIREN database was conducted to characterize the demographics, injury and vehicle characteristics of patients presenting with pulmonary contusion. A procedure was developed to identify cases in the CIREN database that closely matched laboratory-conducted lateral vehicle crash tests. Compression and deflection velocity of the chest wall associated with these crashes were collected from the dummy occupants seated in analyzed crash tests. This data is intended for use as boundary condition data for future mechanistic studies of PC and for computer simulations focused on the study of PC and blunt thoracic trauma in MVCs.

The results showed that patients presenting with PC exhibit significantly greater MAIS, ISS, and mortality than all other cohorts. A separate cohort including only those individuals with a chest injury in the absence of PC were also found to exhibit increased MAIS and ISS values over controls (no chest injury). The mean age of individuals in this group (PC - & Chest +) was significantly greater than the control group. CIREN cases

presenting with PC were disproportionately involved in lateral impacts. A total of 16 CIREN cases were found to match the analyzed crash tests. Seventy-five percent of these cases exhibited AIS 3 or greater chest injury. Half of the matched cases with chest injuries also presented with PC.

The average maximum chest compression and rib deflection velocity from the dummies was slightly greater in vehicle-to-pole type tests (25.3 ± 2.6 % and 4.6 ± 0.42 $m \cdot s^{-1}$) than in vehicle-to-vehicle type tests (23 ± 4.8 % and 3.9 ± 1.1 $m \cdot s^{-1}$). Loading was roughly sinusoidal and symmetric, with peak velocity achieved prior to peak compression. Pole type impacts exhibited significantly greater deflection velocity. Like the total CIREN population, age was found to be a significant factor between cohorts within the matched case sub-population. The PC + & Chest + cohort was significantly younger (33.4 ± 13.0 years) than the remaining cohorts (PC - & Chest + at 53.3 ± 23.9 years and PC- & Chest – at 60.6 ± 32.3 years).

Through correlation with CIREN injury data, the results provide well-quantified chest loading data from MVC resulting in PC. This loading is markedly different than blast type loading, which has been used in some mechanistic studies of this injury. We recommend using equipment that provides loading similar to that provided in this study for future bench-top studies of crash-induced PC. Computational studies of this injury can also utilize these findings to provide realistic boundary conditions for human body models.

Chapter II Acknowledgments

This publication was supported by Grant Number 1 R49 CE000664-01 from the Centers for Disease Control and Prevention (CDC). Its contents are solely the

responsibility of the authors and do not necessarily represent the official views of the National Center for Injury Prevention and Control.

Work was performed for the Crash Injury Research and Engineering Network (CIREN) Project at Wake Forest University School of Medicine in cooperation with the United States Department of Transportation/National Highway Traffic Safety Administration (USDOT/NHTSA). Funding has been provided by Toyota Motor North America Inc. under Cooperative Agreement Number DTNH22-05-H-61001. Views expressed are those of the authors and do not represent the views of any of the sponsors or NHTSA.

The authors gratefully acknowledge the reviewers of this manuscript for their helpful comments during the revision process. The authors wish to thank Matt Craig of NHTSA for his helpful suggestions and assistance in identifying appropriate crash tests for use in this study. Mao Yu of WFU aided in the reviewing process by extracting data from the main CIREN database. Randy Kelly of Denton ATD aided in data collection of EuroSID-2 and EuroSID-2re ATDs.

Chapter II References

1 United States Department of Transportation, National Highway Traffic Safety Administration, Traffic Safety Facts 2006: A Compilation of Motor Vehicle Crash Data from the Fatalities Analysis Reporting System and General Estimates System. DOT HS 810 818, Washington, DC 2006.

2 Blansfield J, Danis D, Gervasini A, et al. Manual of Trauma Care: The First Hour. St. Louis, MO: Mosby; 1999.

3 Cavanaugh KJ. Thoracic biomechanics. In: Nahum A, Melvin J, eds. Accidental Injury Biomechanics and Prevention. New York, New York: Springer-Verlag; 1993.

4 Cohn SM. Pulmonary contusion: A Review of the clinical entity. J Trauma. May 1997;42(5):973-979.

5 Stellin G. Survival in trauma victims with pulmonary contusion. Am Surg. 1991;57(12):780-784.

6 Balci AE, Balci TA, Eren S, et al. Unilateral post-traumatic pulmonary contusion: findings of a review. Surg Today. 2005;35(3):205-210.

7 Allen GS, Coates NE. Pulmonary contusion: a collective review. Am Surg. Nov 1996;62(11):895-900.

8 Miller PR, Croce MA, Kilgo PD, et al. Acute respiratory distress syndrome in blunt trauma: identification of independent risk factors. Am Surg. Oct 2002;68(10):845-850; discussion 850-841.

9 Stitzel J, Gayzik F, Hoth J, et al. Development of a finite element based injury metric for pulmonary contusion, Part I: model development and validation. Stapp Car Crash Journal. 2005;49:271-289.

10 Gayzik FS, Hoth JJ, Daly M, et al. A finite element based injury metric for pulmonary contusion: Investigation of candidate injury metrics through correlation with computed tomography. Stapp Car Crash Journal. 2007;51:189-209.

11 Raghavendran K, Davidson BA, Helinski JD, et al. A rat model for isolated bilateral lung contusion from blunt chest trauma. Anesth Analg. Nov 2005;101(5):1482-1489.

12 Hoth JJ, Stitzel JD, Gayzik FS, et al. The pathogenesis of pulmonary contusion: an open chest model in the rat. J Trauma. Jul 2006;61(1):32-44; discussion 44-35.

13 Knoferl MW, Liener UC, Seitz DH, et al. Cardiopulmonary, histological, and inflammatory alterations after lung contusion in a novel mouse model of blunt chest trauma. Shock. Jun 2003;19(6):519-525.

14 Wang ND, Stevens MH, Doty DB, et al. Blunt chest trauma: an experimental model for heart and lung contusion. J Trauma. Apr 2003;54(4):744-748.

15 Davis K, Fabian T, Croce M, et al. Prostanoids: Early mediators in the secondary injury that develops after unilateral pulmonary contusion. J Trauma. 1999;46(5):824-832.

16 Cohn SM. Experimental pulmonary contusion: Review of the literature and description of a new porcine model. J Trauma. 1996;41(3):565-571.

17 National Highway Traffic Safety Administration, [Vehicle Crash Test Database] Available at: http://www-nrd.nhtsa.dot.gov. Accessed September 1, 2007.

18 Chou C, Aekbote K, Le J. A review of side impact component test methodologies. Int J Vehicle Safety. 2007;2(1-2):141-184.

19 Gabler H, Hackney J. Safety Performance of Production Vehicles in Side Impact. Tenth International Conference on Enhanced Safety of Vehicles. Oxford, England; 1985.

20 Schuster P, Franz U, Stahlschmidt S, et al. Comparison of ES-2re with ES-2 and USSID Dummy, Considerations for ES-2re model in FMVSS Tests. 3rd Annual European Ls-Dyna User's Conference. Bamberg, Germany; 2004.

21 Schneider L, Robbins D, Pflug M, et al. Development of anthropometrically based design specifications for an advanced adult anthropomorphic dummy family. 1983 In: DOT/HS 806 715; Vol 1: Department of Transportation, Washington, DC.

22 Roberts JC, O'Connor JV, Ward EE. Modeling the effect of non-penetrating ballistic impact as a means of detecting behind armor blunt trauma. J Trauma. Jun 2005;58(6):1241-1251.

23 Kent R, Crandall J, Butcher J, et al. Sled System Requirements for the Analysis of Side Impact Thoracic Injury Criteria and Occupant Protection. SAE World Congress (2001-01-0721). Detroit, MI; 2001.

24 Viano D, Lau I. A viscous tolerance criteria for soft tissue injury assessment. J Biomech. 1988;21(5):387-399.

25 Kemper A, McNally C, Kennedy EA, et al. Material property of human rib cortical bone from dynamic tension coupon testing. Stapp Car Crash Journal. 2005;49:199-230.

26 Slice DE, Stitzel JD. Modeling age-related changes in human rib cage geometry. Amer. J. Phys. Anthrop. 2005;126(S40):192.

27 Hoth JJ, Hudson WP, Brownlee NA, et al. Toll-Like Receptor 2 Participates in the Response to Lung Injury in a Murine Model of Pulmonary Contusion. Shock. 2007;28(4):447-52.

28 Byrnes K, Abramczyk J, Berliner J, et al. ES-2 Dummy Biomechanical Responses. Stapp Car Crash Journal. 2002;46:353-396.

Published in: *Stapp Car Crash Journal* Vol. 49; pp. 271-89, 2005

CHAPTER III

DEVELOPMENT OF A FINITE ELEMENT INJURY METRIC FOR PULMONARY CONTUSION, PART I: MODEL DEVELOPMENT AND VALIDATION

Joel D. Stitzel, Ph.D.[1,2]
F. Scott Gayzik, M.S.[1,2]
J. Jason Hoth, M.D.[1]
Jennifer Mercier, .D.V.M. [2]
H. Donald Gage, Ph.D.[1]
Kathryn A. Morton, M.D. [3]
Stefan M. Duma, Ph.D.[1]
R. Mark Payne, M.D.[1,2]

1. Virginia Tech – Wake Forest University Center for Injury Biomechanics, Winston-Salem, NC and Blacksburg, VA
2. Wake Forest University School of Medicine, Winston-Salem, NC
3. University of Utah Health Sciences Center, Salt Lake City, UT

Abstract

Pulmonary contusion is the most commonly identified thoracic soft tissue injury in an automobile crash and after blunt chest trauma and affects 10-17% of all trauma admissions. The mortality associated with pulmonary contusions is significant and is estimated to be 10-25%. Thus, there is a need to develop a finite element model based injury metric for pulmonary contusion for the purpose of predicting outcome. This will enable current and future finite element models of the lung to incorporate an understanding of how stress and strain may be related to contusion injuries.

This study utilizes 14 impacts onto male Sprague-Dawley rats. In 5 of these tests, a calibrated weight (46 g) is dropped from a height of 44 cm directly onto the lungs of intubated, anesthetized rats *in situ*. Contused volume is estimated from MicroPET scans of the lung and normalized on the basis of liver uptake of 18F-FDG. The lungs are scanned at 24 hours, 7 days, and 28 days (15 scans), and the contused volume is measured. In addition, 9 controlled mechanical tests on *in situ* rat lung are used for model development and validation.

Identical impacts are performed on a finite element model of the rat lung. The finite element model is developed from CT scans of normal rat and scaled to represent average rat lung volume. First principal strain is chosen as a candidate injury metric for pulmonary contusion. The volume of contused tissue at the three time points measured using PET is compared to the strain level achieved by a corresponding volume in the finite element model. For PET scans (n=5 scans per time point), the average contusion volume was 4.2 cm^3 at 24 hours, 2.8 cm^3 at 7 days, and 0.39 cm^3 at 28 days. These volumes were used to identify threshold peak first principal strain levels measured by the finite element model. Maximum first principal strain from the finite element model for the three volume levels (4.2, 2.8, and 0.39 cm^3) was 3.5%, 8.8%, and 35% strain, respectively. Furthermore, the lung model exhibited exponential decay in principal strain threshold as more of the lung volume was considered, correlating to the precise and well defined volume of the contusion as it healed.

The results of this study may be used to establish an injury metric to predict pulmonary contusion due to an impact to the lungs. The results may be used to improve finite element models of the human body, which may then be used to tune stiffnesses of interior components of automobiles and tune safety systems for maximum mitigation of this serious injury.

III.1. Introduction

The objective of this study is to explore a finite element-based injury metric for pulmonary contusion. A novelty of this study is the use of inflammation to characterize the injury, something that can only be assessed in living tissue. The approach is to use experimental data on contusion size (volume of contused tissue based on positron emission tomography, or PET) from an animal model and correlate this with mechanical strain measurements from a finite element model simulating the actual impacts onto the lung.

The study proceeds in four parts. First, mechanical testing is performed on rats to generate a controlled pulmonary contusion injury. Contusion volume is measured using the PET imaging modality at 24 hours, 7 days, and 28 days post-injury. Second, model validation tests are performed wherein *in situ* lungs are subjected to controlled impacts and force and displacement are measured. Third, computational modeling is used to recreate the experimental tests. Model validation is performed by matching the force-displacement response to that encountered during experimental testing. This model validation utilizes material parameters from the literature, followed by a parameter identification and optimization algorithm to match the computed force-displacement response to the experimental tests.

Lastly, the mechanically validated computational model of the lungs is subjected to an impact identical to that used for the generation of PET data. First principal strain is chosen as a candidate injury metric. The following approach is used:

1. Volume of contusion measured using PET, which decreases with time, is obtained at 24 hours, 7 days, and 28 days.

2. Peak first principal strains for each element of the impacted lung model are obtained and elements are ranked by peak first principal strain along with individual element volumes and cumulative element volume.

3. A threshold principal strain is chosen for each of the three PET data time points which correlates to volume of contusion measured using PET.

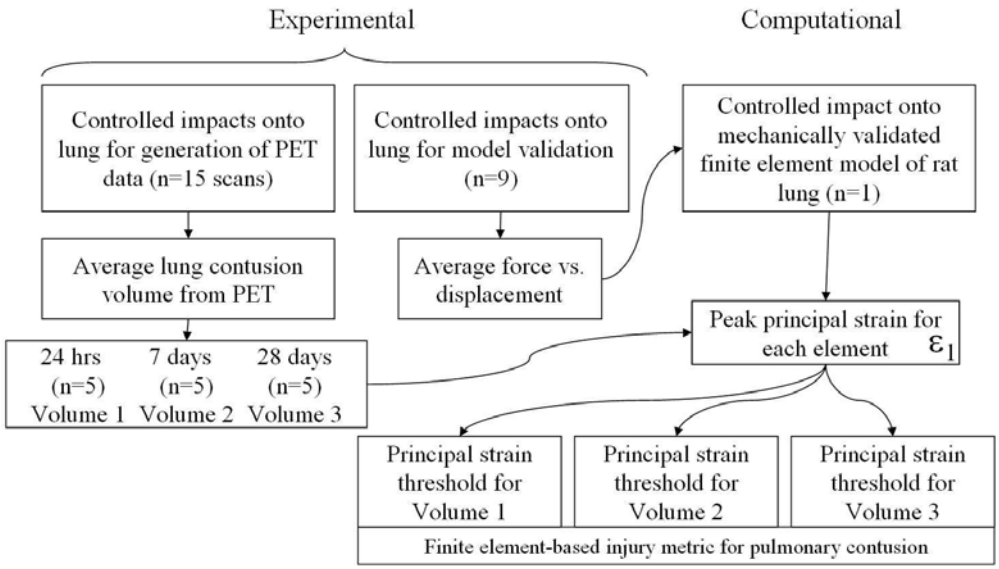

Figure III-1. Outline of study.

III.2. Predictors of Blunt Trauma Induced Lung Injury

There is debate on the best biomechanical predictors of thoracic injury for industry to use in a protective role and government in a regulatory role. Therefore, many injury criteria have been developed. Thoracic impact research has focused on developing global criteria for predicting injury. These include force, acceleration, and chest displacement based criteria, as well as combinations of the above, and much debate exists on the efficacy of the various criteria. (Morgan et al, 1994; Kuppa and Eppinger, 1998). There is a great deal of knowledge about low strain rate pulmonary mechanics and injury from ventilators to the lungs. (Tschumperlin et al, 2000) There are also some criteria for lung

injury resulting from blast-induced shock, with strain rates of 10-100 times that that may be achieved using most blunt impacts. (Choung, 1985) However, injuries to the lungs from car crash loading-rate phenomenon have resulted in no finite element based injury criteria.

A potentially more promising way to predict soft tissue injury is a method based on local stress and strain in the tissues. (Stitzel et al, 2002; Stitzel et al, 2003) There is a continuing trend in government, industry, and academia toward using more localized material properties and soft tissue injury criteria for injury prediction. (Takhounts et al, 2003; Morrison et al, 2003) A finite element (FE)-based injury predictor relating input energy to the lungs and stress and strain in the lung tissue may serve as the best predictor of lung injury. Similar approaches for measures for brain injury have been proposed both in finite element (FE) work (Takhounts et al, 2003) and *in vitro* work correlating mechanical deformation to tissue injury in the brain, coupled with a finite element predictor. (Morrison et al, 2003; Zhang et al, 2004; Hardy et al, 2002)

Current approaches to thoracic injury prediction use global displacement, velocity, acceleration, or combination criteria. (Morgan et al, 1994) Current finite element models of the thorax, therefore, tend to treat the lung structure primarily as a contributing factor to overall chest deformation, and models are still validated based on their response in terms of overall deformation. (Lizee et al, 1998; Ruan et al, 2003; Iwamoto et al, 2002) Chest deformation itself is generally used as a predictor of injury, and is indirectly correlated with various soft tissue injuries that may be incurred. It is widely recognized that soft tissue injury or organ compensation resulting from skeletal fracture is the true threat to life, but soft tissue injuries are also the most difficult to predict. (Viano et al,

1989) Viano et al (1989) points out that lesions to organs (such as pulmonary contusion) and ruptures to vessels present the most significant threat to life. In much of the fundamental injury tolerance work, performed on cadavers, skeletal injuries dominate the response. As such, externally measured variables, and injuries that only manifest themselves in cadavers, are the basis for these injury criteria.

The increasing capability of computers and improvement of the material formulations available to predict trauma have generated a great interest in developing models to predict trauma on a more localized basis. The head is an excellent example. The original head injury criteria (HIC) was designed to predict skull fracture. Subsequent versions of HIC have included other injury measures, relating HIC to probability of concussion, for instance, but future brain injuries have focused on finite element-based predictions. Good examples are the Wayne State brain model (Zhang et al, 2004) and the Simulated Injury MONitor (SIMon) model being developed by the National Highway Traffic Safety Administration (NHTSA). The Wayne State model uses the product of strain and strain rate to predict mild traumatic brain injury (MTBI). SIMon uses three finite element-based measures for predicting brain injury. The brain injuries it attempts to predict are diffuse axonal injury (DAI), contusions, and acute subdural hematoma (ASDH). It does these through finite element-based correlates of cumulative strain damage measure (CSDM), dilatational damage measure (DDM), and relative motion damage measure (RMDM), respectively. (Takhounts et al, 2003) To take one measure in particular, the CSDM was developed with data from Meaney et al (1994) and others (Arbogast et al, 1995; Phelps, 2000) and used animal data to establish the injury threshold for DAI with logistic regression of the CSDM criterion onto various levels of maximum

principal strain to obtain best correlation with experimental data. The CSDM that resulted indicated that 50% probability of concussion would be reached when 55% of the volume of the brain experienced a principal strain level of 15%. This approach can be useful for lung, as a similar approach can be used to correlate peak strains or other measures (to be discussed), and the volume of tissue exceeding those measures, and use these to develop an injury criteria for the lung. Development of such a model would be useful to relate the mechanical strain on the lung to the inflammatory response and may allow prediction of outcome from pulmonary contusion.

Rat Lung Anatomy

Macroscopic Comparative Anatomy

In the human, the right lung has 3 lobes: the right upper lobe (RUL), right middle lobe (RML), and right lower lobe (RLL). The left lung has 2 lobes: the left upper lobe (LUL) and the left lower lobe (LLL). The total volume of the right lung is greater than that of the left lung, a difference attributed to the placement of the heart primarily towards the left side of the chest. In the rat, similarly, the heart rests preferentially to the left side and the left lung volume is less than that of the right lung volume. However, lobar size distribution and architecture is different, with 4 lobes on the right side and one of the left (Zeltner et al, 1990). The total right lung volume on average is 4.52 cc's, and the total left lung volume is 2.58 cc's. The lung model in the current study was scaled to reflect these average numbers and the lung volumes of all rats in the study were assumed to be approximately this size and shape.

Microscopic Comparative Anatomy

Another pertinent difference relevant to potential for injury is alveolar diameter. Lung weight and size is proportional to body weight, as is heart size, however alveolar diameter is proportional to size and to metabolic rate. A relationship for various animals and humans becomes obvious only when alveolar diameter is assumed to be a function of oxygen consumption and normalized to a unit of body weight. Average alveolar diameter in humans is about 200 microns. In rats, average alveolar diameter is 70.2 microns. This has a biologic basis in size of the lungs and the organism, but also has implications for trauma as pressure in the alveoli is a function of initial diameter.

Previous Lung Trauma Research

It has been demonstrated the quantity of contused lung is associated with significant clinical sequelae, including the onset of mechanical ventilation and Acute Respiratory Distress Syndrome (ARDS) (Clark et al, 1988, Gebhard et al, 1997). As estimated by CT, a pulmonary contusion comprising greater than 20% of the total lung volume is associated with a roughly 80% incidence of ARDS (Miller et al). This represents the first actual demonstration of a correlation between the size of contusion and adverse clinical outcomes. Thus, central to the success of the proposed approach is the idea that positron emission tomography, or PET, data is an accurate way to quantify extent of injury.

Positron Emission Tomography (PET) scanning utilizing the glucose analog, [18F]2-fluoro-2-deoxy-D-glucose (FDG), is a relatively new imaging technique that has been shown to be accurate in detecting inflammation in humans. (Zhuang and Alavi, 2002; Rennen et al, 2001). It relies upon the cellular uptake of FDG by metabolically active cells, principally white blood cells of the immune system, in areas of

injury/inflammation. Thus, in addition to quantifying contusion size, PET will provide a global evaluation of the metabolic activity of the lung after injury and add to the general understanding of the role of inflammation in contusion physiology. In trauma patients with pulmonary contusions, PET demonstrated two patterns of inflammation in the lungs: focal uptake at the site of contusion and diffuse uptake that was associated with a more severe systemic inflammatory response. (Schuster et al, 2002; Kaplan et al, 1991) This information suggests that PET can be used to accurately detect inflammation in a contused lung and provide information regarding the host's subsequent inflammatory response based upon the pattern of inflammation. The use of PET in pulmonary contusion could be invaluable in developing models that predict the nature of the ensuing inflammatory response at both the local and systemic levels and clinical outcome after contusion.

Injury Metric vs. Injury Criteria

Previous potential injury metrics for pulmonary contusion have been proposed by Fung (1988). However, at the time less data was available on clinically relevant measures of inflammation. Before an injury criterion can be developed for humans, more data is needed relating car crashes or other well quantified cases of contusion to clinical outcomes. Even for rodent models, an injury criterion will require looking at other finite element-based injury metrics to see whether any of these are better candidates for injury criteria development.

Thus, the first step is to evaluate an injury metric. The structured search for an injury metric will incorporate the ideas given by previous and current researchers for potential candidates. Fung *et al* (1988) searched for a mechanically based mechanism for edema

or hemorrhage in the lung. Fung observed that biological tissues are resilient in compression and a cursory examination revealed a compression wave as the potential mechanism of injury. The hypothesis of injury was that tensile principal strains are induced in the pulmonary alveolar walls. The key question raised was whether alveolar permeability, part of the mechanism of injury, was mathematically correlated on the continuum level to maximum principal strain or another engineering measurement. A tentative decision was made that the maximum principal strain is the most correlated with edema. It is the goal of the current study to correlate this mechanical measure with volume of contused tissue.

III.3. Methods

Overall Approach

Our overall objective is to correlate volumetric contusion levels determined through PET scans to first principal strain levels obtained through computational modeling of direct lung impacts. The methods used to meet this objective are described in this section. First, a description of the experimental methods is presented focusing first on the contusion experimental model and finally on the validation experimental model. Following this, the method used to construct the computational model of the thoracic organs is presented. Finally, the technique used to fit the validation data and the model results are discussed.

Contusion Experiment Model

We have chosen the rat to develop a model of lung contusion for several reasons: 1) It is an extensively used animal with well understood physiology. 2) The genome is well

known and molecular probes are readily available. 3) Their small size makes high-throughput studies possible yet they are large enough for physiological measurements. 4) Mice are too small to obtain adequate imaging resolution in microPET scanners. All animal protocols were reviewed and approved by the Animal Care and Use Committee of Wake Forest University School of Medicine prior to performing any experiments (Protocol Number A05-187).

Sprague-Dawley male rats weighing approximately 320 g in size undergo a right lateral thoracotomy in order to expose the right lung. The rats are anesthetized with 1-1.5% Halothane anesthesia and buprinex 0.1 mg/kg is administered for analgesia prior to the procedure. The rats are orotracheally intubated after induction with Halothane and maintained on a positive pressure respirator (model SAR-830/AP ventilator, CWE, Inc., Ardmore, PA) with a ventilator rate of 55 breaths per minute, a positive airway pressure of 12 cm H_2O, and a continuous positive airway pressure of 1 cm H_2O. Halothane maintenance is continued at 1-1.5% during the procedure. The animal is maintained on a warming pad. The right chest is shaved and sterilized with betadine. The right thorax was chosen as this avoids injury to the heart which occupies a large portion of the left thorax. Care is taken not to injure the lung during this procedure.

Once the right lung has been exposed, the lung is struck during inspiration (physiologic pressure and volume) by a calibrated weight dropped from a specific height to strike the exposed lung with a controlled amount of energy. All of the contusion data presented in this study reflect an injury to the lung from a 26.6 g object traveling 44 cm to deliver the impact (Velocity = 2.8 m/s at impact). The area of impactor surface is 31.7 mm^2, a round impactor with beveled edges (to avoid cutting and tearing tissue at the

interface) of 6.35 mm diameter. The chest then closed using absorbable suture (3-0 Gut), and the skin is closed using 3-0 silk suture. Air is evacuated from the right chest using a small bore catheter which is then withdrawn at the end of the procedure. The animals are allowed to awaken and the ventilator is removed when they are spontaneously breathing.

Pet Data Collection

MicroPET scanning, in a novel application of this technology, will be used in this study to quantify contusion size relative to total lung volume. PET scanning relies upon the cellular uptake of the glucose analog, FDG by cells in areas of inflammation/injury. Therefore, PET not only offers an estimate of the physical size of the contusion, it also gauges the magnitude of the subsequent inflammatory response. To date, no studies have been performed to evaluate pulmonary trauma using PET in rodents.

For PET scans, animals were sedated and maintained on 1.5% isoflurane inhalational anesthetic by nose cone. The animals were monitored to ensure that they remained sedated for the length of the procedure and PET scan. Anesthetized animals were placed in the microPET gantry and positioned via crosshair markers on the chest. Once positioned a 26 minute transmission scan was performed to correct for attenuation. Immediately after the transmission scan, the animal was injected with 1.0 mCi of the radiotracer, [^{18}F]2-fluoro-2-deoxy-D-glucose (FDG) (Bergmann, 1996) via the tail vein. Immediately after injection the rats are imaged for 80 minutes over the thorax to scan the lung.

PET scans were performed on the Concorde Microsystems, Inc., microPET P4 PET scanner. This device has no septa and therefore operates exclusively in three-dimensional imaging mode with axial and transaxial fields of view of approximately 8

and 20 centimeters respectively. The reconstructed resolution is approximately 2.5 mm in all three axes. Data was corrected for attenuation and reconstructed into 16 five minute frames using two-dimensional filtered back-projection with a ramp filter. Image counts/pixel were converted to μCi/ml using a scale factor previously determined by scanning a rodent sized phantom with a known concentration of radiotracer.

We have established protocols to allow comparison of the volume of inflammation in lung across different experiments. A ROI is drawn in the liver to define non-specific tissue uptake. Liver is large and homogeneous in its uptake of glucose. We have found that tracer washout in the liver is similar to that found in the normal lung and reaches similar tissue concentrations after tracer injection. Voxels in the right lung exceeding a threshold defined from the liver ROI (mean + 3 standard deviations) are then defined as inflammation and their volume determined in the lung.

Mechanical Validation Experimental Model

To validate the computational model, experimental force versus deflection data was collected *in vivo* on intubated anesthetized rats. The process of this data collection is outlined in this section. All validation data was collected using an 8-channel data acquisition unit, (WaveBook 516E, IOtech, Cleveland, OH) and strain gauge module (IOtech, Cleveland, OH).

Test Configuration and Instrumentation

Dynamic force versus deflection validation data was obtained using an electromagnetically driven Cortical Contusion Injury device (model eCCI, Custom Design and Fabrication, Richmond, VA). The eCCI was set to deliver impacts

penetrating 6mm beyond the initial point of contact at 2.8m/s. A force transducer (model 208C01, PCB Piezotronics, Depew, NY) and 6.35 mm diameter aluminum impacting anvil were mounted to the end of the shaft. A custom shock adapter was used to mitigate the large tensile forces which occur due to the sudden stop when the impacting shaft reaches the end of its stroke. The test setup is shown in Figure III-2. Built-in velocity monitoring was used to record the velocity of the shaft over the final 8.5 mm of travel. The recorded values show that the average speed 8.5mm before impact was 2.8m/s +/- 0.02m/s for the dynamic tests. The impact depth was set to 6.3 mm, and the speed over the course of the impact was confirmed to be constant. With a constant velocity known, the deflection data was extrapolated from the starting point of contact of the impactor and the lung.

Data were collected at 500kHz, with a total of 20000 scans sampled. The data collection was triggered off the large tensile force spike that occurs due to the deceleration of the impacting shaft. 18000 scans were taken pre-trigger, and 2000 scans were taken post trigger.

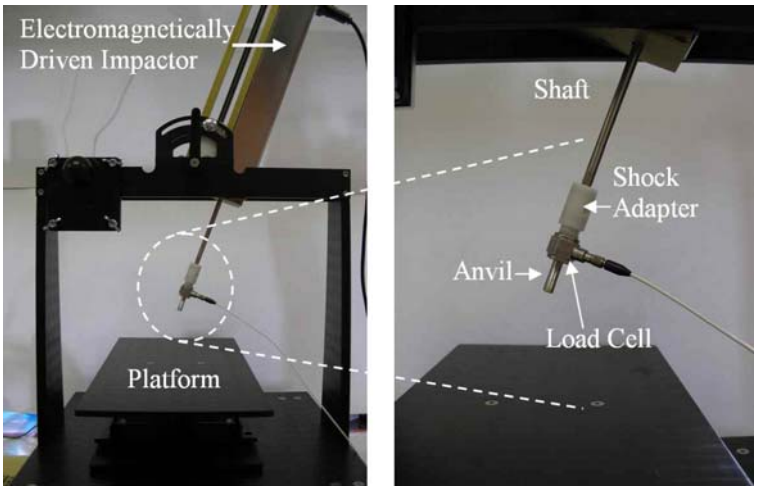

Figure III-2. Mechanical validation data test setup. Electronic cortical contusion injury (eCCI) device (left), enlarged image of impactor, transducer and shock adapter (right).

Test Matrix

The impacts used to collect dynamic validation are shown in Table III-1. A total of 9 impacts were used in order get an adequate number of data points to characterize the response of the lung. One speed only was chosen to keep study size manageable.

Table III-1. Test Matrix for High Speed Impact FE Model Validation Data.

Test No.	Impact Speed (m/s)	Penetration Depth (mm)
1	2.8	6.3
2	2.8	6.3
3	2.8	6.3
4	2.8	6.3
5	2.8	6.3
6	2.8	6.3
7	2.8	6.3
8	2.8	6.3
9	2.8	6.3

Experimental Data Interpretation

<u>High Speed Video Data of Impacts for PET studies</u>

Impacts to the lung were delivered with a 46 g weight which slides freely on a vertical pole. In order to accurately model the same impact in LS-Dyna, the trajectory of the weight during the insult, the maximum penetration depth and initial contact velocity must be known accurately. To collect this data, the impactor was filmed using a high speed camera at 3000 frames/second with a pixel resolution 128x512 (Phantom High Speed Camera, Vision Research Inc., Wayne, New Jersey). No target was included in the high speed video data collection and it was assumed the inertia of the falling weight would cause the same behavior regardless of the presence of the lung tissue. A total of 5 separate events were filmed. The high speed video files were used to track the location of the impactor.

Two separate tracking files were created for each image stack and saved in text files. All subsequent data processing was performed in Matlab. The first file tracks the trajectory of the impactor over the course of the event. The average of these trajectories (n=5) is used as the load curve in the LS-Dyna model of the impact, Figure III-7. This data also is used to find the maximum penetration depth of the impactor, Table III-5. The second set of tracking files was used to find the approach velocity of the impactor. For this set, the position of the anvil was tracked over the final 3ms (10 frames) before impact. The average of these traces is calculated and the slope of the average is considered the impact velocity, Table III-5. The impact velocity was used in the dynamic model validation described later.

Dynamic Validation Data

The following steps were taken to prepare the dynamic impact data for model validation. Because a piezo-electric load cell was used during the dynamic testing, small differences in baselines were offset by subtracting the average of the first 1000 data points.

With the data properly zeroed, the next step in the preparation was to isolate the loading portion of the curve. The lung was within the chest wall and thus could not be filmed to see exact time of contact. Also, the initial position of the lung was slightly variable due to controlled inflation of the lung via the ventilator. At the end of each test, the impactor hit a mechanical stop to immediately stop further movement into the lung. This stop was accompanied by a large inertial spike which was easily identifiable. This spike was correlated to an end-of-loading index, simply the final point before the large tensile force was measured. The beginning index was then chosen as the first zero-slope index below zero, tracing back from the end-of-loading index.

With the start and end of loading known, the data was prepared for filtering. In all cases, before filtering, the data was mirrored and inverted on both sides to avoid inaccurate filtering at the ends of the trace. The data were filtered to SAE J211 channel filter class 1000Hz. The data were inertially compensated using the acceleration of the rigid impactor shaft to account of the effect of mass below the sensitive plane of the transducer. Placing an accelerometer on the impacting shaft assembly close to the load cell was impractical because of shaft balance, weight, wiring, and space considerations. The load cell was placed as close to the impacting surface as physically possible. Inertial compensation was performed by assuming that the impacting rod assembly was a rigid body, and that the force at the impact point was equal to the total mass of the rod assembly multiplied by its acceleration. The masses of each component of this assembly were precisely known by direct measurement or from manufacturer's specifications. The inertially compensated force is the measured force multiplied by the ratio of the total mass of the assembly to the mass between the sensitive plane of the load cell and rear of the assembly. This ratio was 114%, thus all measured forces were multiplied by 1.14 prior to analysis. The mass of the impacting shaft is very high compared to the mass of the lung, and velocity measurements of the impacting assembly confirm that the velocity is constant throughout the duration of impact to within 0.001 m/s, until the shaft hits rigid stops at a chosen impact depth.

Computational Model

Geometry, CT Image Segmentation and Mesh Creation

For mesh creation, normal CT scans of rats were taken using a Lightspeed Pro 16 Scanner (General Electric (GE) Medical Systems, Minneapolis, MN) in common clinical

use throughout the United States. Full resolution CT coronal images were taken of an entire middle-aged rat, at a pixel resolution of 0.2539 mm/pixel. Width and height of scans was 512 x 512 pixels with a pixel depth of 16 bits. Slice thickness was 0.625 mm.

Lung appears black in CT's due to the presence of air, while bony structures appear white to off-white. Image segmentation to isolate the outer surface of the lungs is therefore relatively straightforward. Image segmentation was performed using Amira software (ZIB/Mercury Computer Systems, Berlin, Germany). Multiple dilation and erosion steps were used to isolate the lung, along with some manual isolation to smooth outer surfaces and segmentation artifacts. In particular, overlapping between the heart and lungs and between the lungs and liver/diaphragm required anatomical knowledge and some intervention through manual segmentation. However, initial segmentation efforts were performed using automatic segmentation techniques and Boolean steps to isolate anatomical features from one another.

Automatic outer surface meshing algorithms were then used to form a tetrahedral mesh on the outer surface of the lungs. This mesh, intended for stereolithography model development, was imported into FEMB (Finite Element Model Builder, Engineering Technology Associates, Troy, MI) and splines were used to define and partition the lungs into volumetric segments and create better defined surfaces. The heart was separately meshed, as were the primary bronchi leading to the right and left lungs (Figure III-3). Thereafter, surface and line information was exported to TrueGrid (XYZ Applications, Livermore, CA). TrueGrid was used to create a structured hexahedral mesh within the area. The mesh was subjected to relaxation algorithms to reduce element distortion and result in a higher quality mesh. All elements except those used for the trachea are

hexahedrons with reduced (single point) integration. Trachea was modeled with thin shells.

The final volume of the meshed lungs was very close to the volume of normal rat lungs obtained from the literature. This initial difference between finite element mesh lung volume and published volume for normal rats was less than 9% and all meshes were scaled uniformly to maintain interfaces and to achieve the correct volume of the right lung (4.52 cm^3) for agreement with the 'average' rat anatomy previously described.

The final mesh consists of the right lung, left lung, tissues to represent mediastinum, heart, and trachea, however the mesh also has a sheath to represent the outer chest wall and diaphragm, which was modeled as a rigid boundary with sliding contact (Figure III-3, right). This assumption is valid for modeling the lung since the lung itself is much less stiff than the chest wall or liver, the solid organ below most of the diaphragm.

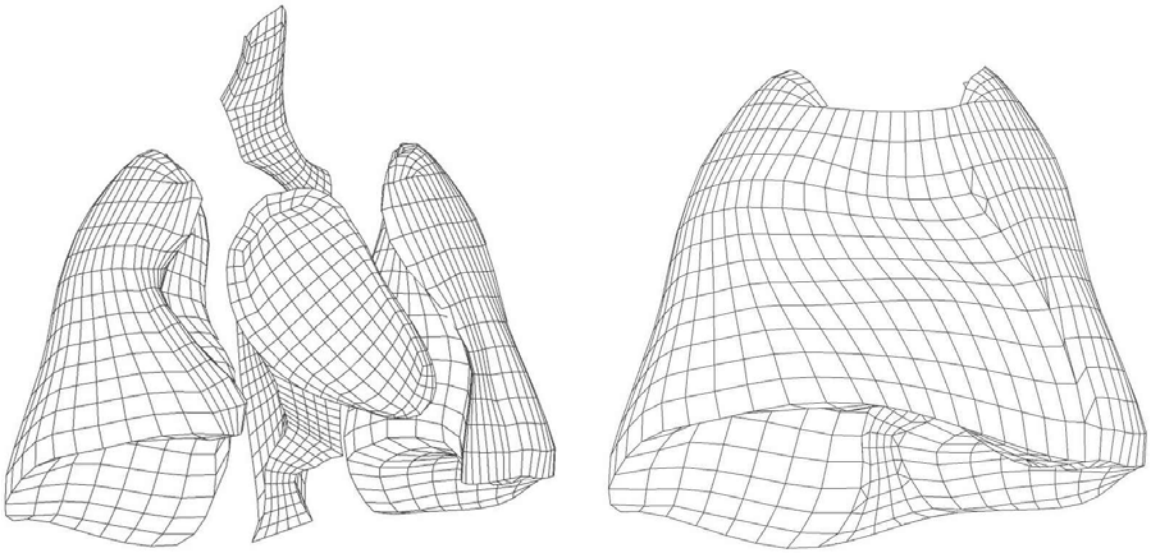

Figure III-3. Exploded mesh of rat lung (left) consisting of lungs, heart, mediastinal tissues, and trachea. The chest wall and diaphragm (right) were modeled as rigid boundaries surrounding the lungs.

Because of the design of the computational aspects of this research (GA and DOE studies), it was important to develop a model with a modest run time. The presented version of the model is a six-millisecond impact event which runs in approximately 1-2 minutes on a PC workstation (Dell Optiplex GX620, P4, 3.4GHz processor with 1GB ram). This allowed for extensive model parameter research via GA, and DOE algorithms. Also, Takhounts et al (2003) described an acceptable run time for a 150 millisecond impact event, and 1 hour was chosen as a goal to allow the parameter variation and other studies. At 1.5 minutes average run time for our 6 millisecond event, a 150 millisecond run would take approximately 40 minutes.

Material Definitions

The model was given material properties to define its response to external forces, and include nonlinear elasticity, finite deformation, and surface tension. Many models are currently available for describing lung tissue, but there is one that is most common in

explicit codes. The material model that was used for the rat lung tissue was a material model originally proposed by Vawter (1980). It is an FE material model that has found much use in current commercial codes as a representation of human lung. Common material properties for this lung tissue and feasible values for the lung material properties are also presented by Vawter (1978). The relationship used for the stresses and strains in human lung is a strain energy functional expressed using the Green Strain (Equation III-1):

$$W(I_1, I_2) = \frac{C}{2\Delta} e^{(\alpha I_1^2 + \beta I_2^2)} + \frac{12C_1}{\Delta(1+C_2)}\left[A^{(1+C_2)} - 1\right] \qquad \text{Equation III-1}$$

$$A^2 = \frac{4}{3}(I_1 + I_2) + 1 \qquad \text{Equation III-2}$$

C, α, β, C_1 and C_2 are material coefficients determined from experiments, and K is the bulk modulus. Delta (Δ) is the typical alveolar diameter when unstressed, $I_1 = e_{11}+e_{22}+e_{33}$ is the first strain invariant, and $I_2 = e_{11}e_{22}+e_{22}e_{33}+e_{33}e_{11}-e_{12}^2-e_{23}^2-e_{31}^2$ is the 2nd strain invariants, where e_{ij} are the Green strains. The 2nd term in Equation III-1 comes from the relationship for the surface energy density (Equation III-3), which is combined with the surface area given in Equation III-2 (Fung, 1988). The relationship of gamma to area is not reported for rats, but approximations such as that presented by Vawter (1975, 1977, 1978, 1980), Equation III-4, can be used. Vawter gives the relationship using C_1 and C_2 experimentally determined constants. Hydrostatic work is given in terms of the bulk modulus, K, and the third strain invariant, J (Equation III-5).

$$E = \frac{12}{\Delta}\int_1^A \gamma(A)dA + constant \qquad \text{Equation III-3}$$

$$\gamma = C_1 A^{C_2} \qquad \text{Equation III-4}$$

$$W_H(J) = \frac{K}{2}(J-1)^2 \qquad \text{Equation III-5}$$

Virtual model validation using isolated rat lung in impact studies

To obtain the correct material properties for the model being developed, it was necessary to use parameter identification processes to adjust material parameters until the model fit experimental data. The lung tissue model initial parameters came from several sources. Bulk modulus or modulus of compressibility has a high effect on the model's response when considered for static loading scenarios. As loading rate increases, the density has a larger effect. The initial bulk modulus and density were taken from Yen et al (1986, 2005) as 0.118 g/ml (1/8.5 times water) and bulk modulus measured by calculation from stress wave propagation speed was 1291 cm H_2O or 0.1266 N/mm^2. In the case of c/delta, alpha, beta, C_1/delta, and C_2, initial parameters are taken from Vawter (1980). Delta, the typical alveolar diameter when unstressed, can be obtained from histologic studies in the literature and for rats is 70.2 +/- 6.6 microns (Tenney, 1963). Initial values of C and C_1 were therefore calculated using this value. For comparison, in humans the average alveolar diameter is over 200 microns. These values were used as initial values for the lung model and then adjusted using optimization algorithms (to be explained) to match force vs. displacement response. Alveolar diameter and density were held constant for all studies undertaken, as these are intrinsic, easily measurable tissue properties. When trying to validate a model using *in situ, in vivo* mechanical data, the approach outlined is one of the best methods available.

Model Response Optimization

Dynamic test data from 2.8m/s impacts on in vivo rat lung were used for validation of the lung model. Statistically significant discrepancies between the simulated and empirical force versus displacement histories required that the nominal model parameters from the literature be adjusted. These parameters are previously described.

A multi-island genetic algorithm (GA) was used to match the simulated force response to the experimental force response. The GA, performed with iSIGHT software (Engineous Software Inc., Cary, NC), works by minimizing an objective function, S (Equation III-6).

$$S = \sum \left(F_{Sim}(\beta_{1-6}) - F_{Exp} \right)^2 \qquad \text{Equation III-6}$$

Here, F_{sim} is the force response from the finite element simulation, F_{exp} is the experimental force response and β is a vector representing the six parameters which are adjusted to tune the model response. These parameters and their upper and lower bounds are shown in Table III-2. The objective function approaches zero when the simulated and experimental force responses become equal.

The multi-island genetic algorithm works like a traditional genetic algorithm, but with sub-populations developing in parallel on a number of different islands. Like most GA's, a fitness value is assigned to each set of parameters, based on the value of the resulting objective function. A set of parameters, or an "individual", is said to be more "fit" as S approaches zero. Each parameter of an individual can be thought of as a chromosome. Each chromosome is a binary encoding of the parameter value between its upper and lower acceptable bounds. The effects of the multi-island algorithm are

introduced as individuals "migrate" from one island to another. This migration allows for a greater range of solution space to be investigated than using cross-over and mutation alone since parallel development on different islands reduces the amount of competition between individuals.

Table III-2. Static and Dynamic parameter design space.

Variable (Unit)	Description	Lower Bound	Nominal	Upper Bound
ρ (kg m^{-3})	Density	-	1.18×10^{-4}	-
K(N m^{-2})	Bulk Modulus	0.0950	0.127	0.158
C (N mm^{-1})	Curve fit parameter	1.72×10^{-5}	1.72×10^{-4}	1.72×10^{-3}
Δ (mm)	Mean alveolar diameter	-	7.02×10^{-2}	-
α	Curve fit parameter	0.0183	0.183	1.83
β	Curve fit parameter	-2.91	-0.291	-0.0291
C1	Curve fit parameter	1.33×10^{-7}	1.33×10^{-6}	1.33×10^{-5}
C2	Curve fit parameter	0.271	2.71	5.0

The parameters used in the genetic algorithm are summarized in Table III-3. The size of the subpopulation, number of islands and number of generations are multiplied together to determine the total number of runs in the GA optimization. The interval and rate of migration determine the number of generations between migrations and the percentage of individuals who will migrate from their island. The probability of mutation is the probability that a gene (a single 1 or 0) will change value. The rate of crossover gives the percentage of individuals whose genetic encoding will be crossed with another individual to produce the next generation. The genetic encoding is determined by the gene size, which in this case is 32bits. To ensure that the best individuals pass on their parameter values, an elite member from each generation is selected from a sub population on each island called a tournament. In this case, the individual with the lowest value of S in a tournament will be selected. The relative tournament size of 50% means that the

elite individual will be selected from a randomly chosen sub-set on each island consisting of 5 individuals.

Table III-3. Parameters used in GA.

Size of sub-population (individuals)	10	Rate of migration	50%
Number of islands	10	Rate of crossover	100%
Number of generations	25	Gene size (bits)	32
Total number of runs to complete GA	2500	Elite Size (individuals)	1
Interval of migration (generations)	5	Relative tournament size	50%
Probability of mutation of a single gene	1%		

Sensitivity Studies

To explore the effects the parameters in the hyperelastic material model have on the simulation outcome, a design of experiments (DOE) simulation was performed using iSIGHT software. In order to perform a DOE study a design space must be delineated. The design space is bounded by the minimum and maximum acceptable values of the parameters from the lung model under study. The optimal Latin hypercube (OLHC) algorithm was used to maximize the effectiveness with which the design space was sampled. The inputs to this algorithm are the desired number of simulations to run and the design space boundaries. Before running the design of experiments, all variables of interest must be specified as either input or output. The purpose of this specification is so the effect of an input variable on an output variable can be explored after the DOE is completed.

In the DOE six parameters were specified as input parameters, the bulk modulus of lung, K, and the following parameters from the constitutive equation of the lung tissue: α, β, C, C1, C2. The minimum and maximum acceptable values of each of these parameters

was taken as +/- 50% of the optimal value as calculated by the GA. A Matlab script is executed at the end of each design trial. This script is part of series of scripts developed in our laboratory to perform various operations on LS-Dyna output files. In this case, the contact force and nodal displacement of the impactor from the LS-Dyna simulation are used to compute the energy imparted to the lung by integrating the force versus deflection curve. This energy is specified as a DOE output variable. The effect of each design variable on the impact energy is discussed in the Results section.

III.4. Results

Experimental Results

Shown in Figure III-4 is a photograph of a right lung removed 24 hours after injury. The black arrows point to the area of contusion, which is well circumscribed by bruising of the lung and has multiple adhesions with the chest wall. The left lung, in comparison, has no outward evidence of injury and the heart is normal in appearance and function because it was not in the field of injury. This is important because bruising of the lung in thoracic blunt trauma is common and contributes to pulmonary dysfunction during post-trauma management (Miller, 2001). The open lung contusion simplifies our model because closed chest contusion in the rodent, and other animal models, may generate severe arrhythmias in the heart resulting from myocardial contusion, indicating involvement of a different organ system in the trauma event, which may complicate interpretation of the data (Wang, 2003).

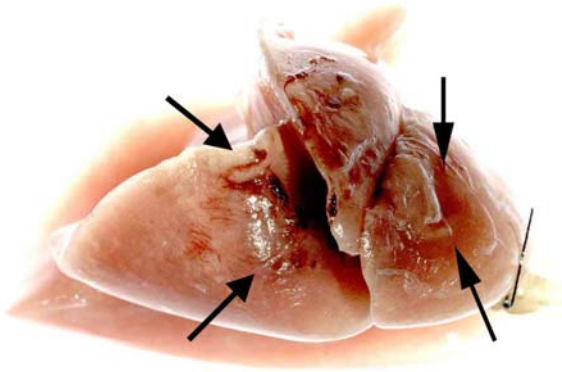

Figure III-4. Pulmonary contusion to right lung. This right lung was exposed through a lateral thoracotomy and struck as described in text. Twenty-four hours later it was removed and inflated to a pressure of 20 cmH_20. The black arrows point to the contusion of the right lung. The left lung is normal in appearance without any evidence of erythema or injury.

PET Experimental Results

Results of PET scanning show a diminished contusion volume over the course of a one month healing period. The impacted lung (right lung), shows an inflammatory response affecting its entire volume at the end of 24 hours. At the end of one week, the volume is markedly diminished. At the end of one month, very little volume remains affected. The volume that does remain affected is the volume closest to the site of impact.

Figure III-5 and Figure III-6 document that the lung contusion can be followed over time by PET scan and the volume of [^{18}F]FDG uptake can be quantified. The results show one animal (out of 5) followed for 1 month after open lung contusion. In Figure III-6, the volumes of [^{18}F]FDG uptake were quantified for 5 animals. To control for variability between animals, the signal intensity was normalized to uptake of [^{18}F]FDG by the liver and the signal at the 7d and 28d times is expressed as a percentage of the initial signal at 1d for each animal. The initial uptake in the contused lung subsides by ~50% 1 wk after injury and is less than 10% of the initial injury 1 mo after trauma (Table III-4). Both the 7d and 28d signals are statistically significant compared to the 1d signal

(p = <0.001). Our interpretation of the decreasing PET signal is that inflammation generates the initial [^{18}F]FDG uptake whereas scar formation is a metabolically less active process.

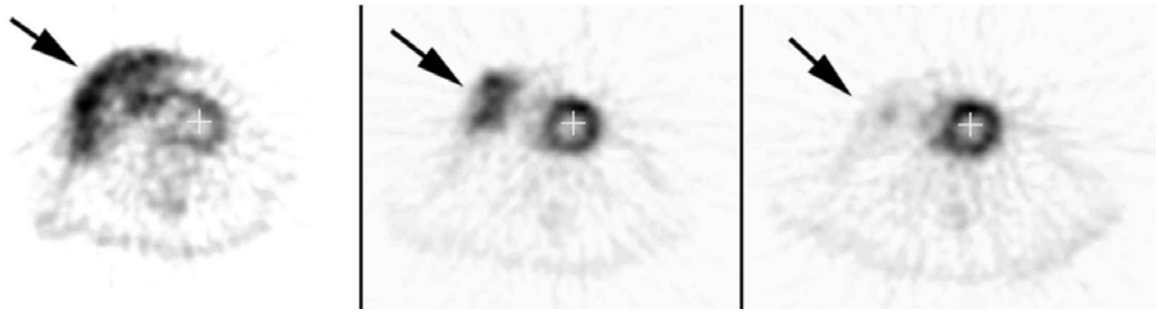

1 Day 1 Week 1 Month

Figure III-5. Sample PET scans (2-D slices) at 24 hrs, 7 days, and 28 days. Arrows indicate areas of contused lung tissue.

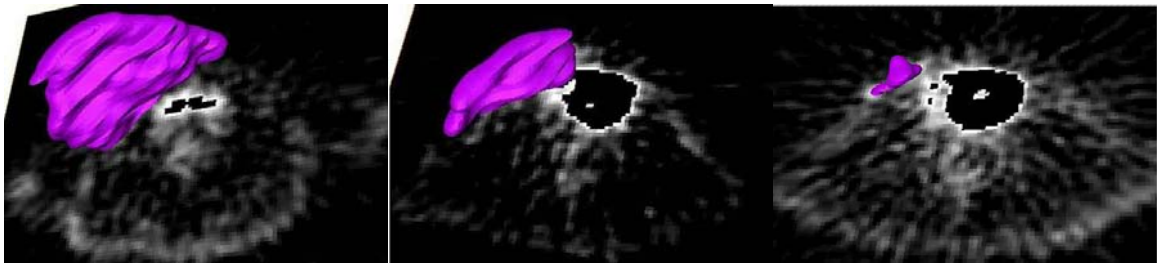

1 Day 1 Week 1 Month

Figure III-6. Volumetric segmentations of contusion volume, for correlation with FE results.

Table III-4. Contused volume from PET scans, used for FE model correlation with principal strains.

PET Scan	1	2	3
Day	1	7	28
Contusion Volume, mm^3			
Test 1	7061	1934	58
Test 2	5590	2578	462
Test 3	8270	3619	238
Test 4	6997	2201	1066
Test 5	6343	3767	123
Average Contusion Volume, mm^3	6852	2819	389
Standard Deviation, mm^3	991	831	408
Coefficient of Variation	0.14	0.29	1.05
Contused Volume PET, cm^3	6.85	2.82	0.39
Contusion Volume for model comparison (Right lung only), cm^3	4.18	2.82	0.39

Mechanical Data Experimental Results

Results of characterization of the system used to impact rat lungs for PET data collection demonstrate a repeatable system. The displacement versus time profile was used to impact the mechanically validated model of the rat lung to correlate maximum peak principal strain (on a volumetric basis) with PET inflammation data (Figure III-7).

Table III-5. Model inputs obtained via high speed video.

Name	Value	Standard Deviation
Maximum Penetration Depth	6.2 mm	0.15 mm
Contact Velocity	2.8 m/s	7.9E-2 m/s

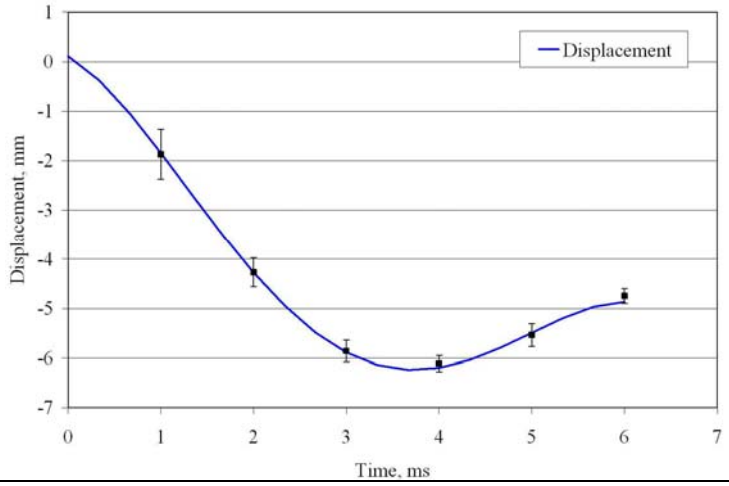

Figure III-7. Displacement vs. time from impacting device used to perform controlled impacts on rat lung for PET data generation (error bars represent n=5 tests).

Finite Element Model Mechanical Validation Data Experimental Results

Results of mechanical testing of rat lung for model validation show that testing conditions resulted in very repeatable impacts to the lung, with a mean peak force of 0.96 N, a mean energy of 4.0 mJ. For comparison with literature, mean energy per unit area of impactor was 126 J/m^2. Energy per unit volume (assuming energy is equally distributed throughout the lung, perhaps not a valid assumption) would be 740 J/m^3. Data are inertially compensated as described previously in the Methods, Experimental Data Interpretation section.

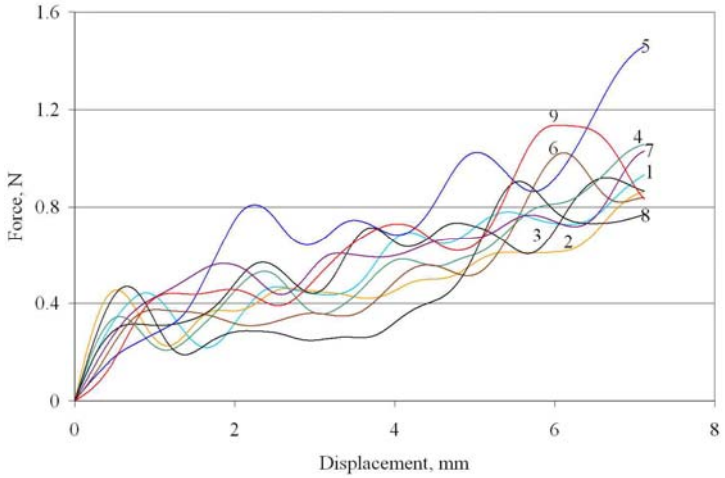

Figure III-8. Experimental impact tests for model validation, filtered CFC 1000, at 2.8 m/s. Numbers indicate test numbers.

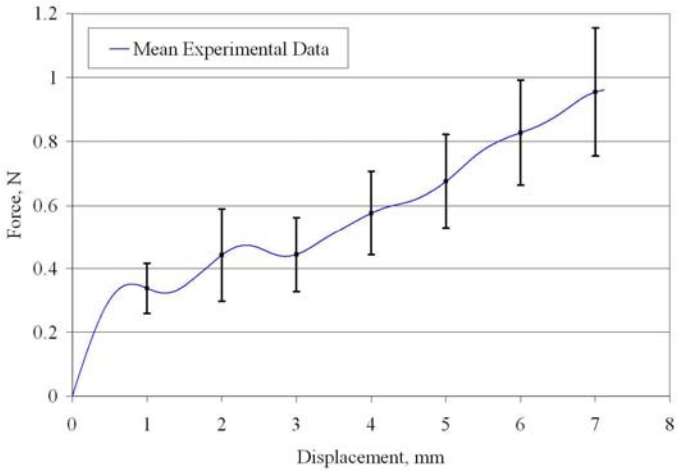

Figure III-9. Force versus displacement from experimental tests at 2.8m/s. Error bars represent +/- one standard deviation.

Table III-6. Mean and standard deviation of peak force and energy from rat lung impacts for finite element model mechanical validation.

	Mean	Standard Deviation	Coefficient of Variation
Peak Force, Newtons	0.96	0.21	0.21
Energy, milliJoules	4.0	0.60	0.15

Modeling Results

Initial results of modeling experiments highlight the large deformation due to lung impact. Large deformation of the finite element mesh is apparent, associated with high first principal strains of greater than 50% (0.5) (Figure III-10). From the model results for the optimized model run with the impact representative of that used for PET studies, the number of elements exceeding a warpage angle criterion is 144/9039, with the angle varying from 20 to 135 degrees. The warpage angle used in the model was 20^{o}, the default value for shell elements. Elements exceeding the warpage angle are found in two parts of the model; the trachea and the layer of zero-mass elements used to apply the surface to surface contact between the lungs and the rigid outer shell. The trachea elements that exceed the warpage angle are due to the mesh in the region of the bifurcation. The warpage that occurs in the zero-mass elements is due to the anvil motion during the impact. It is believed that exceeding the warpage angle default does not negatively affect the model performance. Since the model measures a dynamic impact to soft tissue, large deformations are expected. Such large deformations will inevitably cause warpage angles in some elements to exceed 20^{o}. The default value of the warpage angle is appropriate in materials more rigid than lung. Additionally, despite a number of elements exceeding this warpage angle the model showed robust stability in design of experiment and optimization studies, which solved the model with hundreds of different combinations of material parameters. More on model stability can be found in the discussion of the optimization and sensitivity studies.

A study of hourglass control parameters was conducted to determine the effect of hourglass control on model results. This study consisted of a full factorial investigation

of the hourglass viscosity type and the hourglass coefficient. The hourglass viscosity type was varied between Flanagan-Belytschko integration and Flanagan-Belytschko with exact volume integration. The hourglass coefficient was varied between 0.01 and 0.2 in steps of 0.01. This study showed negligible effect of the hourglass control parameter and type on the threshold values of mechanical strain encountered in the model.

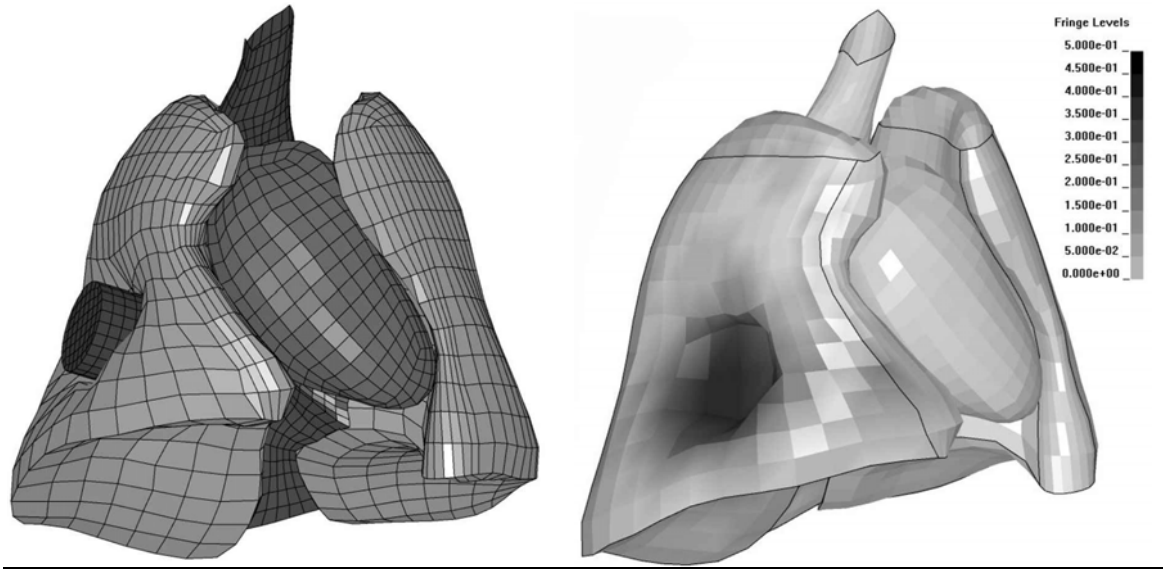

Figure III-10. Maximum displacement of impactor into lung (left) and peak principal strain plots of lung (right). Material surrounding the lungs and diaphragm is not shown here for clarity.

Optimization Results

The GA described previously produced an optimized set of parameters shown in Table III-7. This set of parameters results in a simulated impact whose force displacement response is within one standard deviation of the experimentally measured data for nearly the entire impact. These parameters are from the individual who proved to be most fit (i.e., produced the lowest value of S) after 2500 runs.

Table III-7. Parameters resulting from the GA optimization, based on 2.8 m/s impact.

Parameter Name	Units	Parameter	Value (Optimal fit parameters)
Density*	g mm^{-3}	ρ	1.180×10^{-4}
Bulk Modulus	N mm^{-2}	K	1.124×10^{-1}
Curve fit parameter	N mm^{-1}	C	5.035×10^{-4}
Alveolar Diameter (unstressed)*	mm	Δ	0.0702
Alpha, curve fit parameter	Unitless	α	8.227×10^{-2}
Beta, curve fit parameter	Unitless	β	-2.46
Hyperelastic Coefficient	N mm^{-1}	C1	6.535×10^{-6}
Hyperelastic Coefficient	Unitless	C2	2.876

* Density and alveolar diameter were chosen from literature values and unchanged.

Force versus displacement of optimized model

The results of run optimization produced a lung model response which fell within experimental corridors for the entire the loading regime (Figure III-11). The model notably duplicates the initial inertial spike encountered in experimental runs, and oscillatory effects from the initial impact die out over time as with experimental runs. Nominal values from the literature fell outside the single standard deviation boundary from experimental data after the initial inertial spike. However, optimization of the model resulted in a force-displacement response greatly improved over initial parameter values.

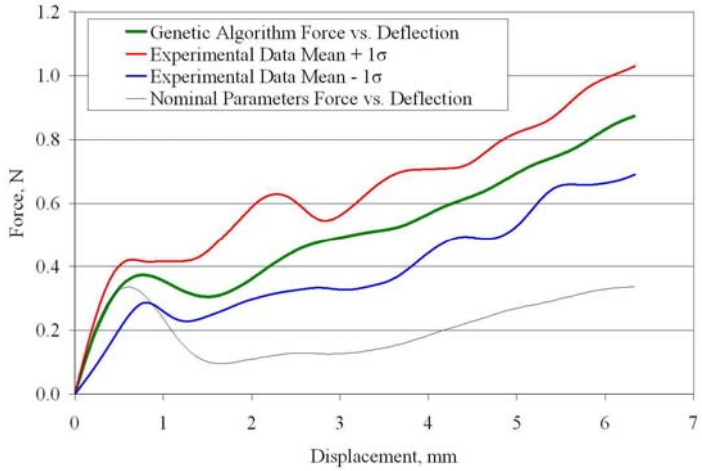

Figure III-11. Force vs. displacement results for optimized model.

Lung Modeling

Percent strain thresholds were obtained for the lung model by ranking element peak principal strains. Modeling results demonstrated that 4.2 cm^3 of lung, nearly the entire right lung, underwent a minimum strain of 3.5%. 2.8 cm^3 of lung underwent a minimum strain of 8.8%. 0.39 cm^3 of lung underwent a minimum strain of 35% (Figure III-12, Table III-8).

Table III-8. Contusion volume measured from PET and corresponding 1st principal strain experienced by that volume of tissue in the finite element model.

Day	1	7	28
Contused Volume from PET	4.2	2.8	0.39
Contused Volume FE	4.2	2.8	0.39
First Principal Strain Threshold (expressed as a percentage)	3.5%	8.8%	35%

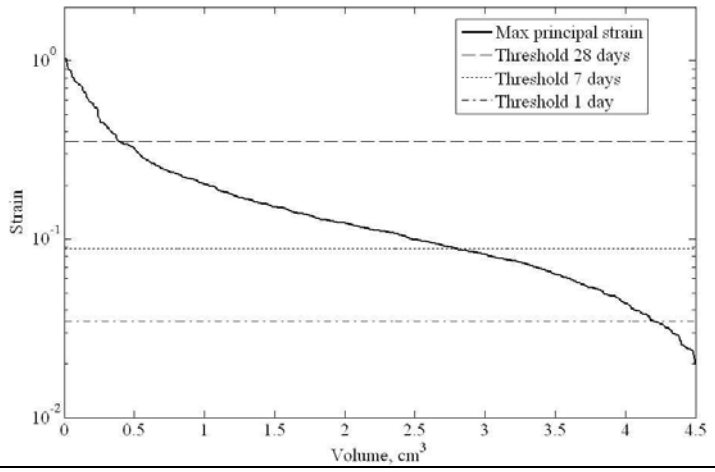

Figure III-12. First principal strain threshold (logarithmic scale) versus cumulative volume. The intersections represent percent strains (Maximum Principal Strain) for volumes of contused lung at 1 day, 7 days, and 28 days.

When cross sections through the impactor and lung (centered on the axis of the impactor and parallel to the line of action of the impactor) are created and principal strain in the cross section is plotted, the results are useful to compare to the results of Figure III-5 showing the PET inflammation measurements (Figure III-13). This series of figures shows evolution of strain during the impact rather than post-impact total volume measurements (used for injury metric development), where a threshold was chosen to correlate to PET. However, it supports a mechanical deformation-based rationale for the presence of greater amounts of inflammation, which persist longer after the impact, in the areas nearest the impactor. It agrees qualitatively with the results provided through positron emission tomography.

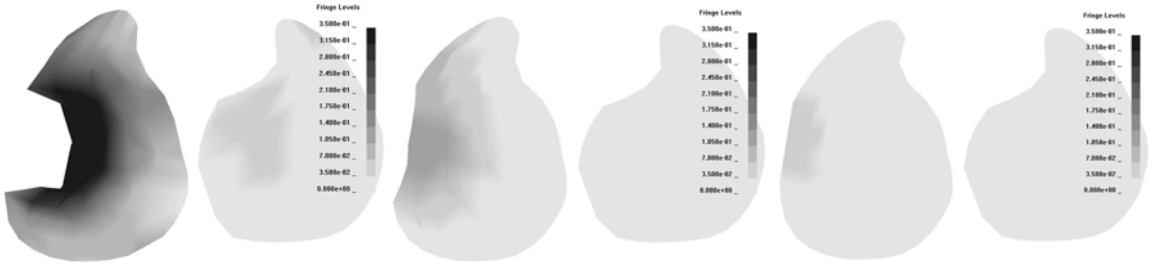

Figure III-13. First principal strain in the lung cross section showing strain field at: A) near maximum deflection, principal strain threshold = 35%, B) principal strain threshold = 8.8%, C) principal strain threshold = 3.5%. Maximum principal strain for all figures is 35% to allow comparison.

Sensitivity Studies

Sensitivity studies were performed to quantify the relationship between material variables and energy of impact (area under the force vs. displacement curve). The parameters in the 500-point sensitivity study (K, C, C_1, C_2, α ,β) were allowed to vary between +/-50% of the value determined by the GA. The Optimal Latin Hypercube Algorithm was used to sample the design space. A least-squares 2nd-order polynomial fit to the experimental data for the 6 inputs versus the single output (energy) yields a set of coefficients describing the polynomial. The polynomial fit contains interaction terms (multiplied terms) between each of the independent variables, as well as squared terms for each of the independent variables. A Pareto plot, shown in Figure III-14 is an ordered bar chart of the normalized coefficients, which represent the percent effect on the total energy. This plot is compiled from results of the design of experiments study and is a convenient way to investigate the effect the parameters have on the energy imparted into the lung. Coefficients whose contribution to the energy was less than 5% are not included, with the exception of alpha, which is included to show its relative importance.

The contribution to impact energy of all interaction terms and squared terms was less than 5%, and are not shown the Pareto plot. The coefficients C_2, Beta, and C and C_1 have the largest effect on the model response in terms of energy (area under the force vs. displacement curve), with the three parameters together accounting for over 30% of the response changes within the ranges of values tested. Bulk Modulus (K) and alpha were shown to have lesser effects.

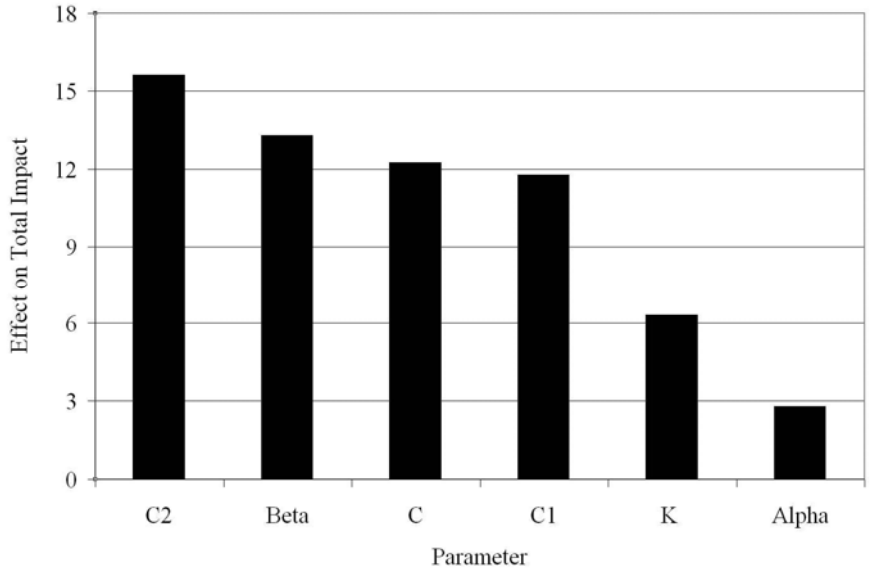

Figure III-14. Pareto plot of effect of individual coefficients on total energy of impact. Terms whose effect on the impact energy was less than 5% are not shown, with the exception of alpha.

III.5. Discussion

Material Model Assumptions

The original data for our lung material model was gathered from the literature, however limited alteration was allowed in lung material parameters in order to better fit the force-displacement response from the computational model to the force-displacement response obtained from the tests with rat lung. This approach may be justified for two reasons. The first is that the hyperelastic model used (with the addition of terms to

account for deformation of alveoli and taking into account surface tension) is a result of a curve fit of a material model to experimental data. From an engineering standpoint, it would be more desirable to test the material in a more controlled environment (control geometry, control the way the tissue is held, etc), but this would result in having to work with postmortem, excised tissue. A major advantage of this study is the use of a living, *in vivo* model to generate both experimental force data, and contusion data.

The material model used was developed to predict the macroscopic stress and strain that lung parenchyma would experience due to an insult (Vawter; 1980). This model uses a continuum assumption treating the lung parenchyma at a more macroscopic level than that represented by a single alveolus and interalveolar septa. Our focus is therefore on effective response of the lung. The model assumes that external loads on the lung are resisted by two distinct factors: the interalveolar septa and surface tension acting on the septa-alveolar interfaces. The presence of air in the alveoli is the physical reason behind including the surface tension term in the material model, however actual airflow between alveoli is not directly modeled and the effect of fluid flow during an impact event is not considered. If the lung alveoli were to collapse, or be filled with liquid such as saline, this term would no longer be valid. The presence of air in the lung is therefore included indirectly via the surface tension term. As a consequence we feel that the current approach is adequate, however our future studies will include CFD or fluid-structure (Lagrangian-Eulerian or ALE) analysis of individual lung parenchyma to help with development of a better continuum model for the mechanical response of the lung.

Genetic Algorithm Results

The genetic algorithm was used to tune the response of the model to the experimental data in a structured manner. It is important to clarify that the parameter set produced by the GA represents an optimized solution to a nearly intractable problem. It is difficult to know if a global minimum of the objective function has been reached. However, a sophisticated GA was selected for this optimization allowing for competition among individuals on a set of isolated islands. This parallel evolution, in conjunction with traditional aspects of GA's such as crossover, mutation, and elite preservation gives confidence that the solution is indeed acceptable. Investigation of the change in the objective function over the final 1000 generations shows that a further reduction of the reported objective function value is unlikely without modifying the approach. Given that the entire trace fits well with the +/- 1 standard deviation envelope of experimental data, it is believed that the parameter set presented here is a good trade off between accuracy and computational cost.

Comparison to Existing Experimental Models

There are no existing models of the lung that have been validated for the rat and used to predict pulmonary contusion. Thus, this is the first lung model that we are aware of that has been used for this purpose.

Very different thresholds for injury have been found for open versus closed chest rat models. To some extent, closed chest trauma work says very little about the susceptibility of the lungs themselves to trauma, and more about the protective effect of the rib cage. In some of the most recent work using the rat as a model to study pulmonary contusion, energies from 1.7 to 6.8 J (Joules, N-m) were administered in a

closed chest model. (Wang et al, 2003) In the low energy group, with energies from 1.7 to 2.4 J, no deaths were reported in 6 tests. In the medium energy group, with energies from 2.9 to 5.1 J, 12/28 rats died, with 23 rats showing some sign of lung injury, either gross or histologic. In the high energy group, 6.8 J, 3 out of 4 rats died and all 4 had lung injury.

These are interesting findings because they demonstrate that average energies of 2.05 J, or almost 660 times more energy is tolerated than that employed by the current work, where direct contact to one lung has been employed. Even if it is assumed that the energy is equally distributed over both lungs in other studies, this difference in energy is multiple orders of magnitude greater than that tolerated by the lungs alone.

It is worth mentioning that the methods of reporting energy in the literature are often suspect. It is sometimes the case in the literature that researchers will calculate energy from velocity and mass or another indirect means, but disregard the effect that a deceleration mechanism used in actual experiments may have had on the total energy transferred to the lung. The only reliable method to measure contact energy is to measure both force and displacement and calculate it from these measurements. However, the variability between different methods points to the need to find one metric that could be used to compare the outcome from all methods. Thus in experimentation there is the same need encountered here in biomechanical model design: one model which will work in a variety of different loading scenarios. The method presented here, a method based on strain in the lungs, is such a method, and it will always require a modeling component or other detailed information about actual deformation of living tissue.

However, the literature does highlight the significant effect that the rib cage has as a protective structure for the lungs. Given that the rib cage absorbs so much of the energy that might otherwise be damaging to the lungs, it is a natural next step to structure the search for a lung trauma metric so that the lungs themselves are isolated. This is accomplished in the current approach. This approach is justifiable, and much of the current work in soft tissue injury is focusing on the soft tissues themselves.

We recommend at the current time that modeling efforts to predict pulmonary contusion be focused on choosing a principal strain threshold for a volume of interest, with principal strain measurements between the 7-day contusion volume and 28 day contusion volume measures being used as a candidate injury threshold. It is apparent since the 1 day contusion volume measurements involve both lungs, and our numbers are based on taking the whole right lung as the contused volume for correlation with the model at 24 hours, the principal strain measurements used as thresholds for the one day volumes are probably not meaningful as an injury criteria. Based on the work of Miller (2004), which identified relative volumes of contusion from Clinical CT scans of admitted trauma patients and related these to outcome, 20% relative volume was identified as a severe pulmonary contusion while less than 20% was identified as less severe. 82% of patients in the high risk group developed ARDS, while only 22% of patients in the lower risk group developed the condition. Our numbers suggest that if PET measurements of contusion at 7 to 28 days are comparable to CT measurements on admission (a correlation that remains to be made in a future work), a tentative criteria could be somewhere between the 8.8% and 36% strain threshold. 28 day PET measurements of contusion volume of 0.39 cm^3 represent about 10% of the right lung's

total volume, while 7 day measurements of 2.8 cm^3 represent about 67% contusion volume. A contusion volume of 20% of the right lung would be about 0.84 cm^3, a volume of lung which experienced a minimal first principal strain of 22%. Thus, a very preliminary estimate of suggested first principal strain level for lung at high rate loading would be 22%. It is readily apparent that many of the assumptions to arrive at this number need additional work, but this is the direction to proceed with this research.

Limitations and Suggestions for Future Work

There are many limitations to the current work. The study is a broad one which contains new data on pulmonary contusion in rat lungs, a new experimental model for controlled impact to create contusions in live rat lungs, a new finite element model which has been developed of the rat lung, and optimization of the model to fit the response of encountered experimentally. Each of these endeavors in itself could be a separate, deeper study. The idea of this study is to set the stage for future research in pulmonary contusion using a more clinically relevant model. At the same time, however, a concerted effort is being made to apply basic clinical science data and new imaging techniques to a practical model that may be used in the future to predict pulmonary contusions in car crash victims.

Future work should include a more in-depth study of pulmonary contusion, and will include blood work, histology, and analysis of other markers of inflammation to investigate more clinically relevant aspects of pulmonary contusion. A drawback of this study is that the finite element model has not been validated quasi-statically or at a range of velocities of impact. To be a fully validated model, additional velocities should be explored and a model should give correct mechanical response for a range of impact

severities and scenarios. Prior to exploring the establishment of an actual stress and strain based injury criteria for the lung, more detailed validation will be necessary. Because of the limitations of an *in vivo* model, stress and strain could not be measured directly within the lung during this study. We have relied on the accuracy of the continuum model and built upon the work of previous researchers to develop the model through matching of force-displacement response. Although the model could be used to look at different injury metrics (i.e. 1^{st} principal strain vs. product of strain and strain rate), an injury criteria will require more detailed validation of stress and strain in the tissues. There are certain drawbacks to using an open chest model, in addition. An open chest model presents an opportunity to measure the mechanics of the lung directly, but the chest wall will play a major role in the transmission and absorption of energy which would otherwise damage the lung. In that sense the current study uses an optimal method to validate a lung tissue model, but additional testing would be necessary to validate the ability of the model to predict pulmonary contusion within the chest wall.

In the future, viscoelasticity may optionally be added to the lung's response, which may improve the range of impacts over which the lung model's response is applicable. A preliminary study incorporating representative linear viscoelastic parameters in an approach similar to that used for brain by Takhounts et al (2003) demonstrates that including linear viscoelasticity does little to change the thresholds determined in the current study. Long term shear modulus (G_∞) values from 5 to 50 kPa were used with time constants of τ=1 ms and 10 ms were tested and results demonstrate that this is particularly true for large values of G_∞. However, the issues of contact interface algorithms, element hourglassing, integration methods, and other control parameters in

the finite element input data must also be addressed. Studies will be made of each of these variables and their effects on element behavior, model stability, and model response.

III.6. Conclusions

This study has introduced many novelties, including a finite element model of rat lung and the rat thorax which did not previously exist, the use of PET data to quantify pulmonary contusion in the rat, new mechanical data on the rat lung, and optimization methodologies for better fitting the response of the rat lung to experimental parameters. In particular the optimization methodologies offer the opportunity to better understand the model's sensitivity to different input parameters, a study which has also been undertaken in the current work. A threshold for contusion volume has been obtained at one day, one week, and one month after contusion, and this threshold has been correlated to a peak principal strain level encountered in the tissue. Also, the inflammatory response to contusion and the long-term PET results are subject to many factors other than the initial stress and strain in the tissues. Since all factors are not considered, the current study is limited. Greater interpretation and more research in the future will allow the establishment of an injury criteria from this or another injury metric. For instance, the 24 hour response may not be of as much interest as response after a week or a month of healing. The correlation of severity of impact with actual outcome is a study that will have to be undertaken with greater numbers of tests and by looking at more clinical measures. The current research, however, provides a framework within which researchers may pursue pulmonary contusion research. Ultimately, the research should help designers not only to mitigate rib fractures using current injury criteria, but also to

mitigate the most common thoracic soft tissue injury encountered in car crashes: pulmonary contusion.

Chapter III Acknowledgements

We would like to thank Livermore Software Technology Corporation for the use of the LS-Dyna software, Engineous, for the use of ISight software, XYZ Applications for the use of TrueGrid software, and Custom Design and Fabrication of Richmond, VA for assistance in customizing their hardware. Additionally we would like to thank Craig McNally of Virginia Tech for designing and machining some of the hardware required for this testing. Jennifer Mercier is now located at North Carolina State University, and R. Mark Payne is now located at Indiana University School of Medicine.

Chapter III References

1. Arbogast, K. B., Meaney, D. F., and Thibault, L. E. Biomechanical characterization of the constitutive relationship for the brainstem. 39, 153-159. 1995. Proceedings of the 39th Stapp Car Crash Conference.

2 Bergmann, S.R., Weinheimer, C.J., Markham, J., and Herrero, P. 1996. Quantitation of myocardial fatty acid metabolism using PET. *Journal of Nuclear Medicine* 37:1723-1730.

3 Choung, C. J. Characterization and modeling of thoraco-abdominal response to blast waves. 6(190811). 1985. DTIC ADA. Biomechanical Model of the Lung.

4 Clark,G.C., Schecter, W.P., and Trunkey, D.D. 1988. Variables affecting outcome in blunt chest trauma: flail chest vs. pulmonary contusion. *J.Trauma* 28:298-304.

5 Fung, Y.C., Yen, R.T., Tao, Z.L., and Liu, S.Q. 1988. A hypothesis on the mechanism of trauma of lung tissue subjected to impact load. *J.Biomech.Eng* 110:50-56.

6 Gebhard, F., Kelbel, M.W., Strecker, W., Kinzl, L., and Bruckner, U.B. 1997. Chest trauma and its impact on the release of vasoactive mediators. *Shock* 7:313-317.

7 Iwamoto, M., Kisanuki, Y., Watanabe, K., Furusu, K., Miki, K., and Hasegawa, J. Development of a finite element model of the total human model for safety (THUMS) and application to injury reconstruction. 31-42. 2002. Proceedings of the 30th International Research Council on the Biomechanics of Impact.

8 Kaplan, J.D., Calandrino, F.S., and Schuster, D.P. 1991. A positron emission tomographic comparison of pulmonary vascular permeability during the adult respiratory distress syndrome and pneumonia. *Am.Rev.Respir.Dis.* 143:150-154.

9 Kuppa, S.M. and Eppinger, R.H. 1998. Development of an improved thoracic injury criterion. *Stapp Car Crash Journal* 42:139-154.

10 Lizee, E., Robin, S., Song, E., Bertholon, N., Lecoz, J.Y., Besnault, B., and Lavaste, F. 1998. Development of a 3D finite element model of the human body. *Stapp Car Crash Journal* 42:115-138.

11 Meaney, D.F., Ross, D.T., Winkelstein, B.A., Brasko, J., Goldstein, D., Bilston, L.B., Thibault, L.E., and Gennarelli, T.A. 1994. Modification of the cortical impact model to produce axonal injury in the rat cerebral cortex. *J.Neurotrauma* 11:599-612.

12 Miller, P.R., Croce, M.A., Bee, T.K., Qaisi, W.G., Smith, C.P., Collins, G.L., and Fabian, T.C. 2001. ARDS after pulmonary contusion: accurate measurement of contusion volume identifies high-risk patients. *J.Trauma* 51:223-228.

13 Morgan, R.M., Eppinger, R.H., Haffner, M.P., Kallieris, D., Miltner, E., Mattern, R., Yoganandan, N., Pintar, F.A., Sances, A., Kuppa, S.M. *et al*. 1994. Thoracic trauma assessment formulations for restrained drivers in simulated frontal impacts. *Stapp Car Crash Journal* 38:15-34.

14 Morrison, B., Cater, H.L., Wang, C., Thomas, F.C., and Hung, C.T. 2003. A tissue level tolerance criterion for living brain developed with an in vitro model of traumatic mechanical loading. *Stapp Car Crash Journal* 47:93-106.

15 Phelps, M.E. 2000. Inaugural article: positron emission tomography provides molecular imaging of biological processes. *Proc.Natl.Acad.Sci.U.S.A.* 97:9226-9233.

16 Rennen, H.J., Boerman, O.C., Oyen, W.J., and Corstens, F.H. 2001. Imaging infection/inflammation in the new millennium. *Eur.J.Nucl.Med.* 28:241-252.

17 Ruan, J., El-Jawahri, R., Chai, Li., Barbat, S., and Prasad, P. 2003. Prediction and Analysis of Human Thoracic Impact Responses and Injuries in Cadaver Impacts Using a Full Human Body Finite Element Model. *Stapp Car Crash Journal* 47:299-322.

18 Schuster, D.P., Anderson, C., Kozlowski, J., and Lange, N. 2002. Regional pulmonary perfusion in patients with acute pulmonary edema. *J.Nucl.Med.* 43:863-870.

19 Stitzel, J.D., Duma, S.M., Cormier, J.M., and Herring, I.P. (2002) A nonlinear finite element model of the eye with experimental validation for the prediction of globe rupture. Stapp Car Crash Journal 46: 81-102.

20 Stitzel, J.D., Cormier, J.M., Barretta, J.T., Kennedy, E.A., Smith, E.P., Rath, A.L., Duma, S.M., and Matsuoka, R. 2003. Defining regional variation of the material properties of human rib cortical bone and its effect on fracture prediction. *Stapp Car Crash Journal* 47:243-266.

21 Takhounts, E.G., Eppinger, R.H., Campbell, J.Q., Tannous, R.E., Power, E.D., and Shook, L.S. 2003. On the development of the SIMon Finite Element Head Model. Stapp Car Crash Journal 47:107-133.

22 Viano, D.C., King, A.I., Melvin, J.W., and Weber, K. 1989. Injury biomechanics research: an essential element in the prevention of trauma. J.Biomech. 22:403-417.

23 Vawter, D.L., Matthews, F.L., and West, J.B. 1975. Effect of shape and size of lung and chest wall on stresses in the lung. *J.Appl.Physiol* 39:9-17.

24 Vawter, D.L. 1977. Stress-free equilibrium volume of the lung. *J.Appl.Physiol* 43:3-7.

25 Vawter, D.L., Fung, Y.C., and West, J.B. 1978. Elasticity of excised dog lung parenchyma. *J.Appl.Physiol* 45:261-269.

26 Vawter,D.L. 1980. A finite element model for macroscopic deformation of the lung. *J.Biomech.Eng* 102:1-7.

27 Wang, N.D., Stevens, M.H., Doty, D.B., and Hammond, E.H. 2003. Blunt chest trauma: an experimental model for heart and lung contusion. *J.Trauma* 54:744-748.

28 Tenney SM, Remmers JE. (1963). Comparative quantitative morphology of the mammalian lung: diffusing area. Nature. 5;197:54-6.

29 Tschumperlin, D.J., Oswari, J., and Margulies, A.S. 2000. Deformation-induced injury of alveolar epithelial cells. Effect of frequency, duration, and amplitude. *Am.J.Respir.Crit Care Med.* 162:357-362.

30 Wang, N.D., Stevens, M.H., Doty, D.B., and Hammond, E.H. 2003. Blunt chest trauma: an experimental model for heart and lung contusion. *J.Trauma* 54:744-748.

31 Yen RT, Fung YC, Ho HH, Buttermann GR. (1986) Speed of stress wave propagation in lung. J Appl Physiol. 61(2):701-5. Erratum in: J Appl Physiol. 2005 Jan;98(1):421.

32 Zeltner, T.B., Bertacchini, M., Messerli, A., Burri, P.H.. (1990) Morphometric estimation of regional differences in the rat lung. Experimental Lung Research 16:145-158.

33 Zhang L, Yang KH, King AI. (2004) A proposed injury threshold for mild traumatic brain injury. J Biomech Eng. 126(2):226-36

34 Zhuang, H. and Alavi, A. 2002. 18-fluorodeoxyglucose positron emission tomographic imaging in the detection and monitoring of infection and inflammation. *Semin.Nucl.Med.* 32:47-59.

Published in: *Stapp Car Crash Journal* Vol. 51; pp 189-209, 2007

CHAPTER IV

A FINITE ELEMENT-BASED INJURY METRIC FOR PULMONARY CONTUSION: INVESTIGATION OF CANDIDATE METRICS THROUGH CORRELATION WITH COMPUTED TOMOGRAPHY

F. Scott Gayzik, M.S.[1,2]
J. Jason Hoth, M.D.[1]
Melissa Daly, M.S.[1]
J. Wayne Meredith, M.D.[1]
Joel D. Stitzel, Ph.D.[1,2]

1. Wake Forest University School of Medicine, Winston-Salem, NC
2. Virginia Tech – Wake Forest University Center for Injury Biomechanics, Winston-Salem, NC and Blacksburg, VA

Abstract

Pulmonary contusion (PC) is the most common thoracic soft tissue injury following non-penetrating blunt trauma and has been associated with mortality rates as high as 25%. This study is part of an ongoing effort to develop a finite element based injury criteria for PC. The aims of this study are two fold. The first is to investigate the use of computed tomography (CT) to quantify the volume of pathologic lung tissue in a prospective study of PC. The second is to use a finite element model (FEM) of the lung to investigate several mathematical predictors of contusion to determine the injury metric that best matches the spatial distribution of contusion obtained from the CT analysis.

PC is induced in-situ utilizing male Sprague Dawley rats (n = 24) through direct impact to the right lung at 5.0 $m \cdot s^{-1}$. Force vs. deflection data are collected and used for model validation and optimization. CT scans are taken at 24 hours, 48 hours, 1 week, and 1 month post contusion. A numerical simulation is performed using an FEM of the rat lung and surrounding structures. Injury predictors investigated include maximum first principal strain, maximum shear strain, triaxial mean strain, octahedral shear stress, and maximum shear stress. Strain rate and the product of strain and strain rate are evaluated for all listed strains. At each post-impact time point, the volume of contused lung is used to determine the specific elements representing pathologic lung. Through this method, a threshold is determined for all listed metrics. The spatial distribution of the elements exceeding this threshold is compared to the spatial distribution of high-radiopacity lung tissue in the CT through a three dimensional registration technique to determine the predictor with the best correlation to the outcome.

Impacts resulted in a mean energy input to the lung of 8.74 ± 2.5 mJ. Segmentation of the imaging data yielded a mean unilateral high-radiopacity tissue estimate of 14.5% by volume at 24 hours with decreasing high-radiopacity lung volume at later time points. Significant differences in the volume of high radiopacity (HR) tissue were noted at 1 week and 1 month post contusion. The best fit injury metric at the 24 hour time point was the product of maximum principal strain

and strain rate, with a value of 28.5 sec^{-1}. The maximum principal strain, and the maximum principal strain rate also characterized the distribution of pathology well with the proposed threshold for injury at 24 hours post-insult being 15.4 % and 304 sec^{-1} respectively.

This study quantifies pulmonary contusion via CT, an attractive modality due to its sensitivity to this lesion and widespread use in trauma centers. The study also presents a novel spatial validation technique for correlation of mathematical predictors to volumetric contusion data; a technique that may be extended to other injuries and modalities as well.

IV.1. Introduction

Pulmonary contusion (PC) is a common lesion occurring in patients sustaining severe blunt chest trauma. The lung, like other air filled organs is particularly vulnerable to injury from dynamic loading (Fung et al. 1988; Viano and Lau 1988). Acutely, injury can lead to ventilation perfusion mismatch, elevated pulmonary shunt, loss of lung compliance and edema. Long term respiratory dysfunction is found in a majority of patients (Allen and Coates 1996). Severe cases may culminate in respiratory failure.

In civilian trauma the predominant cause of PC is motor vehicle crash (MVC). In 2005 in the United States, there were over 6 million police reported crashes, resulting in nearly 2 million injuries and 40,000 fatalities (NCSA 2005). In terms of incidence, chest trauma is second only to head trauma with PC being the most common injury identified following blunt chest trauma. PC affects 10-17% of all trauma admissions. (Blansfield et al. 1999; Cavanaugh 1993; Cohn 1997). The mortality associated with PC is difficult to predict but is estimated to be 5-25% for adults and as high as 43% for children (Allen and Coates 1996; Balci et al. 2005; Stellin 1991). The elevated mortality in these studies was generally associated with the severity of the injury, and other factors including age, flail chest, and associated head trauma. PC has also been demonstrated as an independent predictor of Acute Respiratory Distress Syndrome (ARDS) and pneumonia (Miller et al. 2002).

The first objective of this study is to use computed tomography (CT) to quantify the host response to a known insult using a semi-automatic, attenuation defined segmentation approach. As part of this objective, the spatial distribution of the resulting regions of pathology are also quantified. The second objective of this study is to use the resulting

regions of pathologic, or high radiopacity (HR) lung within the subject as a tool for choosing the most appropriate mathematical descriptor of the pathologic lung volume through the use of a finite element model (FEM) of the rat lung. A registration approach is introduced which compares the normalized extent of the pathology observed through CT segmentation, and the corresponding injury metric from the FEM. A variety of predictive metrics hypothesized to correspond to the volume of pathology such as first principal strain and strain rate are investigated. A volume-based approach is used to determine the injury threshold for these metrics.

Animal Models of Lung Trauma

The rat has been used extensively in previous mechanistic studies of PC. Rats are chosen because of their well understood physiology and anatomy, because their small size makes high throughput studies possible, and they are large enough to achieve adequate resolution through imaging studies. The human lung is several orders of magnitude larger than the rat lung by volume, but on a microscopic scale the difference in average alveolar diameter is much less pronounced; 70.2 microns for the rat versus 200 microns for the human (Tenney and Remmers 1963). Despite morphological differences, the clinical relevance of this model (in terms of the physiological response) has been established in the literature. Lung dysfunction in rats measured by arterial blood oxygen, histology, and immunological markers, has been shown to progress over time, beginning at 3 hours and peaking between 24 and 48 hours post insult as in humans (Hoth et al. 2006; Raghavendran et al. 2005; Wang et al. 2003).

The host response at the cellular level has also been shown to react strongly to a pulmonary insult. Positive influx of neutrophils and other white blood cells suggests an

inflammatory nature to this lesion (Hoth et al. 2006) and the pro-inflammatory process is activated shortly after the insult (Knoferl et al. 2003; Raghavendran et al. 2005). Cellular infiltration at the microscopic level manifests as inflammation and edema visible at the macroscopic level via imaging modalities like CT.

Previous Studies Quantifying Pulmonary Contusion

There has been interest for some time in quantifying the extent of PC following a thoracic insult. CT is frequently used to obtain lung contusion data in the critical care setting, because it provides a three-dimensional dataset that can used to examine the patient, it is sensitive to edema and hemorrhage, and data can be acquired quickly. At many trauma centers throughout the United States, a chest CT is standard protocol following motor vehicle crash. A study utilizing CT has shown that patients with greater than 20% contusion by volume have a significantly higher risk of developing acute respiratory distress syndrome (ARDS) than patients with less than 20% contusion (Miller et al. 2001). The amount of contusion present may also play a role in the risk of developing pneumonia, although complications associated with head injury which correlate with the Glasgow Coma Score (GCS) also contribute (Antonelli et al. 1994; Croce et al. 1998; Miller et al. 2001).

Biomechanical Studies of Lung Trauma

While clinical studies are useful to determine the appropriate treatment course for an individual, it is not possible to know the magnitude of the thoracic insult in these cases. With the link between a mechanical insult and inflammatory response strongly demonstrated in the literature, biomechanical studies quantifying the insult as well as the

outcome are essential to make progress in developing countermeasures for the mitigation of PC.

One hypothesis on the mechanism of lung injury is that proposed by Fung, which is based on the theory that tensile and shear loading is induced in the alveolar septa upon rebound from compressive loading. This rebound occurs because of the presence of air within the lung parenchyma (Fung et al. 1988). When modeling this phenomenon at the continuum level discussed, it was unknown which mathematical quantity the observed increase in permeability of the alveolar epithelium was best correlated. Proposed injury metrics were maximum shear stress, octahedral shear, mean strain, areal strain, and maximum principal strain.

Stitzel et al. (2005) conducted a biomechanical study of blunt lung injury in rats at a loading rate of 2.8 m/s. The purpose of the study was to explore a finite element based injury metric for pulmonary contusion based on contusion volume quantified via Positron Emission Tomography or PET scanning. PET utilizes a radioactive glucose analog injected in the host to quantify the amount of inflammation in a particular region. The study tentatively estimated a strain threshold for pulmonary contusion measured 24 hours post-impact between 8.8 and 36%.

Despite the novel aspects of that study there were limitations. PET is a functional imaging modality, and inflammation volumes were not normalized to the total lung volume since non-inflamed lung tissue was not readily discernable. The lack of a means of normalization makes comparisons between individuals difficult. PET scans also require 15 minutes or more of scan time to formulate an image and since PET is not

commonly used in critical care research, comparisons of experimental results to clinical data are difficult to make.

The current study builds on this foundation utilizing a similar model, and incorporating CT as the imaging modality. Segmentation of CT can be used to determine the ratio of pathologic tissue to healthy tissue, facilitating comparisons across groups. The volume of contusion observed experimentally is used to determine thresholds for various metrics calculated via the FEM. In addition, the spatial distribution of the elements exceeding this threshold are correlated directly to the observed pathology via a CT – FEA (Finite Element Analysis) registration process to determine the most appropriate metric(s) upon which a formalized injury criteria can be based. The methods, results and discussion of the contusion experiment are presented first, followed by the methods, results, and discussion of the computational work.

IV.2. Experimental Methods

Contusion Experiment and Instrumentation

An electronic piston (model eCCI, Custom Design and Fabrication, Richmond, VA) was used to generate a quantifiable insult to the subject lung with an impact speed of 5 $m \cdot s^{-1}$ and a target penetration depth of 6.3 mm. The impacting edge of the eCCI was instrumented with a force transducer (model 208-C02, PCB Piezotronics, Depew, NY) and a 6.35 mm diameter aluminum impacting anvil. A custom shock adapter was used to mitigate the large tensile forces which occur due to the sudden stop when the piston shaft reached the end of its stroke. The eCCI was manufactured with an on-board, 1200 line per inch optical encoder which is used to monitor and control the velocity of the shaft.

All protocols used in this study were approved by the Institutional Animal Care and Use Committee at Wake Forest University School of Medicine. Sprague-Dawley male rats weighing 320-350 g at delivery were used. The protocol used to elicit PC follows that described in previous publications (Hoth et al. 2006; Stitzel et al. 2005). Analgesia was administered prior to the procedure. The animal underwent posterolateral right thoracotomy between the 5^{th} and 6^{th} ribs. Subjects were orotracheally intubated after induction with Halothane and maintained on a positive pressure respirator (model SAR-830/AP ventilator, CWE, Inc., Ardmore, PA).

In preparation for impact, the rat was placed on a platform below the piston, with the posterolateral aspect facing upward (Figure IV-1). The ribs were retracted to maintain the chest wall open and to allow the impactor to directly strike the lung. The impact speed and penetration depth were programmed into the control box. The piston was lowered to a set position relative to the housing (roughly 10cm, letter A in Figure IV-1). This initial point of loading is fixed relative to the housing. Next, the position of the entire housing and the platform on which the rat was set were adjusted relative to the rigid support structure to place the anvil through the opening in the chest wall and in normal contact with the lung. When adequate placement was achieved, the platform and housing were secured, and the piston was withdrawn to its starting position. Capacitors in the piston housing were charged and the piston then rested in a standby state. The ventilator was then placed on constant positive pressure (16 mm H_20) and the lung was slowly inflated. Once the lung adequately filled the pleural space, the impactor was manually activated. Immediately following the impact the chest was closed using

absorbable suture. Air was evacuated from the right chest using a small bore catheter. The ventilator was removed when the animal exhibited spontaneous breathing.

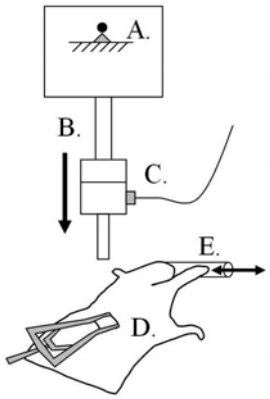

Figure IV-1. Schematic of contusion experiment. A. Electronically driven piston housing, rigidly fixed in space by support structure. B. Sliding piston. C. Load cell assembly with shock adapter, impacting anvil, and cable. D. Impacted subject, with posterolateral thoracotomy. A retracting device was used to maintain the opening in the chest wall. E. Oxygen and anesthesia are provided through a positive pressure ventilator.

A total of 24 rats were used in this study (Table IV-1). Twenty one of these underwent thoracotomy and impact (groups 1-5); three sham animals underwent thoracotomy alone (group 6). Sham animals were handled in exactly the same manner as the impacted animals while on the ventilator. Subjects were further divided into groups based on the CT scanning protocol. Groups 1-4 were scanned at a single time point, groups 4-6 were scanned at progressive time points. The total number scans per time point are shown in Table IV-1.

Table IV-1. Subject grouping for Computed Tomography image collection. A dot represents a time point at which all animals in a given group were scanned.

Group	n	Description	Post Impact Time Point			
			24 hour	48 hour	1 week	1 month
1	4	Impact, 24 hour	●			
2	4	Impact, 48 hour		●		
3	4	Impact, 1 week			●	
4	4	Impact, Longitudinal	●	●	●	
5	5	Impact, Longitudinal	●	●	●	●
6	3	Sham	●	●	●	●
Total Rats	24	Scans at Time Point (Impacted, Sham)	(13,3)	(13,3)	(13,3)	(5,3)

Force vs. deflection data were collected for all applied insults using an 8-channel data acquisition unit, (model: WaveBook 516E, IOtech, Cleveland, OH). Data were collected at 500kHz. Data reduction began by subtracting the average of the first 1000 data points to remove bias error. These points were collected prior to initiation of the impact sequence. The data were plotted and points corresponding to the onset and termination of loading were selected. The onset of loading was selected as the point signaling departure from zero force.

Data were filtered to SAE J211 channel filter class 1000 Hz. Prior to filtering, data were mirrored and inverted at both the initiation and termination of loading to ensure continuity of the slope at the edges of the trace. Data were inertially compensated based on a method used in a previous study utilizing the same equipment to deliver the pulmonary insult (Stitzel et al., 2005). Force versus deflection traces were integrated to determine the energy imparted to the struck organ for all impacts.

Computed Tomography Scanning Protocol

CT data was collected at 24 hours, 48 hours, one week, and one month post-contusion. The protocol resulted in a total of 16 individual scans at each time point, with

the exception of the 1 month time point, where 8 individuals were scanned. Scanning was conducted in an acrylic and PVC imaging and sedation enclosure designed in-house. The enclosure reduced the number of scans required to collect the CT image data by a factor of 4, Figure IV-2. Four 70 mm diameter translucent PVC chambers for housing the subjects fit within the enclosure. The cranial portion of the individual chambers is fitted with a conical inlet to prevent suffocation. The caudal end is open to allow the subject to enter the chamber. Anesthesia was delivered directly to each chamber, a common gas scavenge was used to create circulation throughout the enclosure. Care was taken to ensure that the animals were completely sedated before initializing the scanning protocol. Animals were given roughly five minutes to establish a steady breathing state prior to scanning.

All scans were taken using a Light Speed Pro CT scanner (GE Medical Systems, Minneapolis, MN). Complete scan protocol parameters are listed in Table IV-4 in the appendix. The scans were acquired in axial mode with two images per rotation and a slice thickness of 0.625 mm. The complete procedure including loading, sedation, image acquisition, and unloading of the subjects was accomplished in roughly 10 minutes. Data were initially acquired for a display field of view of 200 mm, allowing for simultaneous viewing of all subjects in the enclosure. The images were retrospectively reconstructed using a narrower region of interest (ROI) to create isolated image stacks of a single subject. Native image acquisition and ROI reconstruction data are provided in Table IV-4 (see appendix).

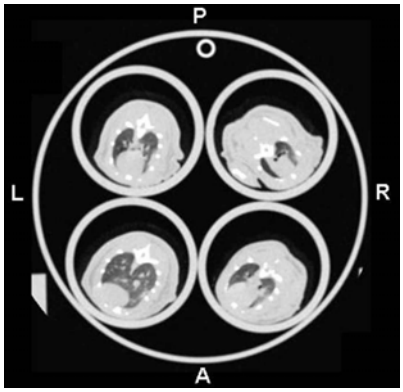

Figure IV-2. A transverse CT image showing four subjects within the sedation enclosure.

Segmentation Protocol

The purpose of the image segmentation protocol was to identify and quantify the volume of contused lung tissue for each subject. A semi-automated, attenuation-defined approach for isolating the lung and segmenting the image data was applied using Mimics (Materialise, Ann Arbor, MI). This approach to isolate the lung tissue was well suited for removing partial volume effects near the edges of the lungs which result from the animal's breathing. Additionally, this method prevented pulmonary arteries and veins from being included in the lung mask, which would lead to inaccurate contusion volume estimation.

For each subject, at each time point, the following protocol was applied: A grouping of pixels, M_1, (hereafter referred to as a *mask*) was created through a thresholding operation containing all pixels in the image stack between the maximum Hounsfield Unit (HU) value in the stack and -370 HU. The Hounsfield Unit scale is the standard scale for measuring radiopacity. A second mask, M_2, was created through a multi-slice dynamic region growing operation by selecting a representative voxel within the lung parenchyma. All adjacent voxels within 225 HU were included in M_2. Small gaps in M_2 were

eliminated through a closing operation. A total lung mask reasonably representing the lung tissue, M_{tl} was then created by subtracting M_1 from M_2. M_{tl} was then modified manually to remove motion artifacts in the region of the diaphragm and the heart, and non-parenchymal features included in M_{tl} such as the trachea and primary bronchi. Contused tissue in the medial portions of the lungs that were not included in M_{tl} were added using the ribs of the subject as a guide.

A fourth mask, M_{low} representing all low radiopacity voxels in the entire image stack (between -1024 and -351 HU range) was created. The Boolean intersection of M_{low} and M_{tl} resulted in a mask containing all voxels representing healthy, or "lung radiopacity" tissue, M_{lr}. Subtracting the latter mask from the total lung mask created a final mask containing "high radiopacity" lung tissue, M_{hr}. The volumes of M_{tl}, M_{lr} and M_{hr} were recorded. The fraction of contusion was calculated for all subjects by taking the ratio of the volume of HR tissue in the right (struck) lung to that of the right lung volume. Boolean operations were also used to separate the resulting masks into right and left components. The coordinate locations of the voxel centers and HU values of all voxels in these masks were exported from Mimics as text files to be analyzed in Matlab (The Math Works, Natick, MA).

A single individual segmented the lung CT data. The intra-observer repeatability of the segmentation algorithm was assessed by having the individual segment the same scan (24 hour post contusion) three times. In addition, a second individual familiar with the rat anatomy and the segmentation protocol repeated the segmentation on a single subject three times.

Contusion Characterization

Geometric characterization was conducted to quantify the extent of the contusion along anatomical directions, i.e., in the anterior-posterior, medial-lateral, and cranial-caudal directions. The distance between the geometric center of the contusion volume and center of the entire lung was also quantified along these dimensions. Since the vast majority of the contusion was noted on the struck (right) side of the lung, characterization was conducted on the right lung only. This data is used in the computational portion of this work, for placement of the impactor and for CT-FEA registration.

Voxel center locations of the right side total lung mask and HR lung masks (M_{tl} and M_{hr}) were imported to Matlab (The MathWorks, Natick, MA.). The coordinate system for the segmented image data is shown in Figure IV-3; with *x* being right to left, *y* being anterior to posterior, and *z* being caudal to cranial. The geometric center of the lung was translated to the origin by subtracting the mean coordinate location in each dimension. The geometric center of the contusion, (Δx_{CT}, Δy_{CT}, Δz_{CT}) was then determined by taking the average coordinate location of the contusion voxels in *x*, *y* and *z* directions. The characteristic length of the lung mask ($l_{x,CT}$, $l_{y,CT}$, $l_{z,CT}$) were determined in each direction by searching along a linear projection passing through the geometric center of the lung to determine its extent in each direction. This procedure was repeated to determine the extent of the contusion volume as well ($c_{x,CT}$, $c_{y,CT}$, $c_{z,CT}$).

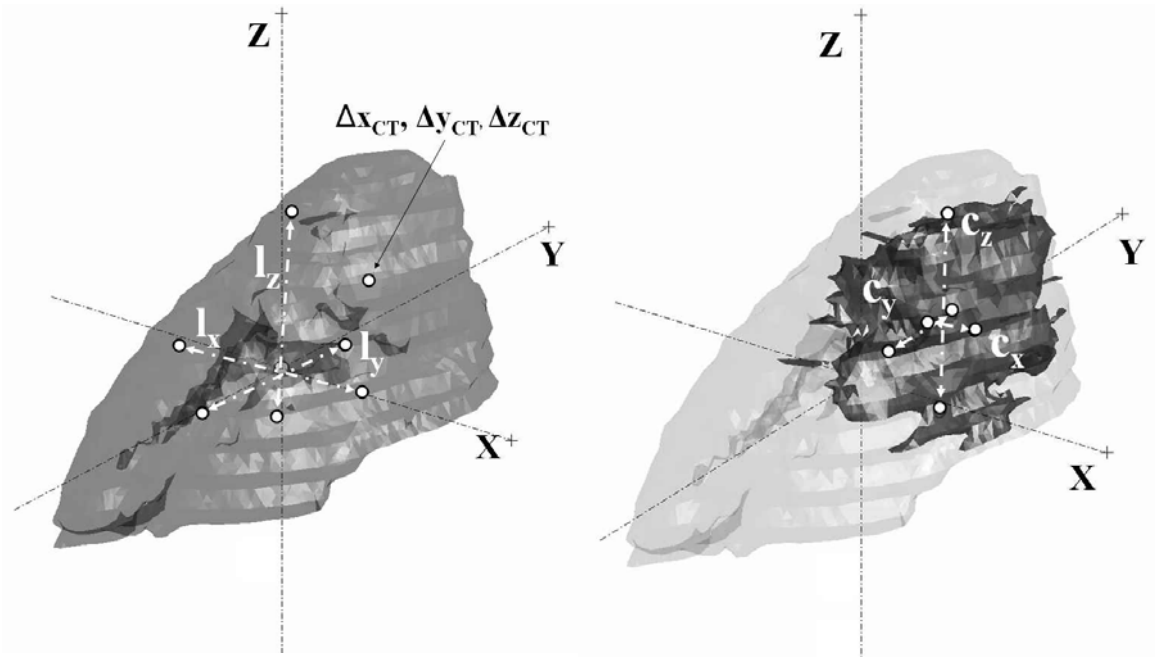

A. B.

Figure IV-3. A. Rendering of exported struck lung mask, M_{tl}. Coordinate axes pass through geometric center. Characteristic lengths, $l_{x,CT}$, $l_{y,CT}$, $l_{z,CT}$ are shown (dashed white lines) along with geometric center of high radiopacity lung tissue mask, M_{hr}. B. Characteristic lengths of M_{hr}, $c_{x,CT}$, $c_{y,CT}$, $c_{z,CT}$ are shown.

IV.3. Experimental Results

Contusion Experiment and Image Analysis

Table IV-5 and Table IV-6 in the appendix summarize the experimental findings, including data on rat weight, impact energy, lung volume and percent HR lung for all animals in the study at all time points. Subjects tolerated the experimental protocol with zero mortality. Force vs. deflection traces from the lung impacts are shown in Figure IV-4. Exemplar force vs. time, velocity vs. time and displacement vs. time plots are found in Figure IV-10 in the appendix. The velocity of the eCCI piston during the final 8.4 mm of its stroke was recorded via the optical encoder and saved to the device's onboard memory. The velocity of the piston was found to be constant throughout the

portion of the stroke where impact occurred (Figure IV-10B in the appendix). With constant velocity, the deflection data from the point of impact was determined by multiplying the impact velocity by the data collection time step.

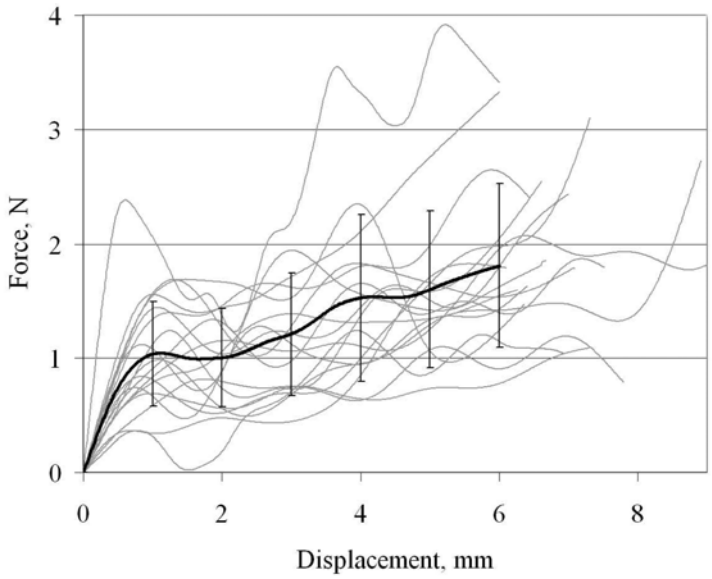

Figure IV-4. Mean force versus deflection trace with error bars representing one standard deviation corridors.

The total mass of the piston and accompanying instrumentation was 108.6 g, much greater than the approximate mass of the rat lung (0.5 g) and therefore, one would not expect the piston to be slowed substantially by the impacting the lung. The average velocity and penetration depth of the impactor were determined to be 5.02 ± 0.035 m/sec and 6.92±1.06 mm, respectively. The average energy imparted to the lung was 8.74 ± 2.47 mJ. Two tests (specimens 15 and 17) were excluded from the remainder of the study because the absorbed energy was greater than three times the standard deviation from the mean (Table IV-5 and Table IV-6, appendix).

Exemplar CT data are shown in Figure IV-5. Figure IV-5A shows a transverse slice of the ROI scan of an individual animal with HR lung highlighted. A three dimensional

reconstruction of the contusion region is shown in Figure IV-5B. Gross motion artifacts were noted in 5 individual scans. Data from these subjects were not included in the remainder of the study. This included one animal at the one week time point, one at the one month time point and one sham animal at 48 hours, one week and one month post-thoracotomy. Excluded animals are marked in Table IV-6 in the appendix.

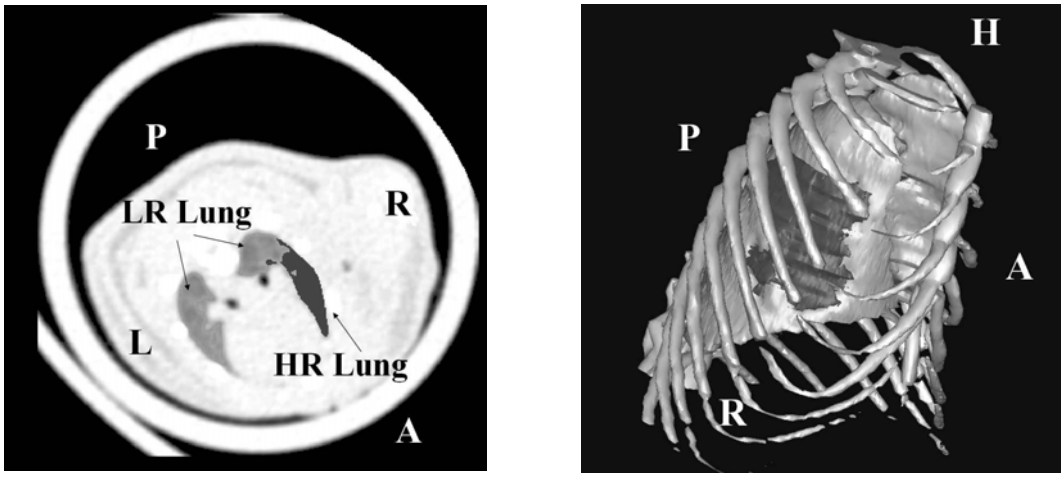

A. B.

Figure IV-5. CT image results, anatomical directions indicated in block letters, P, Posterior, A, Anterior, R, Right, L, Left, H, head. A. Transverse slice showing high and low radiopacity lung volumes. B. 3D reconstruction of high (dark) and low (light) radiopacity lung, rib cage shown but not included in analysis.

The ratio of HR lung volume to the total lung volume for all animals is found in Figure IV-6 and Table IV-6 (see appendix). The greatest average volume of pathology was observed at 24 hours post impact (14.51±5.56 %), with subsequent reduction of the pathologic volume throughout time. A significant reduction in the percent of HR lung compared to the 24 hour time point was noted at one week and one month post insult (t-test assuming equal variance, one tail, $p < 0.001$). No significant difference was noted for this ratio between 24 and 48 hours, although the mean ratio decreased over this time. Differences were noted between the 24 hour and 48 hour time points ($p < 0.001$ and $p = 0.048$ respectively) when comparing sham and contused animals.

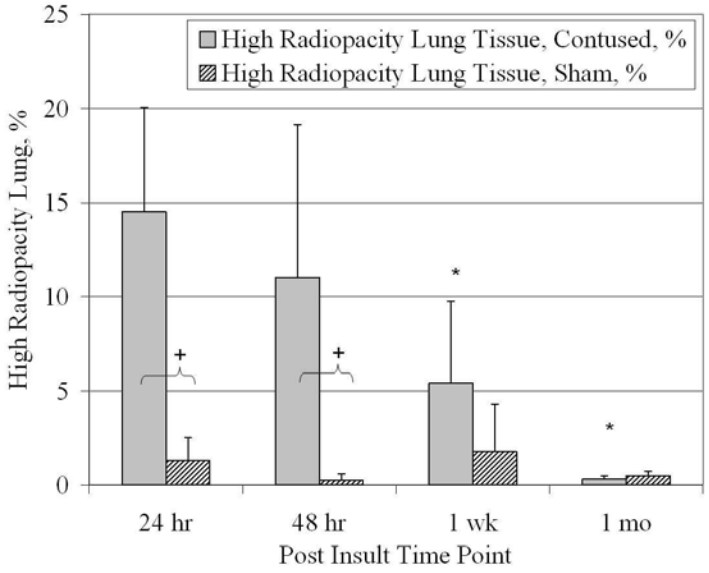

Figure IV-6. Mean percent high radiopacity lung for all time points, normalized by the struck lung. [+]A significant decrease in this ratio was noted from the contused to the sham animal. [*]A significant decrease was noted from the 24 hour time point at 1 week and 1 month post-contusion.

Figure IV-11 in the appendix shows contusion volume versus time for only those animals included in the longitudinal study, and as expected the portion of pathologic lung decreases with time. Percent HR lung versus absorbed energy and peak force were plotted as well (Figure IV-12 and Figure IV-13 in the appendix). When excluding outliers and sham rats, no significant relationship was found between the volume of pathology and parameters describing the magnitude of the insult. The protocol for identifying contusion was found to be repeatable within 10% when comparing the percentage of HR lung calculated between observers. The intra-observer variability of this ratio was within 3 % of the mean value.

The mean characteristic lengths obtained through analysis of the CT masks at 24 hours and 48 hours are shown in Table IV-7 of the appendix. Characteristic lengths at the 1 week and 1 month time point were not assessed due to the significantly diminished volume of pathology at these time points. No significant differences in these lengths

were noted between 24 hour and 48 hour populations (t-test for sample means, assuming equal variance).

IV.4. Discussion of Experimental Results

A prospective study of direct blunt trauma to the lung was presented using a well-validated rat model of PC. The first goal of the experimental portion of the study was to administer controlled and quantifiable insults to the study subjects. The results were encouraging, with an average piston velocity (5.02 ± 0.035 $m \cdot s^{-1}$) and penetration depth (6.92 ± 1.06 mm) both within one standard deviation of their respective target values of 5.0 $m \cdot s^{-1}$ and 6.3 mm. The custom shock adapter on the end of the piston rod may have contributed to the slight increase beyond the nominal penetration depth. The adapter was needed to mitigate the large tensile forces that occurred at the end of the stroke. Increased penetration may also have been related to the position of the lung itself at the instant the impact began. As described in the methods section, the leading edge of the piston had to be withdrawn from the preset point of initial impact in order to charge the capacitors. Thus the surface of the lung may have moved slightly prior to the actual time of impact.

Force vs. deflection data were acquired for each impact. The inertial loading spike typically observed in impact experiments is less pronounced for these data because of the low mass and high compliance of the lung in comparison to the piston apparatus. The average energy for the impacts was 8.74 ± 2.47 mJ, which is reasonable control of the insult when considering the conditions of the experiment (i.e., live subject, small scale, open chest model, individual variability, and dynamic measurement of force on the lung).

Because an open chest model was utilized in this research, the energy calculated from the impact experiment represents energy applied directly to the lung. Using a closed chest model would add a confounding factor since the precise manner in which the applied load was transmitted to the lungs would be unknown. Publications utilizing closed chest models of the rat for the study of PC have reported energy imparted to the animal of up to 2.7 J, (Raghavendran et al. 2005) nearly 300 times the mean energy measured in the present work. As one would expect based on this discrepancy in the absorbed energy, the two outliers in the present study caused by contact of the anvil with the chest wall were easily identified. In addition, the force versus deflection data presented in Figure IV-4 is directly applicable to organ-level validation of an FEA model of the impact.

The percent of HR lung volume was also determined, thereby characterizing both the pulmonary insult and the resulting host response. This data pairing represents a useful addition to the biomechanics literature. The peak percentage of HR lung occurred at 24 hours post contusion. A significant decrease in HR tissue was not noted between the 24 and 48 hour groups. This indicates that computational work based on these findings should utilize data acquired no later than 48 hours post insult. Sham animals that underwent thoracotomy and positive pressure ventilation but were not contused exhibited markedly less contusion, demonstrating that the thoracotomy procedure alone does not cause large scale pathology in the lung. This is an important finding since the open chest model is essential for organ-specific FEM development.

No significant relationship between the absorbed energy or peak force and resulting percent of pathologic lung were reported for any time point (Table IV-6). The existence

of such a relationship can not be ruled out based on these findings alone, in fact previous research has demonstrated a positive correlation between magnitude of the insult and the host response measured through bronchoalveolar lavage (Raghavendran et al. 2005). On the other hand, this finding suggests that the impacts administered in this study were essentially equivalent.

Because pathology is identified using CT in this study, care is taken to avoid describing the HR regions of lung tissue as only "pulmonary contusion". The lack of homogeneity in the pathologic region precludes segmenting the many specific pathologic conditions that can occur following blunt thoracic trauma. These include contusion, atelectasis (collapse of the alveoli), hemothorax and other pathology (Wagner et al. 1988). In order to reduce variation introduced through the segmentation process itself, this analysis was conducted by grouping these entities together and collectively referring to them as HR lung tissue. The approach applied in this research is a compromise between manual segmentation, which could cause extensive user bias, and fully automated methods that have been introduced, but tend to exhibit diminished performance when large amounts of pathology are present (Leader et al. 2003; Sakai et al. 1994).

Experiment Limitations

An inherent limitation of scanning live animal subjects is that breathing can not be controlled. As a consequence, a slight amount of motion artifact was unavoidable. Under the assumption that the lung volume exhibits a sinusoidal deviation about a mean volume, the lung volumes depicted in this study should reasonably represent the average lung volume of the subjects. In addition, the animals were anesthetized immediately

upon entry to the sedation enclosure, and allowed roughly five minutes to establish a steady breathing state.

The data presented is limited in scope since only one impact scenario was tested. While no significant relationship between absorbed energy and the percentage of HR lung tissue was determined for this series of testing, it is certainly possible that a greater range of impact scenarios would result in such a dependency. Future efforts will focus on identifying the effect that variations in impact speed, penetration depth and impactor area have on the resulting quantity of HR tissue. Despite these limitations, the data presented in the first phase of the study represent an important contribution to the biomechanics of lung trauma by quantifying the impact as well as the outcome from a direct pulmonary insult. The data generated in this phase is intended for use in model validation and the direct comparison of computational and experimental findings. With this in mind, the methods, results and discussion of the computational part of this study are now presented.

IV.5. Computational Modeling Methods

Finite Element Model

The finite element model of the rat lung used in this work is an organ-level model of the thoracic viscera of the rat (Stitzel et al. 2005). It consists of the right lung, the left lung, tissues to represent the mediastinum, heart and trachea, and a mesh sheath to represent chest wall and diaphragm. The entire animal was not modeled, only the anatomy pertinent to this study. The geometry of the lung model was developed from a CT of an uninjured mature male rat. The volume of the right lung in the FEA model was 4.52 cm^3. The impact to the lung was modeled with a constant velocity (5.0 $m \cdot s^{-1}$) prescribed motion boundary condition and automatic surface to surface contact. The

impactor penetration depth at the end of the simulation was 6.3 mm. An automatic single surface contact was used between organs. A frictionless surface to surface contact was used between the organs and the chest wall / diaphragm. Viscous type hourglass control was used (Takhounts et al. 2003). The 1.26 ms event requires about 40 seconds to run on a PC workstation (Dell Optiplex GX620, Pentium D, 3 GHz processor with 3.5 GB ram). LS-Dyna build 970 (LSTC, Livermore, CA) was used for the finite element simulation.

The material model used for the lung was taken from the literature and has been implemented in the commercial explicit finite element code LS-Dyna (LSTC, Livermore, CA), (Vawter 1980). The constitutive equation is a strain energy density functional expressed in terms of the invariants of the Green's strain (Equation IV-4, Appendix). This function was developed to predict macroscopic stress and strain within lung tissue over volumes much greater than a single alveolus. Material coefficients include the density, ρ, bulk modulus, K, unstressed alveolar diameter, Δ, and 5 hyperelastic curve fit parameters C, α, β, C_1, C_2.

The location of the impactor in the simulation was determined from experimental results. Impact placement began by determining the characteristic lengths of the right lung of the FEA model in the medial-lateral ($l_{x,FEA}$), anterior-posterior ($l_{y,FEA}$) and cranial-caudal ($l_{z,FEA}$) directions via the same algorithm used to determine the these lengths for the CT masks (Figure IV-7, Table IV-7). The geometric center of the HR lung (Δx_{CT}, Δy_{CT}, Δz_{CT}) was previously determined for all subjects. The analogous location on the FEA model, (Δx_{FEA}, Δy_{FEA}, Δz_{FEA}) was determined using Equation IV-1. The leading edge of the impactor was placed at (Δx_{FEA}, Δy_{FEA}, Δz_{FEA}) and then moved laterally until

it was positioned just outside of the lung volume. The final location of the impactor is also shown in Figure IV-7.

$$\left(\Delta x_{FEA}, \Delta y_{FEA}, \Delta z_{FEA}\right) = \left(\frac{\Delta x_{CT}}{l_{x,CT}} l_{x,FEA}, \frac{\Delta y_{CT}}{l_{y,CT}} l_{y,FEA}, \frac{\Delta z_{CT}}{l_{z,CT}} l_{z,FEA}\right) \qquad \text{Equation IV-1}$$

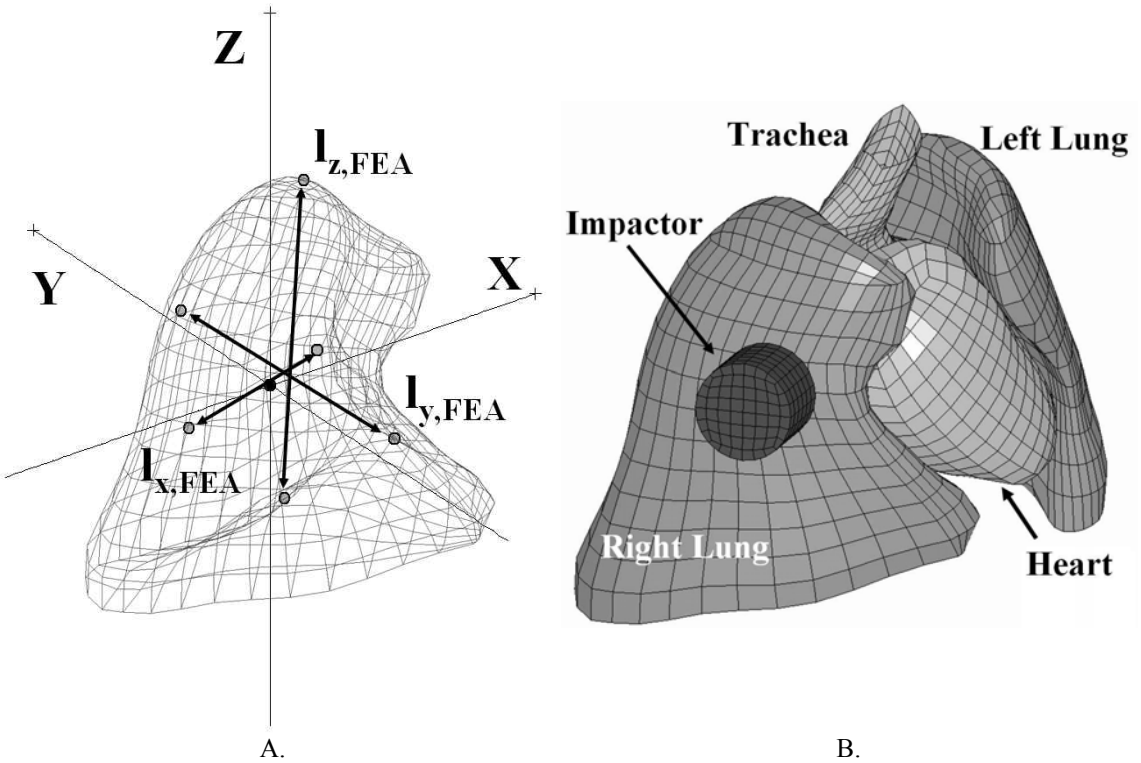

A. B.

Figure IV-7. A. Characteristic lengths of FEA model ($l_{x,FEA}$, etc.). B. Finite element model of rat lung, with thoracic structures labeled (Stitzel et al. 2005). The location of the impactor is based on CT contusion data.

Model Validation and Optimization

Parameters for the material model from the literature (Table IV-8, appendix, Stitzel et al., 2005) were optimized using Isight software v. 10 (Engineous Software, Cary, NC). The nominal parameter set did not produce a model response within the ± 1 standard deviation force-deflection corridors shown in Figure IV-8. A multi-island genetic algorithm (MIGA) was used to optimize the model response by adjusting the parameters

of the model to fit within the experimental data corridors for the 5.0 m/s impact dataset (Stitzel et al. 2005). The MIGA works like a traditional genetic algorithm (GA) in that an individual, in this case represented by one complete set of model parameters, is assigned a fitness, *S*, based on how well the force-displacement response matches the experimentally observed response (Equation IV-2).

$$S = \sum \left(F_{Sim}(\beta_{1-6}) - F_{Exp} \right)^2 \qquad \text{Equation IV-2}$$

By choosing "fitter" parameter sets to pass their genetic information to the next generation, the fitness of the population generally improves over the course of generations. The algorithm was run for 100 individual parameter sets 'evolving' in parallel on 10 islands. A total of 20 generations were tested, resulting in a total of 2000 FEA model runs. The optimization scheme required 16 hours to complete on a PC workstation.

Evaluating Candidate Injury Metrics

Candidate injury metrics calculated by the model were evaluated to determine which best represented the post-impact contusion volume observed in the animal model. Quantities proposed in previous lung research for use as injury metrics were tested (Fung et al., 1988). These include; shear stress, octahedral shear stress, maximum principal strain, maximum shear strain, triaxial mean strain, the rate of these strains, and the instantaneous product of the strain and strain rate. Prior to time differentiation, all strain traces were filtered to SAE J211 CFC 1000 Hz. To evaluate the candidate injury metrics, the simulated impact was run in LS-Dyna. The stress and strain tensor data for all

elements of the struck lung for all time points were imported into Matlab. Metrics were calculated for all elements for all time points.

The maximum value for each element and each metric throughout the simulation was selected. The metric values were arranged in descending order and plotted against the normalized cumulative volume. Since maximum pathologic lung by volume was observed at 24 hour time point, the corresponding percent HR tissue in the struck lung (14.5 %, Table IV-6, appendix) was used to determine thresholds for all candidate injury metrics. Elements whose values for a given metric were above or below this threshold were partitioned into two groups; one representing the predicted volume of injured parenchyma and one representing normal parenchyma. The extent of the model-predicted pathology in the three anatomical directions, ($c_{x,FEA}$, $c_{y,FEA}$, $c_{z,FEA}$) was calculated via the line search algorithm previously described.

By normalizing the extent of CT pathology by the CT characteristic lengths, and calculating the analogous quantity from the FEA model for all metrics, a direct comparison between the FEA and CT results was made. This registration score, S_r, was calculated via Equation IV-3. The lower the score the more favorable the calculated distribution of pathologic lung matched the experimental results.

$$S_r = \sqrt{\left(\frac{c_{x,FEA}}{l_{x,FEA}} - \frac{\overline{c_{x,CT}}}{l_{x,CT}}\right)^2 + \left(\frac{c_{y,FEA}}{l_{y,FEA}} - \frac{\overline{c_{y,CT}}}{l_{y,CT}}\right)^2 + \left(\frac{c_{z,FEA}}{l_{z,FEA}} - \frac{\overline{c_{z,CT}}}{l_{z,CT}}\right)^2} \qquad \text{Equation IV-3}$$

IV.6. Computational Modeling Results

Finite Element Analysis and Evaluation of Metrics

The optimized force versus deflection trace, one standard deviation corridors, and model response with the nominal parameters are shown in Figure IV-8A. The fitness as

a function of run number is shown in Figure IV-8B, which shows an exponential decay towards the lowest attained value. The optimal set of parameters resulted from trial 1965 of 2000 of the MIGA. The optimized material properties used for the remainder of the results are found in Table IV-2.

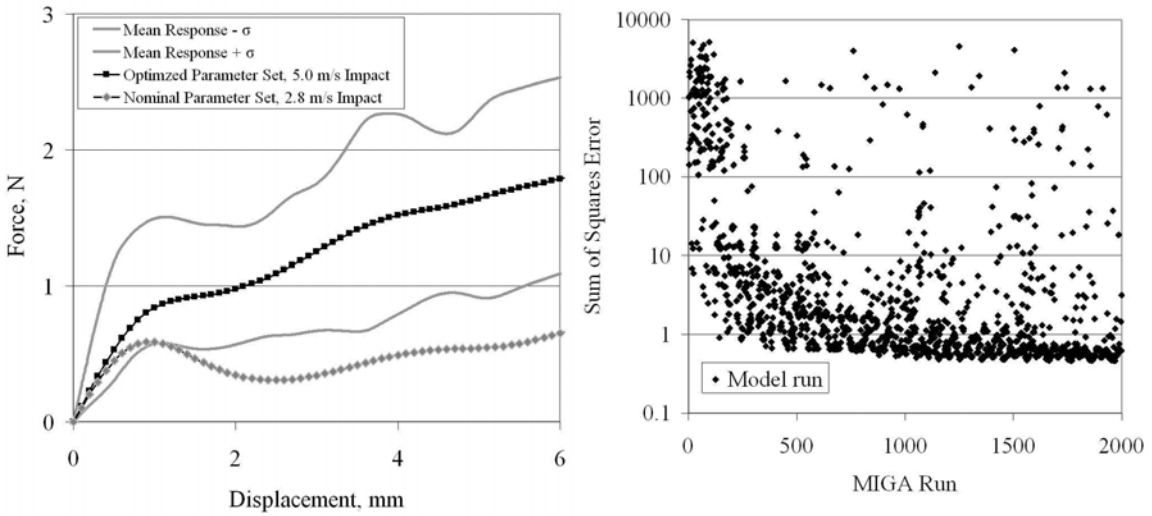

Figure IV-8. A. Force versus deflection data showing ± 1 standard deviation thresholds and optimized model response. B. Improvement in sum of squares error versus model run.

Table IV-2. Optimized parameters for FEA model at 5.0 m/s.

Description	Optimized Value	Description	Optimized Value
Density, ρ (g mm^{-3})	1.180 x 10^{-4}	Curve fit parameter, C (N mm^{-1})	1.187 x 10^{-3}
Bulk Modulus K (N mm^{-2})	1.384 x 10^{-1}	Curve fit parameter, α	4.451 x 10^{-1}
Mean alveolar diameter, Δ (mm)	0.0702	Curve fit parameter, β	-3.95
		Curve fit parameter, C1 (N mm^{-1})	1.949 x 10^{-5}
		Curve fit parameter, C2	1.918

The optimization required 18 hours to complete on the previously described PC. The energy calculated from the optimized model (7.46 mJ) compares favorably to the energy calculated by integrating the mean force versus deflection trace over the first 6.3 mm of piston travel (7.68 mJ). Since the volume of HR lung at 24 hours post insult was used to

determine the injury metrics, it is important to compare the average values from the experimental impact at the 24 hour time point against the model input parameters. The mean value of the velocity and penetration depth for only the specimens of the 24 hour time period (excluding outliers) are 5.02 ± 0.034 $m \cdot s^{-1}$ and 6.64 ± 0.69 mm respectively. These values closely compare to the model input parameters of 5.0 $m \cdot s^{-1}$ and 6.3 mm of penetration.

The threshold value for each of the candidate metrics is shown in Table IV-3. These metrics are ordered by best registration score. The percent increase in this score is given relative to the metric with the best fit; the product of maximum principal strain and maximum principal strain rate. The analysis predicts that within lung parenchyma, contusion will occur should the quantity $\varepsilon_{max} \cdot \dot{\varepsilon}_{max}$ exceed 28.5 sec^{-1}. The corresponding values for ε_{max} and $\dot{\varepsilon}_{max}$ are 15.4 % and 304 sec^{-1} respectively. The threshold selection process is shown graphically in Figure IV-14 in the appendix, where the shaded portion corresponds to 14.5 % of the total right lung volume.

The spatial distribution of elements exceeding the volume threshold is shown in Figure IV-9. Figure IV-9A shows the impactor in its initial position. Penetration of the impactor into the lung model is shown in part B. Parts C and D show the elements exceeding the 24 hour volume threshold shaded and those beneath the threshold semi-transparent. Figure IV-9C shows the best correlated metric, the product of first principal strain and strain rate. The elements that exceed the volumetric threshold are concentrated about the point of contact of the impactor. Figure IV-9D shows the least well-correlated metric, the product of triaxial mean strain and its strain rate, which predicted more diffuse pathology.

Table IV-3. Results of FEA spatial matching technique, with metrics ranked in order of best fit according to the registration score. Each threshold corresponds to the 24 hour post impact volume of HR lung, 14.5 %.

Rank	Metric	24 hour Post-Impact Threshold	Reg. Score	Reg. Score (Percent Increase)
1	Max principal strain · strain rate, $\varepsilon_{max} \cdot \dot{\varepsilon}_{max}$, [sec^{-1}]	28.5	0.320	
2	Max principal strain, ε_{max}	0.154	0.338	6
3	Max principal strain rate, $\dot{\varepsilon}_{max}$ [sec^{-1}]	304	0.345	8
4	Max shear strain rate, $\dot{\gamma}_{max}$ [sec^{-1}]	367	0.346	8
5	Max shear stress, τ_{max} [kPa]	7.10	0.349	9
6	Triaxial mean strain rate, $\overline{\dot{\varepsilon}}$ [sec^{-1}]	58.3	0.382	19
7	Max shear strain, γ_{max}	0.210	0.390	21
8	Max shear strain · rate, $\gamma_{max} \cdot \dot{\gamma}_{max}$ [sec^{-1}]	48.9	0.396	23
9	Octahedral shear stress, τ_{oct} [kPa]	6.00	0.401	25
10	Triaxial mean strain, $\overline{\varepsilon}$	0.0242	0.493	53
11	Triaxial mean strain · strain rate, $\overline{\varepsilon} \cdot \overline{\dot{\varepsilon}}$ [sec^{-1}]	0.700	0.540	67

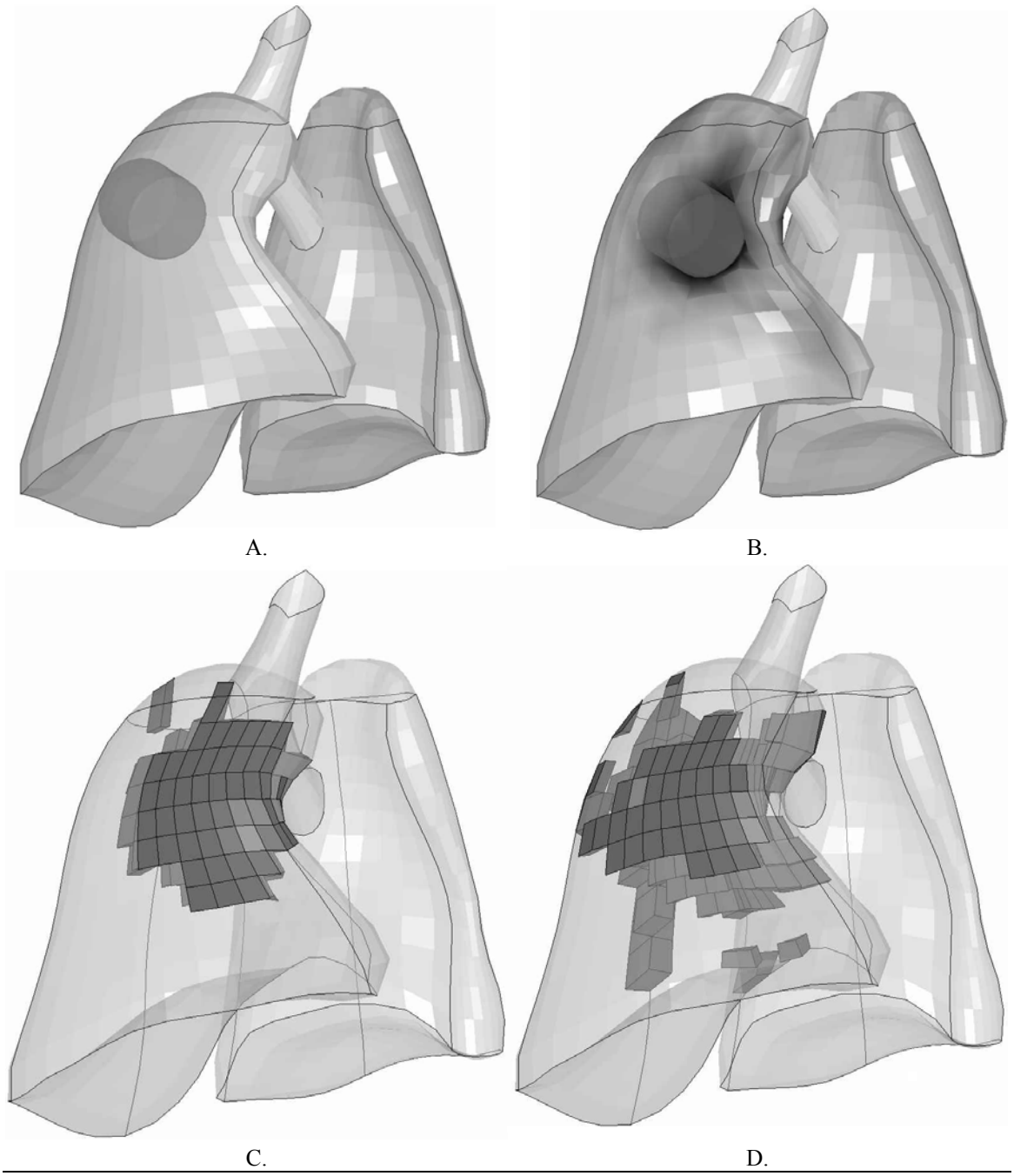

Figure IV-9. Results of FEA model showing indenter at start of simulation (A) and during impact (B). Shaded contours are of maximum principal strain. In (C) and (D), elements that exceed the CT-based volume threshold appear darkened. (C) shows $\varepsilon_{\max} \cdot \dot{\varepsilon}_{\max}$, the best correlated metric, while (D) shows $\overline{\varepsilon} \cdot \overline{\dot{\varepsilon}}$, the least correlated metric. The correlation score (Table IV-3) is determined in part by the measuring the extent of these elements in three anatomical dimensions. The heart and mediastinum are not shown in this figure.

IV.7. Discussion of Computational Results

The goal of this research was to use a combined computational and experimental approach to determine a finite element based injury metric for pulmonary contusion. This combined approach is essential in the study of soft tissue injury, particularly for PC, because due to its inflammatory etiology prospective studies must be based on a living model. The use of a living model restricts the type of model validation data that can be generated, but the open chest technique presented here is considered a good compromise: in-situ force vs. deflection data was collected on a living animal and the animal's response at specific post-insult time points were later quantified using CT. This research is part of a continuing trend towards formulating injury criteria based on localized mechanical deformations within the tissues themselves rather than relying on indirect measures of injury.

The organ level lung model was validated for a single condition using a optimization approach introduced by Stitzel et al (2005). The force-deflection response calculated from the optimized model was well within the one standard deviation of the experimental corridors. The absorbed energy of the simulation was within 3% of the energy obtained by integrating the mean experimental force-deflection trace over the first 6.3 mm of travel. While the absorbed energy from the simulation (7.46 mJ) was well within one standard deviation of the mean absorbed energy of the impact experiments (8.47 mJ), the simulated impact resulted in less energy transfer to the lung. This discrepancy in impact energy occurred because the impactor penetration depth prescribed in the simulation (6.3 mm) was based on the nominal penetration depth input into the eCCI, and this value slightly underestimated the mean penetration depth from the impact experiments (6.92

mm). The lung model also demonstrated good stability. Despite exhibiting large strains (> 50%) in the area of the indenter (Figure IV-9), the model showed robustness when varying the constitutive properties during the optimization. During the 2000 trials of the optimization, the model failed to run to completion in just 2.5 % of cases. For the optimized set, the ratio of internal and kinetic energy to hourglass energy was < 1% for the entire run.

The volume of the right lung in the FEA model was 4.52 cm^3, which closely agrees with a morphological study of the rat lung (4.52±0.1 cm^3, Zeltner, et al. 1990). The average value of the right lung from all sham animals was 3.31±0.35 cm^3 (Table IV-6, appendix). This represents a 26.8% reduction in volume from the model. Relative to this difference in volume, it is important to stress that the lung is an organ that exhibits substantial changes in volume during normal operation. Scaling the volume of the FEA model to match each individual rat would not result in appreciable gains in accuracy since the precise volume of the lung at the moment of impact was not known (pressure was controlled). In addition, this volume surely continued to fluctuate during the healing process. For this reason, all volumetrically based results in this study (CT and FEA) have been normalized to the total volume of the right lung.

The optimization approach was required to tune the model response to the experimental data. Previously published material property values for the constitutive equation used in this model are limited. The nominal parameters used as the basis for model optimization were reported by Stitzel et al.,(2005). To the authors' knowledge, the only additional source for the hyperelastic model parameters (α, β, C, etc.) is the study by Vawter (1980) that introduced the material model. It should be noted that no reference

was provided for the parameters used in this study and they seem to have been chosen only to show the effects of parameter variation. Conducting material testing to obtain such parameters may prove ineffective since the data would have to obtained ex-vivo. The stochastic optimization approach is thus acceptable considering the lack of data. Despite the large amount of variables (6) in the model, and the likelihood of many local minima within the parameter space this approach produced a functional parameter set.

The modeling results of the study introduced novel findings and techniques to the literature for the investigation of PC. Since CT is very sensitive to pulmonary pathology the position of the impacting anvil could be determined based on the experimental results. The relative uniformity of the resulting pathology (Table IV-7, appendix), particularly at the 24 hour time point suggests that the resulting pathology is highly influenced by the insult and that the correlative approach is reasonable. Relatively few FEA models of the lung are found in the literature, and many are intended to study blast induced trauma, which involves significantly higher loading rates than those experienced during MVC. (Grimal et al. 2005; Roberts et al. 2007; Roberts et al. 2005) To the authors' knowledge this research represents the first computational study of pulmonary injury from blunt trauma to use the host response to quantitatively set the boundary conditions and evaluate proposed injury metrics.

The results of the study show that elements exceeding the volume threshold defined by the product of the maximum principal strain and its strain rate correlate best to the distribution of pathology from the CT analysis. The maximum principal strain and its strain rate were the second and third best fitting metrics. There is evidence in the literature to support the notion that lung injury is dominated by the local maximum

principal strains. Maximum principal strain was the metric tentatively proposed by Fung et al. (1988) in their paper investigating the injury mechanism of pulmonary contusion at static loading rates. Under an initially isogravimetric condition where the weight of the lung did not change with time, Fung found that uniform stretching of an excised rabbit lung lead to the formation of edema. He argued that since the expansion was uniform, that stretching of the alveolar walls in this case was occurring in absence of shear strains. However these results were obtained under static loading and using excised tissue.

Limitations of the Computational Model

The computational results presented in this work are limited by the lack of model validation at more than a single loading scenario. The optimal parameter set (Table IV-2) therefore has been validated for this exact experimental condition only, and may not be valid for distributed impacts, or impacts at different velocities, and different penetration depths. These results have important implications for the results of this study. All injury thresholds proposed in this work are the result of analysis of the tissue at a specific continuum level using the constitutive equations described in the appendix. Since the proposed thresholds are dependent on the material model, a more generalized optimization approach which aims to fit the model response to more than a single condition could result in different constitutive parameters and therefore different thresholds.

One potential modification of the model towards general validity would be the addition of rate dependency. Based on the results of this study, there is biomechanical evidence to suggest that this addition is justifiable. The absorbed energy from Stitzel et al., 2005 which was calculated using the same impactor and load cell assembly but with a

reduced impact speed (2.8 ms), was roughly half the value reported in the current work, (4.0 mJ vs. 8.7 mJ). Additionally, the product of first principal strain and strain rate best correlated to the resulting region of pathology in the current study. If rate dependency were included in the model via a Kelvin-Maxwell linear viscoelastic formulation for instance, the effect of shear stress in the model could be amplified. This endeavor unto itself could be a separate, deeper study and at present it is unknown what effect achieving general validity would have on the thresholds presented in this work. Despite this limitation, the approach and thresholds presented in this work represent an important step towards developing a finite element-based injury metric for PC.

IV.8. Conclusions

A mixed computational and experimental approach was presented for the development of finite element-based predictors of injury for pulmonary contusion. In the context of human injury tolerance research, this work is part of a continuing trend towards using computational models to develop predictors of injury based on localized values of strain and stress within the organ of interest.

The experimental work focused on controlling and quantifying pulmonary contusion in a rat model. Thoracic insults with a mean velocity and penetration depth of 5.02 ± 0.035 $m \cdot sec^{-1}$ and 6.92 ± 1.06 mm were applied directly to the lung via an instrumented piston. The study introduced a semi-automated method to quantify contusion and found significantly elevated volumes of pathologic lung in contused subjects at 24 hours when compared to controls (14.51 ± 5.56% vs. 1.32 ± 1.21%, $p < 0.001$). The volume of pathologic lung was also found to decrease over time with significantly reduced values observed at 1 week (5.42 ± 4.33%) and 1 month (0.31 ± 0.15%) post-impact relative to

the 24 hour post-impact volume. Force versus deflection data from the applied insults and a stochastically based optimization scheme were used to validate an FEM of the impact at the nominal test conditions of 5.0 $m \cdot sec^{-1}$ and 6.3 mm penetration. A three dimensional registration scheme was used to determine which computational metric calculated by the FEM best correlated with the size and distribution of observed high radiopacity regions of tissue observed on CT. The product of maximum principal strain and strain rate was found to best characterize this distribution of pathology in the lung, with a threshold for injury at 24 hours post insult of 28.5 sec^{-1}.

Continued research will focus on achieving general validity of the FE model and translating the thresholds developed in the present work for use in the prediction of human lung injury. The thresholds proposed in this work, while preliminary, are ultimately intended for use in evaluating safety countermeasures relative to their ability to prevent pulmonary injury caused by motor vehicle crash and other forms of blunt thoracic trauma. These thresholds, based on a living specimen's response to a quantified insult, represent a novel addition to literature on the biomechanics of lung injury.

Chapter IV Appendix

The strain energy density functional used to describe the stress and strain state of the lung tissue at a continuum level is provided below (Fung et al. 1978; Vawter 1980). Stress arises in the lung tissue due to two phenomena: one is stretching of the parenchyma and another is due to surface tension of the air-septa interface. These effects are modeled via the two terms in Equation IV-4, where I_1 and I_2 are the first and second invariants of the Green strain and A is the ratio of the alveolar surface area in the deformed state to that in the undeformed state within the control volume of interest.

$$W(I_1, I_2) = \frac{C}{2\Delta} e^{(\alpha I_1^2 + \beta I_2)} + \frac{12C_1}{\Delta(1+C_2)}\left[A^{(1+C_2)} - 1\right] \quad \text{Equation IV-4}$$

$$A^2 = \frac{4}{3}(I_1 + I_2) + 1 \quad \text{Equation IV-5}$$

Table IV-4. Summary of Computed Tomography scan acquisition protocol.

	Native Acquisition	ROI Reconstruction
Image Width (pixels)	512	512
Image Height (pixels)	512	512
Reconstruction Diameter (mm)	200	96
Data Collection Diameter (mm)	250	250
Pixel Size (mm)	0.39	0.19
Slice Thickness (mm)	0.625	0.625
KVP (kVolt)	100	-
X ray current (Amp)	300	-
Exposure time (ms)	400	-

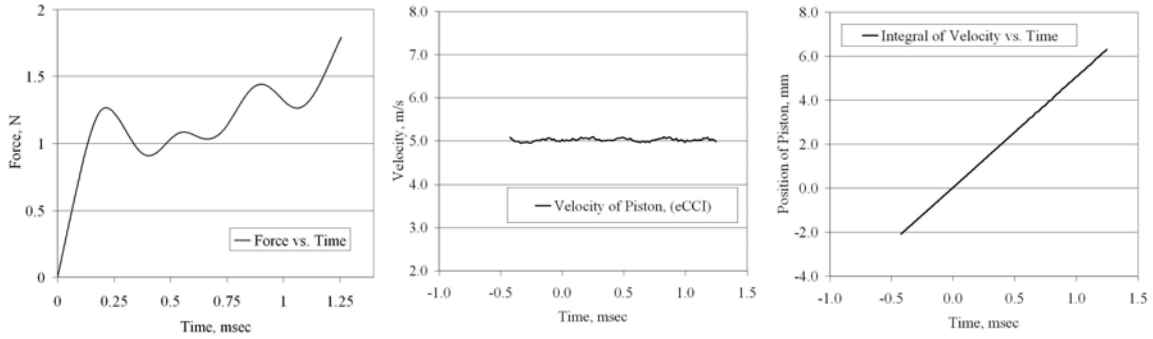

A. B. C.

Figure IV-10. (A) Exemplar Force vs. time (Rat 2, filtered to SAE J211 1000 Hz), (B) Velocity vs. time and (C) Position vs. time plots.

Table IV-5. Summary of impact data. All impacts were conducted using nominal impact speed and penetration depth settings of 5.0 m/s and 6.3 mm respectively.

Subject No.	Grouping	Age at Delivery, weeks	Weight at Scan Time, grams				Impact Experiment		
			24 Hour	48 Hour	1 Week	1 Month	Peak Force, N	Peak Deflection, mm	Absorbed Energy, mJ
1	24 Hour	8-10	314				2.55	6.61	7.97
2	24 Hour	8-10	327				2.44	6.99	9.90
3	24 Hour	8-10	306				1.19	7.79	6.33
4	24 Hour	8-10	328				3.92	5.43	13.24
5	48 Hour	8-10		365			2.74	8.91	9.91
6	48 Hour	8-10		389			1.09	7.29	5.23
7	48 Hour	8-10		339			3.10	7.31	8.95
8	48 Hour	8-10		373			2.08	9.39	13.08
9	1 Week	8-10			393		2.65	6.44	11.02
10	1 Week	8-10			440		3.33	5.12	8.73
11	1 Week	8-10			439		1.83	7.08	10.37
12	1 Week	8-10			405		1.95	6.67	9.15
13	Longitudinal	8-10	314	316	352		1.87	7.51	9.91
14	Longitudinal	8-10	312	313	356		2.35	6.36	9.46
15[a]	Longitudinal	8-10	328	325	360		3.39	8.47	19.67
16	Longitudinal	8-10	344	336	371		1.64	6.41	6.57
17[a]	Longitudinal	8-10	447		450	543	7.82	8.42	39.10
18	Longitudinal	8-10	452		466	537	1.24	6.93	5.02
19[b]	Longitudinal	8-10	470		482	549	-	-	-
20	Longitudinal	8-10	440		444	498	1.60	6.26	7.29
21	Longitudinal	8-10	434		445	570	1.83	6.10	5.23
Mean	**Impacted**		**370±65.5**	**345±28**	**416±45**	**539±26.3**	**2.19±0.77**	**6.92±1.06**	**8.74±2.47**
22	Sham	8-10	454		468	549	0.00	0.00	0.00
23	Sham	8-10	452		460	520	0.00	0.00	0.00
24	Sham	8-10	460		470	528	0.00	0.00	0.00
Mean	**Sham**		**455±4.2**		**466±5.3**	**532±15**			

[a.] Absorbed energy beyond 3 standard deviations of the mean, data from these rats excluded from study. [b.] Impact data not acquired.

Table IV-6. Summary of imaging data.

Subject No.	Grouping	24 Hour			48 Hour			1 Week			1 Month		
		Right Lung Volume, cm^3	Percent HR Lung	Total Lung Volume, cm^3	Right Lung Volume, cm^3	Percent HR Lung	Total Lung Volume, cm^3	Right Lung Volume, cm^3	Percent HR Lung	Total Lung Volume, cm^3	Right Lung Volume, cm^3	Percent HR Lung	Total Lung Volume, cm^3
1	24 Hour	2.95	16.91	5.20									
2	24 Hour	2.46	6.71	4.50									
3	24 Hour	2.12	11.10	4.44									
4	24 Hour	2.22	20.30	4.68									
5	48 Hour				2.16	30.50	4.05						
6	48 Hour				3.19	9.26	5.57						
7	48 Hour				2.49	10.83	5.25						
8	48 Hour				2.94	17.10	4.99						
9	1 Week							2.59	15.01	5.15			
10	1 Week							3.11	2.93	5.69			
11	1 Week							2.68	8.83	5.46			
12	1 Week							2.66	7.66	4.67			
13[c]	Longitudinal[e]	3.12	20.01	6.69	2.77	11.82	5.27	-	-	-			
14	Longitudinal	2.77	10.10	5.64	3.43	2.21	6.13	2.53	1.77	4.84			
15[a]	Longitudinal	2.37	16.54	4.74	1.90	12.21	4.25	1.96	7.26	3.91			
16	Longitudinal	2.94	16.01	5.35	2.37	17.20	4.81	2.15	7.94	3.97			
17[a]	Longitudinal	2.74	24.09	5.32	2.30	31.51	6.02	3.10	3.76	5.67	3.88	0.20	6.66
18	Longitudinal	3.80	13.64	7.91	4.16	6.49	7.49	3.88	2.88	7.68	4.35	0.14	8.18
19[d]	Longitudinal	2.35	24.75	5.96	3.04	4.55	6.94	3.19	3.58	6.74	-	-	-
20	Longitudinal	3.75	9.85	7.40	3.80	4.31	7.13	3.86	1.98	6.83	4.46	0.39	7.97
21	Longitudinal	3.91	10.25	6.87	3.81	7.04	7.44	2.82	6.97	6.42	3.96	0.41	6.90
Mean	**Impacted**	**2.94± 0.64**	**14.51± 5.56**	**5.87± 1.2**	**3.11± 0.65**	**11.03± 8.12**	**5.91± 1.18**	**2.94± 0.57**	**5.42± 4.33**	**5.74± 1.15**	**4.26± 0.26**	**0.31± 0.15**	**7.68± 0.69**
22	Sham	3.27	0.69	6.50	3.49	0.00	6.89	3.34	0.02	5.29	3.86	0.33	6.91
23[b,d]	Sham	3.10	0.57	6.17	-	-	-	3.14	3.58	5.13	-	-	-
24[c]	Sham	2.71	2.72	4.78	3.12	0.49	5.48	-	-	-	3.73	0.66	7.07
Mean	**Sham**	**3.03± 0.29**	**1.32± 1.21**	**5.82± 0.91**	**3.3± 0.26**	**0.25± 0.35**	**6.18± 1.0**	**3.24± 0.14**	**1.8± 2.52**	**5.21± 0.11**	**3.79± 0.1**	**0.49± 0.23**	**6.99± 0.12**

[a.] Absorbed energy beyond three standard deviations of the mean, volumetric data from these subjects were excluded from the study. [b.] CT data at 48 hours contained motion artifact. [c.] CT data at one week contained motion artifact. [d.] CT data at one month contained motion artifact. [e.] Data points were taken at multiple time points.

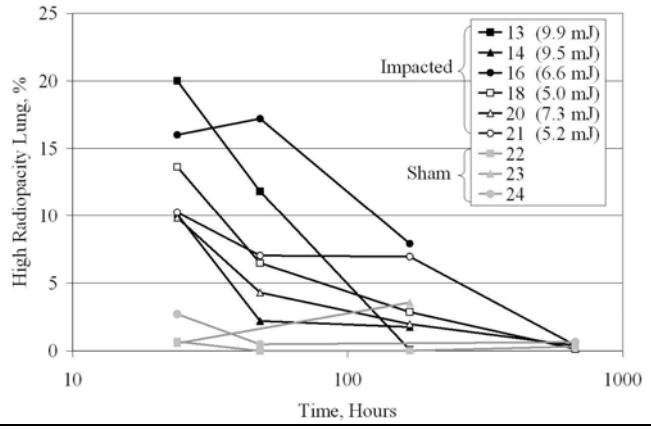

Figure IV-11. Relationship between High Radiopacity lung (normalized by impacted lung volume) and time post insult, for rats where longitudinal data was available. The abscissa is logarithmic based on hours. Test numbers are noted in the legend (Table IV-6). The absorbed energy is shown to the right of the test number in parentheses.

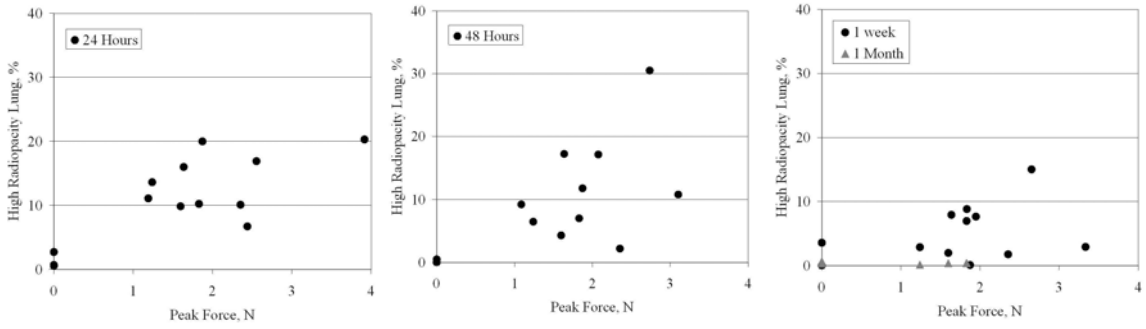

Figure IV-12. High Radiopacity Lung vs. Peak Force from impact at (A). 24 hours, (B) 48 hours, (C) 1 week and 1 Month post-contusion. Sham data included.

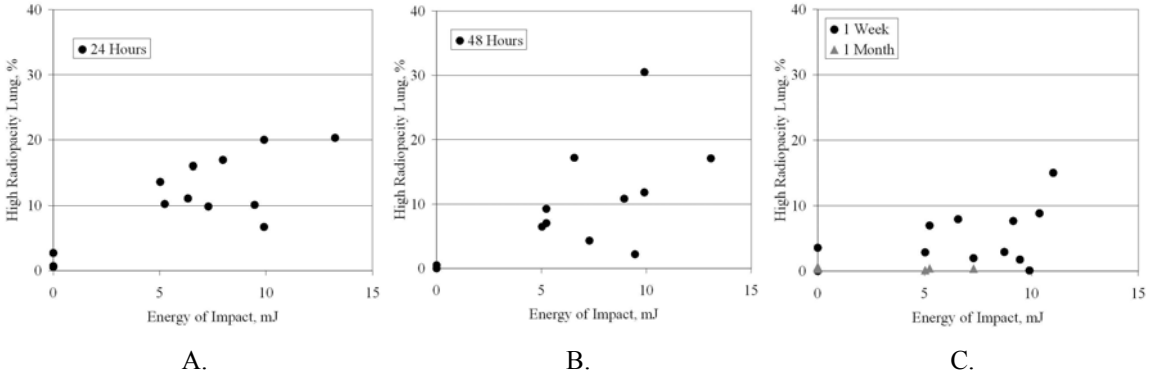

Figure IV-13. High Radiopacity Lung vs. Energy of impact at (A) 24 hours, (B) 48 hours, (C) 1 week and 1 Month post-contusion. Sham data included.

Table IV-7. Results of characteristic length study at 24 hrs and 48 hrs. Axis definitions: x axis, Medial-Lateral, y axis, Anterior-Posterior, and z axis, Cranial-Caudal. All dimension in mm.

Characteristic length	Axis	CT, 24 hours	CT, 48 hours	FEA Model
Right Lung, Total Volume	l_x	13.39±1.98	14.58±4.31	11.58
	l_y	19.96±4.54	18.81±5.35	19.48
	l_z	17.04±4.6	16.94±2.76	23.18
Right Lung, Volume of HR Lung	c_x	5.54±1.81	4.65±2.06	-
	c_y	11.01±3.41	8.19±5.18	-
	c_z	10.96±2.88	9.67±4.05	-

Table IV-8. Finite element model MIGA optimization, nominal parameters and associated constraints on the solution space.

Variable (Unit)	Description	Lower Bound	Nominal	Upper Bound
ρ (kg m^{-3})	Density	-	1.180×10^{-4}	-
K(N m^{-2})	Bulk Modulus	8.43×10^{-2}	1.124×10^{-1}	1.405×10^{-1}
C (N mm^{-1})	Curve fit parameter	5.035×10^{-5}	5.035×10^{-4}	5.035×10^{-3}
Δ (mm)	Mean alveolar	-	0.0702	-
α	Curve fit parameter	8.227×10^{-3}	8.227×10^{-2}	8.227×10^{-1}
β	Curve fit parameter	-24.6	-2.46	-0.246
C1 (N mm^{-1})	Curve fit parameter	6.535 x 10-7	6.535×10^{-6}	6.535 x 10-5
C2	Curve fit parameter	0.2876	2.876	5.0

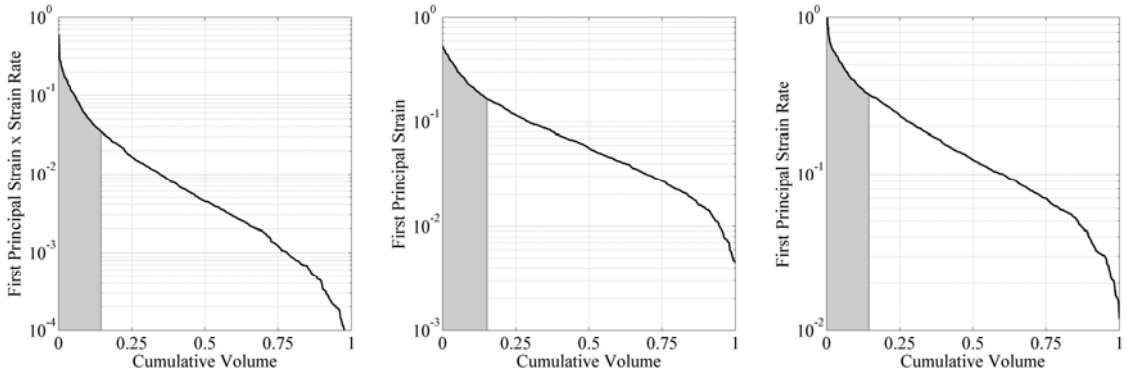

A. B. C.

Figure IV-14. Maximum value for each element, arranged in descending order for metrics found to best correlate with spatial distribution of contusion in animal model at 24 hours post impact. (A) Product of first principal strain and first principal strain rate, (B) first principal strain, and (C) first principal strain rate. Threshold value is 14.5%, which is the average percent volume of the lung that was contused.

Chapter IV Acknowledgements

This publication was supported by Grant Number 1 R49 CE000664-01 from the Centers for Disease Control and Prevention (CDC). Its contents are solely the responsibility of the authors and do not necessarily represent the official views of the National Center for Injury Prevention and Control. Thanks to Ashley A. Ruggles and the Wake Forest University School of Medicine Summer Research Opportunities Program for support of this work. Several software packages were essential for the completion of this study, and we would like to thank the corporations who provided educational / research license discounts. Among them are Livermore Software Technology Corporation for the use of LS-Dyna, Engineous Software for the use of Isight and Materalise for the use of Mimics software.

Chapter IV References

1 Allen, G. S., and N. E. Coates (1996) Pulmonary contusion: a collective review. Am Surg 62:895-900.

2 Antonelli, M., M. L. Moro, O. Capelli, R. A. De Blasi, R. R. D'Errico, G. Conti, M. Bufi, Gasparetto, A (1994) Risk factors for early onset pneumonia in trauma patients. Chest 105:224-228.

3 Balci, A. E., T. A. Balci, S. Eren, R. Ulku, O. Cakir, and N. Eren (2005) Unilateral post-traumatic pulmonary contusion: findings of a review. Surg Today 35:205-210.

4 Blansfield, J., D. Danis, A. Gervasini, and S. Sheehy (1999) Manual of Trauma Care: The First Hour. St. Louis, MO, Mosby.

5 Cavanaugh, K. J. (1993) Thoracic biomechanics in A. Nahum, and J. Melvin, eds. Accidental Injury Biomechanics and Prevention. New York, New York, Springer-Verlag.

6 Cohn, S. M. (1997) Pulmonary contusion: review of the clinical entity. J Trauma 42:973-979.

7 Croce, M. A., T. C. Fabian, L. Waddle-Smith, S. M. Melton, G. Minard, K. A. Kudsk, and F. E. Pritchard (1998) Utility of Gram's stain and efficacy of quantitative cultures for posttraumatic pneumonia: a prospective study. Ann Surg 227:743-751; discussion 751-745.

8 Fung, Y. C., P. Tong, and P. Patitucci (1978) Stress and strain in the lung. ASCE J. Eng. Mech. 104:201-223.

9 Fung, Y. C., R. T. Yen, Z. L. Tao, and S. Q. Liu (1988) A hypothesis on the mechanism of trauma of lung tissue subjected to impact load. J Biomech Eng 110:50-56.

10 Grimal, Q., N. Salah, and A. Watzky (2005) A high frequency lung injury mechanism in blunt thoracic impact. J Biomech 58:1247-1254.

11 Hoth, J. J., J. D. Stitzel, F. S. Gayzik, N. A. Brownlee, P. R. Miller, B. K. Yoza, C. E. McCall, R. W. Meredith, R. M. Payne (2006) The pathogenesis of pulmonary contusion: an open chest model in the rat. J Trauma 61:32-44; discussion 44-35.

12 Knoferl, M. W., U. C. Liener, D. H. Seitz, M. Perl, U. B. Bruckner, L. Kinzl, and F. Gebhard (2003) Cardiopulmonary, histological, and inflammatory alterations

after lung contusion in a novel mouse model of blunt chest trauma. Shock 19:519-525.

13 Leader, J. K., B. Zheng, R. M. Rogers, F. C. Sciurba, A. Perez, B. E. Chapman, S. Patel, C. R. Furman, D. Gur (2003) Automated lung segmentation in X-ray computed tomography: development and evaluation of a heuristic threshold-based scheme. Acad Radiol 10:1224-1236.

14 Miller, P. R., M. A. Croce, T. K. Bee, W. G. Qaisi, C. P. Smith, G. L. Collins, and T. C. Fabian (2001) ARDS after pulmonary contusion: accurate measurement of contusion volume identifies high-risk patients. J Trauma 51:223-228; discussion 229-230.

15 Miller, P. R., M. A. Croce, P. D. Kilgo, J. Scott, and T. C. Fabian (2002) Acute respiratory distress syndrome in blunt trauma: identification of independent risk factors. Am Surg 68:845-850; discussion 850-841.

16 United States Department of Transportation, National Highway Traffic Safety Administration, Traffic Safety Facts 2005: A Compilation of Motor Vehicle Crash Data from the Fatalities Analysis Reporting System and General Estimates System. DOT HS 810 631, Washington, DC 2005.

17 Raghavendran, K., B. A. Davidson, J. D. Helinski, C. J. Marschke, P. Manderscheid, J. A. Woytash, R. H. Notter, P. R. Knight (2005) A rat model for isolated bilateral lung contusion from blunt chest trauma. Anesth Analg 101:1482-1489.

18 Roberts, J. C., A. C. Merkle, P. J. Biermann, E. E. Ward, B. G. Carkhuff, R. P. Cain, and J. V. O'Connor (2007) Computational and experimental models of the human torso for non-penetrating ballistic impact. Journal of Biomechanics 40:125-136.

19 Roberts, J. C., J. V. O'Connor, and E. E. Ward (2005) Modeling the effect of non-penetrating ballistic impact as a means of detecting behind armor blunt trauma. J Trauma 58:1241-1251.

20 Sakai, N., M. Mishima, K. Nishimura, H. Itoh, and K. Kuno (1994) An automated method to assess the distribution of low attenuation areas on chest CT scans in chronic pulmonary emphysema patients. Chest 106:1319-1325.

21 Stellin, G (1991) Survival in trauma victims with pulmonary contusion. Am Surg 57:780-784.

22 Stitzel, J., F. Gayzik, J. Hoth, J. Mercier, H. M. Gage, K, S. Duma, and R. Payne (2005) Development of a finite element based injury metric for pulmonary contusion, Part I: model development and validation. Stapp Car Crash Journal 49:271-289.

23 Takhounts, E., R. Eppinger, J. Campbell, and R. Tannous (2003) On the development of the SIMon finite element head model. Stapp Car Crash Journal 47:107-133.

24 Tenney, S., and J. Remmers (1963) Comparative Quantitative Morphology of the Mammalian Lung: Diffusing Area. Nature 197:54-56.

25 Vawter, D (1980) A finite element model for macroscopic deformation of the lung. J. Biomech. Eng. 102:1-7.

26 Viano, D., and I. Lau (1988) A viscous tolerance criteria for soft tissue injury assessment. J Biomech 21:387-399.

27 Wagner, R. B., W. O. Crawford, Jr., and P. P. Schimpf (1988) Classification of parenchymal injuries of the lung. Radiology 167:77-82.

28 Wang, N. D., M. H. Stevens, D. B. Doty, and E. H. Hammond (2003) Blunt chest trauma: an experimental model for heart and lung contusion. J Trauma 54:744-748.

Published in: *Biomedical Sciences and Instrumentation* Vol. 44; pp 225-230, 2008

CHAPTER V

QUANTITATIVE HISTOLOGY OF CONTUSED LUNG TISSUE WITH COMPARISON TO COMPUTED TOMOGRAPHY

F. Scott Gayzik, M.S.[1,2]
J. Jason Hoth, M.D.[1]
Noel Brownlee, M.D.[1]
Joel D. Stitzel, Ph.D.[1,2]

1. Wake Forest University School of Medicine, Winston-Salem, NC
2. Virginia Tech – Wake Forest University Center for Injury Biomechanics, Winston-Salem, NC and Blacksburg, VA

Abstract

This study presents an image analysis algorithm for quantifying the volume fraction of pathology in serial histology of the rat lung. The right lung of male Sprague-Dawley rats (n=4) was contused using a controlled insult applied via an instrumented, electronic piston. The right (struck) and left lungs were excised at 48 hours post-insult, fixed in 10% formalin. Serial histology was taken at 1.5 mm intervals on the struck lung and 3 mm intervals on the left lung. Sections were stained with H&E and digitally imaged using a fixed, high-resolution digital camera. Immediately prior to sacrifice, computed tomography images of all subjects were also acquired. An automated image analysis program was applied to each image (8-bit, RGB) using morphological (dilatation and erosion), filtering (circular averaging), and thresholding techniques to sort pixels representing healthy lung tissue, pathologic lung tissue, and blood into separate masks. Blood was determined by multi-channel thresholding in the following inclusive ranges: Red (197-240), Green (0-90) and Blue (115-154). After applying the morphological and filtering operations, lung pathology was identified as all pixels exceeding a grayscale value of 85, with 0 being black and 255 being white. The average normalized volume of pathology across the data set was 12.63 ± 11.40 %. The results showed greater volumes of tissue pathology than blood in all subjects indicating a good model for blunt lung trauma. CT segmentation data from the same four animals was used for a related study but was included for the purposes of comparison. These values were determined through a semi-automated approach and resulted in an average pathology volume of 16.92 ± 9.66 %. Normalized pathology did not differ significantly between histology and CT ($p = 0.18$, paired t-test for sample means, $\alpha = 0.05$). In general, the histology analysis algorithm and CT data resulted in similar trends across the data set. This approach can be used to improve the accuracy of both histology-based and CT-based segmentation processes.

V.1. Introduction

In this study, digital histology analysis is used to quantify the extent of pulmonary contusion (PC) following a thoracic insult. Thoracic injuries are exceedingly common in blunt trauma patients and are associated with significant morbidity and mortality. [1, 2] Contusion volume at the time of hospitalization has been shown to be an independent predictor for the development of Acute Respiratory Distress Syndrome (ARDS), with the risk of ARDS increasing sharply with PC in excess of 20% by volume. [3] Computed tomography (CT) is the most frequently used clinical modality for obtaining volumetric lung contusion data, however the segmentation process is labor intensive and can be confounded by the fact that many types of pathology produce image data within the same Hounsfield unit (HU) range. This research presents an image analysis algorithm for the automated identification of lung contusion applied to serial histology sections of the rat lung. The long-term goal of this research is to use histologically-calculated contusion volume as a standard against which CT-calculated contusion volume can be validated.

V.2. Methods

All experimental protocols were approved by the Wake Forest School of Medicine Animal Care and Use Committee. Contusion was generated in Sprague-Dawley male rats (n = 4) using an instrumented, electromagnetically-driven piston, with a nominal impact speed and penetration depth of 5 m s^{-1} and 6.3 mm respectively. Subjects were intubated prior to the procedure. The right lung was exposed via thoracotomy, and was directly struck with the piston. Force and displacement data were collected for each impact. [4, 5] Detailed descriptions of the experimental preparation are available in the literature [4-6] At 48 hours post impact, CT images were acquired and the subjects were

euthanized for histology. The intact lungs were excised and fixed in 10% buffered formalin at a pressure of 15mm H_20 for 24 hours prior to sectioning. Specimens were embedded in paraffin, sectioned, and stained with hematoxylin and eosin (H&E) for examination (Harris Histology, Greenville, NC). The right (struck) lung was sectioned at Δ= 1.5 mm intervals, and the left lung was sectioned at Δ= 3 mm intervals.

The histological specimens were digitally imaged using a rigidly-mounted Fuji S3 105 mm digital camera equipped with a micron-nikkor lens (Fuji, Valhalla, NY; Nikon, Melville, NY). A metric ruler with clear millimeter demarcations was imaged under the same mounting protocol to determine the resolution of the resulting data. All images were saved at high-resolution, resampled to 1064 x 712 pixels, and saved as bitmapped images via a batch process. Resampled images were imported to Matlab (The MathWorks, Natick, MA) as unsigned, 8-bit, RGB images for preprocessing and segmentation. The segmentation algorithm and accompanying graphical user interface used were programmed in house using Matlab.

Images were preprocessed to: 1. clearly distinguish background pixels from lung pixels and 2. translate each so that they were aligned along a common centroid. To accomplish these tasks, the green channel of the image was used because it exhibited the greatest contrast between lung pixels and background pixels, and reduced the computational cost. The monochrome image was converted to binary format and several Matlab image processing functions were employed. Binary format was advantageous during preprocessing since black (0) and white (1) could be used to represent background and lung masks. Because of the porous nature of lung tissue, the *imfill* command was used to ensure that regions of pixels representing alveolar airspace were not considered

background pixels. The *regionprops* command was used to identify boundaries of lung tissue and calculate the centroid (analogous to center of mass) of each region of lung tissue. In cases where more than one distinct region of lung tissue was present in a single slide, a weighted average of the centroids based on the region size was used to determine a single image centroid. Images were then translated to align the entire stack along the centroid. Preprocessing was done separately for the right and left lung and is summarized in Figure V-1.

A.

B.

C.

Figure V-1. Overview, study methodology.

***A*. Dotted lines represent sample serial sections of excised lung tissue collected 48 hours post-insult.**
***B*. Exemplar image (monochrome) of histology section.**
***C*. Total lung reconstruction of centroid-aligned images. Triad shows Anterior-Posterior (A-P), Medial-Lateral (M-L) and Cranial-Caudal (Cr-Ca) directions.**

Images were segmented to categorize the lung pixels into three masks: 1. healthy lung tissue, 2. pathologic lung tissue, and 3. blood. The parameters used in this algorithm are outlined in Table V-1. The segmentation began by determining the quantity of blood in the image. Blood in a given image resulted from the presence of an arterial cross-section or bleeding following the insult. Since it was identifiable by a fairly homogenous RGB range, multi-channel thresholding was used to identify these pixels. Boolean operations were used to remove these pixels from the lung mask. A combination of morphological and filtering operations were then used to identify regions of pathology within the lung mask. The morphological operations used a combination of dilatation and erosion operations on the monochrome image to accentuate regions of pathology. A circular-average filtering operation was then applied to the image to smooth contrast within of the image. A gray-scale threshold was then applied to the processed, monochrome image. Pixels exceeding this threshold were considered areas of pathologic tissue. A Boolean operation was used to separate the pathologic lung tissue from the remaining lung mask, thereby completing the segmentation process. Figure V-2 shows the image processing progression.

Table V-1. Thresholding parameters used to segment blood, pathologic lung tissue and healthy lung tissue.

Blood mask		Pathology mask	
Channel	Range (inclusive)	Operation	Description
Red	(197-240)	Morphologic	Diamond sampling element, 4 pixel axis
Green	(0-90)	Filter	Circular element, 5 pixel radius
Blue	(115-154)	Threshold (0-255)	85

A.

B.

C.

Figure V-2. Segmentation process for determining pathologic tissue.
***A*. Image after morphologic operation.**
***B*. Image after filtering operation.**
***C*. Image after thresholding operation. This binary image shows only pathology. The native monochrome image can be seen in Figure V-1.**

Pathologist Validation

To validate the algorithm, a pathologist blind to the study identified regions of pathology on printouts of the images via a transparency tracing method. High resolution images of specimen 1 were printed in color on standard size 8.5 by 11 inch paper using an HP Color Laser Jet 3550 printer. There were 50 slides in this image stack. Fifty transparencies were provided with the color printouts. The transparencies were carefully aligned with the printouts and the pathologist was asked to mark pathologic regions with a fine tip permanent marker. Following this identification process, the transparencies were scanned and compared to the algorithm results on a pixel by pixel basis. Sensitivity

and specificity of the algorithm were determined on a slide by slide basis. The validation portion of this study was also programmed in Matlab.

V.3. Results

The results of the study are summarized in Table V-2. The subjects experienced similar lung insults and were within a tight weight range (CoV, weight = 5.7%). While the distance between sections (Δ) were uniform for the right and the left sides, the number of sections per individual varied slightly. To aid in comparisons across modalities, pathology volumes identified by the algorithm were normalized to the total volume of the lung on a given side. The precisely quantified image resolution and slice interval enabled volumetric calculations of the segmented histology data. It was assumed that the composition of the section was uniform across Δ. The fraction of contusion determined by the algorithm varied across study subjects, but was always greatest on the struck side. The volume of pathology exceeded the volume of blood in the image stack for all subjects. The pathology identified by the algorithm qualitatively agreed with a preliminary assessment of the full color images.

Table V-2. Study results. All data collected 48 hours post-insult.

Subject No.	1	2	3	4	Mean ± S.D.
Impact Experiment Data [5]					
Impact Energy, mJ	9.91	5.23	8.95	13.1	9.29 ± 3.23
Weight, gr	364	389	339	373	366 ± 20.9
Histology Data					
Distance Between Samples, Right Δ, mm	1.5	1.5	1.5	1.5	
Number Sections, Right	37	45	55	50	
Distance Between Samples, Left Δ, mm	3.0	3.0	3.0	3.0	
Number Sections, Left	23	25	30	24	
Image Resolution, mm/pixel	0.021	0.021	0.021	0.021	
Total Lung Volume, ml	5.61	6.37	7.36	6.37	6.43 ± 0.72
Right (Struck) Lung, Volume, ml	3.06	3.69	4.31	3.89	3.74 ± 0.52
Right Lung Pathology, ml	0.745	0.103	0.106	0.759	0.428 ± 0.37
Right Lung Blood, ml x 10^{-3}	5.46	3.96	16.8	28.7	14.0 ± 12.0
Pathology and Blood, Right, %	24.5	2.90	2.85	20.3	12.63 ± 11.4
Left Lung, Volume, ml	2.55	2.68	3.06	2.47	2.69 ± 0.26
Left Lung Pathology, ml	0.0669	0.0534	0.0270	0.0823	0.057 ± 0.02
Left Lung Blood, ml x 10^{-3}	1.64	6.83	16.3	8.70	8.36 ± 6.0
Pathology and Blood, Left, %	2.69	2.25	1.41	3.69	2.51 ± 0.95
CT Data [5]					
Slice Thickness, mm	0.625	0.625	0.625	0.625	
Image Resolution, mm/pixel	0.190	0.190	0.190	0.190	
Right Lung Volume, ml	2.20	3.19	2.49	2.94	2.70 ± 0.45
Total Lung Volume, ml	4.05	5.57	5.25	4.99	4.97 ± 0.65
Pathology, Right, %	30.5	9.26	10.8	17.1	16.92 ± 9.66

CT data from the same individuals acquired just prior to sacrifice were segmented using a semi automated approach as part of a larger study. [5] The fraction of pathology normalized to the right lung volume determined via CT are also included in Table V-2 and are shown with the histology data in Figure V-3. The histology and CT segmentation approaches agree in that the volume of pathology from subjects 1 and 4 is greater than that in subjects 2 and 3. The total lung volume determined through analysis of the histology data was greater than that determined through CT segmentation for all subjects.

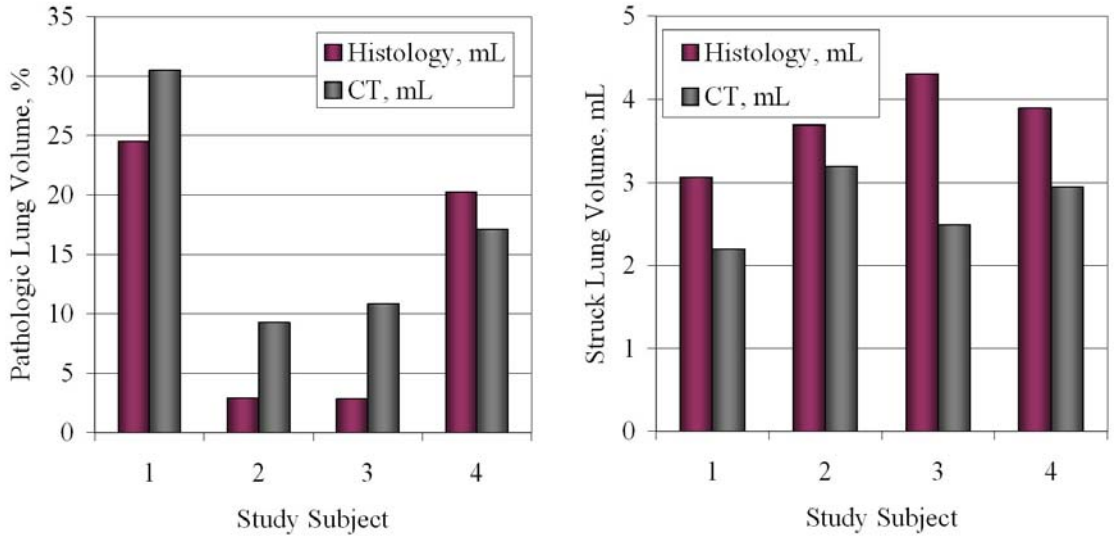

Figure V-3. Comparison of results, histology vs. CT for struck lung. *A.* Volume of pathology normalized by total lung volume. B. Struck lung volume.

The normalized volume of PC outlined by the pathologist for the entire data set was 22.7% whereas the algorithm identified 17.9%. The algorithm demonstrates an excellent mean specificity, 0.99±0.009, but the mean sensitivity was less, 0.57±0.26. This finding is consistent with the gross contusion volume comparison. However, images resulting in low sensitivity typically demonstrated little to no contusion. When analyzing only those scans exhibiting 20% or more PC by volume (n=25, pathologist assessment) the average sensitivity was markedly higher, 70.0%.

V.4. Discussion

Digital histology analysis has become more common as increases in computational resources have allowed for fast and inexpensive processing of high-resolution images. [7, 8] Applications of this approach are numerous. Corneal opacity, [9] regional variation of patellar trabeculae, [10] and tumor invasion and propagation [11, 12] have all been quantified using similar software packages as in the current study. This study presented

an automated algorithm for quantifying the volume of contusion in histological samples of H&E-stained rat lung. The results of this study are encouraging. With respect to the model for pulmonary contusion itself, far more pathology was detected than blood in the tissue samples when comparing gross volumes. This indicates that the method used to elicit contusion is good for generating a blunt rather than penetrating injury mechanism. Normalized pathology values from the histology data were calculated taking the ratio of pathology *and* blood pixel volumes to total lung pixel volumes. The data also suggest (Table V-2, rows 1 and 13) that a relationship may exist between impact energy and pathology volume in the stuck lung. Further studies would be needed to establish significance between these values.

The primary motivation for this study was to compare normalized pathology data from the same subjects across two different modalities; Histology and CT. The results reflected similar trends in the data (Figure V-3A). Normalized pathology did not differ significantly between histology and CT ($p = 0.18$, paired t-test for sample means, $\alpha = 0.05$). For two of the study subjects ($N^{os.}$ 1 and 4) the Histology and CT segmentation found differences in the normalized contusion volume of 6% or less. The remaining subjects exhibited less contusion than their counterparts in both modalities, but discrepancy between modalities was greater. This may be due to a number of factors. First the total volume from the excised tissue (histology data) was greater than the total volume from CT segmentation (Figure V-3B). This may be the result of quasi-static inflation of the tissue after excision beyond its average *in-situ* volume. The implication of this over expansion is that it may have disproportionately increased the volume of normally functioning tissue, thereby decreasing the fraction of pathology. A second

factor is that the CT pathology may not reflect only contusion, but rather a collection of pathologies such as edema and atelectasis which share the same HU range, thus increasing the fraction of pathology. These conditions work to increase the differences between the values determined by the two modalities. Progress in resolving these differences could potentially be made through further refinement of the initial insult to maximize the presence of a specific pathology.

Despite these discrepancies this study outlines a useful approach for improving histology and CT-based segmentation of pulmonary contusion and other pathologies since both the data sets were from the same individuals, collected at the same time, and experienced the same insult. The results of the histology analysis algorithm compared favorably to manual segmentation by a pathologist, exhibiting excellent specificity (0.99±0.009). [13] The algorithms' sensitivity to contusion (the ability to detect true-positives) was less however, (0.57±0.26), and was particularly poor on images with a fraction of contusion less than 20%. This suggests that the algorithm could be improved through optimization of the parameters used in its execution. The values of the parameters used in the present study were taken from the aforementioned work. Future research will focus on applying an automated sampling algorithm to optimize the parameters in Table V-1 to best match the CT data, and to determine which parameters have the largest effect on the resulting estimates of pathology.

V.5. Conclusions

An image analysis algorithm was developed to determine the normalized volume of pathology in histology specimens. Normalized pathology from CT of the same animals from a previous study, taken at the same time point, were used to compare results. The

histology analysis algorithm and CT data found similar trends between individuals. However, the total lung volume estimated via histology was greater than that estimated via CT in all cases, while the fraction of pathologic lung estimated via CT was greater than that estimated via histology in 3 of 4 cases. Future efforts will focus on optimizing the parameters of the segmentation algorithms to improve the match. In conclusion, this approach represents a useful method for improving the accuracy of both histology-based and CT-based segmentation processes.

Chapter V Acknowledgements

This publication was supported by Grant Number 1 R49 CE000664-01 from the Centers for Disease Control and Prevention (CDC). Its contents are solely the responsibility of the authors and do not necessarily represent the official views of the National Center for Injury Prevention and Control. Digital photography services provided by Creative Communications, Wake Forest University Baptist Medical Center, Winston-Salem, NC.

Chapter V References

1 J. Blansfield, D. Danis, A. Gervasini, and S. Sheehy, *Manual of Trauma Care: The First Hour*. St. Louis, MO: Mosby, 1999.

2 S. M. Cohn, "Pulmonary contusion: review of the clinical entity," *J Trauma,* vol. 42, pp. 973-9, May 1997.

3 P. R. Miller, M. A. Croce, T. K. Bee, W. G. Qaisi, C. P. Smith, G. L. Collins, and T. C. Fabian, "ARDS after pulmonary contusion: accurate measurement of contusion volume identifies high-risk patients," *J Trauma,* vol. 51, pp. 223-8; discussion 229-30, Aug 2001.

4 J. Stitzel, F. Gayzik, J. Hoth, J. Mercier, H. M. Gage, K, S. Duma, and R. Payne, "Development of a finite element based injury metric for pulmonary contusion, Part I: model development and validation," *Stapp Car Crash Journal,* vol. 49, pp. 271-289, 2005.

5 F. S. Gayzik, J. J. Hoth, M. Daly, J. W. Meredith, and J. D. Stitzel, "A finite element based injury metric for pulmonary contusion: Investigation of candidate injury metrics through correlation with computed tomography," *Stapp Car Crash Journal,* vol. 51, pp. 189-209, 2007.

6 J. J. Hoth, J. D. Stitzel, F. S. Gayzik, N. A. Brownlee, P. R. Miller, B. K. Yoza, C. E. McCall, J. W. Meredith, and R. M. Payne, "The pathogenesis of pulmonary contusion: an open chest model in the rat," *J Trauma,* vol. 61, pp. 32-44; discussion 44-5, Jul 2006.

7 F. J. Leong and A. S. Leong, "Digital imaging applications in anatomic pathology," *Adv Anat Pathol,* vol. 10, pp. 88-95, Mar 2003.

8 F. J. Leong and A. S. Leong, "Digital imaging in pathology: theoretical and practical considerations, and applications," *Pathology,* vol. 36, pp. 234-41, Jun 2004.

9 J. J. Li, L. Xu, B. C. Sun, Y. J. Chen, and K. Ma, "[The application of digital photography with retroillumination for lens in cataract study]," *Zhonghua Yan Ke Za Zhi,* vol. 39, pp. 278-82, May 2003.

10 H. Toumi, I. Higashiyama, D. Suzuki, T. Kumai, G. Bydder, D. McGonagle, P. Emery, J. Fairclough, and M. Benjamin, "Regional variations in human patellar trabecular architecture and the structure of the proximal patellar tendon enthesis," *J Anat,* vol. 208, pp. 47-57, Jan 2006.

11 N. S. Akella, Q. Ding, I. Menegazzo, W. Wang, G. Y. Gillespie, J. R. Grammer, C. L. Gladson, and L. B. Nabors, "A novel technique to quantify glioma tumor

invasion using serial microscopy sections," *J Neurosci Methods,* vol. 153, pp. 183-9, Jun 15 2006.

12 Q. Ding, J. R. Grammer, M. A. Nelson, J. L. Guan, J. E. Stewart, Jr., and C. L. Gladson, "p27Kip1 and cyclin D1 are necessary for focal adhesion kinase regulation of cell cycle progression in glioblastoma cells propagated in vitro and in vivo in the scid mouse brain," *J Biol Chem,* vol. 280, pp. 6802-15, Feb 25 2005.

13 F. S. Gayzik, N. A. Brownlee, J. J. Hoth, and J. D. Stitzel, "An image analysis method for quantitating pulmonary contusion in histologic specimens," in *Southeast Bioengineering Conference*, Duke University, 2007.

Manuscript currently in preparation for submission to the Journal of Biomechanics

CHAPTER VI

A FINITE ELEMENT BASED INJURY METRIC FOR PULMONARY CONTUSION: GENERAL MODEL VALIDATION AND CONCLUDING EXPERIMENTS

F. Scott Gayzik, M.S.[1,2]
J. Jason Hoth, M.D.[1]
Joel D. Stitzel, Ph.D.[1,2]

1. Wake Forest University School of Medicine, Winston-Salem, NC
2. Virginia Tech – Wake Forest University Center for Injury Biomechanics, Winston-Salem, NC and Blacksburg, VA

Abstract

Concluding experiments to determine the finite element based injury metrics for pulmonary contusion (PC) are presented in this chapter. The main goals of this study were; 1. To generate finite element model validation data at distinct loading conditions using an animal model, 2. To explore the relationship between impact severity and the resulting contusion for these impact conditions, 3. To apply previously-developed model validation schemes to validate the finite element model of the lung against multiple impacts simultaneously and 4. To determine a final set of finite element based predictors for PC, based on first principal strain and first principal strain rate.

The experimental methods of this study are consistent with those presented in the preceding chapters. Sprague-Dawley male rats underwent right-side thoracotomy prior to impact. Insults were applied directly to the lung via an instrumented electronic piston. An integrated anvil and load cell custom-designed for use with the electronic piston was used to collect force data. Five cohorts were tested in this study: one sham group that underwent thoracotomy but was not impacted and four groups that experienced lung insults of varying degrees of severity. The nominal values for impact velocity (V) and penetration depth (D) of the cohorts in this study were: Group 1, (Severe, V = 6.0 $m \cdot s^{-1}$, D = 5.0 mm), Group 2. (Intermediate, V = 1.5 $m \cdot s^{-1}$, D = 5.0 mm), Group 3. (Intermediate, V = 6 $m \cdot s^{-1}$, D = 2.0 mm) and Group 4. (Mild, V = 1.5 $m \cdot s^{-1}$, D = 2.0 mm). CT scans were acquired at 24 hours, 48 hours, and 1 week. A semi-automated segmentation algorithm was used to quantify the volume of contusion within each study subject. Various statistical tests were conducted to determine if significant differences between cohorts existed. Linear regression models were conducted across all cohorts testing the volume of high radiopacity lung versus impact parameters. Finally, based on the method presented in Chapter IV of this dissertation, finite element based injury metrics for pulmonary contusion were determined for contusion at 24 hours and 1 week post impact.

Significant differences in velocity, displacement, peak force during impact, and impact energy were observed between study groups (ANOVA, p = < 0.0001). The volume of high radiopacity lung (HRL) was greatest for the severe impact group (mean HRL = 9.21 ± 4.89) and was significantly greater than all other cohorts at 24 hours with the exception of Group 3. Significant linear regressions for HRL vs. impact energy and peak impact force were established at the 24 hour time point. Nearly all relationships between impact parameters and observed HRL were no longer significant after the 24 hour time point. All groups exhibited falling mean values of HRL with increased post impact time. The concurrent model optimization fit the model output to the validation data from the impact experiments, matching impact energy within one standard deviation for both the Group 1 severe impacts (observed energy = 3.88 ± 0.883 mJ vs. simulation energy = 4.47 mJ) and Group 2 intermediate impacts (observed energy = 1.46 ± 0.403 mJ vs. simulated energy = 1.50 mJ). The optimized computational model showed good stability, with the ratio of hourglass energy to the total energy remaining below 2% for the duration of the simulation for both cases. Based on the validated model output and observed values of HRL for all cohorts, injury metrics for pulmonary contusion were determined at 24 hours and 1 week. The predictive injury metrics at 24 hour post contusion are $\varepsilon_{max} \cdot \dot{\varepsilon}_{max}$ exceeding 94.5 sec^{-1}, ε_{max} exceeding 0.284 and $\dot{\varepsilon}_{max}$ exceeding 470 sec^{-1}. Thresholds for injury to the lung still present at 1 week post-impact were also determined. There were $\varepsilon_{max} \cdot \dot{\varepsilon}_{max}$ exceeding 149 sec^{-1}, ε_{max} exceeding 0.343 and $\dot{\varepsilon}_{max}$ exceeding 573 sec^{-1}. These metrics and the accompanying validated FEA model represent a comprehensive undertaking in developing a predictive metric for pulmonary contusion. Future research will focus on translating these findings to models for human injury prediction. These metrics are valuable additions to the literature for prediction and prevention of PC and will aid in the design of safety systems.

VI.1. Introduction

The purpose of the final study of this dissertation was to build on the findings presented in Chapters III and IV.[1, 2] The methodology for determining the injury metrics for pulmonary contusion (PC) was established in these two chapters. The Sprague-Dawley male rat was determined to be a good model for the contusion experiments. It provided an adequate compromise between image resolution and the ability to conduct high throughput studies. The method for eliciting contusion in this model was also proven. Subjects underwent posterolateral right thoracotomy followed by a prescribed impact with the instrumented electronic piston, model eCCI (Custom Design and Fabrication, Richmond, VA). Computed tomography (CT) emerged as the preferred modality for quantifying contusion in the subjects because of its ability to image both contused and healthy lung tissue. This allowed for the calculation of normalized values of high radiopacity lung (HRL). CT was also preferred over PET because of its fast acquisition time (acquisition time was roughly 2 min. per body scan as opposed to up to 80 min in PET). A CT and finite element analysis (FEA) registration technique was introduced and it was found that the most appropriate variables to use in developing an injury metric were those based on the first principal strain and strain rate. Early biomechanical studies of pulmonary injury support these findings.[3] There were a number of unresolved questions however, which prompted this final study.

One important unexplored aspect was how varying the impact severity affected the primary outcome measure, the volume fraction of HRL of the subject. In previous studies where image data were available, only a single impact condition was tested. Stitzel et al. (2005) impacted subjects at 2.8 $m \cdot s^{-1}$, and used Positron Emission

Tomography (PET) to quantify the values of contusion. Gayzik et al. 2007 impacted subjects at a higher rate (5.8 $m \cdot s^{-1}$) and used CT to quantify the contusion, but comparisons between these datasets are difficult. PET data cannot be normalized by the total volume of the injured lung since only the inflamed tissue is visible. In addition, volumes of contusion determined through PET analysis were normalized by the uptake of the 18F-FDG radioactive tracer in the liver rather than through investigation of the morphology of the organ and corresponding injury as is done in CT segmentation. Thus it was necessary to conduct a study were a single modality (in this case CT) was used to quantify the fraction of HRL between subjects that experienced impacts of varying intensity.

The data presented in Chapter II aided in the design of the four-level test matrix outlining the experiments presented in this chapter. The parameters used to describe the severe and mild cases were derived from analysis of the rib cage module of dummy occupants in lateral crash tests. PC was found to be commonly associated with the lateral crash scenario in the latter study. The two intermediate cases are mixed scenarios where one factor is held at the severe level and the other is held at the mild level. Based morphological measurements of the average rat rib cage width in the coronal plane, the penetration depths presented in this chapter (2.0 mm and 5.0 mm) correspond to 15% and 35% lateral-to-medial penetration respectively.

A limitation of the results of Chapter IV[1] was validation of the finite element model based on a single impact cohort. This limitation is addressed with these final experiments. The experimental design of the current study, with four levels of impact intensity produced a more expansive set of data for model validation. The automated

technique for model validation used in previous studies can be expanded to conduct a 'concurrent' optimization trial where the finite element model is adjusted to match multiple experimental conditions. This technique has been used to fit both dynamic and quasi-static data in previous studies[4, 5] and is employed here.

The methods section is broken into experimental and computational components. The experimental portion is presented first, followed by the computational portion. In keeping with this structure, the results section presents the experimental results, followed by the computational results.

VI.2. Methods

Contusion experiment methods

Detailed information on animal husbandry, preparation, anesthesia and analgesia have been previously published and remained unchanged.[1] The protocol was approved by the Wake Forest University Animal Care and Use Committee (protocol number A05-186). Subjects were aged 8-10 weeks at the time of the impact experiment.

Impacted subjects were intubated and underwent right posterolateral thoracotomy prior to impact. Study cohorts numbers, nominal impact velocity, penetration depth, and sample size are provided in Table VI-1. Impacts were administered with the electronic Cortical Contusion Impact device, model eCCI (Custom Design and Fabrication, Richmond, VA).

Table VI-1. Test matrix for final impact experiments.

Group	Description	Nominal Impact Velocity (m/s)	Nominal Penetration Depth (mm)	Sample (n)
1	Severe	6.0	5.0	11
2	Intermediate	1.5	5.0	9
3	Intermediate	6.0	2.0	6
4	Mild	1.5	2.0	6
5	Sham	-	-	8
			Total Sample =	40

A custom-designed anvil and load cell unit that was specifically designed for the eCCI was used to collect force data during the impact experiments. This new anvil had the same impacting surface area (6.35 mm diameter) as the previous anvil. An aluminum housing held a piezoelectric crystal and was attached to the piston of the eCCI via ¼-28 threading. This load cell exhibits a high frequency response and is robust enough to be used with the piston without the use of a shock mitigation device. A charge amplifier was supplied with this load cell. Details of this anvil and load cell unit can be found in the Appendix, Section A.3. Force data were collected at 500 kHz using the same protocols as described in Gayzik et al., (2007). An updated version of the WaveView software (version 7.14) was used to collect data in conjunction with a WaveBook 516E (Iotech, Cleveland, OH).

Force vs. Displacement data reduction

Data was reduced using the methods described in Gayzik et al., (2007). All data were filtered using the SAE J211 protocol. The filter class varied between impacts. Data from Groups 1 and 3 were filtered to 2 kHz, while data from Groups 2 and 4 were filtered to 1 kHz. Data were inertially compensated according to the load cell manufacturers'

specifications (Appendix, Tables A-3 and A-4). Mean plus-or-minus one standard deviation corridors were calculated for all traces. Impact velocity was recorded from the eCCI control unit. Lung displacement was determined by multiplying the total loading time from the force vs. time trace by the impact velocity. Previous research has demonstrated that the eCCI piston velocity remains essentially constant during the impact sequence.[1] Impact energy was determined through integration of the force vs. deflection traces.

An additional processing step was taken to develop the curves that were used in the objective function of the concurrent optimization. This procedure was done on a group by group basis. The purpose of this step was to ensure that integrating the force vs. deflection trace used in each group's objective function as the 'optimal' trace (see Equation VI-1) yielded the same amount of energy as the average energy from the impact experiments. To accomplish this, the average force value was calculated at each data point, starting at the initiation of loading (loading D = 0) until the end point of the trace with the least lung penetration. From this point on, the curve was linearly extended based on the average slope of the last 100 data points. Curves were extended until the integration of the average force vs. deflection trace was equal to the average energy of the impact group.

CT scanning was conducted using a Light Speed Pro CT scanner (GE Medical Systems, Minneapolis, MN) according to the scanning matrix in Table VI-2. The scanning protocol remained unchanged from the previous work (Table IV-4). Subjects were scanned four at a time using a rodent imaging and sedation enclosure.[1] Image sets were segmented using Mimics v. 11.0 (Materialise, N.V., Lueven, Belgium) according to

the semi-automated segmentation protocol described in Chapter IV.[1] The normalized fraction of high radiopacity lung (HRL) was calculated by dividing the volume of contused lung tissue determined in the segmentation process (voxels exceeding HU = -351) by the total lung volume. This procedure was repeated for the left and right side.

Table VI-2. CT Scanning matrix for final impact experiments.

Group	Description	Total n	Sub-group n	Scan time post-impact		
				24 hours	48 hours	1 week
1	Severe	11	6	●	●	●
			5	●		
		Total scans at time point →		11	6	6
2	Intermediate	9	4	●	●	●
			5	●		
		Total scans at time point →		9	4	4
3	Intermediate	6	4	●	●	●
			2	●		
		Total scans at time point →		6	2	2
4	Mild	6	6	●	●	●
			-			
		Total scans at time point →		6	6	6
5	Sham	8	4	●	●	●
			4	●		
		Total scans at time point →		8	4	4

Statistical tests were conducted on the study results. Tests were conducted to determine if significant differences *between* study cohorts existed for impact energy, peak impact force, impact velocity, and lung displacement using one-way ANOVA. Values of normalized HRL (of the struck lung) at 24 hours, 48 hours and 1 week post-impact were compared *between* study cohorts, also using ANOVA. Tukey's post hoc test was used for pair-wise comparisons of these results. Pair-wise comparisons of HRL *within* cohorts at different time points were conducted using Student's t-tests. All statistical analyses was performed using SAS v. 9.1, (The SAS Institute, Cary, NC) with a significance level of $\alpha = 0.05$. Linear regressions were conducted using Matlab (The MathWorks, Natick, MA). HRL values were regressed onto impact parameter values at 24 hours, 48 hours

and 1 week post-impact. Significance for these regressions were also based on $\alpha = 0.05$. Slope, intercept, R^2, and p-values were reported for all significant regressions.

Computational methods

This section reviews the computational methods used to 1. conduct the concurrent optimization, 2. conduct the design of experiments (DOE) study, and 3. determine the final injury metric values. The finite element model was developed from CT scans of a healthy male rat.[2] Details on this development can be found in Chapter III. The final mesh consists of the right lung, left lung, and tissues to represent mediastinum, heart, and trachea. The mesh also has a sheath to represent the outer chest wall and diaphragm, which was modeled as a rigid boundary with sliding contact.

Model validation

Validation of the model was a combined approach focused on optimization of the material model, investigation of parameter sensitivity, and quality checks of the model once the final parameter values were obtained. Discrepancies between simulations employing the parameters presented in Chapters III and IV, and the experimental force versus displacement histories acquired for this study required that the material model parameters be optimized.

A multi-island genetic algorithm (MIGA) implemented in iSight software, v. 10.0 (Engineous, Cary, NC) was used to optimize the model response. Details of this algorithm can be found in Chapters III and IV (Table III-3). The optimization routine in this case was a concurrent optimization because the objective function was formulated to minimize error from two distinct simulations. The first was a simulation of the impact

applied to Group 1, the second was a simulation of the impact applied to Group 2. The objective function is described in Equation VI-1. These groups were severe and intermediate impacts respectively.

$$S = \sum \left(F_{Sim,Group1}(\vec{\beta}_{1-6}) - F_{Opt,Group1} \right)^2 + \sum \left(F_{Sim,Group2}(\vec{\beta}_{1-6}) - F_{Opt,Group2} \right)^2 \qquad \text{Equation VI-1}$$

Here, the objective function is a two-term sum of squared error function. Error is calculated between the simulated force trace, F_{sim}, which is a function of the current parameter set, and the optimal force trace, F_{opt} based on the experimental findings for the impacts in a particular Group. The optimization was initialized using the parameters in Chapter III (Table III-7). This set was selected because it was the results of optimizing the model for an impact administered at 2.8 m s^{-1}, a velocity in the middle of the impacts of Group 1 (6.0 m s^{-1}) and Group 2 (1.5 m s^{-1}). A total of 4000 model runs were conducted in the optimization (2000 for each model), and the procedure required roughly 30 hours to complete. The optimization trial was run on a PC (Dell Optiplex GX620, Pentium D, 3 GHz processor with 3.5 GB ram). LS-Dyna build 971 (LSTC, Livermore, CA) was used for the finite element simulation. The entire model optimization was run two times to give confidence that a global minimum had been achieved.

Two design of experiment (DOE) parameter studies were conducted following the concurrent model optimization. The parameters used as the basis of the DOE study were the optimal parameters determined in the concurrent trial. Each study required an additional 500 model runs. The purpose of the DOE study was to reveal which parameters have the largest effect on a desired model response. The DOE calculated the effect that material model parameters had on absorbed energy (integration of force vs.

deflection). The design space was bounded by +/- 50 % of the optimized parameter values. Parameter sensitivity was examined via Pareto plot.

Additional model quality checks were performed on the validated (optimized) model. The ratio of hourglass energy to the sum of kinetic and potential energy was determined for both the Group 1 simulation and Group 2 simulation. Plots depicting the optimized force vs. deflection traces from the FEA with the experimental corridors are presented and finally the energy of the simulated impacts were compared to the average energy for each cohort.

Methods for determining injury metrics

The first step in the process of determining the injury metrics was to run the simulations corresponding to the four impacts in Table VI-1 using the validated material model. Following this, the maximum value for a given variable of interest was determined on an element by element basis using a Matlab program developed in house. This procedure is outlined in greater detail in Chapter IV. Data was imported to Matlab from the LS-Dyna *elout* file. Based on the findings of Chapter IV, only three variables of interest were calculated using this approach, they were the product of first principal strain and strain rate, ($\varepsilon_{max} \cdot \dot{\varepsilon}_{max}$), first principal strain (ε_{max}), and first principal strain rate ($\dot{\varepsilon}_{max}$). These three variables were previously found to have the best agreement with the location and spatial distribution of the observed HRL.[1]

The maximum values of these variables for each element were then plotted against their element volume and arranged in descending order to create the cumulative volume plots that are the basis for determining the injury thresholds. Using these plots, the percentage of HRL for each subject (at a given time point, i.e. 24 hours) was used to

determine the corresponding threshold. These individual threshold values were then averaged to determine the finite element based injury metrics for pulmonary contusion. A detailed example of this technique is found in the results section. This process was repeated for both the 24 hour and 1 week post-impact values of HRL.

VI.3. Results

Experimental results

Force versus displacement by Group are shown in Figure VI-1. In these plots, individual test numbers are labeled. The impact experiments are summarized in this Chapter's appendix in Table VI-10 on page 194. Impacts where contact with the chest wall occurred were excluded from the remainder of the study. Mean traces with one standard deviation corridors are shown in Figure VI-2.

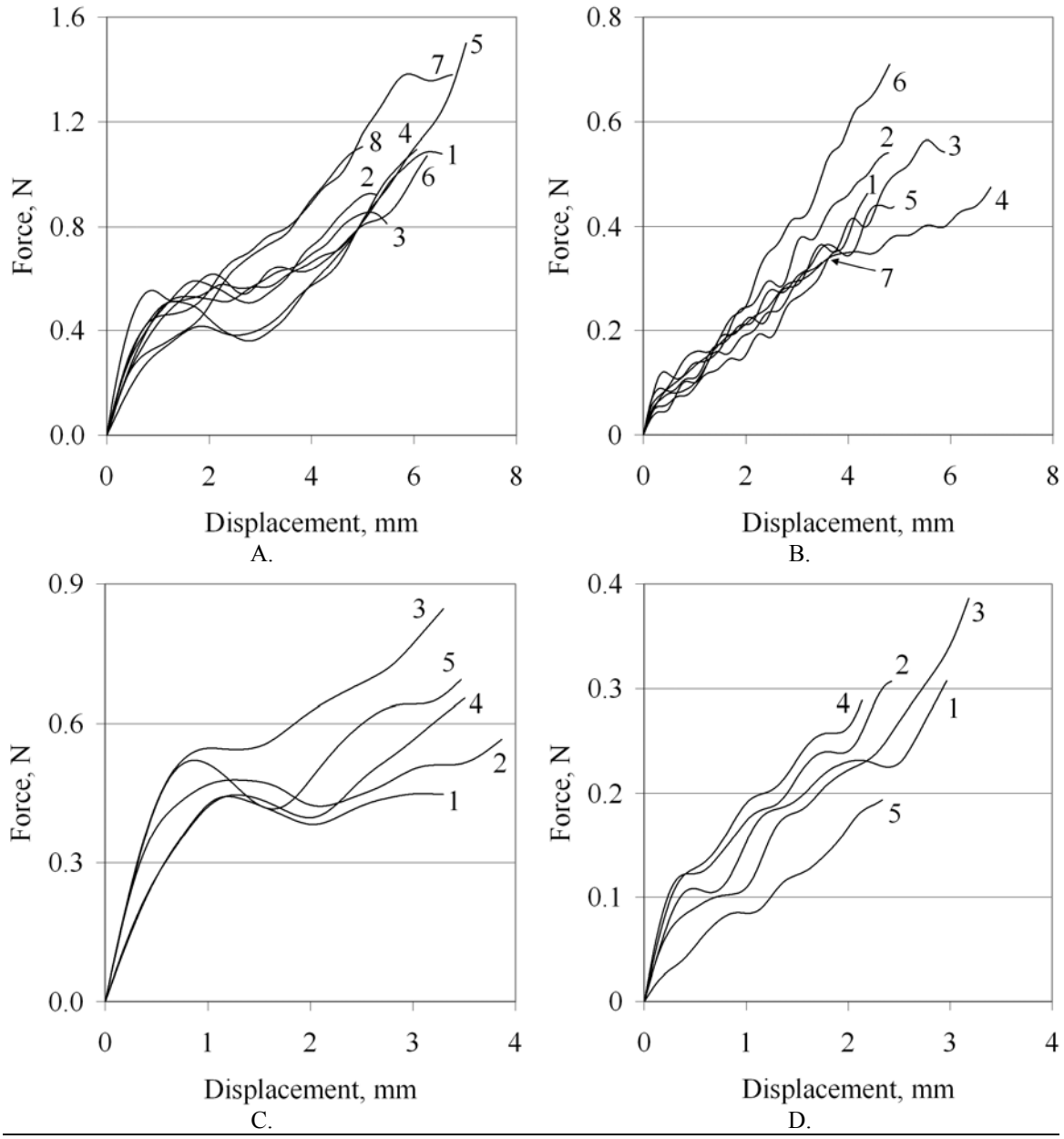

Figure VI-1. Force vs. displacement traces for impact experiments. A. Severe (Group 1; V = 6.0 m/s, D = 5 mm), B. Intermediate (Group 2; V = 1.5 m/s, D = 5 mm), C. Intermediate (Group 3; V = 6.0 m/s, D = 2 mm), D. Mild (Group 4; V = 1.5 m/s, D = 2 mm). Velocity and depth of penetration are nominal values for groups.

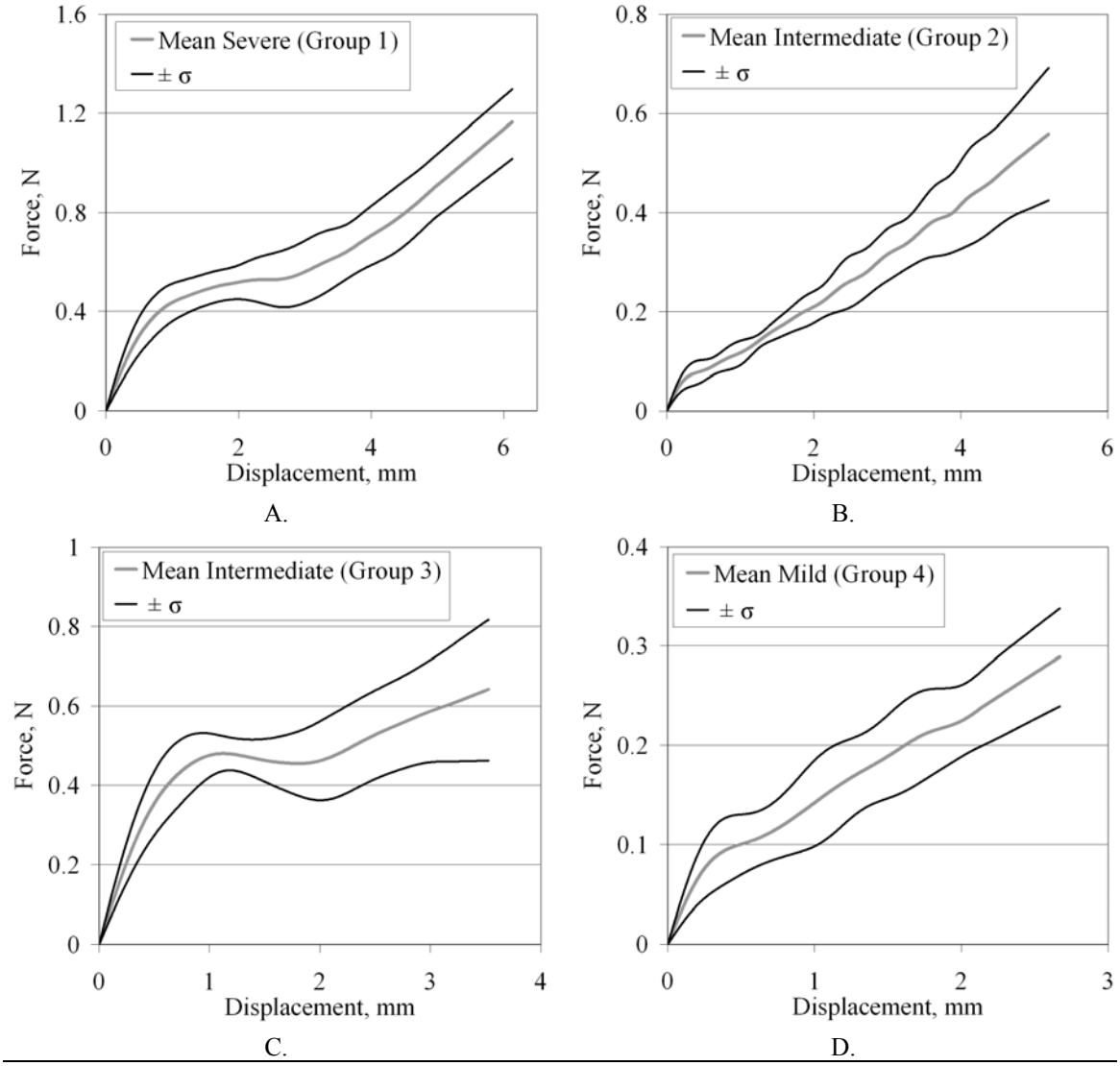

Figure VI-2. Mean force vs. displacement traces for impact experiments showing one standard deviation corridors. A. Severe (Group 1; V = 6.0 m/s, D = 5 mm), B. Intermediate (Group 2; V = 1.5 m/s, D = 5 mm), C. Intermediate (Group 3; V = 6.0 m/s, D = 2 mm), D. Mild (Group 4; V = 1.5 m/s, D = 2 mm). Velocity and depth of penetration are nominal values for groups.

Figure VI-3A shows the mean traces and standard deviation error bars for all groups on the same axes. As expected, Groups 1 and 3 overlap for the initial 2.5 mm of the impact. Similar behavior is observed in Groups 2 and 4. All cases demonstrated slight overshoot from the nominal deflection. This is exacerbated for the high velocity impacts. Table VI-3B shows the mean traces from Group 1 and 2 prepared for use in the optimization algorithm. Again, one standard deviation corridors are shown.

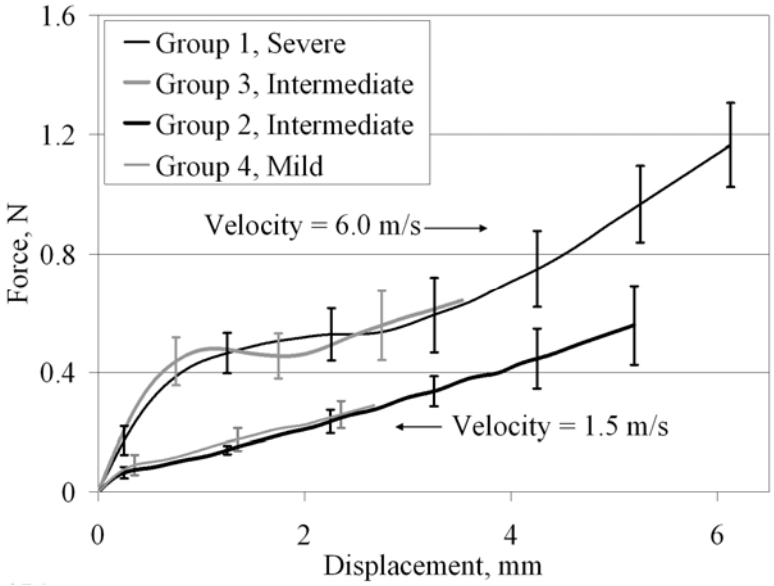

A.

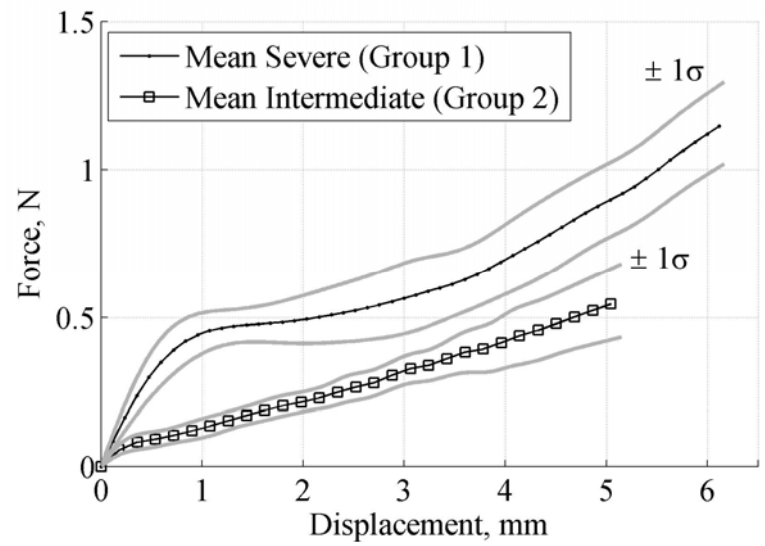

B.

Figure VI-3. A. Mean force vs. displacement for all cases showing one standard deviation error bars. B. Mean force vs. displacement traces used in Multi-Island Genetic Algorithm for concurrent optimization. One standard deviation corridors are also shown.

A summary of the impact experiment results is found in Table VI-3. This table shows the mean velocity, displacement, peak force, and absorbed energy from each study cohort. The data in table is graphically presented in Figure VI-4 (velocity and displacement) and Figure VI-5 (force and energy). Results from the ANOVA between each cohort are presented graphically in the latter figures. The variables input to the

eCCI control module (velocity and displacement) show significant differences between paired groups as intended. Impact energy in Group 1 was greater than all other groups. Groups 2 and 3 were not significantly different with regards to impact energy. All groups exhibited greater impact energy than the mild cohort. Full results from these ANOVA tests can be found in this chapter's appendix, beginning on page 200.

Table VI-3. Summary of impact experiment results, showing mean, standard deviation and coefficient of variation of velocity, displacement, and force for all groups.

Group	n	Velocity, m/s		Displacement, mm		Peak Force, N		Absorbed Energy, mJ	
		μ ± σ	COV	μ ± σ	COV	μ ± σ	COV	μ ± σ	COV
1	8	6.01 ± 0.070	1.2	6.04 ± 0.736	12.2	1.13 ± 0.215	19.1	3.88 ± 0.883	19.1
2	7	1.51 ± 0.022	1.5	5.24 ± 0.900	17.2	0.53 ± 0.112	21.1	1.46 ± 0.403	21.1
3	5	5.98 ± 0.041	0.7	3.48 ± 0.230	6.6	0.64 ± 0.148	23.0	1.62 ± 0.262	23.0
4	5	1.5 ± 0.0089	0.6	2.65 ± 0.429	16.2	0.3 ± 0.0684	23.0	0.45 ± 0.143	23.0

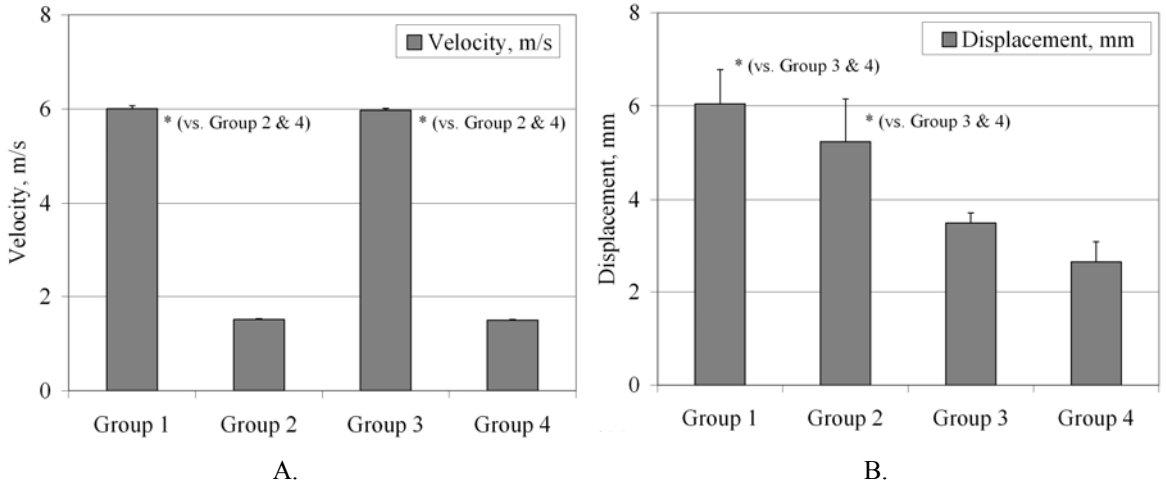

Figure VI-4. Velocity (A) and displacement (B) by cohort groups (Table VI-1). Significant differences are noted. ANOVA, p = <0.0001 for velocity comparisons and p = <0.0001 for displacement comparisons.

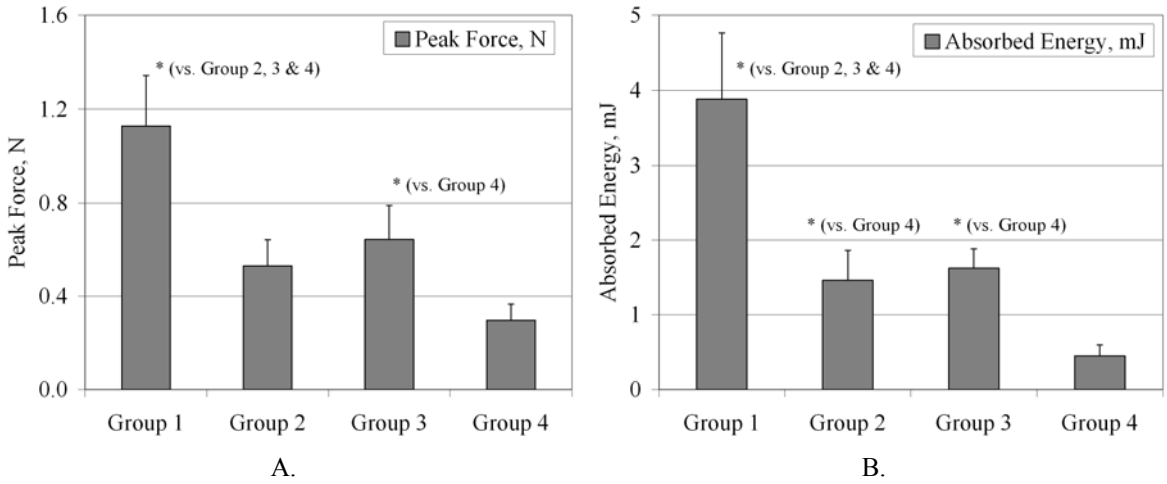

Figure VI-5. Peak force (A) and energy (B) by cohort groups (Table VI-1). Significant differences noted. ANOVA, p = <0.0001 for peak force comparisons and p = <0.0001 for energy comparisons.

At this time, we transition from examining the impact data to examining the resulting image data. Figure VI-6 begins this transition showing the rendered lung mask from subject #1 (Table VI-11). This mask was smoothed using an algorithm in the Mimics v 11.0 software package, with a smoothing factor of 0.5 and 100 iterations.

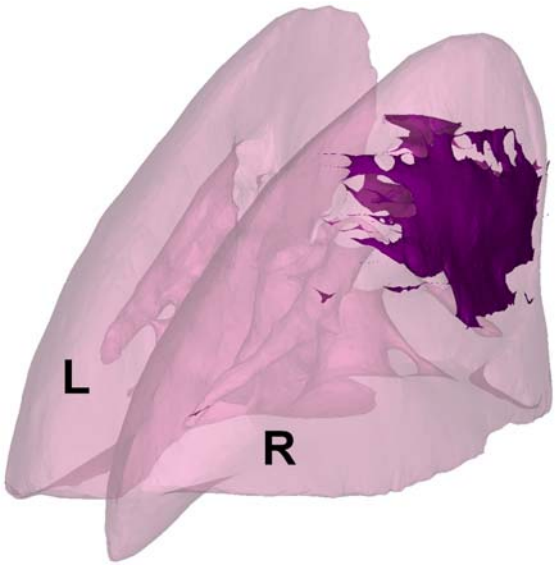

Figure VI-6. Smoothed rendering of a study subject (#1, Severe impact group) viewed posterolaterally showing right and left lungs, and contusion volume (shaded portion).

A summary of the CT segmentation image data by Group and post impact time point is provided in Table VI-4. Sample numbers in this table indicate the number of individuals used in calculating the mean and standard deviation. Table VI-11 through Table VI-13 in the appendix (beginning on page 195) provide all data relative to the segmentation of the scans acquired for this study. Scans where motion artifacts were severe were not included in the calculations of mean HRL. Excluded scans are noted in these tables. The data in Table VI-4 is presented graphically in Figure VI-7. The results from the ANOVA between study cohorts for the 24 hour post-impact time point are shown graphically in Figure VI-7 and found in Table VI-14 in this chapter's appendix. Only the 24 hour post-impact time point demonstrated significant differences between cohorts ($p = 0.0048$). At 24 hours post-impact, Group 1 (severe impact) exhibited significantly greater HRL than groups 2, 4 and 5 (the sham group). The remaining groups did not exhibit significantly elevated HRL from the sham group at 24 hours via ANOVA, although pair-wise t-tests revealed mild significance between Group 2 and the sham group ($p = 0.07$) and significant differences between Group 3 and the sham group ($p =0.04$). The mean values of HRL at 48 hours and 1 week post-impact are shown in Figure VI-8. HRL values approached significance at the 48 hour time point (ANOVA, $p = 0.12$), but not at 1 week (ANOVA, $p = 0.29$). Decreasing values of HRL and wider standard deviations hindered finding significant differences between cohorts at these time points.

Table VI-4. Summary of CT image segmentation results, showing mean, standard deviation and coefficient of variation for percent high radiopacity lung for all groups. Number of scans used in calculation of mean values is provided for all time points.

Group	% High Radiopacity Lung 24 Hours			% High Radiopacity Lung 48 Hours			% High Radiopacity Lung 1 Week		
	n	μ ± σ	COV	n	μ ± σ	COV	n	μ ± σ	COV
1	8	9.21 ± 4.89	53.1	4	5.51 ± 3.72	67.4	4	3.89 ± 4.36	111.9
2	6	4.26 ± 1.93	45.3	2	5.11 ± 5.09	99.6	2	0.92 ± 1.17	126.7
3	4	5.01 ± 2.38	47.5	3	1.63 ± 0.88	53.7	3	1.45 ± 0.59	40.7
4	5	3.401 ± 2.33	68.6	5	2.11 ± 1.46	69.3	5	0.91 ± 0.98	108.2
5	7	2.66 ± 1.61	60.3	3	0.71 ± 0.33	47.0	3	0.26 ± 0.29	108.0

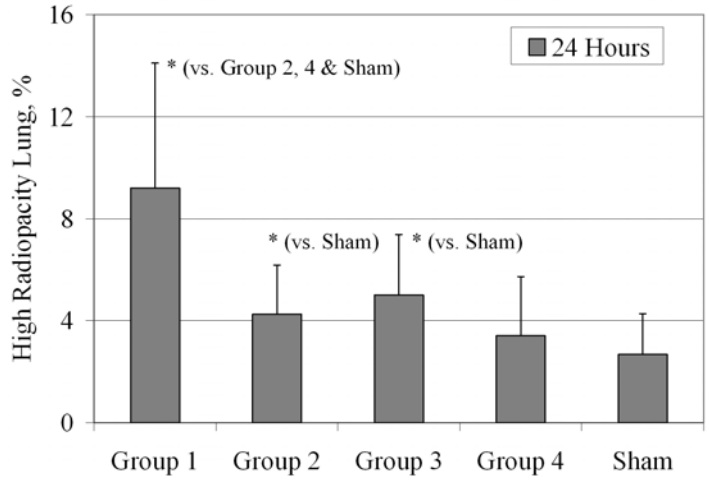

Figure VI-7. Percentage of high radiopacity lung in the struck lung by cohort groups at 24 hours post impact. Significant differences between cohorts are noted.

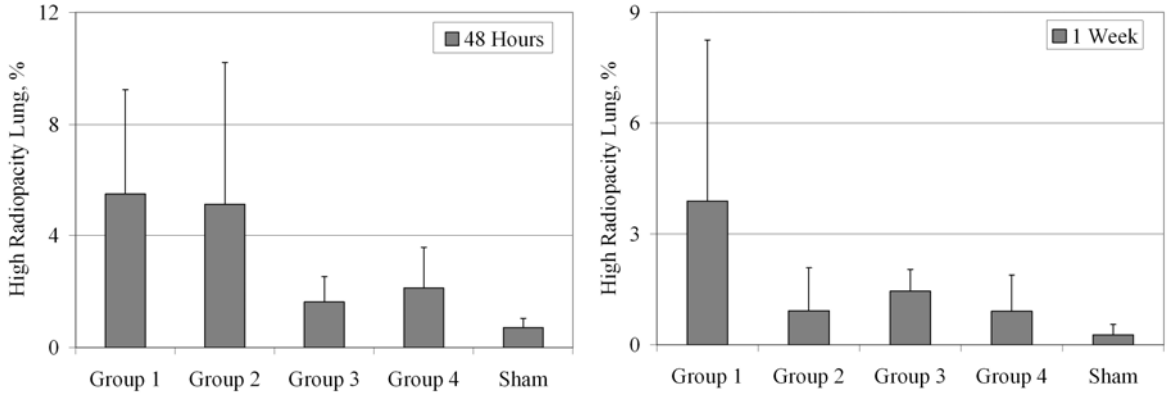

Figure VI-8. Percentage of high radiopacity lung in the struck lung by cohort groups at 48 hours and 1 week post impact.

Figure VI-9 shows the HRL for all Groups for all time points. Significant reductions in HRL are identified (t-test, $\alpha = 0.05$). P-values for these tests are found in Table VI-19 on page 201 in this chapter's appendix. The value of HRL at 1 week post-impact was significantly less than the value at 24 hours in most Groups at a significance level of $\alpha = 0.05$. The exception was the decrease in Group 1, which was mildly significant, $p = 0.09$. The 48 hour time point shows a transitional quality, in some cases the value is significantly less than the HRL value at 24 hours (Group 3) and in others, HRL lung actually increases (Group 2).

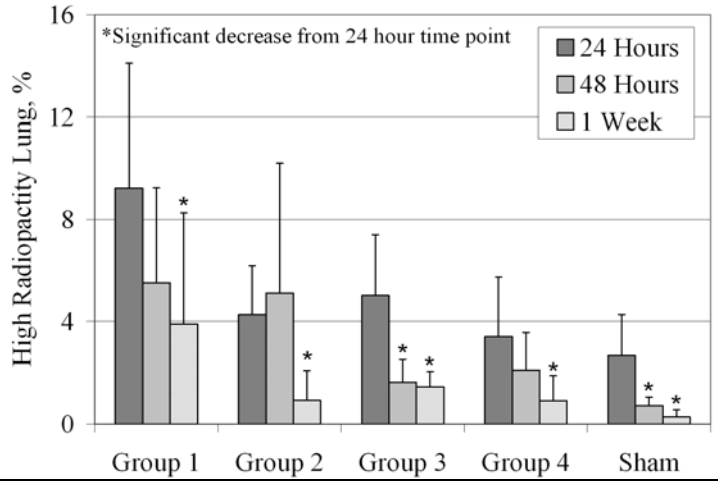

Figure VI-9. Percentage of high radiopacity lung in the struck lung by cohort groups and time point. Significant differences between cohorts are noted. Student's t-test was used for pair-wise comparisons, $\alpha = 0.05$. (Table VI-19).

The results of the linear regression of HRL at 24 hours onto impact variables are shown in Figure VI-10. While the coefficient of determination (R^2), does not approach one for any of the plots shown in this figure, the regressions are significant ($p < 0.05$) in all cases. This indicates that while none of these variables alone account for the resulting volume of HRL, all are significant factors. Peak force of the impact showed the best correlation, with a $p = 0.003$. The slope and intercept of these relationships are provided in Table VI-5. Regressions at both later time points did not yield significant results, but

the plots for these are found in the appendix of this chapter, in Figure VI-21 and Figure VI-22.

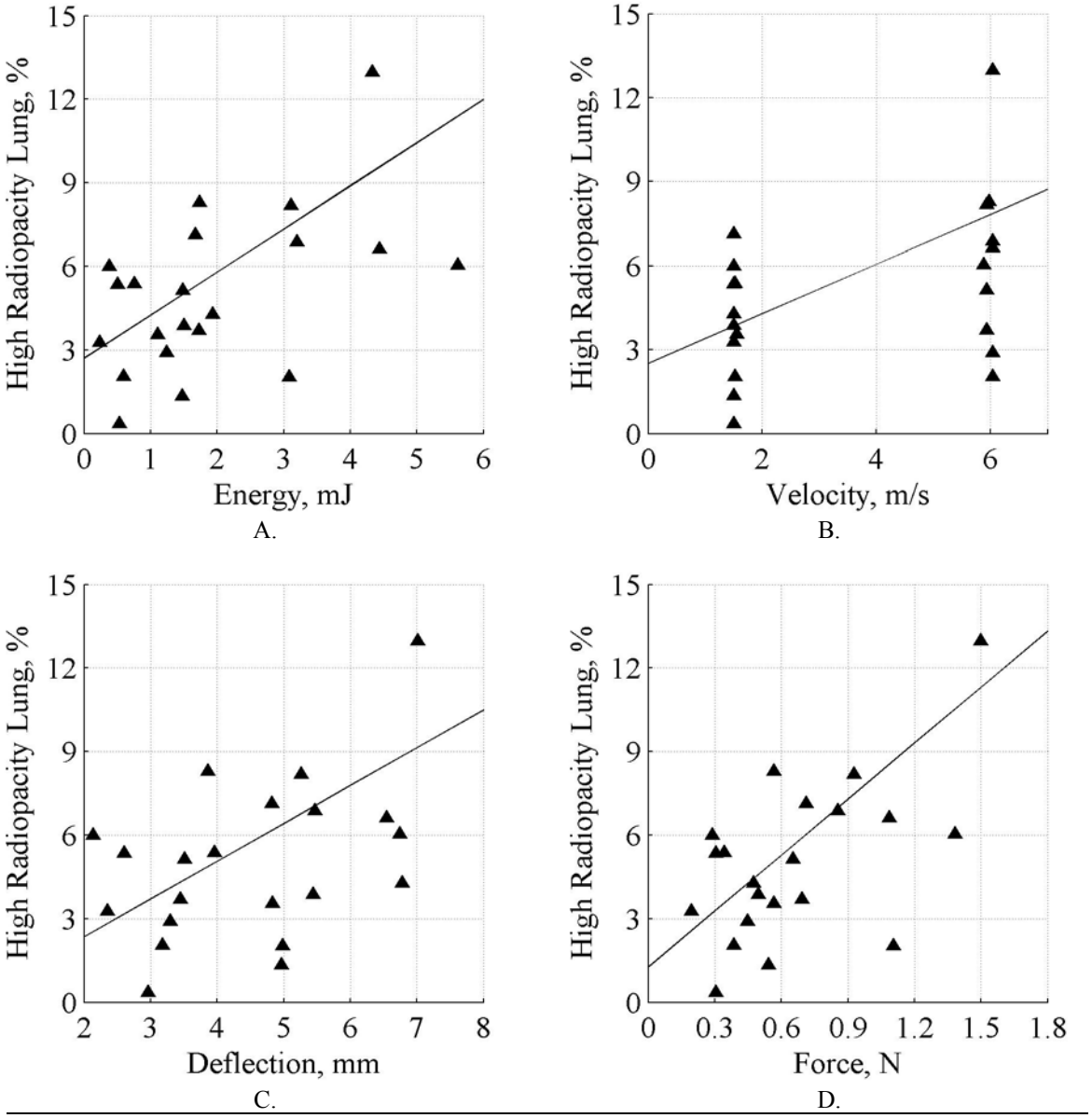

Figure VI-10. Normalized high radiopacity lung (percent of struck lung) vs. A. Absorbed energy, B. Impact velocity, C. Displacement, D. Peak Force during impact. All traces are from 24 hour post-impact scans.

Table VI-5. Summary of linear regression analysis of high radiopacity lung (HRL) vs. impact experiment parameters. Significant relationships are highlighted. Slope, m (% HR Lung / unit) and intercept, b (% HRL) are provided for significant relationships.

		Absorbed Energy, mJ	eCCI Velocity, m/s	Peak Displacement, mm	Peak Force, N
24 Hours	p	**0.005**	**0.014**	**0.027**	**0.003**
	R^2	0.31	0.26	0.21	0.35
	m	1.55 % HRL/ mJ	0.885 % HRL/ (m/s)	1.36 % HRL/mm	6.70 % HRL/mm
	b	2.70 % HRL	2.52 % HRL	-0.359 % HRL	1.26 % HRL
48 Hours	p	0.272	0.584	0.106	0.101
	R^2	0.10	0.03	0.20	0.21
1 Week	p	0.120	0.153	0.109	0.050
	R^2	0.19	0.16	0.20	0.28

Computational Model Results

In this section, we review the results from the computational aspects of this study, including the finite element injury metrics derived from this data. Figure VI-11 graphically summarize the results of the concurrent optimization, with part A showing the results from the simulation of the severe impact (Group 1) and part B showing the results from the intermediate impact (Group 2). Impact traces are shown with 1 standard deviation and two standard deviation corridors. Improved instrumentation led to more repeatable impacts and lower standard deviations. An inertial response over roughly the first third of the simulation causes the model response to actually exit the corridors briefly in both simulations. This discrepancy is minor however, and overall the model appears to be well-validated. As noted in Table VI-6, the input parameters describing the boundary conditions and the impact energy are within one standard deviation of the experimentally observed values for both Groups.

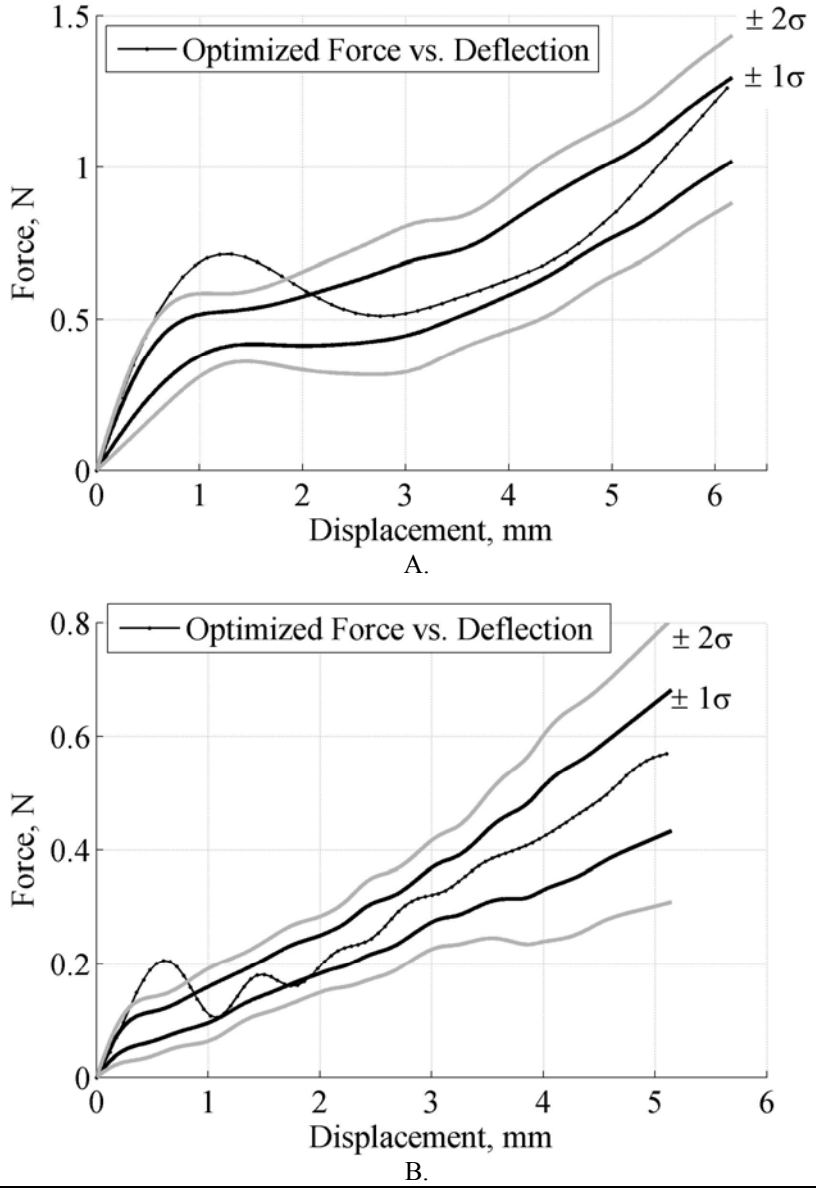

Figure VI-11. Optimized force vs. displacement traces from model for severe (Group 1, V = 6.0 m/s, D = 5 mm) and intermediate (Group 2, V = 1.5 m/s, D = 5 mm) impact scenarios.

Table VI-6. Velocity, displacement and impact energy from impact experiments and corresponding simulation values by group.

Group	Mean Input & Output Variables	Experimental Average	Simulation Value
Group 1	Velocity, m/s	6.01 ± 0.070	6.00
	Peak Displacement, mm	6.04 ± 0.736	6.16
	Impact Energy, mJ	3.88 ± 0.883	4.47
Group 2	Velocity, m/s	1.51 ± 0.0223	1.50
	Peak Displacement, mm	5.24 ± 0.900	5.12
	Impact Energy, mJ	1.46 ± 0.403	1.50
Group 3	Velocity, m/s	5.98 ± 0.041	6.00
	Peak Displacement, mm	3.48 ± 0.230	3.58
	Impact Energy, mJ	1.62 ± 0.262	2.19
Group 4	Velocity, m/s	1.5 ± 0.0089	1.50
	Peak Displacement, mm	2.65 ± 0.429	2.77
	Impact Energy, mJ	0.45 ± 0.143	0.54

The material parameters determined through the concurrent optimization are provided in Table VI-7. This parameter set should be used in subsequent modeling efforts since it has been validated in multiple impact scenarios. The values of these parameters relative to values in the literature by Vawter et al. and those used by Stitzel and Gayzik et al (2005) are presented in Figure VI-12. The results of the two design of experiment (DOE) studies conducted are shown in Figure VI-13. DOE studies were conducted (one for the Group 1 simulation and another for the Group 2 simulation) to examine how parameters sensitivity affects impact energy. Commentary on the relative scaling of these parameters and the implications of the DOE are reserved for the discussion.

Table VI-7. Material model parameters resulting from concurrent optimization.

Description	Optimized Value	Description	Optimized Value
Density, ρ (g mm^{-3})	1.180×10^{-4}	Curve fit parameter, C (N mm^{-1})	0.239×10^{-3}
Bulk Modulus K (N mm^{-2})	0.8485×10^{-1}	Curve fit parameter, α	6.292×10^{-1}
Mean alveolar diameter, Δ (mm)	0.0702	Curve fit parameter, β	-1.143
		Curve fit parameter, C1 (N mm^{-1})	2.20×10^{-5}
		Curve fit parameter, C2	1.42

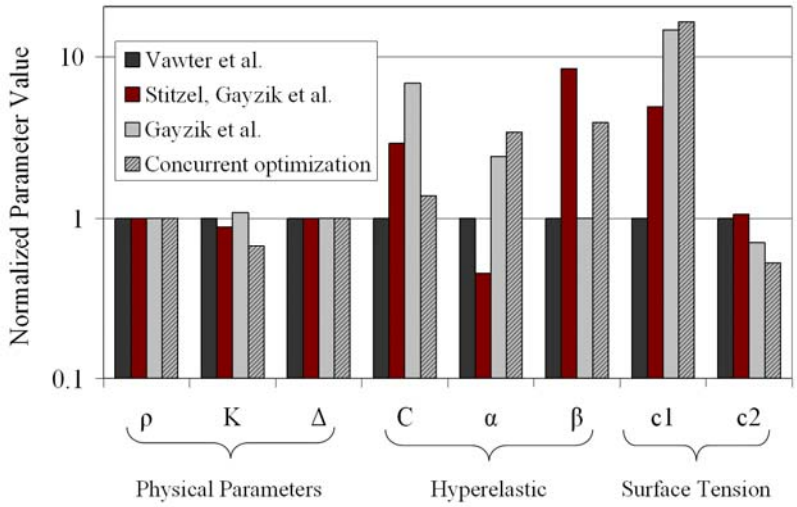

Figure VI-12. Normalized values of hyperelastic lung model material parameters from Vawter et al. (1980), Stitzel, Gayzik et al. (2005), Gayzik et al. (2007) and the concurrent optimization.

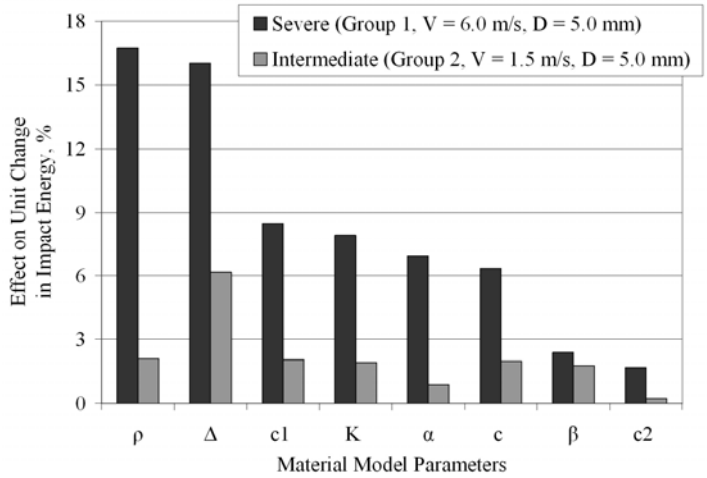

Figure VI-13. Pareto plot showing the effect material property parameters have on a unit change in impact energy.

The optimization routine was run a second time (an additional 4000 model executions) to verify that the parameters resulting from the first trial indeed represented a global minimum for the search space. The results of this repeated trial are found in Table VI-8. Nearly all parameters were identical, with the exception of α, which was within 3% of the initial optimization value, giving further confidence in the results.

Table VI-8. Parameter variation between repeated optimization runs.

Parameter	Optimization 1	Optimization 2	% Difference
Bulk modulus, K (N mm^{-2})	0.08485	0.08551	0.77
Curve fit parameter, C (N mm^{-1})	0.000239	0.000239	0.00
Curve fit parameter, α (-)	0.6292	0.6089	-3.33
Curve fit parameter, β (-)	-1.143	-1.143	0.00
Curve fit parameter, c_1 (N mm^{-1})	2.20×10^{-5}	2.20×10^{-5}	0.00
Curve fit parameter, c_2 (-)	-1.42	-1.42	0.00

In addition to verifying the results of the optimization routine itself, checks of the resulting model quality were conducted. Figure VI-14 shows the results of a study of hourglass energy, showing the ratio of the hourglass energy vs. the sum of kinetic and potential energy for the Group 1 and Group 2 simulations. The ratio was greater for the higher velocity simulation. While the energy ratio increases throughout the simulation, it never exceeds 2%. It is generally recommended that this value remain below 5% for the duration of the simulation.

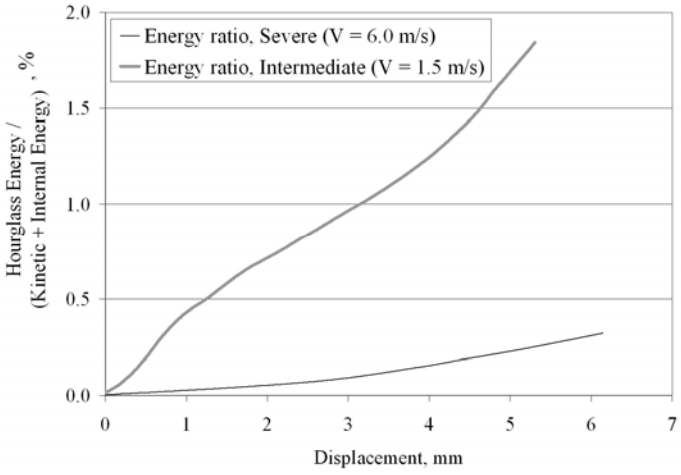

Figure VI-14. Ratio of hourglass energy to the sum of the kinetic and potential energies vs. impactor displacement for the severe impact (Group 1) and intermediate impact (Group 2) simulations.

Figure VI-15 provides an overview of the model execution, with part A showing the model and impactor prior to the initiation of the impact. Following this, windows B and

C show the first principal strain in the model for the mild impact and severe impact respectively. Fringe levels are provided and are scaled equally for both images.

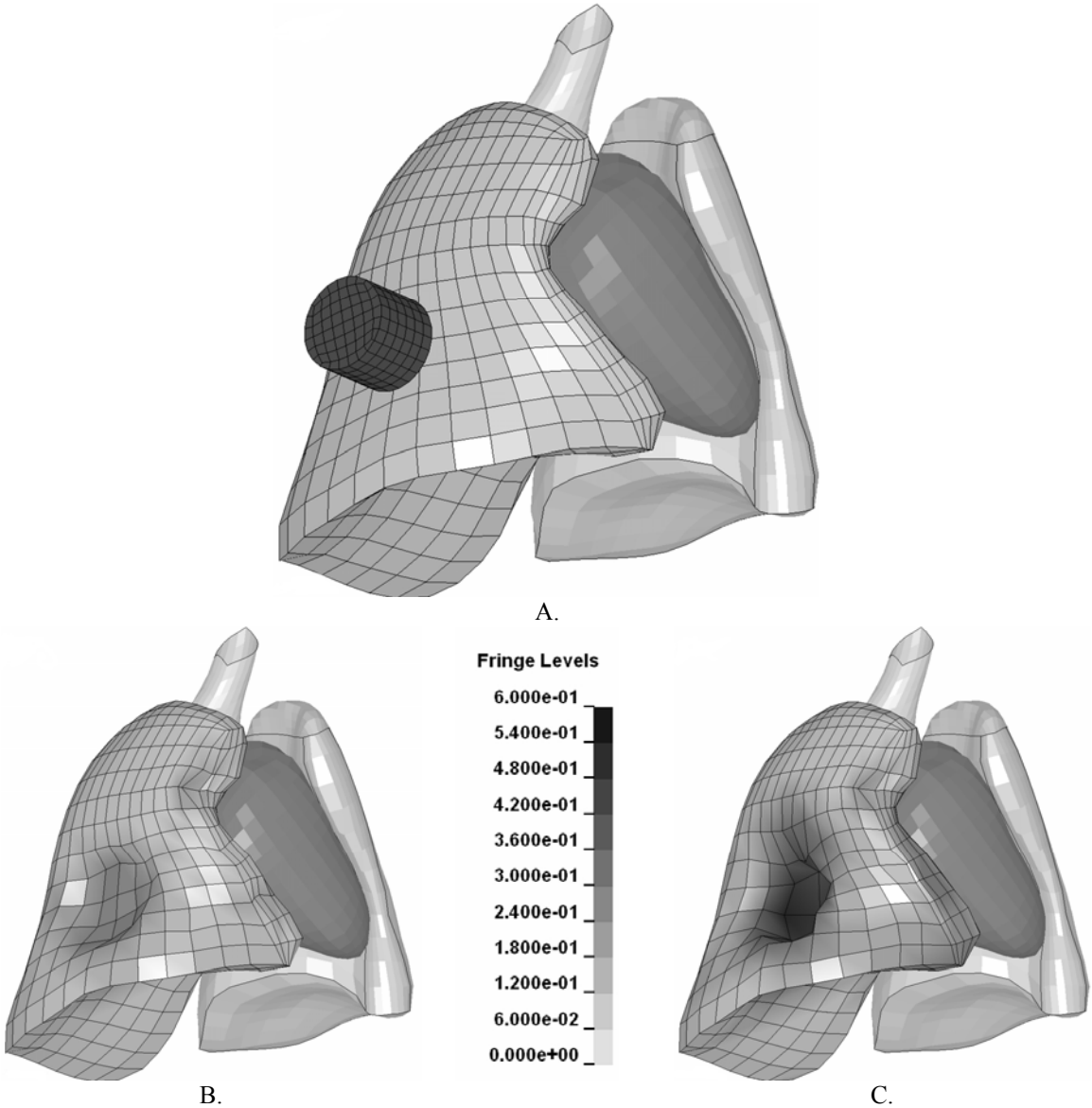

Figure VI-15. Finite element simulation results summary. A. Model with impactor prior to impact initiation, B. Mild impact simulation at maximum penetration, C. Severe impact simulation at maximum penetration.

Determining Injury Metrics

The final aspect of the study was to synthesize the experimental and computational results to determine the finite element-based injury metrics. The procedure for determining these metrics is shown graphically in Figure VI-16.

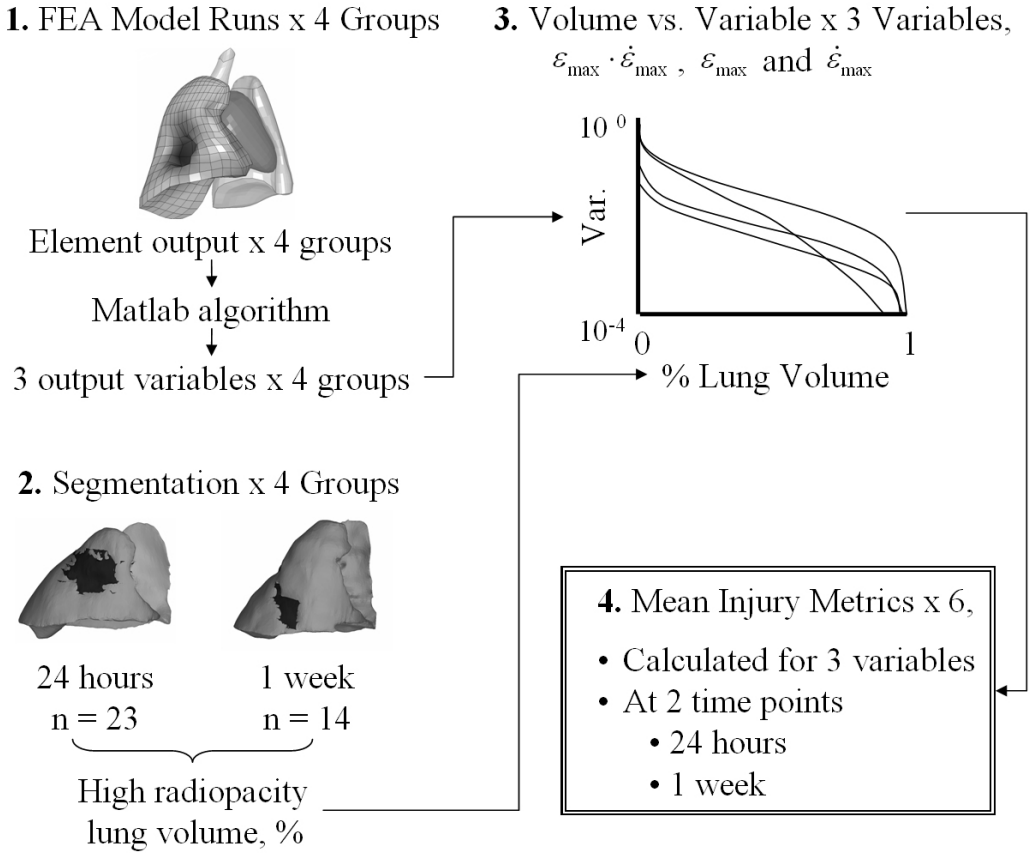

Figure VI-16. Schematic of process used to determine finite element based injury metrics.

The process in Figure VI-16 is briefly reviewed here with references to the study results. The optimized FEA model was run once for each study group (4 model runs, Part 1 of the Figure). The LS-Dyna *elout* file from each simulation was imported into the Matlab algorithm presented in Chapter IV. For each group, for each variable of interest (the product of first principal strain and strain rate, first principal strain, and first principal

strain rate), the algorithm output the maximum value that occurred in each element, and paired it with the element's volume. A total of 12 traces were output (3 variables x 4 groups).

The HRL volumes at 24 hours, and 1 week were then collected (Part 2). This included 23 data points for the 24 hour time point and 14 data points for the 1 week time point. These time points were selected because significant reductions from 24 hours to 1 week were noted for all groups. Next, the threshold for contusion was determined for each individual HRL value by reading the threshold from the output variable vs. lung volume plot (Part 3). One of these plots is shown below in Figure VI-17. Here, the product of first principal strain and strain rate is plotted against cumulative lung volume. The plots for the remaining metrics are found in this chapter's appendix (Figure VI-24).

The following is an example of how one individual threshold was determined. Since study subject #1 (Figure VI-6, Table VI-11) was in the severe impact group, its corresponding threshold for PC would be read from the "Severe" curve in Figure VI-17. The HRL value of 6.6% by volume for this individual corresponds to a $\varepsilon_{max} \cdot \dot{\varepsilon}_{max}$ threshold of 156 sec^{-1}. All other study subjects' corresponding values would be determined this way.

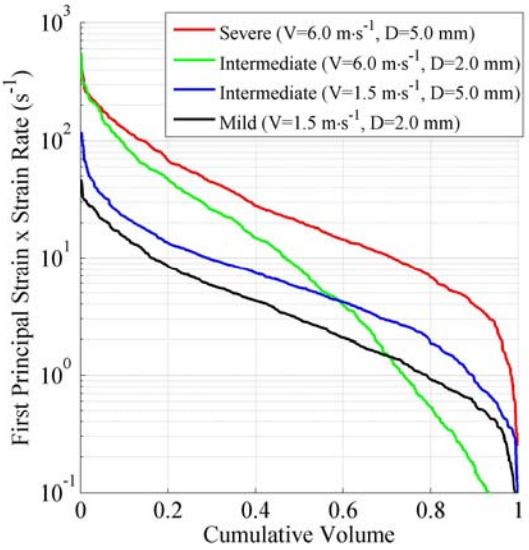

Figure VI-17. Maximum value of the product of first principal strain and strain rate in each element vs. element volume.

In the fourth and final step in this process, the individual thresholds determined through this method were averaged to calculate the mean the injury metrics for each variable. The injury metrics are provided in Table VI-9. Box plots summarizing the range of these variables are provided for all time points and output variables in Figure VI-18.

Table VI-9. Finite element based injury metrics for pulmonary contusion based on first principal strain.

Metric	Mean threshold for 24 hours	Mean threshold for 1 week
Max principal strain · strain rate, $\varepsilon_{max} \cdot \dot{\varepsilon}_{max}$, [sec^{-1}]	94.5	149
Max principal strain, ε_{max}	0.284	0.343
Max principal strain rate, $\dot{\varepsilon}_{max}$ [sec^{-1}]	470	573

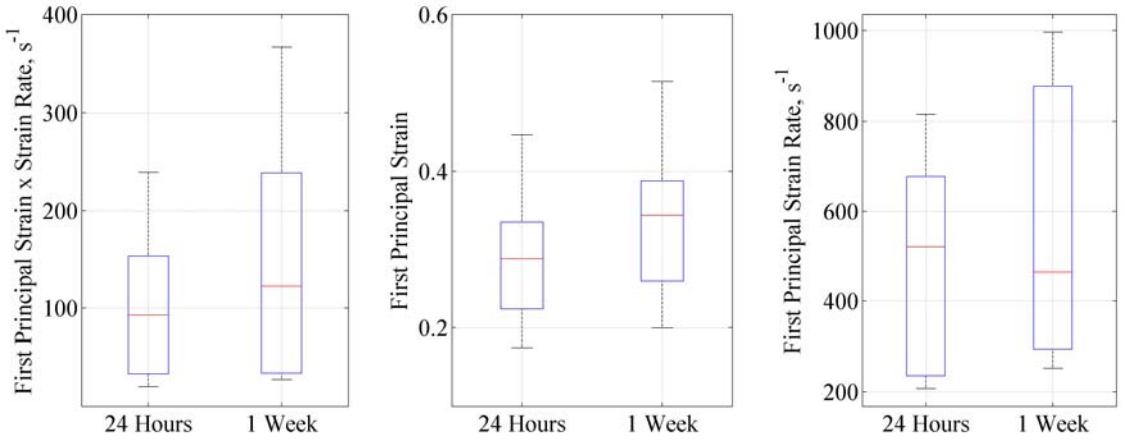

A. B. C.

Figure VI-18. Distribution of finite element-based thresholds for pulmonary contusion for 24 hours and 1 week post impact.

VI.4. Discussion

In this Chapter, finite element-based injury metrics for pulmonary contusion were developed using a combined experimental and computational approach. This approach recognizes that a living model must be used in the study of PC because it is an inflammatory response to blunt force trauma.[7, 8] The injury metrics in Table VI-9 are the culmination of several research studies working towards fulfilling this aim. Figure VI-19 displays the predicted PC in the finite element model and two renderings of the corresponding image data. In this figure, panels B and D show finite element results with elements of predicted contusion shaded. Panels A and C show segmentation results from corresponding study groups.

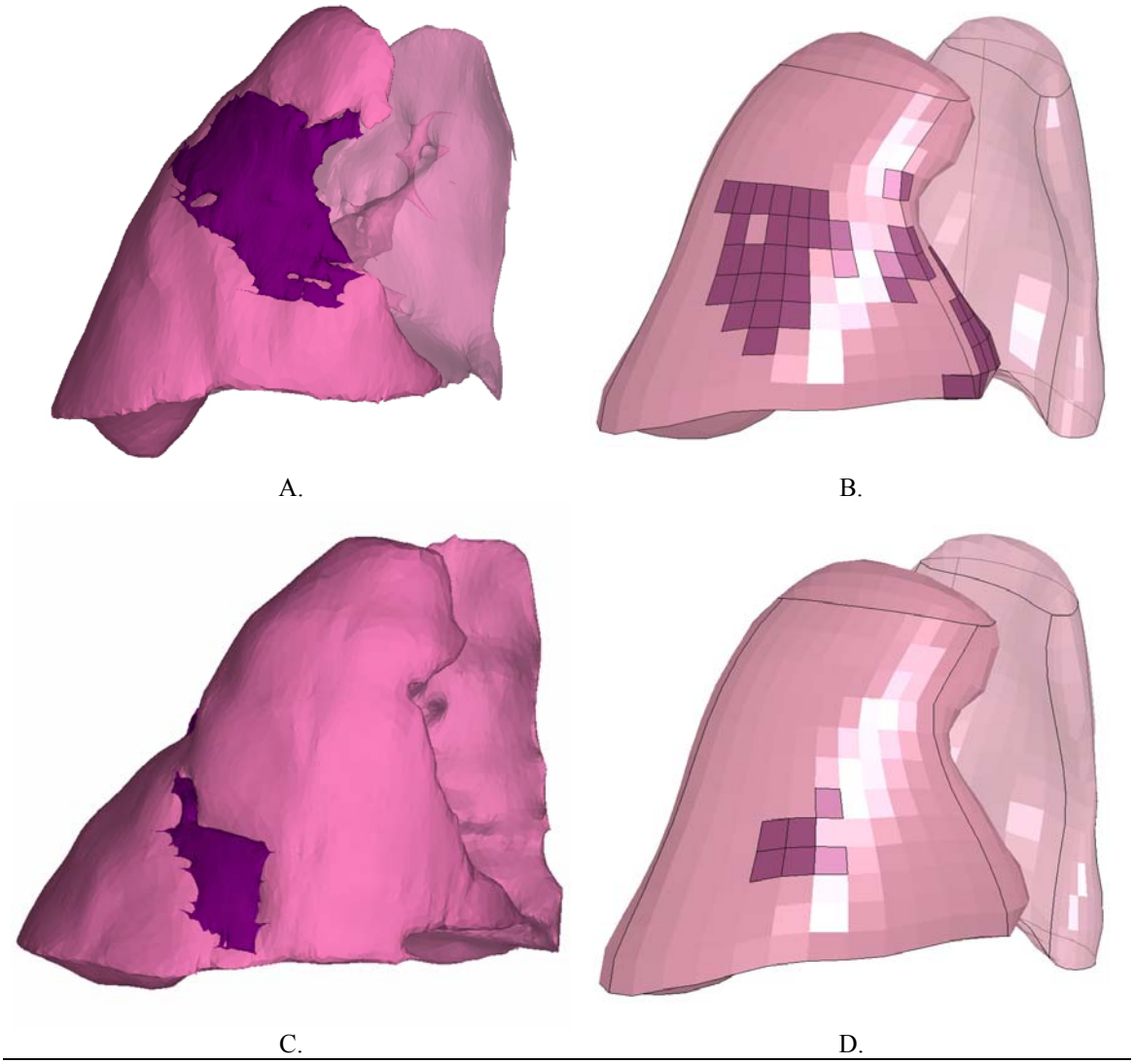

Figure VI-19. Rendering of segmentation masks and corresponding finite element model results. A. Severe (Group 1) impact CT reconstruction, B. Severe impact FEA simulation showing contusion (shaded portion), C. Intermediate (Group 2) CT reconstruction, D. Intermediate impact FEA simulation. Thresholds for strain x strain rate used, Table VI-9.

The metrics presented above in Table VI-9 have several advantages over metrics presented in previous iterations. The first study employing many of these techniques (Chapter III) reported a preliminary first principal strain for PC threshold of 22%. This figure however was based on a volume of HRL from the literature, since normalized values of inflamed lung tissue could not be determined from PET scans. In addition, the sample population of this first study was limited to 5 rats.

The injury metrics presented in Chapter IV were limited in that a single impact scenario was modeled. This scenario is similar to the severe case that was investigated in the present study, however the updated instrumentation used herein yielded tighter force vs. deflection corridors. This is evidenced by a comparison of Figure IV-4 and Figure VI-2. In addition, since the integrated anvil and load cell did not require a shock mitigation device, greater control of the lung displacement was achieved.

This study was able to demonstrate that a rat model of pulmonary contusion can be used to demonstrate significant relationships between impact parameters and the resulting values of HRL. Significant differences in the volume of HRL were noted between study groups at 24 hours post impact. In addition, a number of significant regressions showed that impact velocity, displacement, energy, and peak force all are significant predictors for the volume of contusion. These results have important implications in the study of PC using full human body models.

There is evidence to support the findings that local principal strains and their strain rates are good predictors for this injury. In early lung injury research, Fung et al. reasoned that first principal strain was responsible for an increase in edema in tests using excised rabbit lung tissue.[3] Fung noted that edema increased under quasi static pressure increase. Since the pressure increase was occurring uniformly, he proposed that alveolar rupture at the microscopic scale was occurring in the absence of shear stress, and therefore in a computational sense, principal tensile strains should be the best mathematical predictors. It should be noted however that Fung did not investigate rate effects.

While there are few if any finite element models of the lung for investigating blunt trauma found in the open literature, there have been numerous studies focused on soft tissue injury. Many of these studies are focused on modeling the brain and its behavior under dynamic loading. In surveying the findings of these studies there are again some interesting parallels based on first principal strain. In a study utilizing the Simulated Injury Monitor (SIMON) brain model[9], Takhounts et al. demonstrated that diffuse axonal injury could be correlated to cumulative strain. A similar approach is taken with the lung model in this work, where a diffuse injury, in this case PC, is modeled by determining which elements surpass a particular threshold based on first principal strain. In another study focusing on brain injury, King et al, found that the product of strain and strain rate at the midbrain region provided the strongest correlation to mild traumatic brain injury (MTBI).[10] Strain rate was also a good injury predictor in this study. The authors of the latter study used the Wayne State Head Model. Like King's work, we also utilized the product of strain and strain rate in determining the lung injury metrics. While the injury mechanism between brain and lung injury are vastly different, these parallels are interesting and speak to the utility of using FEA to determine localized injury criteria in soft tissue.

The optimized material model presented in this chapter will be a good basis for continuing research. The model showed good stability in that of the 2000 trials that were run in the optimization trial for each model, only 57 model failures were encountered (3 % of all runs) for the severe impact simulation and 14 model failures (<1% of all runs) were encountered at the low speed simulation.

As this research progressed, variation between optimized parameter sets were noted. This variation is plotted in Figure VI-12. Values in this plot were normalized by the parameters used as the basis for the concurrent optimization presented in this chapter. In order analyze these results it is helpful to break the material model parameters into three groups: 1. Parameters that can be physically quantified and describe the lung, 2. Curve fit parameters that describe the hyperelastic response of the material model (Equation IV-4) and 3. Curve fit parameters that describe the response of the material model due to surface tension of the alveoli (Equation IV-4 and Equation IV-5).

The first group includes the density, ρ, the alveolar diameter, Δ and the bulk modulus, K. These parameters were by and large unchanged by the optimization algorithm because they have been reasonably well quantified through experimental methods.[6, 11] It should be noted that density and alveolar diameter were left out of the optimization routine. The values of the second group of parameters, C, α, and β resulting from the concurrent optimization showed departures from the literature values and the values determined in previous work. The decrease in the relative weight of C is owed to the increase in the weight of c_1. This changing of magnitude correlates to decreasing the effect of the Fung-type hyperelastic term in the strain energy density functional (first term, Equation IV-4) and increasing the effect due to surface tension at the alveolar septa – air interface (second term, Equation IV-4). The increase in the weight of α relative to β places more emphasis on the first strain invariant, which is a function of the principal strains than the second strain invariant which factors in shear effects. This may be a consequence of the type of loading that the material model experiences, which is the most severe along the axis of the impactor. The final group of parameters, c_1 and c_2 also

showed departures from the previous work. The increase of c_1 continues the trend of increasing the relative weight of the surface tension term. The variation of c_2 is considered relatively inconsequential given the results of the Pareto plot, which is discussed in greater detail below.

The design of experiments studies served two important purposes. The first was to show that the computational model is stable despite perturbations of the material parameters. The second was to determine how these perturbations affect the model response. With respect to the former, perturbations of ± 50 % of the optimized values produced no model runs that terminated in error, thus showing good model stability in the region of the optimum. With respect to the latter, impact energy was chosen as the response variable and a Pareto plot showing the effect of each material model parameter was presented (Figure VI-13). The impact energy was chosen since it encompasses the force traces of the impact and is, in effect, an indication of model stiffness.

As expected the effect of the parameters varies between severe and intermediate impact model runs. The parameters that tend to have the largest influence on stiffness of the model are physical descriptors of the lung, i.e., density (ρ), bulk modulus (K) and alveolar diameter (Δ). This relationship is again highlighted in the charts shown in Figure VI-20 below. In each of these plots, the contribution to a unit change in impact energy is plotted for all parameter sets. The figure shows that the combined influence of these three parameters that are physical descriptors of the lung was always greater than any of the hyperelastic curve fit parameters. In the case of the concurrent optimization, these parameters account for nearly 70% of a unit change in energy.

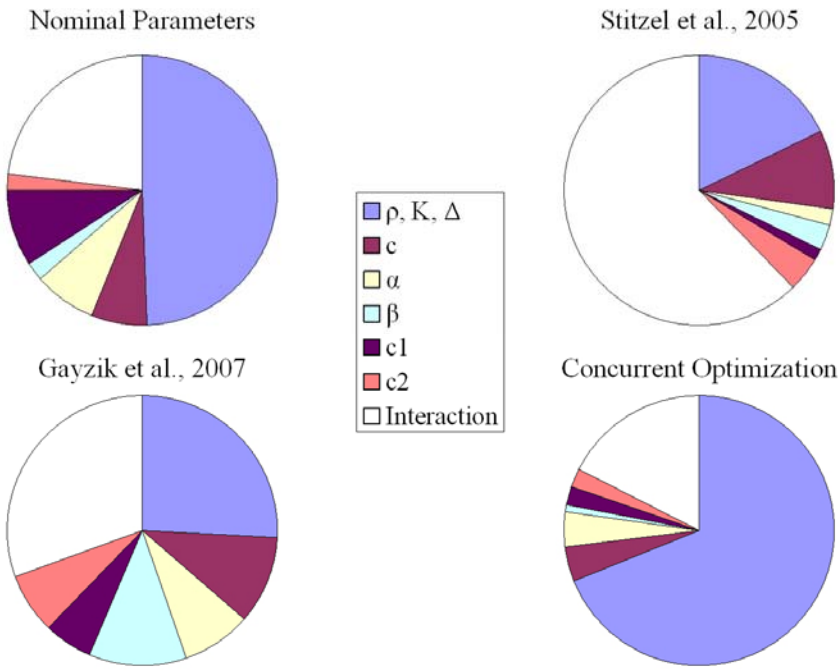

Figure VI-20. Total effect on unit change of impact energy from simulation of the severe impact condition for all presented parameter sets. Nominal parameters refer to Vawter et al. (1980). Physical parameters describing the lung model (ρ, K, Δ) are grouped separately. Interaction terms (α x β, etc.) are also grouped together.

Returning to the results of the concurrent optimization found in Figure VI-13, the relative importance of the surface tension term is shown with the magnitude of the effect of the c_1 parameter. This is to be expected since the hyperelastic model term is typically used to describe solid soft tissues. It is the presence of the surface tension term that makes the model response like that of the lung, an organ with a significant contribution from the air-filled alveoli. As expected, the density of the model takes on greater importance relative to all else when the impact speed increases. The parameter that has the largest influence on the model response at both high and low impact speeds was the alveolar diameter, Δ. The fact that the alveolar diameter and lung density play a large role in the behavior of the lung model shows promise that the transition from a model of

the rat lung to a model of the human lung will be fairly straightforward, since these physical quantities are already known.

The parameter study findings help steer the discussion back to the overall modeling approach. This research is founded on the fact that the behavior of the lung in dynamic loading can be accurately recreated with a continuum model. Clearly, the FEA lung model presented in this research is a simplification of the complicated microscopic structure of the lung. When developing the material model, Fung stated, "Let us define macroscopic stress and strains as local averages taken over small volumes that are, however, large enough to encompass a [large] number of alveoli."[12] As we have seen, Fung went on to develop a model with two terms for the deviatoric strain energy; the response due to the alveolar septa, and the response due to surface tension at the air-septa interface. The alveolar diameter is a factor in both of these terms (Equation IV-4). The composition of the lung model is considered uniform throughout its geometry and each of the elements in the model consists of a network of interconnected septa and alveolar spaces.

While this is a simplification of the true microscopic anatomy of the lung, one must bear in the mind that this model is a good response to the specific aims of this research. We intend to implement these findings in a full human body FEA model or a regional model of the human thorax for the prediction of pulmonary contusion. The only practical approach in the development of the injury metrics was to utilize the continuum type model developed by Fung and Vawter. While the precise injury mechanism of PC is due to rupture of the alveolar septa due to overexpansion due to passing pressure waves, modeling this type of interaction was not practical at this time. Many assumptions of the

behavior of the microscopic structures would be necessary and perhaps more importantly, a model of this injury mechanism would require elements orders of magnitude smaller than those found in current state of the art models.[13] In closing, the hyperelastic lung model, validated finite element model, and corresponding injury metrics developed in this Chapter represent the culmination of a number of research studies and are intended for use in predicting pulmonary contusion due to blunt chest trauma. These results may be used to argument the injury assessment capabilities of finite element models of the human body. Ultimately, the findings of this research may be used to tune safety systems for maximum mitigation of pulmonary contusion.

VI.5. Conclusions

This chapter presented the concluding experiments in developing a finite element based injury metric for pulmonary contusion utilizing a rat model of the injury. A concurrent optimization routine employing a multi-island genetic algorithm was used to tune the model response of a finite element model of the rat lung to experimental data from four distinct impact severities. The resulting FEA model showed good agreement with the experimental data, and was found to be very stable. The final values for the injury metrics were determined for three variables that were found to have a high correlation to the spatial distribution of PC in a previous study. The predictive injury metrics at 24 hours post-impact found were: $\varepsilon_{max} \cdot \dot{\varepsilon}_{max}$ exceeding 94.5 sec^{-1}, ε_{max} exceeding 0.284 and $\dot{\varepsilon}_{max}$ exceeding 470 sec^{-1}. Thresholds for HRL still present at 1 week post-impact were also determined. There were $\varepsilon_{max} \cdot \dot{\varepsilon}_{max}$ exceeding 149 sec^{-1}, ε_{max} exceeding 0.343 and $\dot{\varepsilon}_{max}$ exceeding 573 sec^{-1}. These metrics and the accompanying

validated FEA model represent the most comprehensive undertaking in developing a predictive metric for pulmonary contusion to date. Concluding remarks on the dissertation work as a whole are found in Chapter VII.

Chapter IV Acknowledgements

Work conducted by FSG and JJH was funded in part by a grant from the American Lung Association. Kerry Danelson and Jon Wells assisted in the experimental procedures described in this chapter. Portions of this work were also supported by Grant Number 1 R49 CE000664-01 from the Centers for Disease Control and Prevention (CDC). Its contents are solely the responsibility of the authors and do not necessarily represent the official views of the National Center for Injury Prevention and Control. Engineous Software and LSTC provided software at an educational discount.

Chapter IV Appendix

Additional data from the concluding experiments can be found in this appendix. It is intended to supplement the main portion of this chapter. The following is a listing of tables and figures found in this appendix.

Listing of Tables and Figures in this Appendix

Table VI-10. Impact experiment data for all cases.

Subject	Group	eCCI Velocity, m/s	Peak Displacement, mm	Peak Force, N	Absorbed Energy, mJ
1	1	6.04	6.547	1.087	4.440
2	1	5.94	5.263	0.927	3.110
3	1	6.04	5.472	0.856	3.200
4	1	6.10	6.051	1.096	3.398
5+	1	5.98	5.990	0.752	3.260
6+	1	5.04	4.395	0.882	2.200
7	1	6.04	7.019	1.500	4.338
8	1	5.98	6.255	1.072	3.861
9*	1	6.04	7.120	1.989	6.140
10	1	5.88	6.750	1.383	5.615
11	1	6.04	4.990	1.106	3.084
12	2	1.56	4.836	0.566	1.107
13	2	1.50	4.968	0.542	1.478
14	2	1.52	5.882	0.565	1.750
15*	2	1.52	3.498	1.476	0.531
16	2	1.50	6.783	0.475	1.939
17	2	1.50	5.448	0.498	1.505
18	2	1.50	4.827	0.713	1.677
19*	2	1.50	3.600	0.169	0.377
20	2	1.52	3.967	0.344	0.762
21**	3	-	-	-	-
22	3	6.04	3.300	0.449	1.240
23	3	5.98	3.860	0.566	1.740
24	3	5.98	3.300	0.846	1.910
25	3	5.94	3.510	0.654	1.485
26	3	5.94	3.450	0.694	1.732
27	4	1.50	2.964	0.307	0.530
28	4	1.50	2.607	0.307	0.509
29	4	1.52	3.183	0.386	0.601
30*	4	1.52	3.171	0.718	1.650
31	4	1.50	2.136	0.289	0.386
32	4	1.50	2.352	0.195	0.238
33-40 (Sham)	5	-	-	-	-

+ Ecci malfunction

* Chest wall contact

** Fatality during procedure (prior to impact)

Table VI-11. CT scanning data for all cases, 24 hours.

Subject	Group	Weight at Scan Time, g	Total right lung vol., cm^3	Percent HR Lung, %	Total left lung vol., cm^3	Percent HR Lung, %	Total lung vol., cm^3	Trapped air, cm^3
1	1	310	3.18	6.63	2.98	0.10	2.98	0
2	1	252	3.28	8.18	3.06	0.11	3.06	0
3	1	310	3.22	6.88	3.06	0.27	3.06	0
4	1	307	2.52	15.61	3.10	0.24	3.10	0
5+	1	336	2.43	20.85	2.81	3.26	5.24	0
6+	1	351	2.90	9.49	2.53	0.88	5.43	0
7	1	323	2.89	12.98	2.45	2.05	5.34	0
8	1	338	2.54	15.33	2.51	1.42	5.04	1.30
9*	1	326	1.89	58.82	2.28	9.82	4.17	0.57
10	1	343	3.20	6.04	3.26	0.53	6.46	0.08
11	1	337	3.91	2.03	3.45	0.02	7.36	0.08
12	2	336	2.78	3.56	2.78	0.85	5.57	0
13	2	325	3.54	1.35	3.24	0.19	6.78	0
14++	2	311	2.39	19.18	1.90	10.56	4.30	0
15*	2	311	2.60	6.68	1.25	6.81	3.86	1.97
16	2	319	3.25	4.28	2.98	0.25	6.23	0
17	2	319	3.13	3.87	2.69	1.01	5.83	0
18	2	316	2.79	7.13	2.78	2.33	5.57	0.03
19*	2	315	2.88	2.47	2.59	0.51	5.47	0
20	2	354	2.89	5.37	2.44	2.17	5.14	0.06
21**	3	-	-	-	-	-	-	-
22	3	332	3.27	2.90	2.56	1.68	5.83	0
23	3	336	2.94	8.29	2.78	2.67	5.72	0
24++	3	327	2.75	21.15	2.38	10.88	5.13	0.03
25	3	356	2.87	5.14	2.82	1.38	5.69	0
26	3	339	3.36	3.70	2.95	0.68	6.31	0
27	4	316	3.96	0.35	3.22	0.09	7.18	0
28	4	316	2.77	5.35	2.62	1.43	5.39	0.86
29	4	315	2.89	2.04	3.30	0.25	6.19	0
30*	4	312	3.42	3.79	2.70	2.07	6.12	0
31	4	314	2.74	6.00	2.94	0.28	5.68	0
32	4	325	3.07	3.27	2.69	1.87	5.76	0
33	5	343	3.76	1.85	2.62	0.63	6.37	0
34	5	332	3.40	1.94	2.76	0.23	6.15	0
35	5	311	2.98	4.28	2.17	5.34	5.15	0
36	5	311	2.34	4.49	3.05	0.90	5.39	0
37	5	316	3.87	0.06	3.13	0.00	7.00	0.02
38	5	328	2.93	3.83	2.69	2.38	5.62	0
39‡	5	313	2.37	13.89	2.11	0.00	4.48	0
40	5	313	2.95	2.19	2.73	0.00	5.68	0.02

+ eCCI malfunction
++ Breathing artifact during scan
* Chest wall contact
‡ Adhesion to chest wall
** Fatality during procedure (prior to impact)

Table VI-12. CT scanning data for all cases, 48 hours.

Subject	Group	Weight at Scan Time, g	Total right lung vol., cm^3	Percent HR Lung, %	Total left lung vol., cm^3	Percent HR Lung, %	Total lung vol., cm^3	Trapped air, cm^3
1	1	310	3.17	0.93	2.99	0.00	6.16	0
2	1	252	3.58	5.98	3.27	0.08	6.85	0.06
3	1	310	2.85	5.14	2.46	2.36	5.30	0
4	1	307	2.99	9.99	2.24	3.21	5.23	0
5+	1	333	-	-	-	-	-	-
6+	1	350	3.31	5.78	2.89	0.67	6.20	0
12	2	328	2.74	8.71	2.59	1.98	5.33	0
13	2	315	3.09	1.51	2.76	0.96	5.85	0
14++	2	315	2.33	16.63	2.20	8.34	4.53	0.72
15*	2	298	3.12	1.79	2.10	2.43	5.23	0.32
21**	3	-	-	-	-	-	-	-
22	3	325	3.09	1.49	2.36	1.72	5.44	0
23	3	327	3.21	0.84	3.00	0.56	6.21	0
24	3	319	2.89	2.58	2.75	1.66	5.65	0
27	4	308	4.13	0.17	3.08	0.02	7.21	0
28	4	307	3.84	2.13	3.49	0.06	7.33	0.04
29	4	316	3.12	2.64	2.09	1.77	5.21	0
30*	4	320	3.31	0.40	2.48	0.55	5.79	0
31	4	300	2.74	4.12	2.62	0.73	5.36	0
32	4	331	2.80	1.47	2.76	0.98	5.56	0
33	5	331	3.85	0.38	3.56	0.07	7.40	0
34	5	328	3.32	1.05	2.69	0.18	6.01	0
35‡	5	309	2.43	10.75	2.49	3.04	4.92	0
36	5	307	3.16	0.70	2.75	1.18	5.91	0

+ eCCI malfunction
++ Breathing artifact during scan
* Chest wall contact
‡ Adhesion to chest wall
** Fatality during procedure (prior to impact)

Table VI-13. CT scanning data for all cases, 1 week.

Subject	Group	Weight at Scan Time, g	Total right lung vol., cm^3	Percent HR Lung, %	Total left lung vol., cm^3	Percent HR Lung, %	Total lung vol., cm^3	Trapped air, cm^3
1	1	338	3.99	0.97	3.24	0.56	7.23	0
2	1	305	3.36	0.44	3.59	0.24	6.95	0
3	1	352	3.15	4.25	3.34	0.18	6.49	0
4	1	338	2.90	9.92	3.10	0.40	5.99	0
5+	1	345	3.11	1.02	2.77	0.39	5.88	0
6+	1	372	3.14	2.66	2.88	0.11	6.02	0
12	2	353	3.79	1.74	2.69	2.76	6.48	0
13	2	345	3.68	0.10	3.23	0.13	6.91	0
14++	2	349	2.96	6.67	2.60	2.43	5.56	0
15*	2	339	2.62	7.61	2.35	1.96	4.97	0
21**	3	-	-	-	-	-	-	-
22	3	343	2.92	1.79	2.43	1.48	5.36	0
23	3	344	3.20	0.77	2.88	0.46	6.08	0
24	3	344	3.16	1.80	2.82	1.37	5.98	0
27	4	337	4.28	0.05	3.16	0.02	7.44	0
28	4	328	3.46	0.36	3.21	0.35	6.68	0
29	4	344	3.11	2.53	2.44	0.55	5.55	0
30*	4	329	2.77	4.26	2.59	0.87	5.36	0
31	4	360	2.88	1.06	2.51	0.56	5.40	0
32	4	362	3.78	0.52	3.06	0.47	6.84	0
33	5	350	4.46	0.01	3.41	0.07	7.88	0
34	5	345	3.45	0.22	3.21	0.03	6.66	0
35‡	5	334	3.30	6.52	2.00	1.73	5.30	0
36	5	328	3.34	0.57	2.69	0.81	6.03	0

+ eCCI malfunction
++ Breathing artifact during scan
* Chest wall contact
‡ Adhesion to chest wall
** Fatality during procedure (prior to impact)

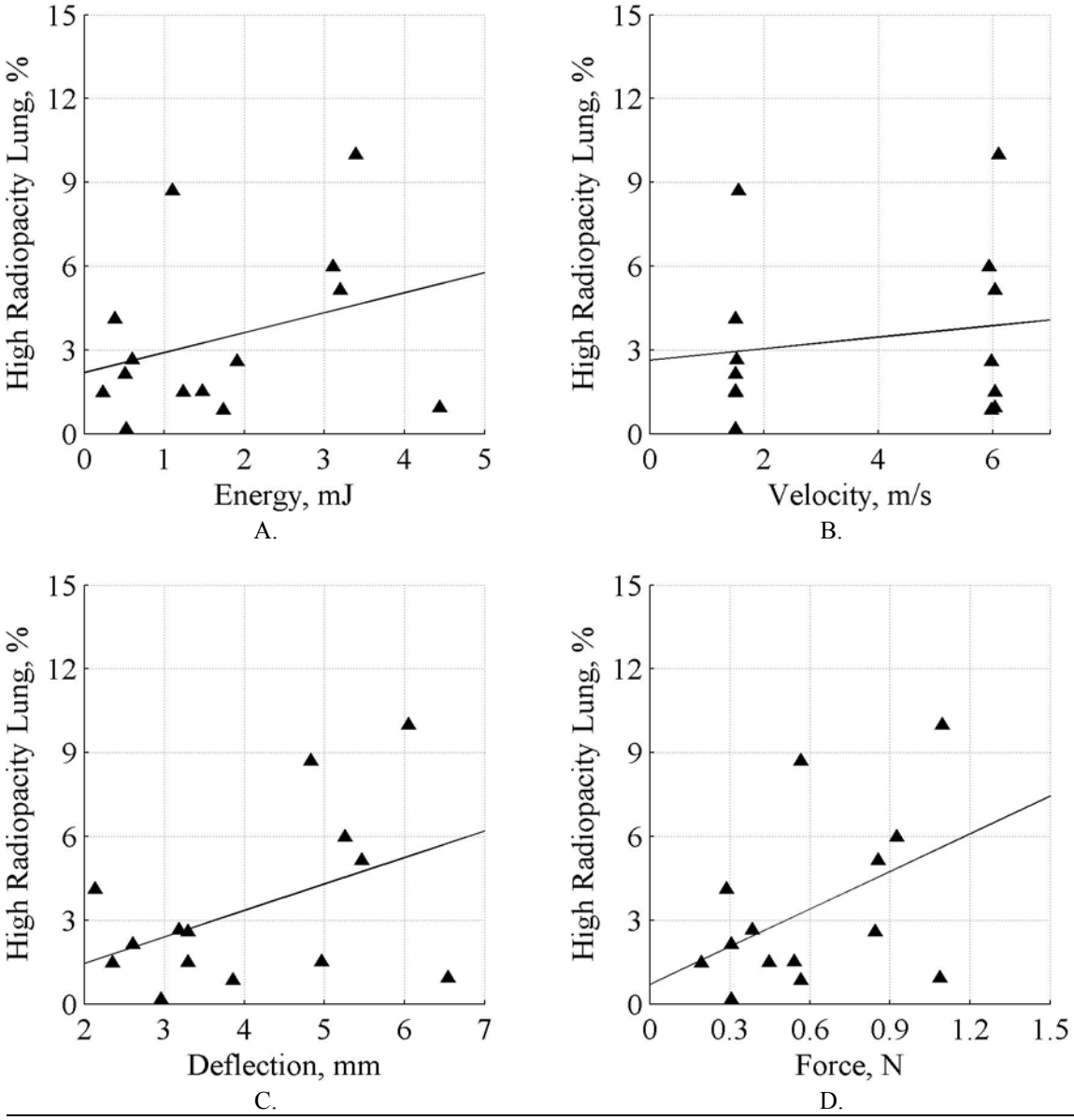

Figure VI-21. Normalized high radiopacity lung (percent of struck lung) vs. A. Absorbed energy, B. Impact velocity, C. Displacement, D. Peak Force during impact. All traces are from 48 hour post-impact scans. None of the relationships are significant.

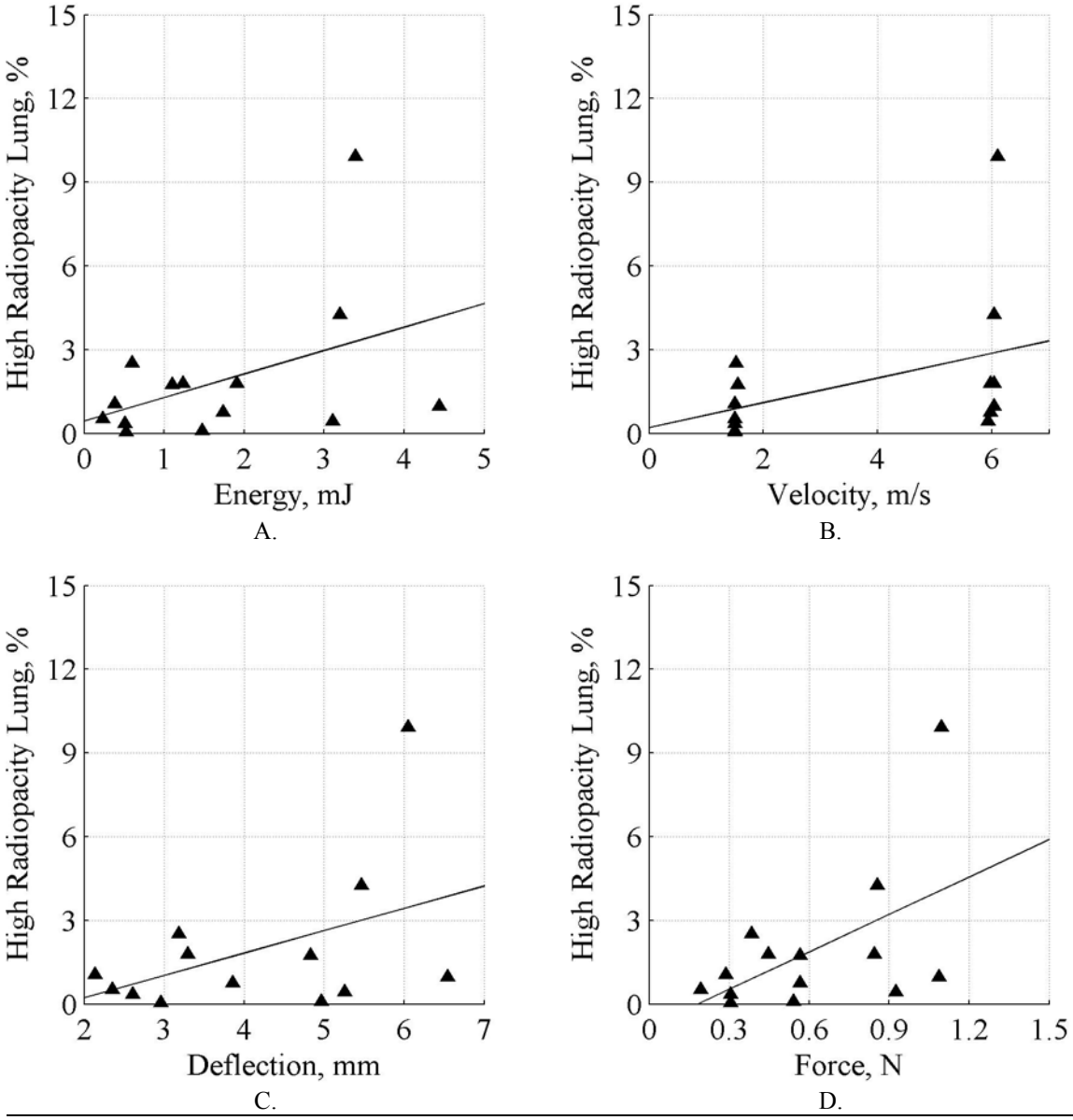

Figure VI-22. Normalized high radiopacity lung (percent of struck lung) vs. A. Absorbed energy, B. Impact velocity, C. Displacement, D. Peak Force during impact. All traces are from 1 week post-impact scans. None of the relationships are significant.

Table VI-14. ANOVA results testing 24 hour post-impact contusion volume (% High radiopacity lung) between study cohorts. Significant differences between cohorts are denoted by ●. Pair-wise comparisons made using Tukey's post-hoc test (See Figure VI-7).

Variable:	24 hour post-impact contusion (%)			**p:**	0.0048
Cohort:	**Severe**	**Intermediate**	**Intermediate**	**Mild**	**Sham**
Nominal V, m/s	6.0	1.5	6.0	1.5	-
Nominal D, mm	5.0	5.0	2.0	2.0	-
Group	1	2	3	4	5
1 vs.		●		●	●
2 vs.					
3 vs.					
4 vs.					

Table VI-15. ANOVA results testing impact energy between study cohorts. Significant differences between cohorts are denoted by ●. Pair-wise comparisons made using Tukey's post-hoc test (See Figure VI-5).

Variable:	Impact energy		**p:**	<0.0001
Cohort	**Severe**	**Intermediate**	**Intermediate**	**Mild**
Nominal V, m/s	6.0	1.5	6.0	1.5
Nominal D, mm	5.0	5.0	2.0	2.0
Group	1	2	3	4
1 vs.		●	●	●
2 vs.				●
3 vs.				●

Table VI-16. ANOVA results testing peak force between study cohorts. Significant differences between cohorts are denoted by ●. Pair-wise comparisons made using Tukey's post-hoc test (See Figure VI-5).

Variable:	Peak force from impact		**p:**	<0.0001
Cohort	**Severe**	**Intermediate**	**Intermediate**	**Mild**
Nominal V, m/s	6.0	1.5	6.0	1.5
Nominal D, mm	5.0	5.0	2.0	2.0
Group	1	2	3	4
1 vs.		●	●	●
2 vs.				
3 vs.				●

Table VI-17. ANOVA results testing lung displacement between study cohorts. Significant differences between cohorts are denoted by ●. Pair-wise comparisons made using Tukey's post-hoc test (See Figure VI-4).

Variable:	Displacement		**p:**	<0.0001
Cohort	**Severe**	**Intermediate**	**Intermediate**	**Mild**
Nominal V, m/s	6.0	1.5	6.0	1.5
Nominal D, mm	5.0	5.0	2.0	2.0
Group	1	2	3	4
1 vs.			●	●
2 vs.			●	●
3 vs.				

Table VI-18. ANOVA results testing velocity between study cohorts. Significant differences between cohorts are denoted by ●. Pair-wise comparisons made using Tukey's post-hoc test (See Figure VI-4).

Variable:	Impact velocity		**p:**	<0.0001
Cohort	**Severe**	**Intermediate**	**Intermediate**	**Mild**
Nominal V, m/s	6.0	1.5	6.0	1.5
Nominal D, mm	5.0	5.0	2.0	2.0
Group	1	2	3	4
1 vs.		●		●
2 vs.			●	
3 vs.				●

Table VI-19. Summary of statistics from t-tests for pair-wise comparisons of high radiopacity lung percentage within cohort groups at all time points (See Figure VI-9).

Group: Description:	1 Severe	2 Intermediate	3 Intermediate	4 Mild	5 Sham
24 hrs. vs. 48 hrs. (p-values)	0.216	0.715	0.070	0.323	0.078
24 hrs. vs. 1 week (p-values)	0.097	0.021	0.021	0.059	0.038
48 hrs. vs. 1 week (p-values)	0.593	0.374	0.374	0.166	0.154

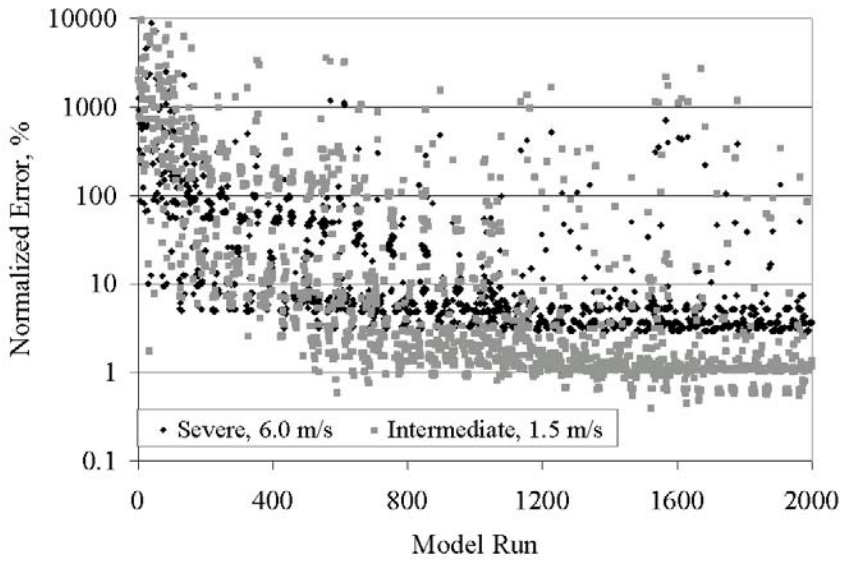

Figure VI-23. Progression of normalized error against optimization run. Error is normalized by the sum of the optimal energy squared and expressed as a percent.

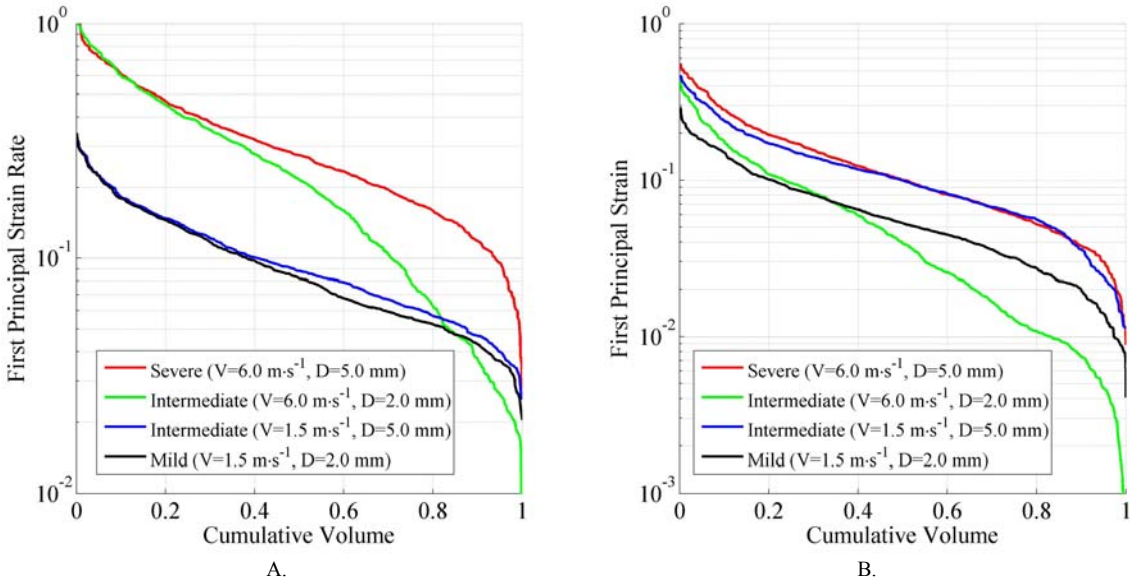

A. B.

Figure VI-24. Maximum values for first principal strain rate (A.) and first principal strain (B.) for all elements in finite element model.

Chapter IV References

1. Gayzik FS, Hoth JJ, Daly M, Meredith JW, Stitzel JD. A finite element based injury metric for pulmonary contusion: Investigation of candidate injury metrics through correlation with computed tomography. *Stapp Car Crash Journal.* 2007;51:189-209.

2. Stitzel J, Gayzik F, Hoth J, et al. Development of a finite element based injury metric for pulmonary contusion, Part I: model development and validation. *Stapp Car Crash Journal.* 2005;49:271-289.

3. Fung YC, Yen RT, Tao ZL, Liu SQ. A hypothesis on the mechanism of trauma of lung tissue subjected to impact load. *J Biomech Eng.* Feb 1988;110(1):50-56.

4. Gayzik FS, Hoth JJ, Stitzel JD. Optimization Methods for Finite Element Model Validation: Fitting Lung Biomechanical Model Data to Injury Corridors. Paper presented at: Icrash 2006, International Crashworthiness Conference; July 4-7, 2006; Athens, Greece.

5. Gayzik FS, Hoth JJ, Stitzel JD. Optimization Methods for Finite Element Model Validation: Fitting Lung Biomechanical Model Data to Injury Corridors. Paper presented at: 5th World Congress of Biomechanics; July 29th - August 4th, 2006; Munich, Germany.

6. Vawter D. A finite element model for macroscopic deformation of the lung. *J. Biomech. Eng.* 1980;102:1-7.

7. Hoth JJ, Hudson WP, Brownlee NA, et al. Toll-Like Receptor 2 Participates in the Response to Lung Injury in a Murine Model of Pulmonary Contusion. *Shock.* Jun 7 2007.

8. Mannick JA, Rodrick ML, Lederer JA. The immunologic response to injury. *J Am Coll Surg.* Sep 2001;193(3):237-244.

9. Takhounts E, Eppinger R, Campbell J, Tannous R. On the development of the SIMon finite element head model. *Stapp Car Crash Journal.* 2003;47:107-133.

10. King A, Yang K, Zhang L, Hardy W. Is head injury caused by linear or angular acceleration? *IRCOBI*. Lisbon (Portugal); 2003.

11. Vawter D, Fung Y, West J. Elasticity of excised dog lung parenchyma. *J. Appl. Physiol.* 1978;45:261-269.

12. Fung YC, Tong P, Patitucci P. Stress and strain in the lung. *ASCE J. Eng. Mech.* 1978;104(EM 1):201-223.

13. Yang KH, Hu J, White N, King AI. Development of numerical models for injury biomechanics research: A review of 50 years of publications in the Stapp Car Crash Conference. *Stapp Car Crash Journal.* 2006;50:429-490.

CHAPTER VII

CONCLUSIONS

VII.1. Contributions

This work has contributed many findings to the injury biomechanics literature relative to the study of pulmonary contusion. In Chapter II, we presented a crash epidemiology study utilizing CIREN data and vehicular crash tests. Using a procedure to identify cases in CIREN that matched key parameters from the vehicle crash tests, the average deflection velocity and medial lateral compression from pole-type impacts and vehicle-to-vehicle-type impacts were determined. Through correlation with CIREN injury data, the results provide well quantified chest loading data from MVC resulting in lung contusion. The loading during crash scenarios was found to be markedly different than blast type loading, which has erroneously been used in mechanistic studies of pulmonary contusion employing murine models.

The study presented in Chapter III while broad in scope, introduced several novel techniques to the study of lung injury biomechanics. The study set the fundamental framework for the remaining thesis work; introducing the finite element model of the rat lung, the use of the Sprague-Dawley rat, the use of imaging data (in this case PET data) to quantify the inflammatory response of the host, mechanical validation data from direct impact to the rat lung, and an automated model optimization and parameter sensitivity approach that tuned the model response to the experimental results. While the results of

the study were limited, a preliminary threshold for pulmonary contusion was provided at 22% true strain.

The follow up study to Chapter IV was built on the foundation of Stitzel et al. (2005), but utilized CT instead of PET to obtain image data. A number of the technical aspects of this study should also be considered original contributions to the injury biomechanics literature. Chief among them is the registration scheme that was used to determine which computational metric calculated from the FEA model best correlated with the location and spatial distribution of high radiopacity regions of tissue observed in CT segmentations. Among many variables tested, the product of maximum principal strain and strain rate was found to best characterize pathology in the lung. The maximum principal strain and its strain rate were also highly correlated. This study was the first to present a threshold for lung injury based on the results of this registration technique. The study found that elements whose value of $\varepsilon_{\max} \cdot \dot{\varepsilon}_{\max}$ exceeded 28.5 sec^{-1} at any point in the simulation indicated the presence of contusion in that volume. However, these findings were based on a model that was validated only in a single impact condition. A similar approach was taken in Chapter VI of this dissertation, but four cohorts of varying impact severity were used to develop a more robust set of injury metrics for pulmonary contusion.

Chapter V was an extension of Gayzik et al. (2007) that presented a short study of histological image data from a subset of the data presented in Chapter IV. A novel aspect of this study was segmented image data of a single subject taken at roughly the same time point (48 hours post-insult) using two very distinct imaging techniques; CT and digital histology. Serial sections of histology were digitally imaged and analyzed using an

original algorithm programmed in Matlab (The MathWorks, Natick, MA). Calculated contusion volumes from histology across study subjects showed general agreement with CT. When compared to a pathologist's assessment of the contusion volume the algorithm showed excellent specificity and good sensitivity in slides where the contusion was in excess of 20% by volume.

Chapter VI represented the synthesis of the computational and experimental methods of this dissertation. Using refined instrumentation, four distinct levels of impacts were applied to study subjects using the protocols outlined in the previous studies (Chapters III and IV). The results demonstrated significant relationships between the normalized volume of contusion at 24 hours post-impact and both impact energy ($p = 0.005$) and peak impact force ($p = 0.003$). A concurrent optimization technique was applied to tune the model response to impacts at two distinct impact speeds, severe (6.0 $m \cdot s^{-1}$) and mild (1.5 $m \cdot s^{-1}$). The force deflection traces resulting from the optimized models matched the mean experimental values of the corresponding cohorts' impact energy within one standard deviation. Using the FEA model results and the normalized values for contusion observed in the experimental subjects, injury metrics for pulmonary contusion were determined using this well-validated model. Based on the results from the CT-FEA registration technique presented in Gayzik et al., (2007) injury metrics were determined for the product of the maximum principal strain and strain rate, the maximum principal strain, and the maximum principal strain rate.

Based on the experimental findings presented in Chapter VI, the values for these thresholds were respectively, $\varepsilon_{max} \cdot \dot{\varepsilon}_{max} = 94.5\ sec^{-1}$, $\varepsilon_{max} = 0.284$, and $\dot{\varepsilon}_{max} = 470\ sec^{-1}$. In simulations of dynamic impact events using this material model for lung, elements

wherein these variables exceed the above thresholds should be anticipated to exhibit contusion at 24 hours post-insult. Thresholds based on the percentage of contusion at 1 week post-insult are also provided. These thresholds were slightly elevated from the 24 hour post-insult thresholds presented above.

Since many of the techniques used in determining these injury metrics can be applied to other organs and systems of the human body, in a broader sense the techniques outlined in this dissertation may be applied to related research to help reduce the risk of death or trauma associated with accidental injury. In an ever modernizing world, where an increasing portion of the global population has access to vehicular transport and lives in urban centers, the importance of improving safety systems is perhaps greater today than ever.

VII.2. Directions for Future Research

The central focus of the next phase of this research will be demonstrating that the injury metrics developed in this dissertation can be used to predict pulmonary contusion in humans. This type of translational research is unavoidable when using an animal model in the early stages of a research project. While the injury metrics established in this dissertation in Chapter VI are robust and result from a model validated in multiple impact conditions, numerous challenges remain in translating these results to a human model.

First among them will be demonstrating that the material model is valid for the human lung. The rat has long been established as a good model for pulmonary research, but there are vast differences between the rat and human lung at the macroscopic level.. Fortunately, these differences are diminished as one moves to the microscopic level. One

example is alveolar diameter. Gross volume differences between species are several orders of magnitude, but the alveolar diameter is relatively close in size (70 μm in the rat vs. 200 μm in the human). Considering that this diameter is a parameter in the material model, and has been shown to have a significant effect on the force vs. deflection response of the organ, material model validation could potentially be done using fresh excised tissue in a similar experimental technique as used in Chapters III-VI of this dissertation. But this approach would only be useful for verifying the resulting force vs. deflection response. Prospective studies designed to quantify the insult and outcome of such experimental techniques could not be obtained using excised human lung tissue.

The avenue with the best potential for obtaining such relationships could be through examining and simulating well-documented, real-world vehicle crashes. This once again brings to the forefront the importance of Chapter II of this dissertation, which provides well quantified loading data precisely at the thorax resulting from severe lateral impact crashes. This data could be used in conjunction with PC+ cases in the CIREN database that match the vehicle crash tests. For these cases, detailed radiology will be available for segmentation and analysis in order to complete the link between the insult (determined through computational modeling of the event) and the outcome (the patient radiology). While these concepts are only now in the planning phase, the conclusions from this research have set a strong foundation for continuing research in mitigating and preventing pulmonary contusion.

APPENDIX

A. IMPACT EXPERIMENT TEST EQUIPMENT

This appendix catalogs the test equipment and instrumentation used in the impact experiments conducted in this thesis. This section serves as a reference for details on the equipment used to: impact the test subjects, record the force and deflection traces, and acquire the experimental data. Some of this information is included in the journal publications that comprise this thesis. Data that did not appear in these manuscripts, such as calibration values, can be found in this appendix.

A.1. Electronic Cortical Contusion Device

In Chapters III-VI of this thesis, data was generated through impact testing with the electronic Cortical Contusion Injury Device or eCCI. The device was manufactured by Custom Design and Fabrication, in Richmond, VA (tel. 1-800-828-2998). The eCCI is an electromagnetically-driven piston capable of achieving impact speeds up to roughly 6.5 m/s when instrumented. Peter Robinson of CDF was the engineer responsible for building the eCCI unit. The piston, control tower and stage are shown in Figure A1.

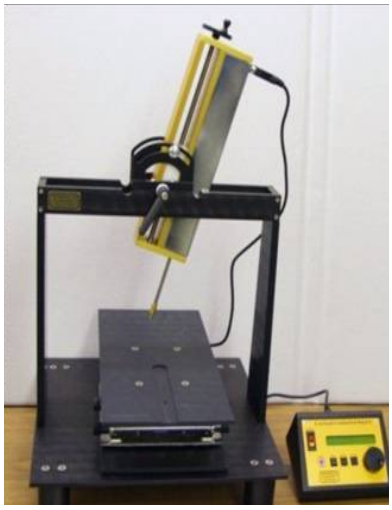

Figure A-1. Electronic Cortical Contusion Device, or eCCI. Showing piston, control box and stage.

A.2. Data Acquisition

Data was acquired with an Iotech® Wavebook 516E data acquisition system (DAS), (Iotech, www.iotech.com, Cleveland, OH). The Wavebook 516E is an Ethernet-based portable high speed waveform acquisition unit. It has a 16-bit/1-MHz Analog to Digital converter. In the application used in this thesis, a single channel was used and data were acquired at 500 kHz. Piezoelectric load cells were used for all data acquisition. All load cells were connected to Channel 1 of the DAS through BNC type connectors. All load cells worked in conjunction with external charge amplifiers. Wave View software, V 7.9-15. also from Iotech, was used to configure data acquisition settings. Various load cells were used in conducting this research, some commercially available, and one custom-designed load cell and anvil combination.

A.3. Commercial Load Cell Calibration and Testing

This section reviews calibration and checks on the commercially available load cells used in this research. These load cells manufactured by PCB Piezotronics (www.pcb.com, Depew, NY). Models 208-C01 and 208-C02 were used. These models are designed for measuring force in dynamic events. A charge amplifier was used to amplify the high-impedance output from the crystal in these load cells (PCB Piezotronics) to a low impedance voltage signal. A shock adapter built by Custom Design and Fabrication (CDF) was used to mitigate large tensile strains in the crystal housing. A custom anvil attachment, manufactured by Faircloth Machine Shop (Winston-Salem, NC) was used on the impacting edge of the anvil. Figure A-2 shows an image of the PCB model 208-C02, mounted to the eCCI via the custom shock adapter.

Figure A-2. PCB load cell with shock adapter and aluminum anvil attachment.

Calibration file data

Table A-1 and Table A-2 contain the calibration data used collecting data with the 208-C01 and 208-C02 load cells. Scale factors were determined from calibration curves provided by the manufacturer.

Table A-1. Calibration file data for the commercial load cell 208-CO2 by PCB electronics.

Units	Newtons
Scale factor (slope)	96.099998 N/V
Scale factor (intercept)	0 N
Range	-96.1 N to 96.1 N
Trigger	Channel 1 Analog, -80N, falling
Sample rate (pre- and post-trigger)	500 kHz
n Samples pre-trigger	18,000
n Samples post-trigger	82,000
Filename	impact_CO2_100k_samples.cfg

Table A-2. Calibration file data for the commercial load cell 208-CO1 by PCB electronics.

Units	Newtons
Scale factor (slope)	9.225 N/V
Scale factor (intercept)	0 N
Range	-9.2 N to 9.2 N
Trigger	Channel 1 Analog, -8N, falling
Sample rate (pre- and post-trigger)	500 kHz
n Samples pre-trigger	18,000
n Samples post-trigger	82,000
Filename	impact_CO1_100k_samples.cfg

Calibration testing

A weight-lifting technique was used to verify the anvil calibration. A mass of known value was placed on the rigidly mounted sensor. The sensor was allowed to equilibrate over a five minute time period (State 1). Once equilibrated, the weight was quickly removed from the sensor (State 2) and the change in force, ΔF, was recorded. A mass of m_1 = 168.4 g, F = 1.65 N was used in the lifting test. Data were collected at 1 kHz and triggered automatically. A schematic of the lifting test is shown in Figure A-3 of the Custom Load Cell appendix. One test was performed with each sensor to verify the calibration used in the tests, Figure A-4 and Figure A-5.

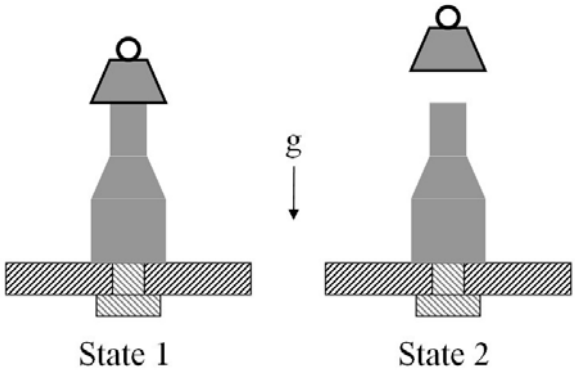

Figure A-3. Weight lifting test schematic showing two states. The first state the mass is placed on the load cell and allowed to equilibrate. In state two, the mass has been quickly removed.

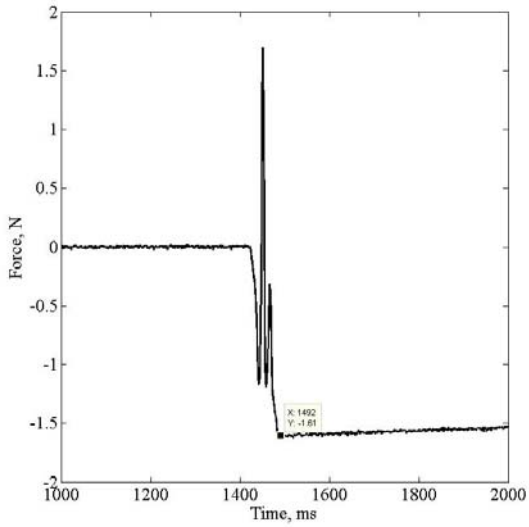

Figure A-4. Weight lift test with 1.65 N weight, 208-CO2.

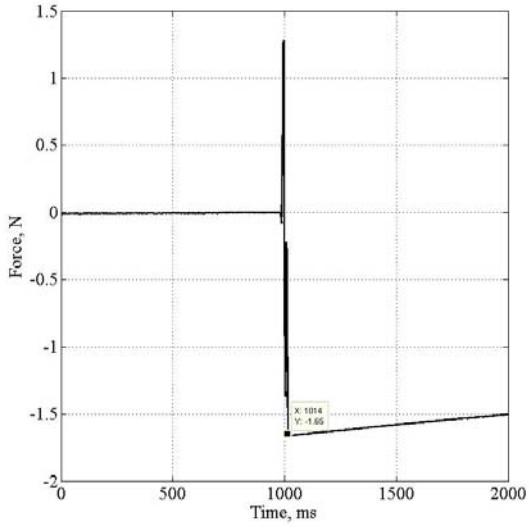

Figure A-5. Weight lift test with 1.65 N weight, 208-CO1.

Custom shock adapter design

When the eCCI reached the end of its stroke it rapidly decelerated from the impact speed (roughly 5.0-6.0 m/s) to rest. The custom shock adapter built by CDF was employed to mitigate the large tensile force induced in the load cell. The absorber

contains a 2.5 mm thick, medium hardness rubber o-ring. This same assembly was used in collecting validation data for Chapters 2 and 3. Figure A-6 provides for further detail. A photograph of the shock adapter can be found in Figure A-2.

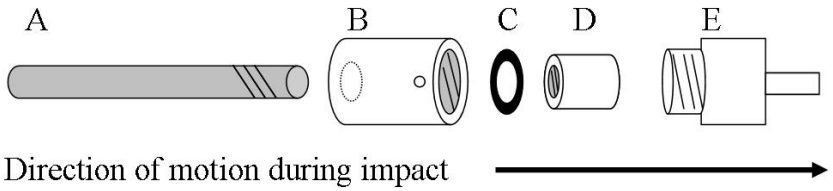

Figure A-6. Schematic of shock adapter. A. Shaft of piston, threaded on the end closest to the point of impact. Piston housing not shown. Threading matches with part D. B. Outer shock adapter housing, with opening on left side to allow shaft to slide through and threaded opening on the right side. Threading matches E. C. Shock absorbing O-ring. D. Anchor for upper housing, threading matches A. E. Load cell assembly, threading matches B, threads so that the o-ring (C) is pressed between B and D.

A.4. Custom Load Cell Calibration and Testing

This section reviews calibration checks for the custom anvil supplied by Custom Design and Fabrication (CDF) of Richmond VA for the impact testing performed in Chapter 6 of this thesis. This piece of equipment is an integrated anvil and load cell and was designed specifically for use with the eCCI. Figure A-7 shows an image of the custom load cell.

Figure A-7. Integrated load cell and anvil from Custom Design and Fabrication.

The custom load cell and anvil is manufactured with a piezoelectric crystal, providing a high frequency response and is fitted with ¼-28 threading so that it can be screwed directly to the impacting shaft of the eCCI. No shock absorbing material was needed for this anvil. Calibration data is in Table A-3 and was provided by the manufacturer.

Table A-3. Custom anvil specifications.

Scale	1V = 1Kg
Range	+- 4.6 Kg = +- 45 N
High Frequency Cutoff	50 kHz (< % error)
Housing	Aluminum
Impacting Edge Radius	6.48 mm
Effective Mass (with portion of cord)	18.59 g

Calibration file data

Table A-4 shows the data in the calibration file used with the custom load cell. The Wavebook-516E DAS was used to collect this data. The custom load cell was provided with a custom charge amplifier.

Table A-4. Calibration file data for the custom load cell.

Units	Volts (Kilograms)
Scale factor (slope)	1 V = 1 kg
Scale factor (intercept)	0 V = 0 kg
Range	-10 to 10 V
Trigger	Automatic, 1V, falling
Sample rate	500 kHz
n Samples pre-trigger	18,000
n Samples post-trigger	82,000
Filename	Impact_integrated_100k_samples.cfg

Calibration testing

The custom anvil was tested via the weight-lifting technique described above to verify the manufacturer's calibration. Two different masses (m_1 = 8.3 g and m_2 = 168.4 g) were used in the lifting test. Data were collected at 5 kHz and triggered manually. A

schematic of the lifting test is shown in Figure A-8. Three lifting tests were performed with each weight for a total of 6 tests. Lifting test results are provided in Figure A-8.

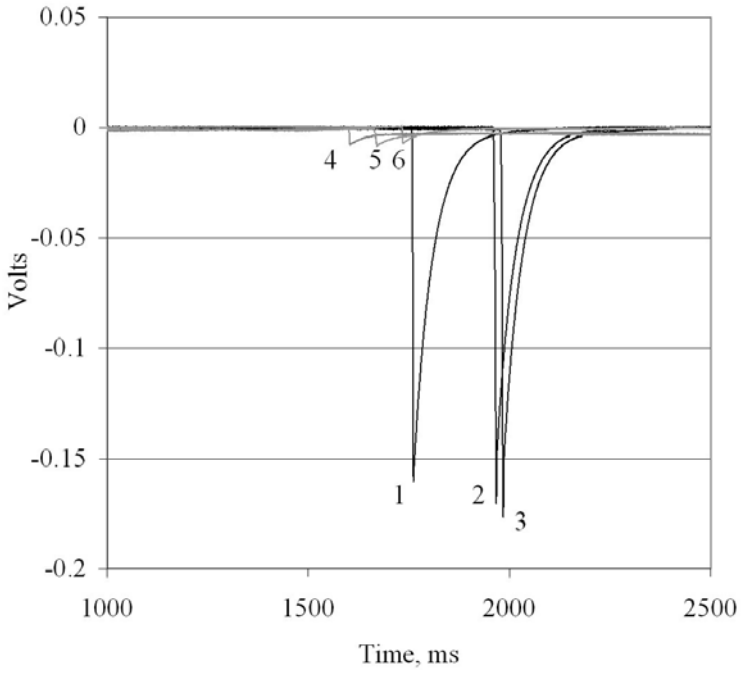

Figure A-8. Weight lift test traces for custom anvil and load cell.

Following the lift test data the observed values of ΔF were plotted against the calibration curve for the actual ΔF values calculated by multiplying the test mass by g (9.806 $m \cdot s^{-2}$). These are shown in Figure A-9. The coefficient of determination (R^2) was determined for these 6 measures and was found to be $R^2 = 0.98$.

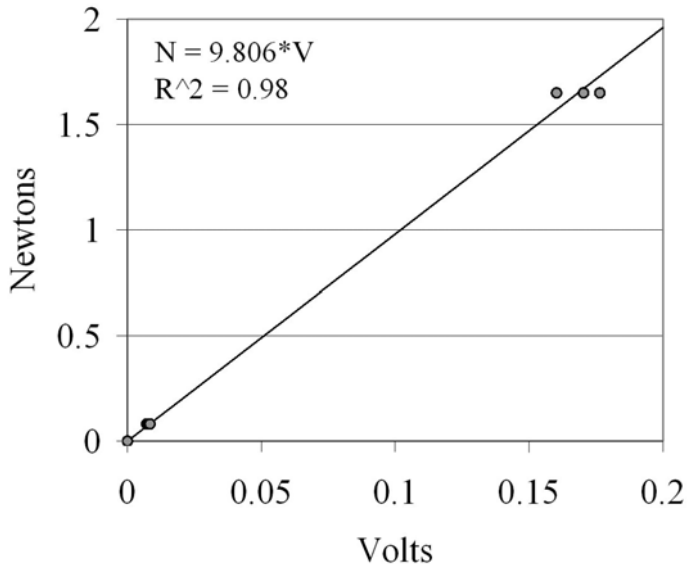

Figure A-9. Regression for calibration based on scale factor of 9.806 N/V.

A.5. Inertial Compensation

Data from both load cells were inertially compensated using D'Alembert's principal. This technique is used to compensate for mass below the sensitive plane of the transducer. The inertial compensation factor is given by Equation A-1.

$$IC = \frac{m_T}{m_T - m_{IC}} \qquad \text{Equation A-1}$$

Here, m_T is the total mass of the system in motion, including the mass of the eCCI shaft assembly (75 g), and mass of the load cell assembly. The second mass in this equation, m_{IC} is the mass below the sensitive plane of the load cell. The values for m_{IC} varied between load cells and were provided by the manufacturers in all cases. In the design of the custom load cell, the crystal has 5 mm of aluminum below its sensitive plane, equating to m_{IC} = 1.78 g. For the PCB load cells, the mass below the sensitive plane was m_{IC} = 13.7 g. This mass included the aluminum anvil. The mass of the custom shock adapter (8 g) was included in the inertial compensation factor for the commercial

load cells. The IC factors were 1.14 and 1.019 for the PCB and custom load cells respectively. Force traces from these load cells were multiplied by these IC factors.

SCHOLASTIC VITA

F. Scott Gayzik
3549 Summerfield Lane, Winston-Salem, NC, 27106
Phone: 540-818-3968, Email: sgayzik@wfubmc.edu

Education

Wake Forest University & Virginia Tech, Winston-Salem, NC *August* 2008
Ph.D. Candidate, School of Biomedical Engineering and Sciences
Dissertation: *Development of a finite element-based injury metric for pulmonary contusion*
Advisors: Dr. Joel D. Stitzel (Primary Advisor), Dr. H. Clay Gabler, Dr. Stefan M. Duma
Virginia Tech – Wake Forest University Center for Injury Biomechanics

Dr. J. Jason Hoth, Dr. Robert S. Martin
Wake Forest University School of Medicine, Surgical Sciences

Virginia Tech, Blacksburg, VA
M.S. Mechanical Engineering, QCA: 3.8/4.0 Aug 2004
Thesis: *Optimal control of thermal damage to biological materials*
Advisor: Dr. Elaine P. Scott, Thermal and Inverse Characterization Laboratory

B.S. Mechanical Engineering, Spanish Minor, QCA: 3.6/4.0 *(Magna Cum Laude)* May 2002

Current Academic Title

Ph.D. Candidate and Graduate Research Assistant
Virginia Tech – Wake Forest University Center for Injury Biomechanics,
Department of Biomedical Engineering,
Wake Forest University School of Medicine, Winston-Salem, NC

Highlighted Skills

- Dynamic and static finite element analysis, nonlinear material modeling, analytical programming, and shape analysis
- Experimental research, including high-speed impact data collection (force, pressure, video etc.), data reduction and analysis
- Excellent written and oral communication skills, numerous peer reviewed publications and conference abstracts

Journal Publications

1. **Gayzik, F.S.**, Martin, R.S., Gabler, H.C., Hoth, J.J., Chang, M.C., Miller, P.R., Duma, S.M., Meredith, J.W., Stitzel, J.D., Characterization of crash induced thoracic loading resulting in pulmonary contusion. J Trauma; 2008 (*In press*) *July 2008*

2. **Gayzik, F.S.**, Yu, M., Danelson, K.A., Slice, D.E., Stitzel, J.D., Quantification of age-related change of the human rib cage through geometric morphometrics. J Biomech; 41(7):1545-54 *April 2008*

3. **Gayzik, F.S.**, Hoth, J.J., Daly, M.D., Meredith, J.W., Stitzel, J.D., A Finite Element-Based Injury Metric for Pulmonary Contusion: investigation of candidate metrics through Oct. 2007

correlation with computed tomography. Stapp Car Crash Conference; 51: 189-209

4. Daly, M., Miller, P.R., Carr, J.J., **Gayzik, F.S.**, Hoth, J.J., Meredith, J.W., Stitzel, J.D., Traumatic pulmonary pathology measured with computed tomography and a semi-automated analytic method. Clinical Imaging; (*In Press*) — Feb. 2008

5. Stitzel J.D., **Gayzik F.S.**, Hoth J.J., Mercier J., Gage H.D., Morton K.A., Duma S.M., Payne R.M., Development of a finite element-based injury metric for pulmonary contusion Part I: Model development and validation. Stapp Car Crash Journal; 49: 271-289 — Nov. 2006

6. Hoth, J.J., Stitzel, J.D., **Gayzik, F.S.**, Brownlee, N.A., Miller, P.R., Yoza, B.K., McCall, C.E., Meredith, J.W., and Payne, R.M., The pathogenesis of pulmonary contusion: an open chest model in the rat. J Trauma; vol. 61, pp. 32-44; discussion 44-5 — Apr. 2006

7. **Gayzik, F.S.**, Loulou, T., Scott, E.P., Experimental validation of an inverse heat transfer algorithm for optimizing hyperthermia treatments. Journal of Biomechanical Engineering; 128: 505-515 — Aug. 2006

Peer-Reviewed Conference Papers

1. **Gayzik, F.S.**, Hoth, J.J., Stitzel, J.D. Quantitative histology of the injured rat lung and comparison to computed tomography. Submitted to Biomedical Sciences and Instrumentation; (*in press*) — Apr. 2008

2. Lambert, C.C., **Gayzik, F.S.**, Stitzel, J.D., Characterization of the carotid and adjacent anatomy using non-contrast CT for biomechanical model development. Biomedical Sciences and Instrumentation; 43: 330-5 — Apr. 2007

3. **Gayzik, F.S**., Hoth, J.J., Stitzel, J.D., A comparative study of optimization techniques for tuning a finite element model of the lung to biomechanical data. Biomedical Sciences and Instrumentation; 43: 212-7. — Apr. 2007

4. **Gayzik, F.S.**, Bostom, O., Ortenwall, P., Duma, S.M., Stitzel, J.D., An experimental and computational study of blunt carotid artery injury. Annu Proc Association for the Advancement of Automotive Medicine; 50:13-32 — Oct. 2006

5. **Gayzik, F.S.**, Loftis, K.L., Slice, D.E., Stitzel, J.D., A finite element study of age-based size and shape variation in the human rib cage. Biomedical Sciences and Instrumentation;42:19-24 — Apr. 2006

6. **Gayzik, F.S.**, Tan, J.C., Duma, S.M., Stitzel, J.D., Mesh Development for a Finite Element Model of the Carotid Artery. Biomedical Sciences and Instrumentation; 42:19-24 — Apr. 2006

Conference Abstracts and Scientific Exhibits

1. Danelson, K.A., Yu, M. , **Gayzik, F.S.**, Geer, C.P., Slice, D.E., Stitzel, J.D. "Geometric Scaling Factors for the Pediatric Brainstem," Biomedical Sciences and Instrumentation, 2008; 44 — April 2008

2. Ruggles, A.A., **Gayzik, F.S.**, Stitzel, J.D., "Biomechanical analysis of pulmonary contusion in motor vehicle crash victims: A Crash Injury Research and Engineering Network (CIREN) study." Summer Research Opportunities Program Poster Session, Wake Forest University Baptist Medical Center, Winston-Salem, NC — July 2007

3. **Gayzik, F.S.**, Danelson, K.A., Bonivtch, A.R., "A biofidelic lung surrogate for anthropomorphic test devices to predict pulmonary contusion following motor vehicle crash." Enhanced Safety of Vehicles, Student Competition, Lyon, France — June 2007

4. **Gayzik, F.S.**, Daly, M., Stitzel, J.D., "A method to determine pulmonary contusion severity through analysis of Hounsfield unit frequency." ASME Summer Bioengineering Conference, Keystone, CO — June 2007

5. **Gayzik, F.S**., Stitzel, J.D., Hoth, J.J., Brownlee, N.A., Daly, M., Meredith, J.W., "Correlation of pulmonary contusion volumes using computed tomography, histology and finite element analysis." American Thoracic Society International Conference, San Francisco, CA — May 2007

6. **Gayzik, F.S.**, Brownlee, N.B., Hoth, J.J., Stitzel, J.D., "An image analysis method for quantitating pulmonary contusion in histologic specimens." Southeast Bioengineering Conference, Durham, NC — May 2007

7. Stitzel, J.D., Tan, J., **Gayzik, F.S.**, Daly, M., Carr, J., Martin, S., Hoth, J.J., Miller, P., Meredith, W., "3-D real-time CT reconstruction: a tool for analyzing CIREN data." 34th International Workshop on Human Subjects for Biomechanical Research, Dearborn, MI — Nov. 2006

8 **Gayzik, F.S.**, Bostrom, O., Duma, S.M., Stitzel, J.D., "An experimental and finite element study of the porcine carotid artery under dynamic loading." Proceedings of the 30th American Society of Biomechanics, Blacksburg, VA — Oct. 2006

9. **Gayzik, F.S.**, J. J. Hoth, and J. D. Stitzel, "Optimization methods for finite element model validation: Fitting lung biomechanical model data to injury corridors (dynamic loading)." 5th World Congress of Biomechanics, Munich, Germany — Aug. 2006

10. **Gayzik F.S.**, J. J. Hoth, and J. D. Stitzel, "Optimization methods for finite element model validation: Fitting lung biomechanical model data to injury corridors (quasi-static and dynamic loading)." Icrash 2006, International Crashworthiness Conference, Athens, Greece — July 2006

11. **Gayzik F.S.**, Hoth J., Mercier J., Gage, H.D., Morton, K.A., Duma, S.M., Payne, R.M., Stitzel, J.D., "Development of a finite element injury metric for pulmonary contusion, Part I: Results of preliminary studies with rat lung." 4th SBES Research Symposium, Meadows of Dan, VA — May 2005

12. **Gayzik, F.S.**, Scott, E.P., Loulou, T., 2004, "Optimal control of thermal damage to targeted regions in a biological material." Proc. of ASME Heat Transfer/Fluids Engineering Summer Conference, Charlotte, NC — June 2004

Additional Presentations and Professional Meetings

Gayzik, F.S., Hoth, J.J., Stitzel, J.D. "Quantitative histology of the injured rat lung and comparison to computed tomography." *Invited Speaker*, The Ohio State University's 4th Injury Biomechanics Symposium, Columbus, OH — May 2008

Stitzel, J.D., Kilgo, P., Martin, S., **Gayzik, F.S.**, Meredith, W. "Age Thresholds for Chest Injury: Rib Fractures and Pulmonary Contusion." Presenter, 2008 SAE Government-Industry Meeting, Washington, DC — May 2008

McNeel Associates, *Rhinoceros Level 1 training*, Miami, FL — Dec. 2007

Gayzik, F.S., Duma, S.M., Stitzel, J.D., "Biomechanical analysis of arterial loading: Carotid injury biomechanics." *Invited speaker*, 5th Virginia Tech Injury Biomechanics Symposium, Blacksburg, VA — Mar. 2007

Livermore Software Technology Corporation, *LS-Dyna Training*, Livermore, CA — Feb. 2007

Gayzik, F.S., Duma, S.M., Stitzel, J.D., "Update: task 3, Carotid artery regional model development", *ARC Far-side Group Meeting*, Washington, DC — Jan. 2007

Gayzik F.S., Duma, S.M., Stitzel, J.D., *Carotid artery model update*, ARC Far-side Group Meeting, Melbourne, Australia — Jan. 2006

FDA Medical Device Seminar, Roanoke, VA — Apr. 2005

Research Experience

Graduate Research Assistant, School of Biomedical Engineering & Sciences
Sept. 2004 – Present

Virginia Tech - Wake Forest Center for Injury Biomechanics, Winston-Salem, NC

- Led experimental and computational lung injury research efforts
  - Developed a Matlab and LS-Dyna based model validation system using iSight integration software
  - Conducted impact experiments to gather mechanical validation data and physiological response data following pulmonary injury
  - Coordinated Computed Tomography and Positron Emission Tomography imaging research efforts
- Developed organ-level and regional-level finite element model of the carotid artery for blunt impact studies
  - Worked on fluid-solid interface simulations using LS-Dyna Lagrangian-Eulerian formulation
  - Conducted material model study for carotid artery model
- Led computational efforts in geometric morphometrics research
  - Aided in development of shape analysis software suite in Matlab
  - Coordinated lab efforts in collecting anatomical landmark data for study of thoracic shape change
- Led development of the Wake Forest University Pulmonary Surrogate (crash test dummy lung)
  - Developed functional prototype including pressure data acquisition system and GUI
  - Worked with industry partners to deliver final product under budget constraints
  - Won first prize in international student design competition sponsored by Dept. of Transportation and National Highway Traffic Safety Administration

Graduate Research Assistant, Virginia Tech, Department of Mechanical Engineering
Jan. 2003 – Sept 2004

Thermal and Inverse Characterization Laboratory

- Programmed inverse heat transfer algorithm in Matlab for determining appropriate thermal dose for heating biological materials
- Conducted thermal ablation experiments on biological material (albumin), data collected via LabView

Summer Research Assistant and Intern, l'Ecole des Mines d'Albi-Carmaux, France
May – Aug 2003

Thermal and Inverse Characterization Group, *Advisor: Dr. Tahar Loulou*

- Developed Matlab algorithms for solving inverse heat transfer and optimization problems

Undergraduate Research, Virginia Tech, Department of Mechanical Engineering

Finite Element Group, *Advisor: Dr. Robert West* Sept. 2001 – May 2002

- Surveyed methods of soft-tissue modeling in finite element applications

Material Characterization Laboratory, *Advisor, Dr. Larry Mitchell* Feb. – May 2000

- Quantified frequency dependent elastic modulus of rubber-like material for tire OEM

Other Appointments and Institutional Service

Teacher's Assistant, Virginia Tech – Wake Forest University SBES

Injury Physiology Feb. 2007

- Gave lectures on lung injury physiology

Introduction to Biomedical Engineering Nov. 2006

- Gave lectures on injury biomechanics

Machine Shop Training for Incoming Students Sept. 2006 – Present

- Trained incoming students on shop safety

Vice Chair, IEEE Engineering in Medicine and Biology Oct. 2006 – Present
Wake Forest University Club
- Organized new student welcome picnic and social activities

Honor Code Representative, Department of Biomedical Engineering, Sept. 2006 – Present
Wake Forest School of Medicine, Winston-Salem, NC

Teacher's Assistant, Department of Mechanical Engineering, Aug. 2002 – May 2003
Virginia Tech, Blacksburg, VA
- Graded thermodynamics section homework and tests

Study Abroad, Centro Politécnico Superior, University of Zaragoza, Spain Aug. 2000 – June 2001
- One year student exchange to study mechanical engineering

Calculus Tutor, Center for Academic Enrichment and Excellence Aug. 1999 – Dec.1999
Virginia Tech, Blacksburg, VA

Mechanical Engineering Work Experience

Consultant, Winston-Salem, NC Nov. 2006
- Performed finite element analysis of biomaterial patent

Engineering Assistant, Mechanical Solutions, Inc., Whippany, NJ
- Team resolved rotational imbalance of multi-stage compressor installation Nov – Jan 2001-02
- Performed computational fluid dynamics analysis of journal bearing May – Aug 2001
- Assisted with on-site vibration analysis of centrifugal pump May – Aug 2000

Engineer in Training, Eastman Chemical Co., Kingsport, TN
- Performed thermodynamic analysis on process equipment May – Aug. 2002
- Performed structural analysis of rotating heat-exchange equipment

Programming Intern, Dow Jones & Co., Inc., South Brunswick, NJ
- Loaded software and configured Macintosh computers for employees nationwide May – Aug. 1999
- Created database with Access to facilitate preparation of payroll documents May – Aug. 1998

Computer Skills

Programming Languages:	MATLAB, SAS
Simulation Software:	LS-Dyna, MATLAB, Mathematica
FEA Pre/Post Processing Software:	LS-PrePost, HyperMesh, TrueGrid, Z Print
Optimization / Process Integration:	Isight
Image Analysis Software:	TeraRecon, Mimics, Image J
Data Acquisition & Real-Time Control:	MATLAB, WaveView
High Speed Video:	Phantom
NURBS modeling:	Rhinoceros

Honors and Awards

Association for the Advancement of Automotive Medicine
John D. States Student Paper Award Oct. 2006

Biomedical Sciences Instrumentation Symposium (Rocky Mountain Bioengineering Symposium)
Anthony Sances Jr. Award of Merit Apr. 2008
First Place, Ph.D. Student Presentation Apr. 2007
Third Place, Ph.D. Student Presentation Apr. 2006
Third Place, Ph.D. Student Poster Apr. 2006

National Highway Traffic Safety Administration
First Place, International Student Design Competition, 20th Enhanced Safety of Vehicles
Wake Forest University Pulmonary Surrogate July 2007
National Collegiate Inventors Hall of Fame
National Finalist, Collegiate Inventors Competition Oct. 2007
Wake Forest University Pulmonary Surrogate
National Institutes of Health
National Graduate Student Research Festival, Bethesda MD. Sept. 2008
Stapp Car Crash Conference
First Place, Student Paper Competition Oct. 2007
United States Department of Defense
Alternate, Science and Mathematics Academic Research for Transformation (SMART) Fellow June 2007
Virginia Tech
Virginia Tech Scholar Scholarship 1998-2000
Dean's List: College of Engineering Fall 1997, Spring 2000, Spring 2002
Dean's List w/Distinction: College of Engineering Fall and Spring 1999, Fall 2000, Fall 2001
Virginia Tech, School of Biomedical Engineering and Sciences
Outstanding Masters Presentation Award, SBES Apr. 2004
Wake Forest University, Graduate School of Arts and Sciences
Alumni Student Travel Award Sept. 2006, Oct. 2007
Wake Forest University, School of Biomedical Engineering and Sciences
Outstanding Ph.D. Poster Presentation Award, SBES May 2007
Outstanding Ph.D. Presentation Award, SBES May 2008

Patents and Copyrights

"Pulmonary Surrogate and Related Methods including Pressure Sensors," July 2007
U.S. Provisional Patent, Gayzik, F. S., Danelson, K.A., Bonivtch, A.R., Stitzel, J.D.

"Code for Lung Surrogate Analysis Graphical User Interface: A Matlab Algorithm for the Determination of Impact Magnitude for an Instrumented Pulmonary Surrogate
U.S. Copyright Pending, Gayzik, F.S. July 2007

Professional Memberships

Association for the Advancement of Automotive Medicine Feb 2008 – Present
Socieity of Automotive Engineers (SAE) student member May 2008 – Present
IEEE Engineering in Medicine and Biology Society July 2005 – Present
Pi Tau Sigma, National Mechanical Engineering Honors Society Jan 2002 – Sept. 2004
National Society of Collegiate Scholars Aug. 2001

Referee of Peer Reviewed Journals

Journal of Anatomy
International Journal of Crashworthiness
Journal of Biomechanics
Internal Journal of Heat and Mass Transfer

Community Activities

Coach, SBES Departmental Softball, Winston-Salem, NC 2006, 2007, 2008
SBES Departmental Flag Football, Winston-Salem, NC 2005 – 2007
Member, Wake Forest University Cycling Club, Winston-Salem, NC 2006, 2007
Regular Columnist, The Collegiate Times, Blacksburg, VA 2003, 2004